A study of the interface stresses in trans-tibial sockets. (A comparison of PTB and Hydrocast sockets)

Noor Azuan Abu Osman
Dip.(Mech.), BEng (Mech.), MSc (Bioeng.)

This thesis is presented in fulfillment for the degree of Doctor of Philosophy
at the Department of Bioengineering, University of Strathclyde , Glasgow

June 2005

Declaration of Author's Right

ACKNOWLEDGEMENTS

I am especially indebted to my wife, Liana and my three kids, Nadia, Erwin and Natli whose encouragement, patience, and understanding helped make completion of this degree possible. I am grateful beyond words.

I would like to acknowledge with gratitude to my supervisors, Mr W.D Spence and Mr S.E Solomonidis for invaluable supervision, cooperation, encouragement throughout this work, criticism and revision of my writing. I am extremely grateful.

My appreciation is also to Professor J.P Paul for his advice and comment during writing up of the thesis.

I wish to express my thanks to Mr Steve Murray, Mr Ian Tullis, Mr John Maclean, Mr David Robb, Mr Robert Hay, Mr Willey Tearney, and Mr Dave Smith who applied their professional expertise in the fabrication of the sockets and transducers.

I would like to thank all the ten subjects who participated in this study.

I would like to acknowledge the financial support from the Malaysian Government administered through University of Malaya, Malaysia, Department of Biomedical Engineering, University of Malaya, Malaysia and Bill Spence's personal research fund, Department of Bioengineering, University of Strathclyde, UK.

ABSTRACT

The concept of loading "pressure tolerant" areas and relieving load from "pressure sensitive" areas of a below knee stump as applied by a Patellar Tendon Bearing (PTB) socket, was based on logical biomechanical principles. (Radcliffe and Foort, 1961) Inconsistencies during rectification of the PTB cast remain a source of error during production of a socket. Kristinsson (1992) described the use of the Icelandic Roll on Silicone Socket (ICEROSS) (or silicone liner). During this casting process, placing a container over the stump allows the air around the stump to be pressurized and thus the cast is formed. Kristinsson (1993) claimed that in most cases, the concept of load transfer to areas such as the patellar tendon, medial flare and condyles of the tibia is ineffective and uncomfortable. His belief is that the most effective socket is one that relies on "hydrostatic principles" for transfer of load. The current study presents a method of producing a socket called 'Hydrocasting', which was originally introduced by Murdoch (1965) as the 'Dundee socket'. The concept behind the 'Hydrocast socket', whereby water is used as a medium to apply uniform pressure around the stump whilst the applied plaster bandage sets, results in a mould of the stump suitable for socket production with minimal or no subsequent cast rectification. The major difference between the conventional PTB socket and the hydrocast socket is that the hydrostatic cast is minimally rectified or not rectified at all.

The aim of this study was to investigate the interface pressure distribution between the residual limb and the prosthetic socket of ten trans-tibial amputees and the principal objectives were (a) to design and develop transducers which would enable simultaneous dynamic measurement of pressure and shear stresses. (b) to determine the variation in pattern of pressure distribution associated with various positions of the patellar tendon bar indent in a trans-tibial socket and (c) to measure stump/socket interface pressure and shear stresses for the PTB and hydrocast socket designs.

Two new custom made transducers, in addition to two previously described transducers, for the measurement of stump/socket interface stresses were designed and

developed. The transducers, constructed using electrical resistance strain gauge technology, are capable of measuring normal and shear stress simultaneously when mounted on a prosthetic socket. One design of transducer allows the measurement of normal and shear stress to be undertaken, and the other design, in addition, allows the sensing surface at the patellar tendon to be translated by, up to, 10 mm from the neutral position for the purpose of examining the effect of patellar tendon bar indentation on the pressure distribution at the interface.

Subjective feedback from all participants indicated that when tendon bar was in the relief position this was preferred. The position of the patellar tendon bar had no significant effect on the pressure distribution around the socket indicating that it is an unnecessary feature, which, is proposed, may be eliminated during manufacture of a trans-tibial socket.

The hydrocast socket compared to PTB socket shows a more even distribution of pressure in the socket and the values for pressures and shear stresses are lower. Subjective feedback from all participants also favoured the hydrocast socket. It is believed that lower, more evenly distributed pressure enhances the comfort of the prosthesis user.

PUBLICATIONS

The research described in this thesis had led to the presentation and publication of the following papers:

(1) N A Abu Osman, W.D Spence, S.E Solomonidis, A.M Muir, 2005. Patellar tendon bar! Is it a necessary feature? J Rehabil Res Dev. (in prep.)

(2) N A Abu Osman, W.D Spence, S.E Solomonidis, A.M Muir, 2005. Transducers for the determination of the pressure and shear stress distribution at the stump/socket interface of trans-tibial amputees. Journal of Engineering in Medicine. Part H. Instn. Mech Engrs. (in prep.)

(3) N A Abu Osman, W.D Spence, S.E Solmonidis, A.M Muir, 2004. The patellar tendon bar – the case for or against! ISPO UK NMS, York, 2004
(BLESMA Award winner)

(4) N A Abu Osman, W.D Spence, S.E Solomonidis, A.M Muir, 2004. A simple and low cost method of producing a prosthetic socket for trans-tibial amputees. IEE 3rd Seminar on Appropriate Medical Technology for Developing Countries. London, 2004, pp 33/1 - 33/4. ISSN 0963-3308-reference no: 03/10408

(5) N A Abu Osman, W.D Spence, S.E Solomonidis, A.M Muir, 2004. Interface pressure measurement of Hydrocast and PTB sockets. 11th World Congress of the International Society for Prosthetics & Orthotics. Hong Kong, 2004. pp 32. ISBN 988-97974-1-0

(6) N A Abu Osman, W.D Spence, S.E Solmonidis, A.M Muir, 2004. The patellar tendon bar – the case for or against! 11th World Congress of the International Society for Prosthetic & Orthotics. Hong Kong, 2004. pp 33 ISBN 988-97974-1-0

(7) N A Abu Osman, W.D Spence, S.E Solomonidis, A.M Muir, 2004. Design and development of transducers for the measurement of trans-tibial stump/socket interface stresses. Kuala Lumpur International Conference on Biomedical Engineering. 2004. Proc. of the International Federation for Medical and Biological Engineering (IFMBE Proc.) 2004; 7: 315-318. ISBN 983-2085-68-3

(8) N A Abu Osman, W.D Spence, S.E Solomonidis, A.M Muir, 2004. A simplified method of producing trans-tibial prosthetic socket. Kuala Lumpur International Conference on Biomedical Engineering. 2004. Proc. of the International Federation for Medical and Biological Engineering (IFMBE Proc.) 2004; 7: 327-328. ISBN 983-2085-68-3

(9) N A Abu Osman, W.D Spence, S.E Solomonidis, A.M Muir, 2003. Pressure distribution in PTB and Hydrocast sockets. A preliminary study. ISPO UK NMS, Newcastle, 2003. pp 18

Content

Chapter 6: Methods

Chapter 7: Results

Chapter 8: Discussion

CHAPTER 1: INTRODUCTION

1.1 Overview and hypothesis

The amputation of a lower limb may be brought about by severe traumatic injury, infection, vascular disease, tumour and severe deformity. (Murdoch, 1970; Marquardt and Correll, 1984). In a statistical study of 6000 amputees in the United States of America, (Kay and Newman, 1975) showed that 92% of all amputations involve the lower limb and that trans-tibial amputations accounted for 54% and trans-femoral amputations 33% of all amputations. In the United Kingdom (UK), out of 5298 new referrals of lower limb amputees to limb centres, 52% were at the trans-tibial level. (NASDAB, Edinburgh 2003). The next most common level of amputation was trans-femoral accounting for 39%. The overall total showed a 6% increase in amputee referrals from the previous year thus indicating an increasing trend in the number of amputations performed. This trend is reflected globally.

The causes of amputation may have a different prevalence in other parts of the world. In India, for example, 82% of amputations are due to trauma (Narang and Jape, 1982). In the UK, amputee referrals to the limb centres has risen from 3500 per annum in 1961 to 5298 in 2002 (Ham et al, 1989; NASDAB, Edinburgh 2003). This trend is also seen in other countries, such as, the USA, from 33000 amputations in

1965 (Ham and Cotton, 1991) to 118,000 in 1983 (Rutkow and Marlboro, 1986); and Sweden from 170 per million population in 1962 to 410 per million in 1977 (Renstrom, 1981). Even though these statistics are somewhat out of date, they clearly show that there are numerous amputees and their number is growing.

Rehabilitation treatment for the trans-tibial amputee may include an external prosthesis to restore walking function and normal appearance to the individual. Engineering principles have been adapted and applied to the design of substitute limbs resulting in the appearance of a wide variety of joint mechanisms and prosthetic feet. New methods of manufacture have rapidly advanced the design and performance of lower-limb prostheses. However the design of the interface between the residual limb and the prosthetic socket is a crucial factor in determining the amputee's mobility and independence. It is highly dependent on the quality of fit and comfort of the prosthesis. The aim of the prosthetist is to provide a comfortable prosthesis, which will minimize residual limb tissue damage and provide adequate stability. A thorough understanding of the stress distribution between the residual limb and prosthetic socket is critical to the design process, as the shape of the resulting socket directly effects the transmission of forces between the stump and the prosthesis. Currently it is estimated that 25 % of prosthetic sockets manufactured in the UK are either rejected as ill fitting or are severely modified in order to achieve an acceptable 'fit'. (Spence, 2005).

With the exception of prostheses fitted using the osseointegration techniques of Branemark et al (2001) most lower limb prostheses must transmit ground reaction forces through the soft tissues of the residual stump to the underlying skeleton. Prior

to amputation these soft tissues would have been unaccustomed to bearing such loads, they are therefore vulnerable to damage occurring from the use of the prosthesis. It is the task of the prosthetist to ensure that a prosthesis is designed, for the amputee, in such a way as to transmit the loads associated with locomotion and yet minimise, if not obviate, the risk of damage to the tissues.

A survey showed that 23% of amputees complained that their limbs were uncomfortable (McColl, 1986). The main cause of these problems was a poor prosthetic socket fit. The interface pressure distribution is important, excessive loading on the tissues can lead to pain and discomfort or, more seriously, insufficient circulation causing tissue damage. Residual limb tissue damage can have a dramatic effect on an amputee's lifestyle. If severe blisters or pressure sores occur, an amputee may be unable to wear the prosthesis until the tissue has healed. Since loads are transferred from the prosthesis to the residual limb through the socket, the socket design is critical in keeping tissue damage minimal. Continued use of a prosthesis following tissue breakdown and tissue trauma can lead to further disability and intolerance to the prosthesis (Levit, 1981). For the very severe cases amputation to a higher anatomical level may be required.

Studies have been conducted to investigate the role of both normal pressure and shearing force as factors in pressure sore formation. Most of the studies concerned pressure sore formation on the buttocks of paraplegics and quadriplegics and these results may be applied to the loading of the tissues of the residual limb of an amputee. Lindan et al (1985) and Mooney et al (1971) conducted research on the pressure distribution during sitting, related to wheelchair cushion design, utilising a

variety of transducers (a capacitance transducer; a bed of compression springs and a pneumatic cell pressure transducer). However all of these studies were limited to consider normal pressure measurement only.

The understanding of the complex interplay of normal and shear stresses between the stump and the socket is seen as fundamental to developing a biomechanical model and therefore a way in which improvements in socket design can be progressed. Meaningful interface pressure measurements require a proper measurement technique, the use of accurate and reliable transducers, and appropriate placement of the transducer at the stump/socket interface and the correct data acquisition and analysing capabilities. An ideal system would be able to continually monitor both normal and shear stresses without significant interference to the original interface condition.

A socket is custom-designed, unlike the shank and foot which are, normally, commercial components. Despite their importance in causing tissue breakdown, residual limb/prosthetic socket interface stresses have been measured by relatively few investigators. Previous studies of the stump/socket interface have mainly focused on pressure. It is believed that further useful information applicable to prosthetic design could be obtained from an investigation of relationships between pressure and shear stresses. Analysis techniques such as Finite Element may be used to predict both normal and shear stresses, however the techniques must be verified/validated by experimental measurement.

Prosthetists, when fitting a socket rely on a visual assessment of the stump/socket relationship; this is clearly a limitation on objectivity since it is a non quantitative procedure and relies on the experience of the prosthetist. According to Sanders (2000) it is not clear which pressure / shear combinations will provide a comfortable prosthetic socket and which will cause tissue breakdown. This lack of knowledge is a severe limitation on fitting techniques and may, in part, be responsible for the reported, (Livingstone et al, 1994); 38 % incidence of infection or skin breakdown on the stump. This study aims to address the lack of objectivity and provide information on both normal and shear stress occurring at the stump/socket interface.

1.2 Objectives

The interface pressure distribution between the stump tissues of a trans-tibial amputee and the socket is believed to determine the comfort of the prosthesis, therefore, should be considered in the design of the socket. Socket design should be based on a full understanding of the stump/socket interface biomechanics. The study described in this thesis aimed to develop and understand the interface biomechanics as a basis for socket design. The main aim was to investigate the interface pressure distribution between the residual limb and the prosthetic socket of the trans-tibial amputee and the principal objectives of the research area are as follows:

a. To design and develop transducers which would enable simultaneous dynamic measurement of pressure and shear stresses.
b. To determine the variation in pattern of pressure distribution associated with various positions of the patellar tendon bar indent in trans-tibial socket.
c. To measure stump/socket interface pressures and shear stresses for the Patellar Tendon Bearing (PTB) and hydrocast socket designs for 10 trans-tibial amputees.

1.3 Outline of thesis

The outline of the remainder of this thesis is as follows: Chapter 2 gives a basic introduction to trans-tibial prosthetics, the conventional PTB and contemporary Hydrocast prostheses. In Chapter 3 the literature on various approaches and equipment that have been used to examine socket interface stresses in trans-tibial amputees is reviewed. Chapter 4, details the design, manufacture and development of the custom-made transducers which enable simultaneous dynamic measurement of pressure and shear stresses at the stump/socket interface to take place. Chapter 4 also contains details of the commercial pressure measurement system, F-Socket™ system from Tekscan, Inc. South Boston, MA, USA that was used in this research, including the customized calibration technique. Chapter 5 describes the calibration and performance of the custom designed transducer. Chapter 6 describes the methodology used to address the specific aims of the research including socket manufacturing and experimental procedure. Chapter 7 presents the experimental results obtained from this study. Chapter 8 presents the discussion of the work undertaken here and suggests further research. Finally, the conclusion are summarised in Chapter 9.

CHAPTER 2: TRANS-TIBIAL PROSTHETICS

2.1 Introduction

In the walking gait of normal person, body support forces are transmitted directly to the skeleton through soft tissues of feet accustomed to doing so while for the subject who has undergone amputation; those support forces are to be transmitted through soft tissues unaccustomed to this role. Whatever level of amputation either above knee or below knee, it will affect prosthetic fittings, later rehabilitation requirements and also quality of life of the patient. In effect the stump plays similar role to the foot of a healthy limb.

2.2 Trans-tibial Amputation Surgery

This section describes, briefly, the basic procedures of trans-tibial amputation surgery. Individuals who have undergone amputation of the leg/foot at a level through the tibia/fibula are referred to as trans-tibial amputees. Causes of such amputation are described in Chapter 1. Beside the need to stabilise the trauma or disease condition, the surgery aims at fashioning a residual limb, with a healthy skin envelope, to which a prosthesis can be fitted and thus restore functional mobility or ambulation.

One of the main aims in trans-tibial amputation is the preservation of the knee joint. The advantages of preservation of the knee joint are highlighted by

Castronuova (1980). The presence of the knee joint could enable an amputee with average stump length to produce a gait similar to that of a normal subject. The trans-tibial amputation takes place below the knee approximately 140 mm from the tibial plateau; but more often, as a guide, the lower leg is divided into three equal parts and two thirds are removed. Too short or too long a stump creates difficulties in a fitting prosthesis and a knee flexion contracture greater than 15 degrees is unsuitable for a prosthetic device (Ham and Cotton, 1991).

When a below knee amputation is confirmed, there are currently two major choices of surgical technique practiced. The Long Posterior Flap, (Burgess, 1968) and the Equal Flap methods (Robb et al, 1965; Termansen, 1977 and Robinson, 1988). These are general techniques which have their variations. The Long Posterior Flap method is most often used as the posterior tissues are generally better vascularised by collateral arteries than the anterior tissues. Where there is insufficient viable posterior tissue, through trauma or ulceration, the Equal Flap method is used. Robinson (1988) and McCollum et al (1985) suggest that the skewed sagittal flaps version of the Equal Flap method may usefully divide the limb into an anteromedial flap supplied by the saphenous artery and a posterolateral flap supplied by the sural artery. The Long Posterior Flap has since been refined by Burgess (1969) (Figure 2.1) and Equal Flap by Robinson (1988) (Figure 2.2).

2.2.1 The Long Posterior Flap technique

For the Long Posterior Flap method the anterior skin incision is made to the level of the deep fascia, 8-12 cm distal of the tibial tuberosity. The level of the transection is somewhat dependant on the viability of the tissues and the blood supply. An optimal length of 12-18 cm with a minimum of 8 cm is suggested (Burgess, 1985 and Vitali et al, 1996). Quesada and Skinner (1992) suggest that any extra length of the limb retained at surgery theoretically reduces the average normal stress experienced by the limb in a socket. Too long a stump may cause prosthetic problems as the muscle flap used to pad the distal end of the tibia, becomes tendonous over its distal third, thus providing poor soft tissue coverage and a boney stump.

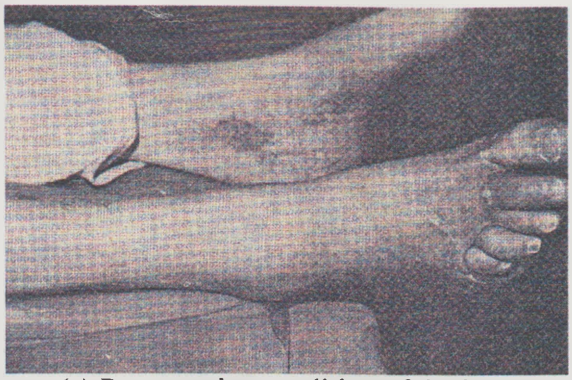

(a) Preoperative condition of the leg

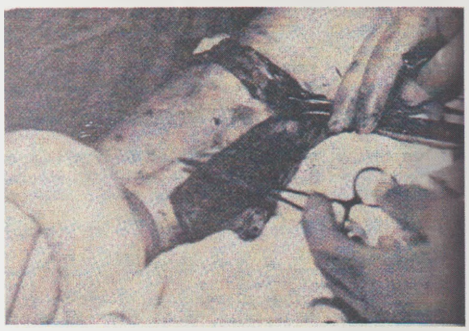

(b) Skin incision with provision for Long Posterior Flap

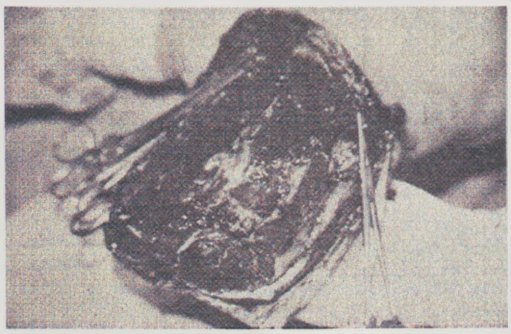

(c) Tibia and fibula sectioned level of anterior skin incision

(d) Tibia rounded to provide good stump contour

Figure 2.1 Long Posterior Flap method for trans-tibial amputation. (Reproduced from Burgess,1969).

(e) Flap ready to be brought forward and approximated

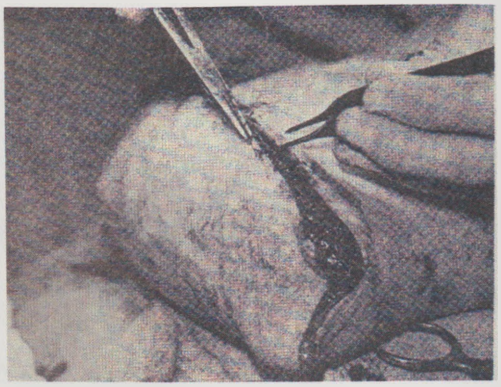

(f) Deep fascia-posterior muscular flap has been sewn

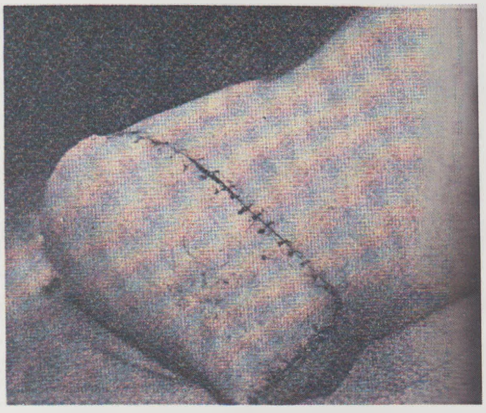

(g) Appearance of stump at time of closure

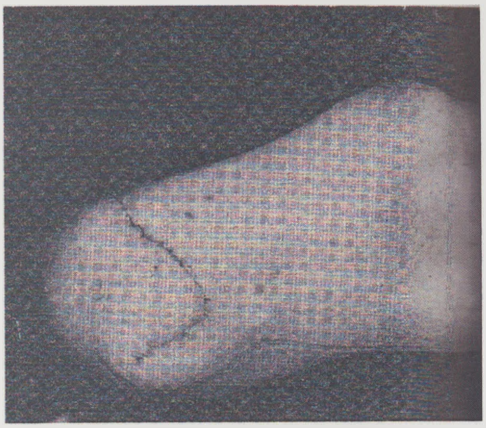

(h) Stump at twenty five postoperative day.

Figure 2.1 Long Posterior Flap method for trans-tibial amputation.
(Reproduced from Burgess,1969).

Continued from page11.

2.2.2 The Equal Flap technique

With the Equal Flap method, the skin incision is begun 10 – 14 cm distal from the tibial plateau, 2 cm lateral of the tibial crest, and 2 cm distal from the proposed tibia transaction. The fibula is sectioned 2 - 4cm proximal of the proposed tibial transection. It is considered advantageous to retain the fibula to create a triangular shaped residual limb, which is more resistant to rotation in the prosthetic socket. The periosteum around the tibia is divided and elevated on the anterior aspect. Care must be taken to avoid disturbance of the precarious anterior blood supply. Tibial division is followed by the cutting of a bevel on the anterior surface of the distal end, which is rounded by file. For the Long Posterior Flap method, the distal part of the limb is removed by dissection of muscle from the posterior surfaces of the tibia and fibula. The deep flexor muscles are sectioned 3 cm below the level of the tibial section, and the underlying peroneal and tibial vessels ligated and sectioned. Angel (1979) and Burgess (1985) recommend bevelling the remaining gastroenemius-soleus muscle flap from just distal to the deep flexor muscles to the level of the fascia at the distal end of the flap. However, others (Waddell, 1981; Little, 1985; and McCollum, 1989) advocate the complete removal of the soleus muscle, as it derives its blood supply from the anterior arteries which may be weak.

(a) Skin incision, section of anterior tibial muscle groups. Ligate and section arteries and nerves

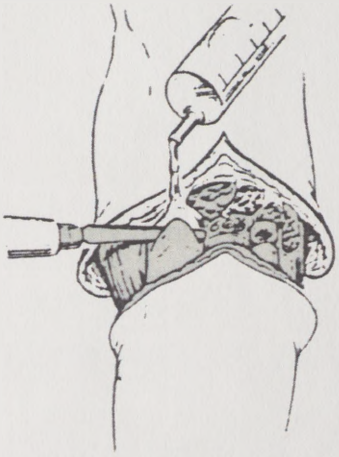

(b) Section tibia and fibula.

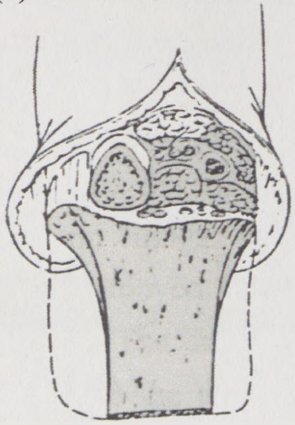

(c) Section lateral muscle group, ligate vessel and nerves

Figure 2.2 Equal Flap method for trans-tibial amputation.
(Reproduced from Robinson, 1988).

(d) Suture muscle tongue to muscle or bone

(e) Suture skin

Figure 2.2 Equal Flap method for trans-tibial amputation.
(Reproduced from Robinson, 1988).

Continued from page14

2.3 Prosthetic design

As this study concerns interface pressure distribution as related to prosthetic socket design, some background information regarding methods of trans-tibial prosthetic design and manufacture appear warranted. In general, a trans-tibial prosthesis consists of a socket with an optional liner, adapter hardware to attach the socket to modular endoskeletal components, and appropriate artificial foot. In addition, the prosthesis may include some sort of auxiliary suspension sleeve.

2.4 Design of the socket

The early socket for a lower limb amputee was a simple inverted cone shape which accommodated the conical stump. Details of stump anatomy and biomechanics were not considered. Radcliffe and Foort (1961) of the University of California, following the studies on possible load-bearing principles, developed the Patellar Tendon bearing (PTB) socket in the 1950s. This design provided a more efficient distribution of pressures around the stump than any other socket in that day. The load is chiefly taken by the load-tolerant areas: patellar tendon, medial tibial flare, and the posterior aspect of the stump. The patellar tendon forms a major weight-bearing area. Relief is given to the sensitive areas, such as the crest of the tibia, tibial tubercle, fibula head and cut ends of the fibula and tibia. A leather cuff encircles the distal thigh in the supracondylar area.

Kristinsson (1992), described the use of the Icelandic Roll on Silicone Socket (ICEROSS) (or silicone liner) in their socket. During the casting process, the subject's limb is held in full extension with the subject seated. Build-ups of silicone padding are added over the bony areas of the stump, such as the anterior-distal aspect of the tibia and the fibular head. The silicone liner is rolled onto the stump and a plaster wrap cast is applied without applying localised pressure. Placing a pressure container over the stump allows air to be pressurised and thus the cast is formed to the stump. Kristinsson (1993) claimed that in most cases, the concept of load transfer to areas such as the patellar tendon, medial flare and condyles of the tibia is ineffective and uncomfortable. His belief is that the most effective socket is one that relies on "hydrostatic principles" for transfer of load.

2.4.1 Patellar Tendon Bearing socket

The PTB socket became the most commonly prescribed prosthesis for trans-tibial amputees in the developed world. The concept of loading the "pressure tolerant" areas and relieving load from the "pressure sensitive" areas was based on logical biomechanical principles. Whilst this has been successfully worn by many amputees over the decades; a high degree of skill is necessary to take a wrap cast and rectify the positive mould in order to produce a satisfactory socket. A PTB socket in cross section is shaped like a triangle and its medial and lateral walls are higher than the anterior and posterior. The posterior wall has a flare to accommodate knee flexion and to make the socket more comfortable in the sitting position. Radcliffe and Foort

(1961) and Barclay (1970), reported the fabrication of a PTB socket which can be summarised as follows:

(a) A thin wet cast sock is pulled over the stump. The fit must be snug to prevent shifting of the cast sock, which would distort the marker locations.

(b) To emphasize the bony prominence, help define the patellar tendon and locate the insertions of the hamstring tendons, the stump is held in 20° flexion during marking and wrapping.

(c) The mediolateral and anteroposterior dimensions are measured (at the level of the apex of the femoral condyles, and from the patellar tendon to the popliteal fossa, respectively) with a calliper. The distance from the distal end of the stump to the patellar tendon is also measured.

(d) The following markings are made: *(a)* outline of the patella, *(b)* patellar tendon, *(c)* tibial tubercle, *(d)* apex of the head of the fibula, *(e)* anterior crest of the tibia, *(f)* distal end of the fibula, *(g)* distal end of the tibia, *(h)* medial flare and *(i)* medial border of the tibia. (See Figure 2.3).

(e) A plaster of Paris wrap is applied with light finger pressure. (See Figure 2.4). Light finger pressure is applied over the patellar tendon and popliteal area. (See Figure 2.5).

(f) After the wrap has dried, the cast is removed.

(g) Using the cast as a mould, a positive model of the stump is produced. Rectification is performed, plaster is removed in the appropriate areas to produce a "pre-compressed" state in the tissues of the patellar tendon and popliteal area.

(h) Plaster is removed over the medial and lateral flares of the tibia. Relief are required to prevent impingement on the hamstring tendons during knee flexion. The patellar tendon area is modified by cutting a groove between the inferior edge of the patellar and the superior edge of the tibial tubercle at right angles to the line of progression. This groove should have a minimum depth of 12mm. and a maximum height of about 25mm and more normally about 18mm. (See Figure 2.6 and Figure 2.7). The groove is then curved to outline the patellar. Rectification is performed by adding or removing some plaster in appropriate areas. This modified cast is a plaster positive of the socket. Finally the 'hard' plastic shell of the socket itself is formed over the plaster model.

(i) Once the socket has been successfully formed, the remaining components of the prosthesis are selected, and the final prosthesis assembled.

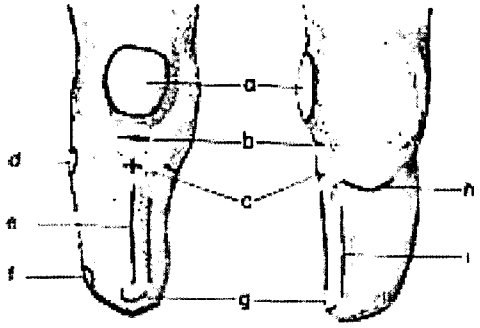

Figure 2.3 Markings location.

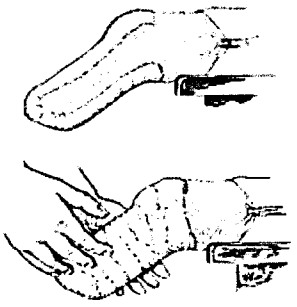

Figure 2.4 Plaster of Paris applied.

(Reproduced from Radcliffe and Foort, 1961).

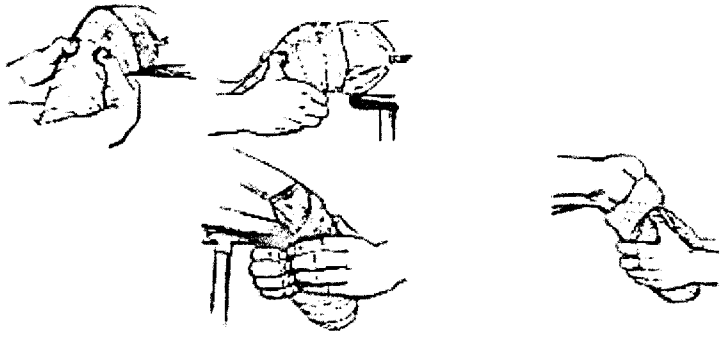

Figure 2.5: Light pressure applied.
(Reproduced from Radcliffe and Foort, 1961).

Figure 2.6: Finger pressure being applied to the plaster wrap

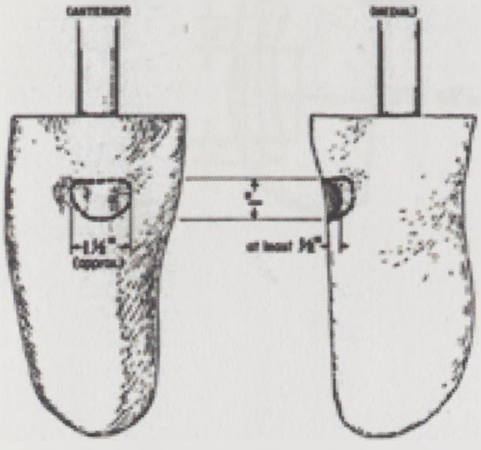

Figure 2.7: Approximately dimensions to produce the patellar tendon indent. (Reproduced from Barclay, 1970).

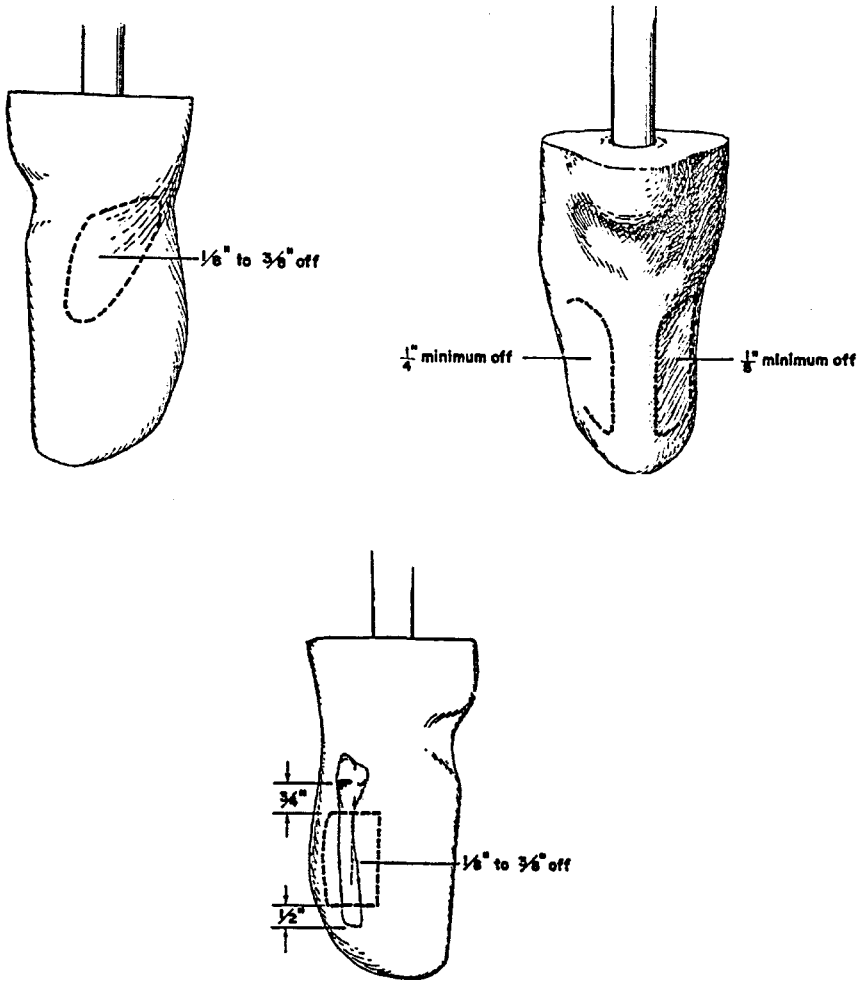

Figure 2.8: Area and the depth of rectification of PTB cast.
(Reproduced from Barclay, 1970).

2.4.2 The Hydrocast socket

This study presents a method of producing a socket which does not require the expertise of a skilled prosthetist and probably involves minimal capital expenditure. This technique, called 'Hydrocasting', was originally introduced by Murdoch (1968) as the 'Dundee socket'. The idea is to eliminate inconsistencies using the hand casting technique i.e. minimizing an element of human error. This system ensures total contact over the entire stump area, whilst still maintaining the ability for cast rectification to provide areas of high and low pressure tolerance such as at the patellar tendon bar. The concept behind the 'Hydrocast socket', whereby water is used as a medium to apply uniform pressure around the stump whilst the applied plaster bandage sets, results in a mould of the stump suitable for socket production with minimal or no subsequent cast rectification. However, in this study the hydrocasts socket are produced without patellar tendon bars. Murdoch (1968) describes the manufacturing process of a Hydrocast socket in the following steps:

a) The patient places the stump into a tank, sharing their weight evenly between the amputated limb and the natural limb. (See Figure 2.9).

b) Water is added to the tank until the patient is balanced and the amputated side is immersed in the tank approximately three inches above knee level.

c) Patient was then removes the stump and a nylon stockinette is placed over the stump. Layers of thin stump sock, impregnated with plaster, are then pulled over the stump.

d) The patient's knee is set in the tank at approximately 10^0 flexion, until the plaster has hardened.

d) Once hardened, the negative cast is removed from the stump to generate a positive cast and the socket is fabricated using standard techniques.

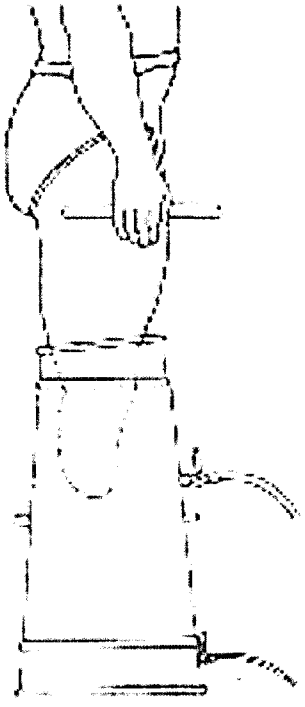

Figure 2.9: Hydrostatic casting method. (Reproduced from Murdoch, 1968).

2.4.2.1 Pressurised hydrostatic tank – fabrication of the hydrocast socket

The pressurised hydrostatic tank system used in this study consists of a cylindrical tank, pressure gauge, membrane and water. The tank with an opening at one end is sealed with the membrane which allows placement of the stump within the tank, but separated from the water, following application of the plaster wrap cast. The subject is then asked to stand in his normal standing position and water was introduced into the tank until full. (See Figure 2.10). The subject is then asked to transfer full body weight to the stump in order to obtain uniform hydrostatic pressure. Once the plaster had hardened, the system is depressurised by removing the water from inside the tank and the stump with the plaster wrap is then removed from the tank. The plaster wrap is removed from the stump to generate a positive cast and the socket is fabricated using standard techniques with no or minimal rectification being performed by the prosthetist.

Figure 2.10: Subject standing in hydrostatic tank.

The major difference between the conventional PTB socket and the hydrocast socket is that the hydrostatic cast is minimally, or not at all rectified. This study aimed to compare both socket designs.

2.5 Prosthesis alignment

The alignment of a prosthesis refers to the position of the socket and limb relative to the foot. The adaptor hardware used to attach the socket to the endoskeletal components, and to the foot, typically allows a range of alignments. Alignment of the prosthesis consists of both static and dynamic stages. A typical static alignment of the socket places the knee in approximately 5^0 of flexion to prevent hyperextension and increase pressures on the anterior surface of the limb, and 5^0 of shank abduction to concentrate pressures in the medial tibial condylar region. (Barclay, 1970; Pearson et al, 1973; Zahedi et al, 1986). In addition, the top plane of the prosthetic foot is set in the horizontal plane, the pylon is vertical, and the alignment in the parasagittal plane should be such that a plumb line at the projection of the centre of the greater trochanter intersects the mediolateral axis of the knee, and lines up with the anterior surface of the pylon (i.e. no tendency for the knee to buckle during stance). Dynamic alignment is based on an analysis of the amputee's gait both anteriorly, posteriorly and laterally. Zahedi et al (1986) found that an amputee can adapt to several alignments ranging from as much as 148 mm in shifts and 17^0 in tilt. This tolerance of alignment variability was believed to be related to the degree of control that an amputee has over the prosthesis (i.e. the retention of the knee joint in a below-knee amputee allows the body to compensate more readily to malalignments). However in

the real clinical environment, prostheses are routinely aligned by prosthetists without any quantitative force measurement, merely "by eye"

2.6 Suspension devices

With most trans-tibial prostheses, some type of suspension system is needed to hold the prosthesis on the stump during the swing phase of gait by resisting gravity and inertia forces. This system should not restrict the normal motion of the knee, and should allow comfortable function of the knee muscles. The suspension system may also be used as a control against hyperextension of the knee during heel strike Hughes, (1970).

Cuff suspension is most commonly utilized for the PTB prosthesis. This cuff fits tightly around the femoral condyles with its distal edge slightly above the proximal border of the patella. The tabs are fitted such that tension is maintained over 60^0 knee flexion, but relaxes enough to allow the knee to flex to 90^0 when sitting. Barclay (1970) and Pritham (1979) review the suspension devices as well as presenting alternative socket designs which utilize different suspension systems.

2.6.1 Supra Condylar Supra Patellar PTB socket

In the supra-patellar supra condylar socket the proximal brimline is extended to completely enclose the patella anteriorly and the femoral condyles both medially and laterally. The anterior brimline is brought in direct contact with the patellar

tendon and eliminates the need for any suspension above this level. (Wilson, 1970). In addition the higher brimline is believed to provide mediolateral stability, prevent knee hyperextension and reduce pistoning action between the stump and the socket.

2.6.2 Supra Condylar wedge suspension socket

The supra condylar (SC) wedge suspension socket is very similar to the supra-patella supra condylar socket, except that the patella is not enclosed. As such the mediolateral stability is equally effective. Suspension is aided by a removable wedge which covers the medial aspects of the knee from just posterior to the patella including the posterior medial face of the femoral condyle. In the case of a stump with extremely prominent bones, especially the head of the fibula, a lateral wedge may also be inserted.

2.6.3 Suction socket.

There are three variations of suction sockets (Staats and Lundt, 1987)

(a)Total surface bearing (TSB) socket is a "tension socket" in which the socket is made volumetrically smaller than the residual limb. The aim of the TSB socket is to distribute weight-bearing over the entire surface of the stump, including those areas which, in the past, have been considered pressure sensitive. The accuracy of fit, is achieved through the use of transparent check sockets.

(b) The silicone suction socket is an "atmospheric suspension". A prefabricated suction sleeve is rolled onto the residual limb prior to casting. Check sockets are used to test the pinning of the sleeve into the distal end of the socket. When the prosthesis

is unloaded, the suction sleeve collapses around the residual limb, and this distal coupling of the socket and the sleeve provides suspension for the prosthesis.

(c) PTB suction (active compression) socket in which the socket interface is made of an elastic or elastomeric material that is stretched or rolled over the residual limb, thereby gripping the skin through compression as well as through friction created between the skin and socket. This minimization of the movement between the socket and the soft tissues is believed to prevent skin breakdown usually caused by the sliding of the prosthesis of the skin (Roberts, 1986; Grevsten and Eriksson, 1974; Staats and Lundt, 1987).

Kristinsson in 1985 demonstrated using a silicone liner which is rolled onto the residual limb and he claimed that it provides a good overall contact. The silicon layer is thick at the distal end of the socket. After being turned inside out and rolled over the stump, the silicone sleeve pulls the stump in a distal direction, stabilising soft tissue and minimising pistoning. The ICEROSS system is primarily used for suspension, Kristinsson (1993) believes that it has also considerably improved the weight-bearing capability of the prosthesis and the interface between prosthesis and user. He firmly believes that a trans-tibial socket, designed to transfer loads primarily to limited areas of the limb such as the patellar tendon and the medial flare and condyles of the tibia, for instance, is in most cases both ineffective and uncomfortable. The most effective socket is one that relies on the hydrostatic principle for load transfer.

CHAPTER 3: LITERATURE REVIEW

3.1 Introduction

In this chapter, the literature related to stump/socket pressure distribution at the prosthetic socket/stump interface is reviewed. Various types of force and pressure transducers have been used to measure interface pressures for a variety of interface systems i.e. buttock/cushion, foot/shoe and stump/socket. As the application may vary, transducers appropriate for pressure measurements in one system may not be suitable for another. Interface stresses can be described in terms of normal stresses (pressure) and shear stresses. Transducers used to measure interface stresses can either be inserted between the stump and the socket liner, or they can be mounted within the socket wall. The placement has a dramatic effect on the sensor's measurement capabilities. Also, the accuracy of measurement depends on the type of transducer used and the method of calibration (Silver-Thorn et al, 1996). In addition, most sensors utilised in this field are only capable of pressure measurement, although newer developments in transducers allow for simultaneous measurements of both pressure and shear stresses (Silver-Thorn et al, 1996).

3.2 Interface assessment techniques: Interface Pressure

Hydraulic transducers were used to measure stump/socket interface pressures during walking. In a study by Van Pijkeren et al, (1980) a hydraulic pressure transducer was manufactured and used. The transducer bag is made by heat sealing two disks of PVC, 0.25mm thick and 30 mm in diameter, which was filled with low viscosity silicone oil. An oil filled tube then connects the bag to a National Semiconductor pressure transducer LX 1600. The total thickness of the fluid filled bag was approximately 0.6mm. The flexibility of the bag was reported to be able to meet both flat and convex or concave surfaces in prosthetic sockets (Figures 3.1 and 3.2). The application of force on the bag will cause an increase in fluid pressure which will be sensed by the external transducer. Van Pijkeren et al, (1980) reported one of the main difficulties experienced with oil filled bag transducers was that extreme care was required during oil filling to ensure air was excluded. This was a study of dynamic interface pressures on trans-femoral amputees.

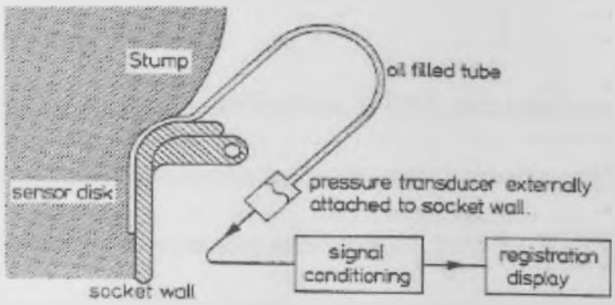

Figure 3.1: Principle of interface pressure measurement system. (Adapted from VanPijkeren et al, 1980).

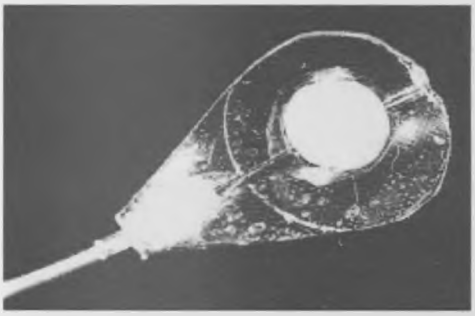

Figure 3.2: Finished transducer.
(Adapted from Van Pijkeren et al, 1980)

Isherwood (1978) used a polyvinylchloride (PVC) welded bag, filled with water, connected to an external silicon diaphragm pressure transducer with a 3 mm short bore tube. The difference between Van Pijkeren and Isherwood's methods, was that Isherwood (1978) mounted these PVC sensors in recesses in the socket wall, and

covered them with 5 mm of PElite. Possible sources of error that were not addressed by either group were the effect of tube protrusion into the skin on transducer performance.

Barbenel and Sockalingham (1990) measured pressure beneath bandages by using temperature compensated low cost, pressure transducers with direct electric outputs; and using large area sensor cells from Talley Group LTD, UK. (See Figure 3.3). Each cell was made from 0.25mm PVC sheet heat sealed to form a 28mm diameter chamber. The lead tube was 1m long, 2mm inner diameter and 3mm outer diameter. The pressure transducer used was a piezoresistive gauged silicone diaphragm (SCX05DN, Sensor Technics, UK). The transducer linearity was approximately ±0.23mmHg (0.03kPa), while hysteresis was less than 0.06kPa. For a long duration period (i.e. 10 month), calibration on 16 occasion showed that the calibration constant varied by less than 2 %.

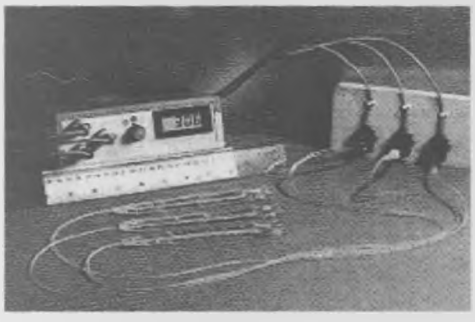

Figure 3.3 Conditioning and output display unit with three sensors.
(Adapted from Barbenel and Sockalingham, 1990).

Appoldt (1967) investigated two types of resistive gauge for stump/socket interface pressure measurement, the Micro systems (semi conductor gauge) and the New York University design. In the New York University design (Appoldt, 1967) one end of a piston with a diameter 6.35 mm was the sensing surface (Figure 3.4). The other end was attached to the centre of a small steel deflection beam oriented perpendicular to the piston axis. Both ends of the beam were rigidly attached to the transducer frame. Strains measured with four strain-gauges mounted in opposite pairs on the beam were proportional to the normal load on the sensing surface. For dynamic interface normal stress measurement on trans-femoral amputees, Appoldt (1967, 1968, 1969) placed mounts in the socket wall. Transducers were positioned in the mounts so that their sensing surfaces were flush with the inside socket surface and rested directly on the stump. No interface liner was worn by the amputee. Maximum measured pressures during constant velocity walking on trans-femoral amputees were approximately 6.9 kPa at mid-stump locations and 172 kPa near the brim. Step-to-step variations in peak interface stresses were minimal except after several hours of testing when the subject became fatigued. Brim location magnitudes, however, showed high sensitivity to alignment changes. For standing test results, Appoldt (1967) stated that "The brim load is roughly 40 percent of the maximum load developed in walking".

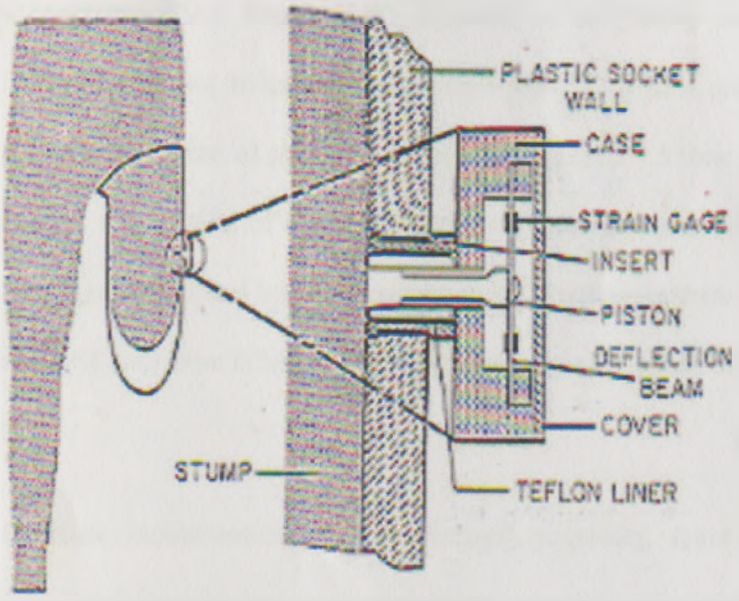

Figure 3.4: NYU transducer assembly.
(Adapted from Appoldt and Bennett, 1967).

The concept of a diaphragm pressure transducer, generally developed and designed for fluid pressure measurements, appears to be the most common choice for stump/socket interface pressure studies. They are based on the theory that, a fluid pressure difference between the internal and external of the device causes a deflection of the diaphragm. The surface strains of the diaphragm are then sensed by strain gauges bonded to the inner surface of the diaphragm. Calibration allows conversion of these strain values into normal pressures. Diaphragm transducers are typically of rigid construction.

Appoldt and Bennett (1967) used both the piston force gauge and diaphragm transducers mounted in the socket wall to measure stump/socket interface pressure for trans-femoral amputee. (See Figure 3.4). Appoldt et al (1969) used the same transducers in their pressure transducer protrusion study (1.6 mm protrusion), and concluded that overestimation of pressure frequently exceeded 1.5 times at areas near bony prominences. Calibration of both sensors was by gas pressure behind a rubber diaphragm, which was checked by dead weight loads. Hysteresis error was given as 3% of the indicated load or ± 0.5psi (± 3.4 kPa). No shear or temperature sensitivity was assessed.

For interface measurement on trans-femoral amputees, several researchers inserted Kulite (New Jersey) pressure transducers (models LP-125 and LQ-125) between the stump and the socket. The transducers were held in place with medical tape either directly over the sensing surface (Pearson et al, 1973; Pearson et al 1974), or over the ribbon cable near the sensor (Rae et al, 1971; Sonck et al, 1970; Winarski et al, 1987). The cables exited at the socket brim.

Pearson et al (1973) in their study of trans-tibial amputees used diaphragm transducers to measure stump/socket interface pressures for several postural stance positions (prosthetic limb suspended, weight on both limbs, and weight borne by the prosthetic leg only). The Kulite semiconductor transducer, 0.76 mm. thick, was placed between the socket and the stump i.e. directly to the patellar tendon, medial and lateral, tibial condyles, and the distal anterior tibia. No mention was made of any calibration procedures.

Pearson et al (1974) then developed an analytical model for predicting stresses in Patellar Tendon Bearing (PTB) suction sockets. The model was verified by performing actual pressure measurements. The positive pressures were measured with the same transducers (Kulite, New Jersey, USA model LQS-125-500), while negative pressures - in the distal socket cavity - were measured with another commercial pressure transducer (TKM-1 Borfors AG, Germany) mounted externally. Again, there was no mention of any calibration procedures.

Ferguson-Pell (1976), using an Instron testing machine, evaluated a Gaeltec (Skye, UK) transducer of similar design to the Kulite sensor (model LQ125) except the Gaeltec transducer was encapsulated in silicone rubber. Repeatability tests showed the coefficient of variation for the sensor reading and Instron measurement to be up to 80% for stresses below 4.3 kPa. Between 4.3 kPa and 26.1 kPa, the coefficient of variation was approximately 10%. He also thought the variation at low loads was probably due to changes in the surface load distribution since hydrostatic calibration showed very repeatable performance.

Rae and Cockrell (1971) used both square and linear arrays of five diaphragm transducers to determine stump/socket interface pressure levels and distributions of a trans-tibial amputee. These pressure transducer matrices were placed between the stump and socket, as was the ribbon cable connecting the transducers to the amplifiers. (See Figure 3.5). Two areas, namely the kick point i.e. anterior distal end and the patellar tendon area were of interest. PTB sockets were used in the study, and the maximum peak pressures for the two areas respectively were 104 kPa and 276 kPa.

Figure 3.5: Pressure transducers in a linear array applied to a stump.
(Adapted from Rae and Cockrell, 1971).

Sonck et al (1970) used the same pressure transducer set-up as Rae and Cockrell (1971) to investigate the effect of various liner materials on interface pressures. The gel liner was developed in the University of Michigan Prosthetic shop by Joseph Giacinto, Henry Sturza, and Richard McUmber in an attempt to smooth and reduce both normal and shear pressures. Comparison of normal pressures measured using these transducers for a gel liner, a sponge rubber insert and a conventional hard socket (i.e. no prosthetic liner) demonstrated lower average peak pressures during gait when the subject wore a socket with a gel liner. However, the distortion effects of the transducers and cable placements were most likely influenced, to varying degrees, by the compliance of the prosthetic liner/socket system. In addition, pressure transducer calibration should have been evaluated for each different interface material.

The patellar tendon depression of the socket wall in a PTB prosthesis was isolated by Mizrahi et al (1985) in order to measure the stresses imposed on it. Vachranukunki et al (1986) from the same group reported a section 5 x 2.5cm section

was cut from the socket and mounted on an external frame. This group fitted an experimental prosthesis with a two-directional load cell at the patellar tendon indent (which was cut out of the hard shell), attached to an adjustable mounting part of a frame. A strain-gauged plate behind the section registered axial and radial stresses applied to the section. Figure 3.6 illustrates this arrangement; Mizrahi et al (1985) observed that approximately 33% of ground reaction forces are directed through the patellar tendon shelf. They suggested that a 7mm indentation gave the optimum result. Vachranukunki et al (1986) also observed that subjects could tolerate up to 60% body weight in normal stress at the patellar tendon without pain. and that gait performance and stability increased with increased load. Additionally to the biaxial stress measurement, force plates measured ground reaction forces and kinematic equipment recorded kinematic data. It has been proposed that a convenient area to transfer some of the load between the stump and the socket is the patellar tendon area, which can withstand relatively high loads without causing pain or tissue damage. (Mizrahi et al, 1985).

Figure 3.6: Biaxial stress measurement on the patellar tendon.
(Adapted from Mizrahi et al, 1985).

Chino et al (1975) used a thin Kulite diaphragm pressure transducer to investigate distal socket pressures during gait for trans-tibial amputees wearing a rubber suspension sleeve. The use of the suspension sleeve appeared to slow the leakage of negative pressure during swing phase

Steege et al (1987) also settled on miniature strain gauge based diaphragm transducers mounted within the socket wall to measure stump/socket interface pressures. Kulite transducer (model XTM-190), in collars were positioned in holes cut in the hard socket. The transducer sensing surface rested directly on an intact PElite liner. Measured pressures on trans-tibial amputees during static equal weight-bearing ranged from 0 to 128 kPa for one subject and from 0 to 300 kPa for a second subject.

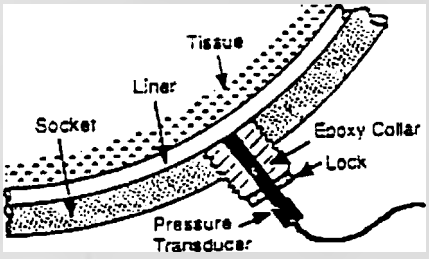

Figure 3.7: Kulite transducer (XTM-190).
(Adapted from Steege et al, 1987).

Prior to this selection, they also considered hydraulic "bag-type" pressure transducers (Sci-medics) and force sensitive resistors (FSR). The FSR material, sandwiched between two conductors was of the appropriate stiffness (i.e. approximately the same as that of the socket wall) and demonstrated fast response. However, results were not repeatable, were nonlinear, exhibited hysteresis, and were temperature sensitive. The diaphragm pressure transducer was finally selected as it

demonstrated fast, repeatable response, and had compliance similar to that of the socket wall.

Lee et al (1997) and Goh et al (2003) used strain gauge based diaphragm transducers mounted within the socket wall of a PTB socket to evaluate stump/socket interface pressure profiles. The transducer used was a load cell from Entran International, USA (model ELFM-B1-FL,). The specification of the Entran transducers used are shown in Table 3.1.

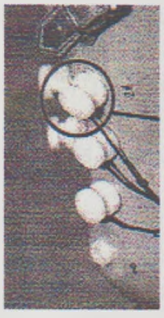

Figure 3.8 Transducer assembly. (Adapted from Goh et al, 2003)

Range	5 lbs (25 N)
Non-linearity	± 0.25 FS
Hysteresis	± 0.25 FS
Sensitivity	1.777 mV/FS
Operating temperature	-50 to 120 ° C
Thermal sensitivity shift	0.02% / ° C

Table 3.1: Entran specification (Adapted from Goh et al, 2003)

3.3 Interface assessment techniques: Shear Stresses

Sanders and Daly (1989) and Sanders et al (1990) combined the use of a diaphragm pressure gauge and a biaxial strain gauge (cantilever beam) to measure both normal and shear stresses for trans-tibial amputees during walking. These custom designed transducers were placed in mounts affixed to the external surface of the socket so that they projected through holes in the socket wall. A strain-gauged diaphragm for detection of normal stresses was fixed on the end of a cantilever beam, which detected biaxial shear stresses. A disc of liner material was affixed to the end of the diaphragm and the transducer was inserted through a hole cut in the socket wall until flush with the inner socket face. The diaphragm measured 6.4mm diameter by 0.17mm thick and the cantilever beam was 1.6mm square. The transducer sensing surface was a PElite disk which lay flush with the surrounding liner. (Figure 3.9 and 3.10). Calibration was by static loading. Hysteresis error for the shear axes was 0.3% and for the normal axes 3%.

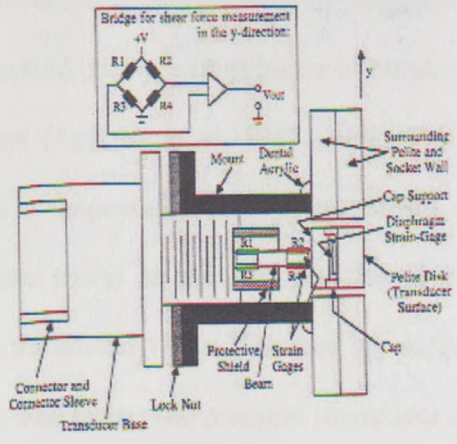

Figure 3.9: Schematic drawing of interface
stress transducer. (Adapted from Sanders and Daly, 1993)

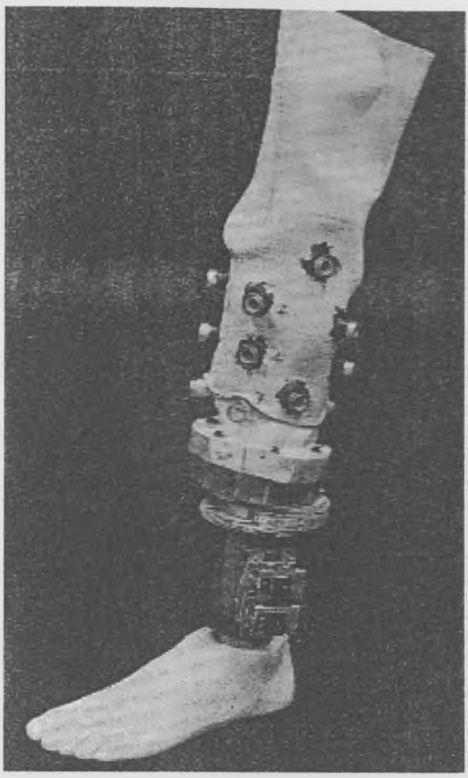

Figure 3.10: Instrumented prosthesis
(Adapted from Sanders et al, 1998)

Appoldt et al (1970) were also interested in the tangential pressures (shear and friction). They placed tangential pressure transducers in mounts which ordinarily held normal pressure transducers (Appoldt et al, 1967, 1968, 1969). They used both a diaphragm transducer and a tangential transducer to obtain normal and tangential stress distributions (separate trials) at the stump/socket interface of trans-femoral amputees during gait. The transducer was a T-shaped bar supported by two 0.41 mm thick strain-gauged beams. The tangential pressure transducer consisted of four strain gauges bonded to a thin steel bending beam such that they responded to application of a load along the load sensitive axis, and cancelled any on-axis compressive load. As normal loads tend to influence tangential pressure results, stiff beams were used to

severely limit such deflection. The transducers were mounted within the socket wall, with the sensor surface flush with the skin such that the location of the sensitive axis corresponded to the direction of interest (i.e. horizontal or vertical).

A group of Japanese workers (Moore et al, 2000) attempted to fabricate a tri-axial transducer which could measure the force acting on the residual limb. The transducers were constructed using six shear strain gauges from Kyowa Electronic Instruments, Tokyo, model SKF-5668. (Figure 3.11). The transducer was not described in detail. However it was reported that the transducer demonstrated linearity in all three directions with very minimal cross-talk. There was no mention of any calibration or experimental procedures.

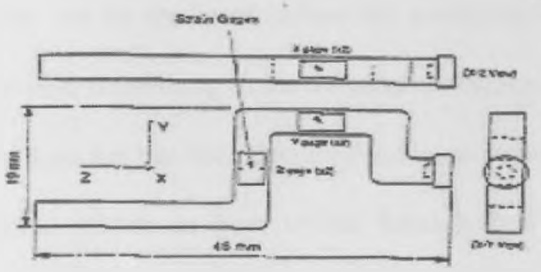

Figure 3.11: Triaxial transducers with six strain gauge used.
(Adapted from Moore et al, 2000)

3.4 Interface Assessment Techniques: Finite Element approach

Another approach for calculating interface stresses uses finite element (FE) analysis techniques. Finite element analysis is a method of analyzing structures of a complex nature. By dividing the structure into small elements of regular polygonal shapes, the behaviour of the structure can be approximated by summing the response of each element. All of the elements combined compose the finite element mesh. Each finite element is defined by a number of nodes, which in turn define the overall geometry of the structure. In addition, each element is assigned material properties, and boundary conditions are applied at appropriate nodes. Loading parameters must also be defined. Generally, an exact solution cannot be obtained for complex structures, but the FE method provides an approximate solution (Silver-Thorn et al, 1996).

One of the most significant benefits of FE modelling is that interface stress distributions can be predicted before the prosthesis is actually fabricated. Computer models are time consuming in the development stage, but may save time over the long term. Once a socket has been designed using computer-aided methods, fabrication can be completed within an hour unlike hand-crafted methods, which take days for fabrication (Zachariah and Sanders, 1996). Fabrication time may vary depending on the manufacturing establishment for example in the Bioengineering Unit, University of Strathclyde a PTB socket may only take some hours not days. Modification of the socket shape is also made easier by the use of computer models since prosthetists can view a graphical display of the socket. Prosthetists can use the predicted stress distribution to rectify the socket shape, thereby relieving areas of low load tolerance and loading areas of high tolerance (Zachariah and Sanders, 1996).

For more than a decade, finite element models have been the primary means for modelling the residual limb and prosthetic socket interface. However, there are several limitations to this approach. Due to the complexity of residual limb tissues, it can be very difficult to select appropriate material properties for the model. It has been shown that soft tissues behave in a non-linear viscoelastic manner (Pathak et al, 1998). However, FE models are often simplified by modelling tissues as linear elastic materials, which greatly reduces the accuracy of the model. Sophisticated models would have to incorporate non-linear viscoelastic materials with properties (e.g., stiffness) that vary regionally due to callusing and scarring, as well as tissue thickness and stiffening effects in regions that are in close proximity to bony structures. Another challenge with FE modelling is determining appropriate boundary conditions, which can be very complex and may vary with time. It has been shown that interface stresses and slip are sensitive to the coefficient of friction parameters (Zhang et al, 1995). However, frictional slip is seldom incorporated into FE models of the stump/socket interface. Finally, comparison of FE results with experimental data is the only method of testing the validity of these models.

The use of sensors positioned within the socket wall may also be limited (Sanders et al, 1995). Problems due to material incompatibility between the interface, skin and transducer are greatly reduced when sensors are mounted within the socket wall. A potential source of error arises when a socket liner is used, which is generally the case for below-knee amputees. With use of a socket liner, a transducer mounted within the socket wall measures stress between the liner and the socket, which differs from the stress between the skin and liner at that position. Therefore, a relation between these two stress measurements must be determined if a liner is to be used.

3.5 Interface assessment techniques: Force Sensitive Resistor

Force sensing resistors (FSR) rely on electrical resistance to indicate pressure. An FSR is basically an assembly of two sheets of polymer, usually with the top sheet coated with an elastomer containing carbon or metal powder while the lower sheet has a silk screened pattern of silver conductors (figure 3.12). The application of force on the FSR causes an increase in contact area resulting in a decrease in electrical resistance. Examples of such system are the Rincoe Socket Fitting System from R. G. Rincoe & Associates, Inc. CO, USA and F-Socket™ system from Tekscan, Inc. South Boston, MA, USA.

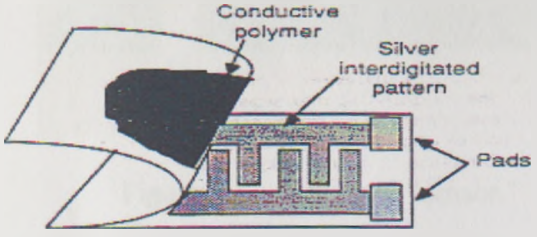

Figure 3.12: FSR construction. (Adapted from Olson, 1991)

The F-Socket™ system developed by Tekscan, Inc. has recently been used for experimental socket pressure measurements. Each F-Socket™ sensor contains 96 individual cells (16 rows by 6 columns) covering a total sensing area of 15480 mm^2. (Figure 3.13). The sensors are designed in such a way that they may be trimmed into

independent sensing strips in order to better fit the curved shape of the residual limb and minimize wrinkling. They measure 0.15 mm (0.007 in) in thickness, which minimizes alterations to socket fit. Each sensor comprises of two thin, flexible polyester sheets. Electrically conductive electrodes are deposited onto each sheet such that a column pattern is formed on one sheet and a row pattern is formed on the other sheet. These rows and columns are then coated with thin semi-conductive ink. When one sheet is placed over the other, a resistive layer is formed at each intersection of the electrical rows and columns. Each of these intersections represents an individual sensing cell. The F-Socket™ sensors can then be calibrated in order to define a relation between applied force and changes in current flow at each cell.

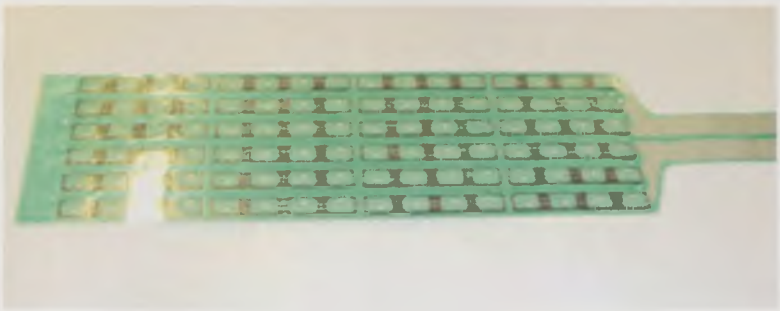

Figure 3.13: F-Socket™ sensor.

Buis and Convery (1997) examined calibration problems associated with the force-sensing resistor. A pressure rig was developed that was designed to load the sensors with either static or cyclic uniform pressure. Analysis of the F-Socket™ sensor output over time, as a constant load was maintained on the sensor, confirmed the presence of a drift artifact during static loading. Dynamic sensor response was

tested with an Instron testing machine. Sensor output stabilized after approximately 10 cycles, and corresponded well with the applied load. Hysteresis increased as the load range increased. Convery and Buis (1999) quantified the socket/stump interface dynamic pressure distributions within a conventional patellar tendon-bearing (PTB) socket and a hydrocast socket. Within a single subject, they found that pressure patterns within the hydrocast socket were distinctly different in comparison to the PTB hand cast socket.

A summary of the peak stresses measured, by the investigators, from various sites around the trans-tibial stump is presented in Table 3.2

Authors / Year / Items	Schrock et al 1968	Sonck et al 1970	Rae and Cockrell 1971	Meier et al 1973
No. of Subjects	2	23	1	10
Types of Socket	a. Rigid plaster dressing (RPD) b. PTB	PTB	PTB with liner	PTB
Transducers used	Pressure transducer (Sensotec)	Pressure transducer (Kulite)	Diaphragm transducer array (Kulite)	Dye-impregnated socks Pressure transducer
Analysis of ?	Pressure	Pressure	Pressure	Pressure
Measurement point	RPD : Proximal, middle, distal end, lateral and medial PTB : Proximal, middle and distal	Patellar Tendon, Anterodistal, Medial tibial condyle, Lateral tibial condyle	Patellar Tendon Anterodistal	Anterodistal Medial tibial condyle Lateral tibial condyle
Maximum stresses	PTB : End bearing (110kPa)	Anterodistal (827 kPa)	Anteriordistal (104 kPa) Patellar Tendon (276 kPa)	N/A

Table 3.2: Summary of the peak stresses measured at any site on the limb.

Table 3.2: Summary of the peak stresses measured at any site on the limb

Continued from page 50

Authors / Year / Items	Pearson et al 1973	Chino et al 1975	Isherwood 1978	Steege and Childress 1988
No. of Subjects	10	9	-	2
Types of Socket	PTB	Total contact with gel liner	PTB with liner	PTB
Transducers used	Diaphragm transducer (Kulite)	Diaphragm transducer (Kulite)	Hydraulic transducer	Diaphragm transducer (Kulite)
Analysis of ?	Pressure	Negative pressure	Pressure	Pressure
Measurement point	Patellar Tendon Anterodistal Medial tibial condyle Lateral tibial condyle	Distal end Medial Poaterior	Anteromedial tibial Popliteal Fibular shaft Distal Patellar Tendon Anterolateral tibial	Distal end Popliteal Medial tibial condyle Patellar tendon bar Medial Flare prox. tibia Fibular shaft
Maximum stresses	Patellar tendon	-7 to -31 kPa	Patellar tendon (303.9 kPa)	Popliteal area (81 kPa)

Authors / Year / Items	Silver-Thorn et al 1992	Sanders et al 1992	Buis 1997	Ming-Zhi 1999	Goh et al 2003
No. of Subjects	5	3	1	1	4
Types of Socket	PTB with liner	PTB with liner	PTB Hydrocast	PTB Hydrocast	PTB
Transducers used	Diaphragm transducer (Kulite)	Custom diaphragm transducer (Micro-measurement)	FSR (Tekscan)	FSR(Tekscan)	Pressure transducer (Entran)
Analysis of ?	Pressure	Pressure and shear stress	Pressure	Pressure	Pressure
Measurement point	Distal end Distal anterior tibia Distal medial tibia Medial tibial flare Medial tibial condyle Lateral tibial flare Popliteal Patellar tendon Fibular head	anterior posterior lateral	Anterior Posterior Lateral Medial	Anterior Posterior Lateral Medial	Anterior Posterior Lateral Medial
Maximum stresses	Distal medial tibia (202.6 kPa)	Posteroproximal (205kPa) Shear (54 kPa)	Patellar Tendon (PT) PT bar (244 kPa) Hydrocast (126 kPa)	PTB- Patellar tendon bar (335kPa) Hydrocast-(1/3 prox. lateral) (164 kPa)	Popliteal (110.5kPa)

Table 3.2: Summary of the peak stresses measured at any site on the limb

Continued from page 51

3.6 Summary

In recent years, much advancement has been made toward a better understanding of the stress distribution at the stump/socket interface for trans-tibial amputees. There is currently no appropriate technology available to measure shear stresses over a large region of the residual limb during gait. Three direction stress measurements are limited to specific transducer sites only. Experimental techniques have more practical clinical applications than computer models, and they are the only way for determining the actual stump/socket interface stresses. To obtain accurate socket pressure measurements using sensors, a careful calibration procedure must be adopted.

CHAPTER 4: THE TRANSDUCERS

4.1 Introduction

In order to satisfy the aim of this research i.e. obtain the measurements of normal and shear stresses at the stump/socket interface it was necessary to use four types of transducer.

The desire to measure, simultaneously, normal pressure, longitudinal and tangential shear stresses at as many sites as possible around the trans-tibial socket prompted the author to design the transducers presented in the thesis. Previous designs (Appoldt, 1970; Williams et al, 1992; Sanders et al, 1993) were deemed to be too bulky and therefore restricted the number of potential measurement sites. The transducers designed by the author offer improved accuracy, smaller size and are lighter, thus more measurement sites can be targeted without burdening the test subject with excessive weight.

This chapter describes the design and manufacture of the four types of transducer together with associated instrumentation. A fourth system, the F-Scan, is also described in this chapter.

4. 2 Interface Normal and Shear Stresses

Transducers were mounted, on average, at 16 sites around the socket of a trans-tibial prosthesis. Normal and shear stresses were measured at the sites during subject standing and walking along a 7 metre walkaway. Data signals from the transducers were transmitted by cable, via junction boxes, to two 16 channel strain gauge amplifiers, model

DAQN-Bridge (Dewetron, Austria) with PCMCIA Lab View DaqCard 700 (National Instruments, Austin, TX) for data acquisition and a Dell Inspiron PIII for data storage with Lab View version 6.1 as analyzing software. Figure 4.1 illustrates a block diagram of the instrumentation used in this study.

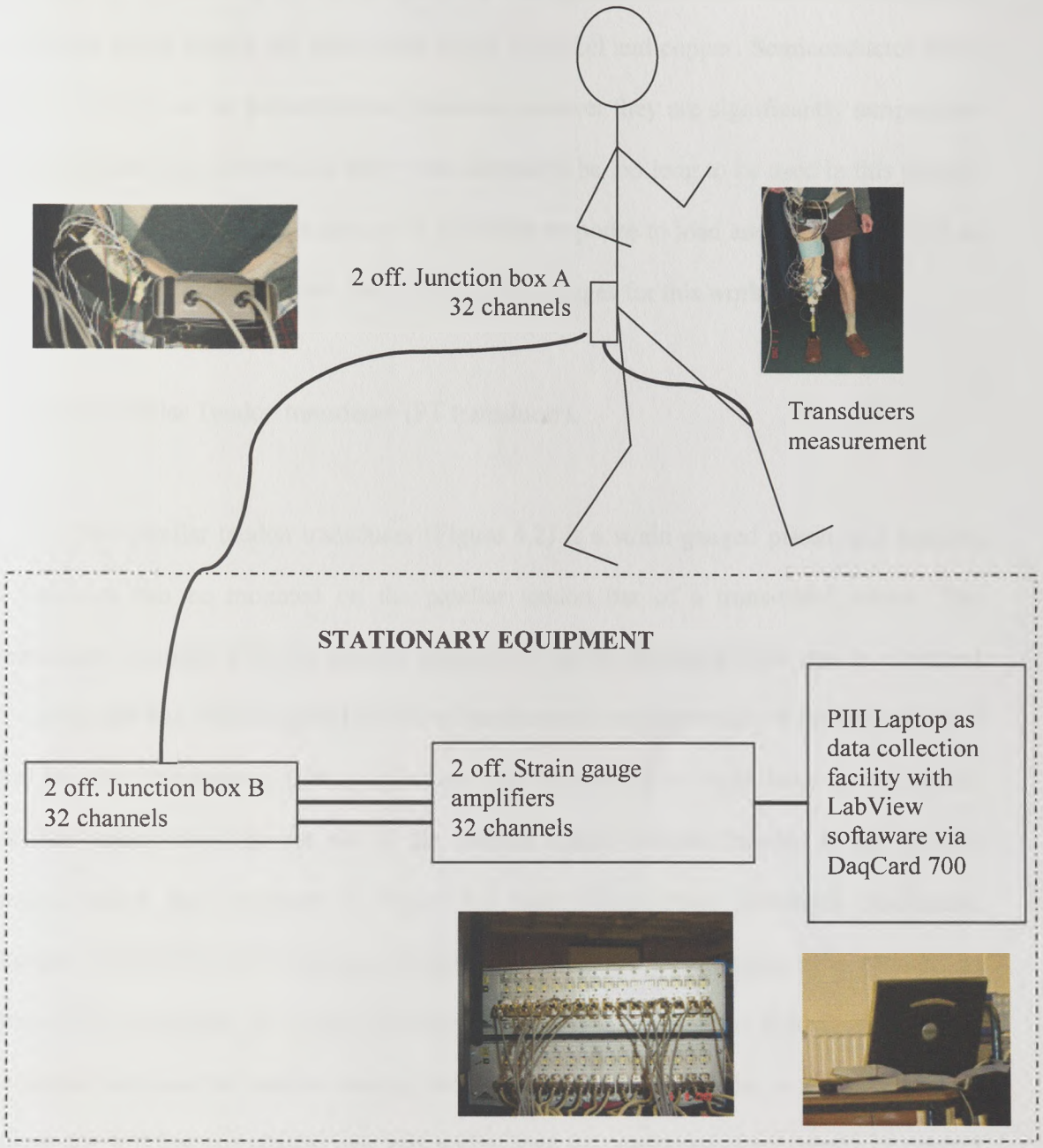

Figure 4.1: Instrumentation block diagram.

4.3 Transducers design.

Strain gauges combined with cartilever beams have been frequently used to measure interface shear stresses. (Appoldt et al, 1970). Metal electrical resistance strain gauges exhibit a variation in resistance primarily due to changes of dimension. An increase in length or decrease in cross-sectional area will increase the resistance. Most electrical resistance strain gauges are made from alloys of nickel and copper. Semiconductor strain gauges operate on the piezoresistive principle, however they are significantly temperature dependent and due to their size they were deemed to be too long to be used in this project. An advantage of metal strain gauges of a linearly response to load and very low cost. The distinct were the prime reasons for choosing these gauges for this work.

4.3.1 The Patellar Tendon transducer (PT transducer).

The patellar tendon transducer (Figure 4.2) is a strain gauged piston in a housing device that can be mounted on the patellar tendon bar of a trans-tibial socket. The transducer complete with the patellar tendon bar can be displaced ± 10 mm in a normal direction and has been designed to make simultaneous measurements of the normal force and the two components (viz. longitudinal and tangential) of shear force acting on the patellar tendon bar. The cut out of the patellar tendon bar was bonded to the patellar tendon holder face as shown in Figure 4.3 using Akemi-Putty (Ottobock Healthcare, GmbH, DUDERSTADT, Germany). Thus it was possible to incorporate the device into other PTB prostheses by simply changing the patellar tendon bar holder. The radial clearance between the patellar sensing surface outer diameter and the socket was 1.5 mm when the PT bar transducer was not under load or compression ensuring no contact between the transducer/patellar sensing surface and the remainder of the socket.

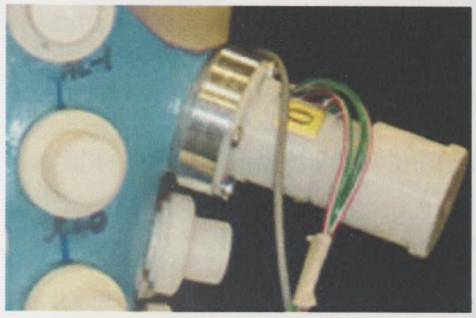

Figure 4.2: Patellar Tendon transducer.

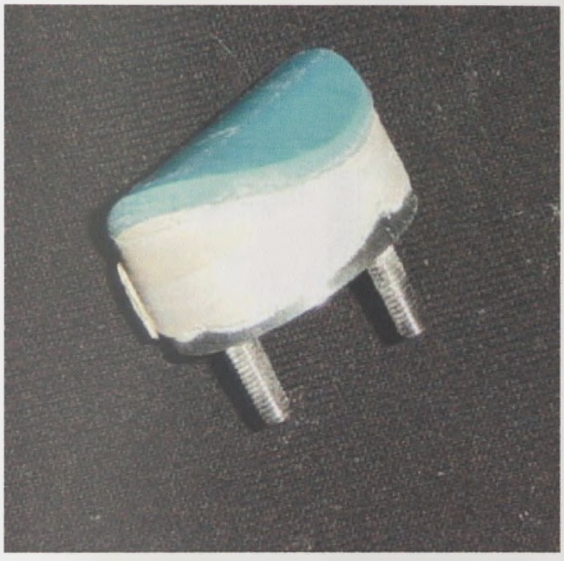

Figure 4.3: Cut off patellar tendon bar curvature sensing surface bonded to the patellar tendon bar holder by Akemi-Putty (Ottobock Healthcare, GmbH, DUDERSTADT, Germany).

The patellar tendon bar sensing surface holder was 25mm in diameter. This diameter was selected because it covered the central part of an average size of patellar tendon bar without appreciably distorting the socket curvature. To accurately position the centre of the patellar tendon bar, the centre of the tendon of each subject was marked on the stump, transferred to the negative cast, then to the positive cast and finally to the socket. A metal insert to hold the PT transducer was attached to the positive cast before lamination of the socket. The marked position was then drilled using a special jig to

produce the 25mm Ø cut out on the socket. The socket was made to accommodate the PT transducer flush with the interior socket wall when in the neutral position. The transducer was able to give quantitative information on each load component. The loads obtained were divided by the transducer projected area to give stress in kPa. A schematic diagram for the PT transducer and its components is shown in Figure 4.4.

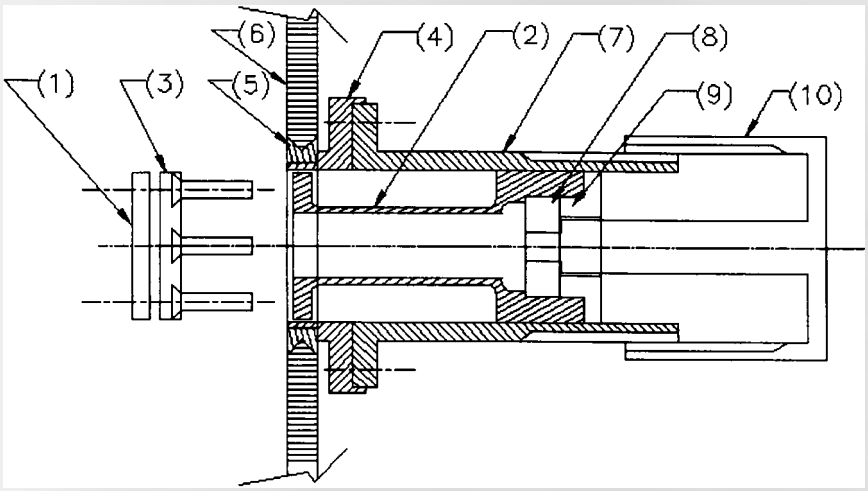

Figure 4.4: Schematic diagram of the custom designed transducer. (Drawing not to scale) (1) 25.0 mm Ø sensing surface, (2) strain gauged piston, (3) patellar tendon bar holder, (4) socket mount, (5) metal insert, (6) laminated socket (7) housing, (8) ball bearing, (9) piston push rod, (10) control knob

A single row radial ball bearing was used in the PT bar device for converting rotational motion to translation of the strain gauged piston i.e. when the piston push rod is rotated by use of the controlling knob, the strain gauge piston will not rotate but will only translate either inwards or outwards depending on the direction of rotation of the controlling knob. By using a thread with 1mm pitch, each full turn of the control knob corresponds to 1 mm translation. The PT bar device was designed to be capable of translating the strain gauge piston by ± 10 mm, from the neutral position. The strain gauge piston and the piston push rod were designed to give a sliding bush fit with the acetal housing. To minimize weight of the device, the PT bar device components were made

from aluminium and acetal material. The complete PT transducer has a mass of 102 grams.

4.3.2 The Normal/Shear or Bioengineering Shear transducer (B.E.S.T.)

The Bioengineering Shear transducer B.E.S.T. (Figure 4.5) is a strain gauged type device designed to measure three forces in the three principal directions (tangential stress σ_x, normal stress σ_y, and longitudinal stress σ_z) simultaneously at any location in a socket of interest. The design of these transducers uses the same gauge types as the PT transducer, the only difference (beside the size and geometry), being that the B.E.S.T. transducer piston cannot be displaced inwards and outwards. The strain gauge arrangement is the same as that in the PT transducer. The size of the sensing surface is 5.60 mm in diameter and the mass of the assembly 89 grams. The B.E.S.T. was formed with three full Wheatstone bridge strain gauges which were attached to the piston using a heat curing adhesive (M-Bond 610, Micro-Measurements, Raleigh, NC) on a 11 mm diameter and a thickness of 1 mm of cross section aluminium tube. Details of the transducers are given in Figure 4.6.

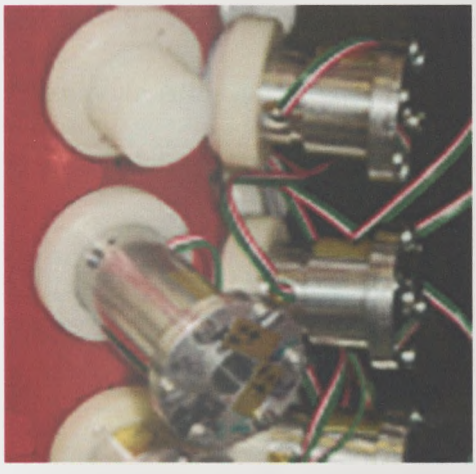

Figure 4.5: Pressure and shear transducers (B.E.S.T.) mounted on socket.

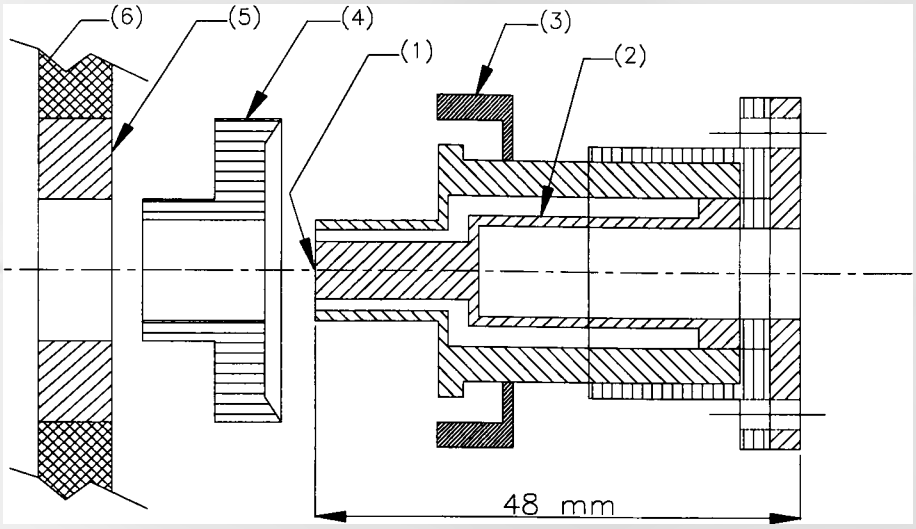

Figure 4.6: Pressure and shear transducer (B.E.S.T.), exploded assembly drawing. - (1) 5.6 mm Ø sensing surface, (2) strain gauged piston, (3) lock nut, (4) socket mount, (5) metal insert, (6) laminated socket.

The strain gauge piston material for both PT bar and B.E.S.T. transducers was machined from aluminium alloy (BS 1474: 1987 and tempered, T6). It is commonly known as "HE30". The material has an ultimate tensile strength of 310 MPa (minimum) and has 0.2% proof stress of 260MPa (minimum). The mechanical properties of an Aluminium Alloy are Modulus of elasticity, E = 68.9 GPa. Poissons ratio, $\nu = 0.26$ and the Shear Modulus, $G = E / 2(1+\nu) = 27.3$ GPa.

The gauges were supplied by Micro-Measurement Group UK Ltd with a gauge factor, k = 2.0 and resistance of R = 120Ω for the axial gauge (type: EA-06-062TT-120). For the shear gauge, the values were k = 2.0 and resistance of R = 120Ω (type: EA-12-062TH-120). The gauging was performed on a single area with two series of full bridges,

each responsible for one single component of the load acting upon the device: i.e. there is a bridge for tangential shear stress Fx, for normal stress Fy and longitudinal shear stress Fz. The normal load was obtained using 2 rosettes in each arm of the full bridge equi-spaced around the periphery, therefore monitoring the direct compressive stress produced by the normal load, Fy. The shear loads, Fx and Fz were measured by rosette gauges aligned at 45^0 to the main axis of the gauge. (See Figure 4.7). A 3 volts power supply was used for the excitation of the bridges for Fx and Fz however 6 volts were necessary for bridge Fy which has double resistor. All gauges were covered with a thin layer of silicone coating for mechanical protection, waterproofing and to reduce noise. The distance between gauge centres was 12.5mm for the PT transducer and 10mm for the B.E.S.T. (See Figure 4.8).

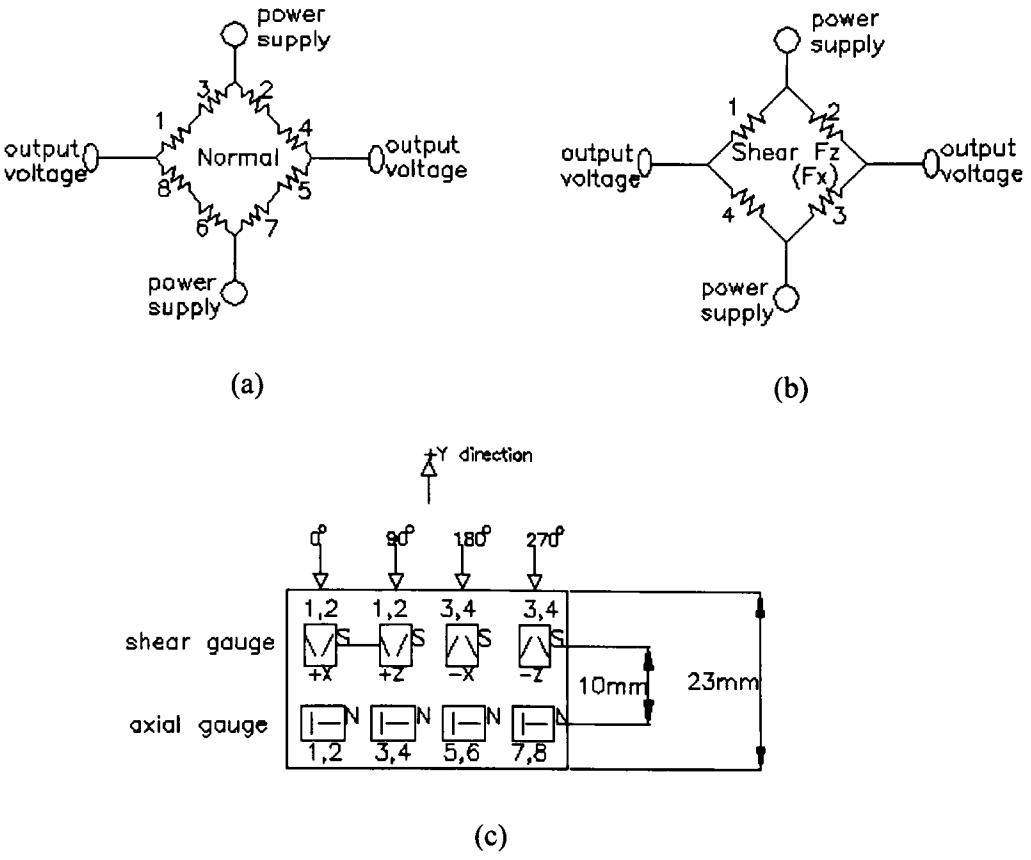

Figure 4.7: Strain gauge orientation for B.E.S.T. and PT transducers. (a) Bridge for normal force measurement in the y-direction. (b) Bridge for shear force measurement in the z and x-directions. (c) Development of the transducer surface showing strain gauge positions.

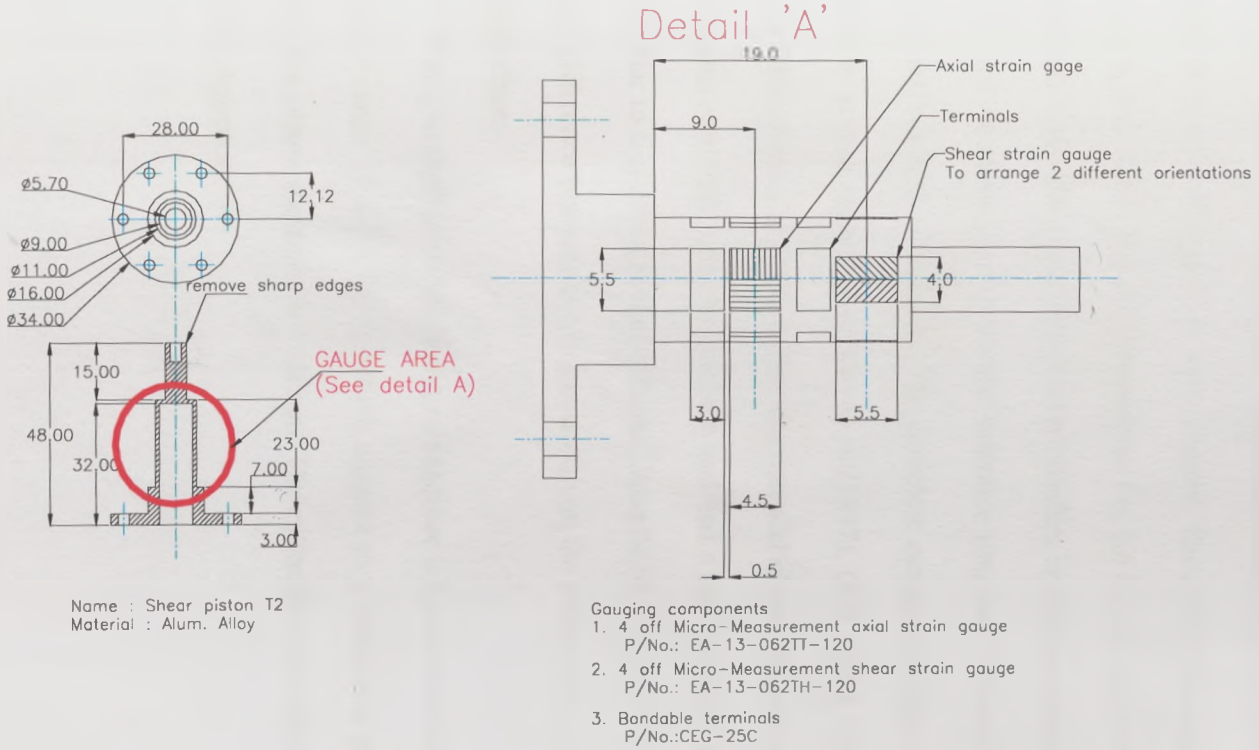

Figure 4.8: Normal / Shear Strain gauge configuration.

4.3.3 Pressure load cell device

The Pressure load cell is a piston in a housing device incorporating an 'Entran' ELFM-B1-5L load cell (Entran International, New Jersey, USA). It has a sensitive diaphragm onto which miniature electrical resistance strain gauges in a full Wheatstone bridge configuration were bonded. The piston (sensing surface) used was the same as that of the B.E.S.T. transducer i.e. 5.6 mm in diameter that kept contact continuously with the diaphragm which transfers normal pressure from the stump to the load cell. It measures the normal interface pressure between the stump and the socket at any location of interest. The complete assembly of the Entran-based device was similar to that described in Lee et al (1997). (See figure 4.9). In an attempt to minimise disturbance of the interface the material chosen for the sensing surface was acetal as this was light, easy to machine and had a low coefficient of friction (0.22 – 0.31) similar to that of the socket material, Acrylic (0.12 – 0.45). Thus there would be minimal difference between the forces acting on the socket wall and on the transducer sensing surface.

The specification of the Entran transducer is given in table 4.1. The transducer had a load range of 0 – 8.89 N, which equates to a maximum pressure of 361 kPa based on the piston diameter of 5.60 mm. The calibration procedure and results can be viewed in Appendix B6.

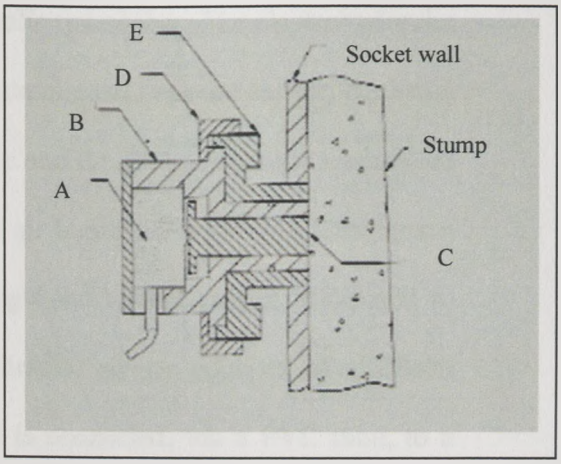

(a) (b)

Figure 4.9: Entran-based device assembly. (a) attached to socket.
(b) schematic drawing; A-Load Cell, B- Mount, C-Piston, D-Locking ring, E-Adapter (Adapted from Lee et al, 1997).

Range	2 lbs (8.89 N)
Non-linearity	± 0.5% FSO
Hysteresis	± 0.5% FSO
Sensitivity	4.735mV/FSO
Operating temperature	-40-120^{O}C
Thermal sensitivity shift	± 5% FSO
Frequency range	0-900 Hz

Table 4.1 Entran pressure sensor specification.

4.3.4 The electrohydraulic transducer

It is difficult to measure the interface pressures at the distal end of the stump/socket due to the shape of the stump. It is impossible to use the B.E.S.T. transducer due to the distal end being the location of the prosthesis shank attachment.

It was therefore decided to utilise an electrohydraulic transducer. The electrohydraulic transducer consists of a sensor bag, a tube and a commercial pressure sensor, Barbenel and Sockalingam (1990). The sensor bag, the tube and the pressure sensor were filled with paraffin oil, care being taken to eliminate all air bubbles. Paraffin oil was chosen due to its viscosity and density, which is amongst the lowest values, compared to other fluids i.e. vegetable oils. The electro-hydraulic sensor consists of a 28mm diameter; 2 mm thick oil filled PVC bag which is connected, via a PVC tube, to a strain gauged diaphragm transducer (RS Components, Ltd, UK). The tubing was 100mm long, with an internal diameter of 2mm and wall thickness of 0.5mm. (Figure 4.10). The electrohydraulic transducer used a pressure vessel to apply uniform pressure on the sensor bag and the calibration results show linear output. (See Appendix B7).

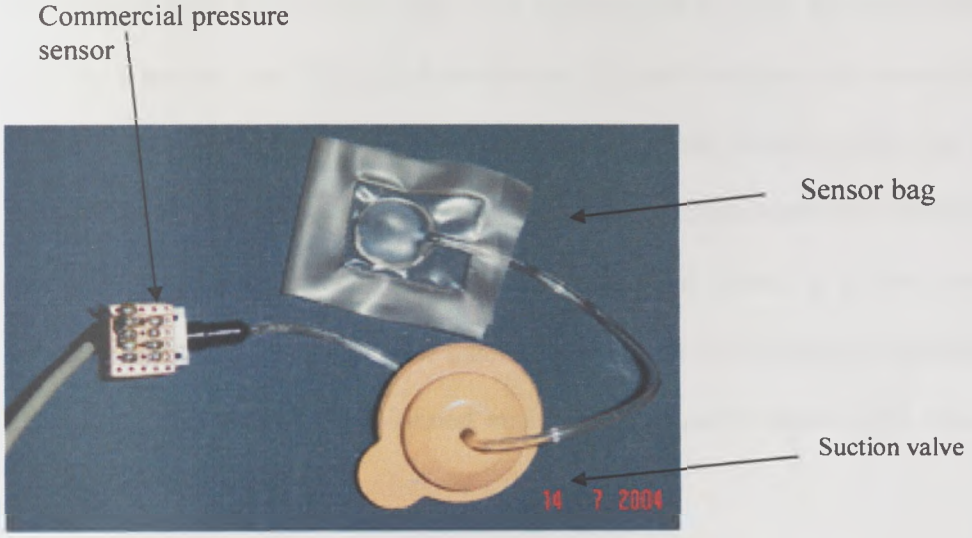

Figure 4.10 Electrohydraulic transducer: (Sensor bag with pressure sensor and suction valve).

4.4 Socket pressure measurement techniques – F-Socket™

4.4.1 Introduction

In addition to the measurement of pressure using the Entran based transducers and B.E.S.T. transducers, it was decided to measure the interface pressure using F-Socket™ socket sensors model 9811 from the Tekscan Inc. (USA).

The flexibility and the thin nature of the sensors minimized any major changes in socket fit during testing. In addition, the F-Socket™ sensors have a high resolution and data can be collected at a wide range of frequencies. Investigators that have previously used the Tekscan F-Socket™ sensors (Figure 4.11) used only two sensors at a time (Convery and Buis, 1998, 1999). The two sensors were placed over half of the residual limb for one trial, then were repositioned to cover the other half of the limb for a second trial. The data from the two different walking trials were combined to provide the pressure distribution over the entire limb. In this study, four sensors were affixed to the inner walls of each socket, however data were only recorded from two positions, (Anterior and posterior and medial and lateral) at a time due to the limitations of the system. However this ensured no or minimal damage occurred to the sensors as they were not re positioned, and thus 'first' quality results were obtained.

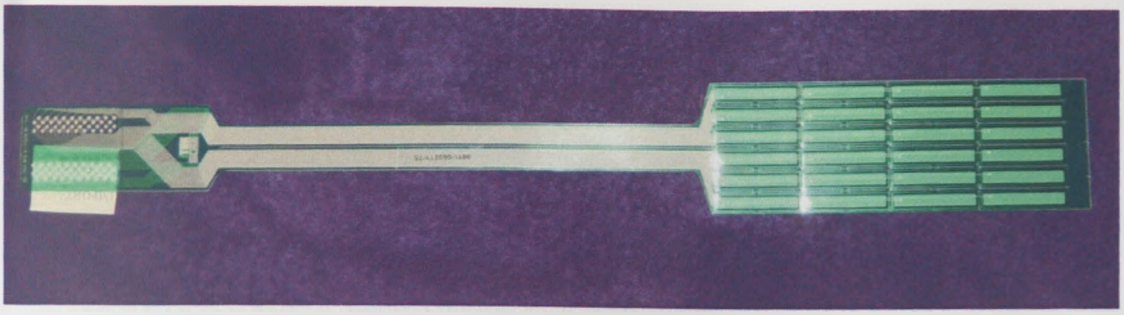

Figure 4.11: F-Socket™ Sensor. (Tekscan, Inc. (USA), product 9811).

4.4.2 Sensor Drift

Drift in the output signal is a common concern associated with force-sensing transducers. A study was conducted in order to assess the amount of drift in the F-Socket™ sensors and to develop a strategy for minimizing error due to drift. A sensor was equilibrated (to reduce inter-cell variation while uniform pressure is applied to the transducer, as recommended by the manufacturer and Convery and Buis (1998)) and calibrated at a pressure of 100 kPa using the F-Scan software program as per the manufacturer's recommended procedure. The pressure of 100 kPa was chosen because it was the average pressure expected during the interface pressures studies with trans-tibial amputees. The frequency of cyclic loading was 1 Hz that is 120 steps per minute for cadence. In a study by Finley and Cody (1970), 534 men and 572 women, during gait analysis, produced cadences of 111 ± 10 steps/min for men and 117 ± 11.7 steps/min for women.

Sensor equilibration and calibration were carried out in the following manner. A sensor was placed within the F-Scan chamber box (Figure 4.12) and a 50 kPa load was applied for 10 seconds at 1Hz. This period of cyclic loading was immediately followed by 10 seconds of static loading, a 20 seconds period of cyclic loading and a 20 seconds period of static loading. At the end of this pre-loading period, recording of the F-Socket™ Sensor output data was obtained of the 50 kPa static load for 120 seconds. The pre-loading was repeated and then a recording was made for 120 seconds whilst a 50 kPa load was applied cyclically at 1 Hz. This entire procedure was repeated for loading levels of 100 kPa and 200 kPa. This allowed the output of the sensor to be observed over time, including the moment the sensor was loaded. The reason for this sequence of cyclic and static loading before executing the equilibration or calibration command was to compensate for some of the air in the bladder which will be withdrawn during cyclic loading when air is in the pressure transfer medium. In this situation, not all of the sensors can receive the same loading condition. A total of three trials were recorded. The average sensor output over the 96 cells was analyzed at 1, 5, 10, 20, 30, 60 and 120 seconds after the load was applied.

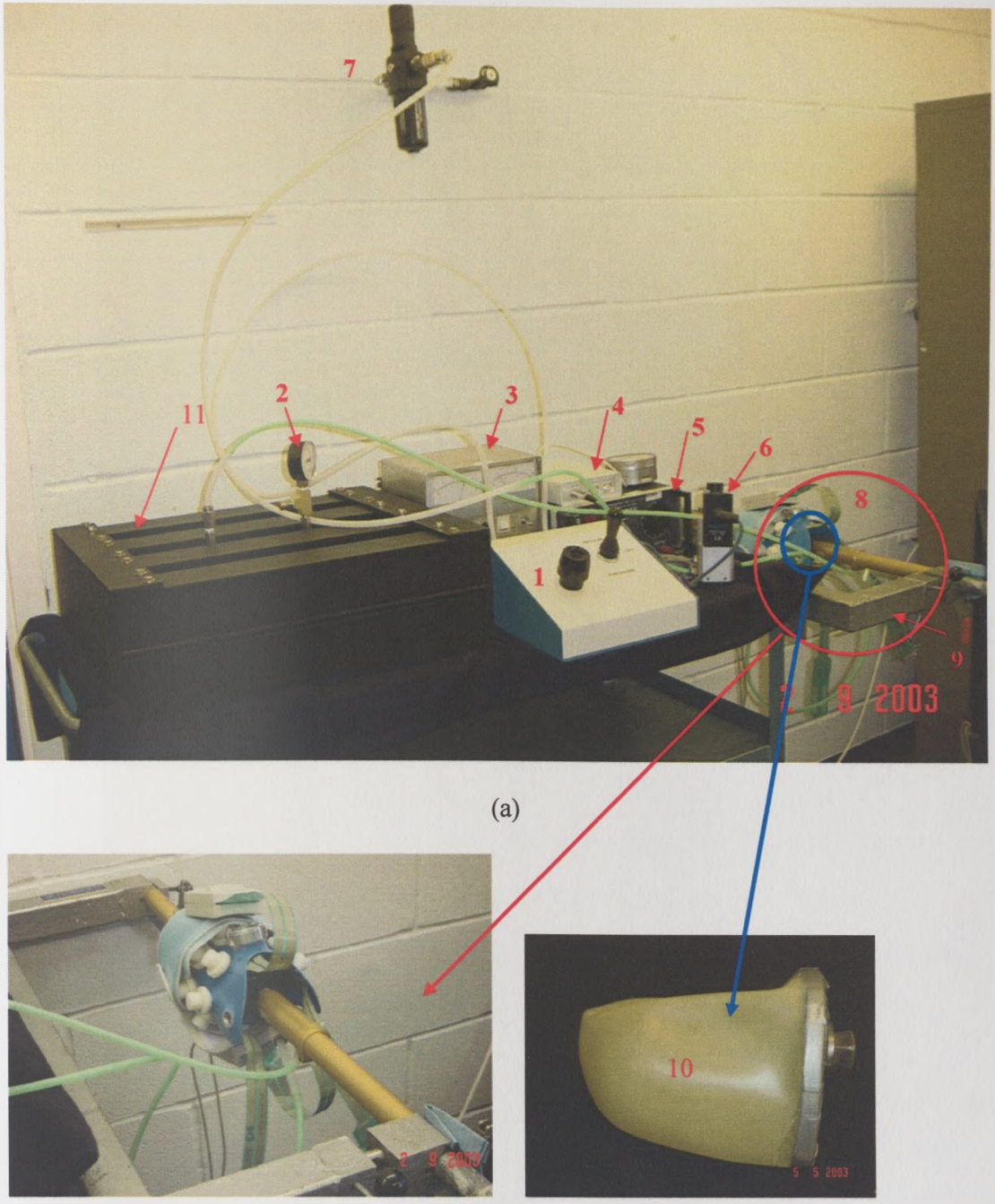

Figure 4.12:In-situ custom calibration setup of F-Socket™ sensor. (a) Complete view of components of the set-up. (b) Enlargement view of the socket attached to the pressure rig. (c) Custom fabricated sealing template with latex balloon bladder.

Legend:

(1) F-Scan pressure regulator controller

(2) Pressure gauge

(3) Power supply

(4) Junction box

(5) Dynamic controlling input generator

(6) Proportional pressure regulator

(7) Compressed air filter

(8) Socket attached securely to the pressure rig

(9) Pressure rig calibration frame.

(10) Custom fabricated sealing template with latex balloon bladder

(11) F-Scan chamber box

4.4.3 Results of sensor drift.

The initial test for sensor drift revealed a dramatic increase in the signal over the first 20 seconds, after the 50, 100 or 200 kPa load was applied (Figure 4.13 and Table 4.2). The results for dynamic load are also presented in figure 4.14 and table 4.3. The pressures remained relatively consistent during the 60 to 120 seconds period, with a range of average values as shown in table 4.2 and table 4.3 over the minute long interval. Sixty seconds after the load was placed on the sensor, the sensor output was expected to match the applied load. This is because the calibration was captured after 60 seconds static and cyclic loading.

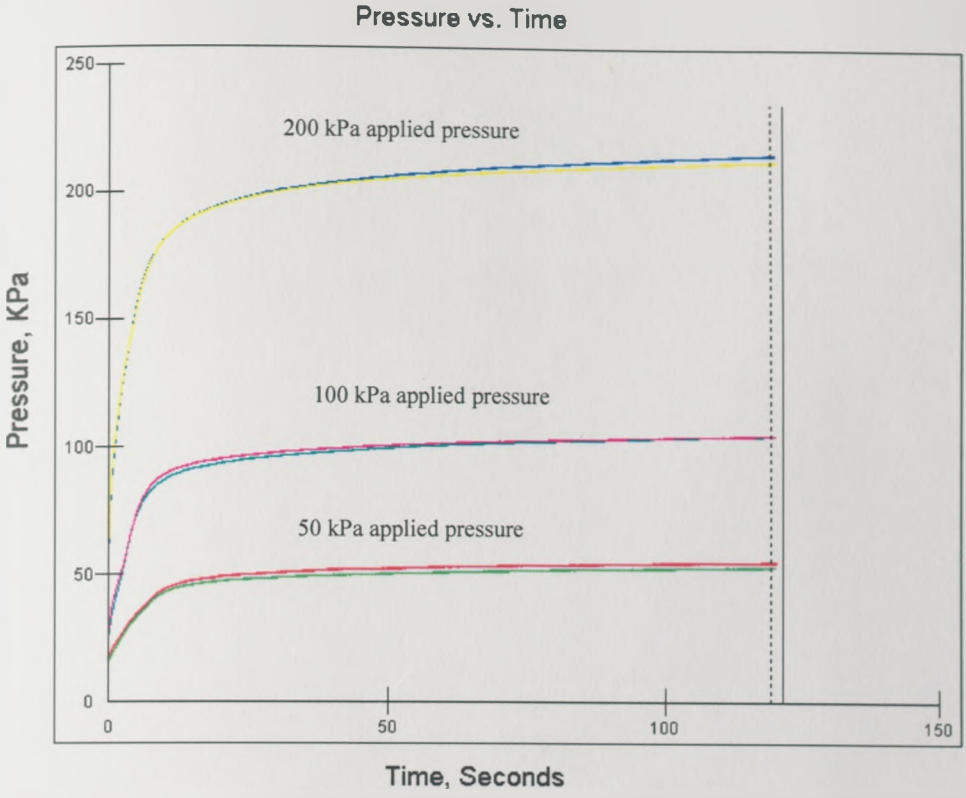

Figure 4.13: Example of F-Socket™ sensor drift (static loading) from 0 to 120 seconds at 1Hz.

	Average pressures		
	Applied pressure of 50 kPa	Applied pressure of 100 kPa	Applied pressure of 200 kPa
Time (s)	Measured pressure aver. ± 1 SD (kPa)	Measured pressure aver. ± 1 SD (kPa)	Measured pressure aver. ± 1 SD (kPa)
1	20 ± 6	37 ± 3	93 ± 4
5	34 ± 4	74 ± 3	156 ± 5
10	44 ± 3	88 ± 5	182 ± 6
20	48 ± 3	95 ± 4	195 ± 5
30	50 ± 4	97 ± 4	197 ± 4
60	51 ± 3	102 ± 3	202 ± 3
120	53 ± 4	103 ± 3	208 ± 4

Table 4.2: F-Socket™ sensor drift up to 120 seconds of static loading at 1 Hz.

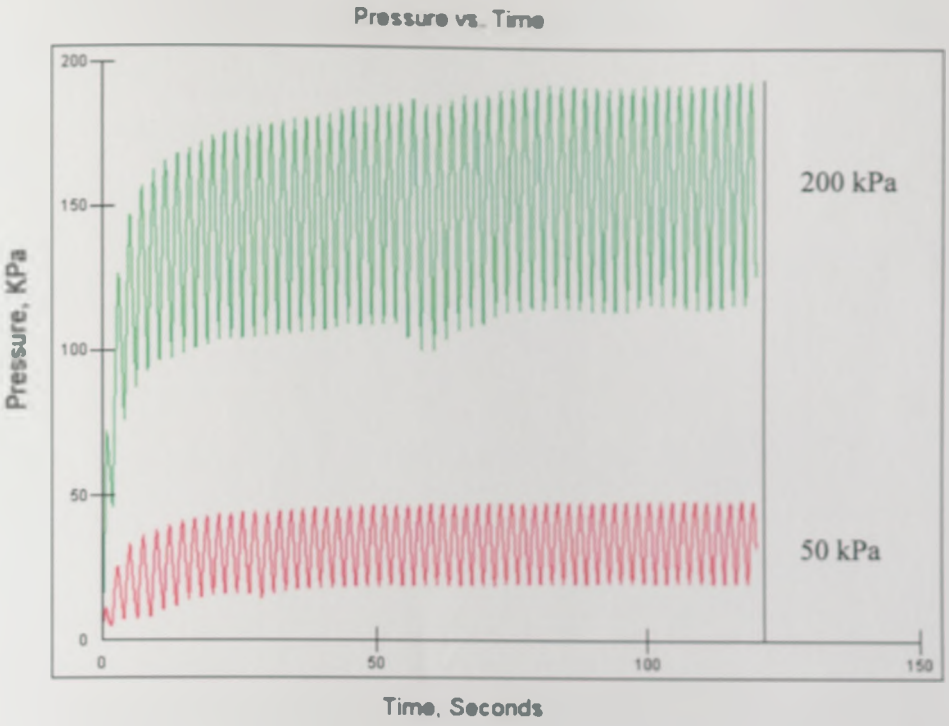

Figure 4.14: Example of F-Socket™ sensor drift (dynamic loading) from 0 to 120 seconds at 1Hz.

	Average pressures	
	Applied pressure of 50 kPa	Applied pressure of 200 kPa
Time (s)	Measured pressure aver. ± 1 SD (kPa)	Measured pressure aver. ± 1 SD (kPa)
1	9 ± 4	84 ± 5
5	33 ± 3	137 ± 4
10	36 ± 4	144 ± 3
20	40 ± 4	163 ± 5
30	43 ± 3	172 ± 3
60	49 ± 4	197 ± 4
120	51 ± 3	202 ± 4

Table 4.3: F-Socket™ sensor drift up to 120 seconds of dynamic loading at 1 Hz.

Sensor drift was strongly influenced by the specific loading conditions. The sub-study findings indicated the importance of closely matching the loading conditions applied during calibration to the loading conditions occurring in the study. The drift in the sensor signal was substantially reduced after 60 seconds of static and dynamic pre-loading. Based on these results, it was predicted that accurate pressure readings could be achieved provided that the sensors were pre-loaded for at least 60 seconds prior to both the calibration and socket pressure trials.

4.4.4 Customized Calibration

Initial results from a pilot study indicated that in order to obtain the appropriate measurements with the Tekscan system a customized calibration procedure was required. A detailed description of this custom calibration procedure development and implementation is provided in this section.

4.4.5 Methods

A photography overview of the calibration system is shown in figure 4.12 and is repeated in a block diagram in figure 4.15

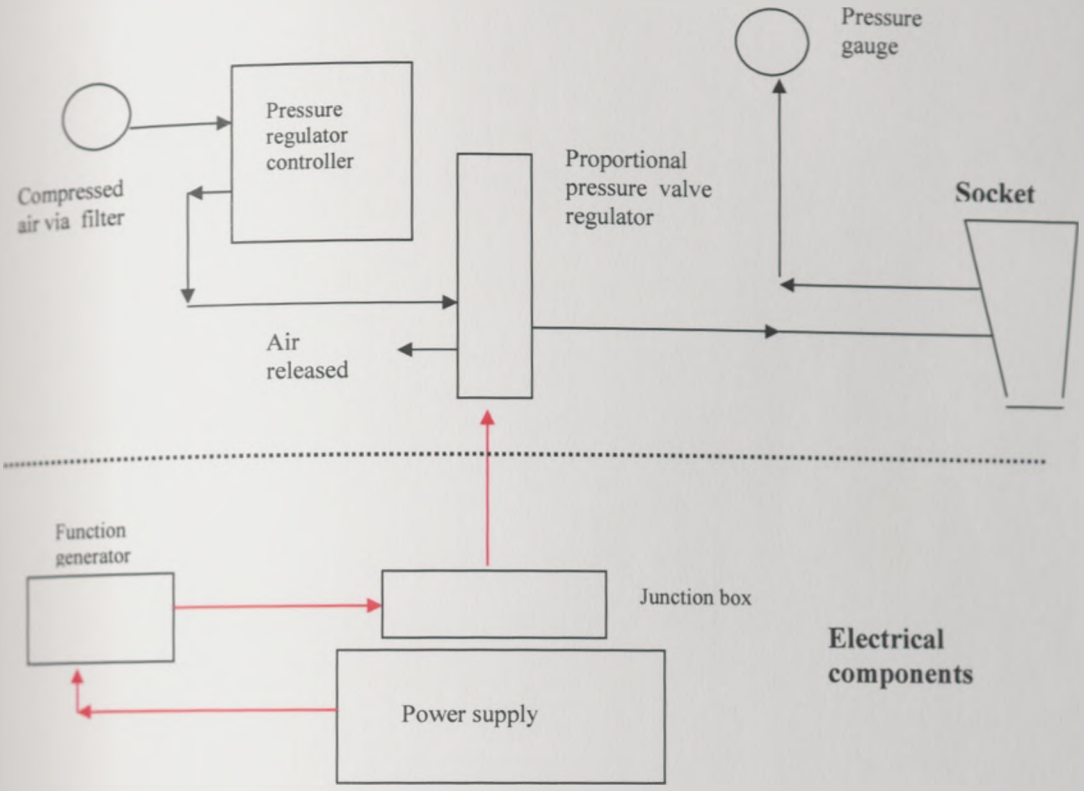

Figure 4.15: Block diagram of customized F-Scan socket calibration. (Air impulse generating system) .

The F-Scan User's Manual, Version 3.8 suggests that to reduce or minimise inter-cell variation encountered on any given F-scan transducer, equilibration must be performed before calibration. In order to mimic the system's operational environment to achieve the highest accuracy, a device originally developed by Buis (1997) was used for equilibration and calibration. This was later modified for use in this study.

Due to the curvature of the interface affecting the response of the F-Socket™ sensor, all F-Socket™ sensors were stick to the hard socket by 3M Spray Mount adhesive. Each equilibration and calibration procedure was conducted on 2 sensors simultaneously. The first pair were located at the anterior and posterior aspects of the socket and the second pair were located at the medial and posterior aspects. All of the F-Socket™ sensors were located below the level of the patellar tendon.

Before equilibration and calibration, the air outlet of the system was connected to a Bourdon pressure gauge to confirm the pressure was correct. The Bourdon pressure gauge was compared to the current complete system pressure gauge (figure 4.12 (a 2)) to confirm accuracy. The comparison results are shown as in table 4.4.

(kPa)	Static measured pressure (kPa), n = 5		Dynamic peak measured pressure (kPa), n = 5	
Applied pressure	Bourdon pressure gauge	Current system pressure gauge	Bourdon pressure gauge	Current system pressure gauge
50	50	50	50	50
100	100	100	100	100
150	150	150	150	150

Table 4.4: Comparison of static pressure and dynamic pressure using current system pressure gauge and Bourdon pressure gauge.

Buis and Convery (1997) designed a pressure rig to apply a cyclic load to the sensors. They applied a cyclic pressure of 100 kPa at 0.5 Hz for a total of 30 cycles. A static load of 100 kPa was then applied for another 5 seconds, at which time the

calibration was recorded. According to their comparison with Entran strain gauges, the researchers reported results within 2% of the applied load. However, it appears that they evaluated the sensor output at different loading rates. Their calibration procedure involved cyclic loading at 0.5 Hz, while in the current study, the rate of socket loading was 1 Hz. The range of 0.5 to 1 Hz is representative of a typical trans-tibial amputee population. In addition, Buis and Convery (1997) applied a static load to the sensor for 5 seconds prior to calibration. An iterative method that could be used to compensate for underestimated pressures was proposed. This suggests that Buis and Convery (1997) may have encountered pressure measurements that were lower than the pressures applied, although this wasn't discussed explicitly. The potential for sensor drift during their calibration procedure could be one explanation for their underestimated pressures.

A test was performed to compare the accuracy of the F-Socket™ sensors results pre and post subject experimentation using the custom calibration set-up (Figure 4.12). Four sensors on each aspect, posterior, anterior, medial and lateral were calibrated using the latex balloon bladder as a pseudo stump and the procedure outlined for dynamic calibration (figure 4.16) i.e. 10 seconds cyclic loading, 10 seconds static loading, 20 seconds cyclic loading and 20 seconds static loading, then the equilibration or calibration command was executed. Once the calibration data were obtained, dynamic trials were recorded. A recording was then triggered after which a cyclic peak load/dynamic load of 80 kPa at 1 Hz over 96 cells of the sensor (a 16 by 6 cell area) was applied for approximately 60 seconds. Average pressures recorded over the entire sensor were compared to the known applied loads. This entire procedure was repeated at the conclusion of subject testing to determine if any changes in the sensor's characteristic had occurred.

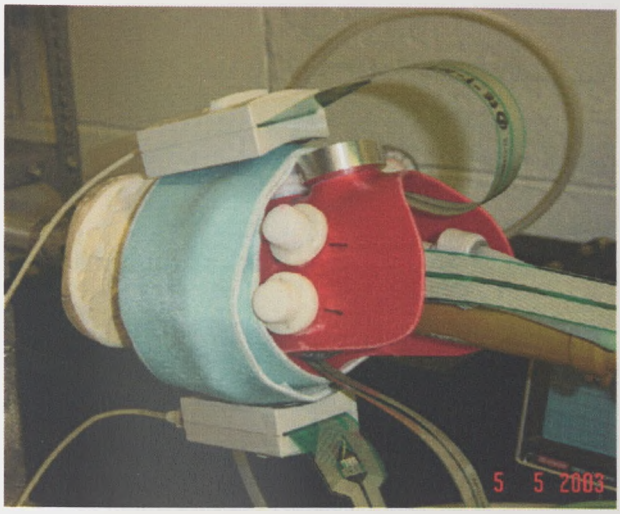

Fig. 4.16: Four F-Socket™ sensors at the posterior, anterior, medial and lateral aspects situated within a test socket.

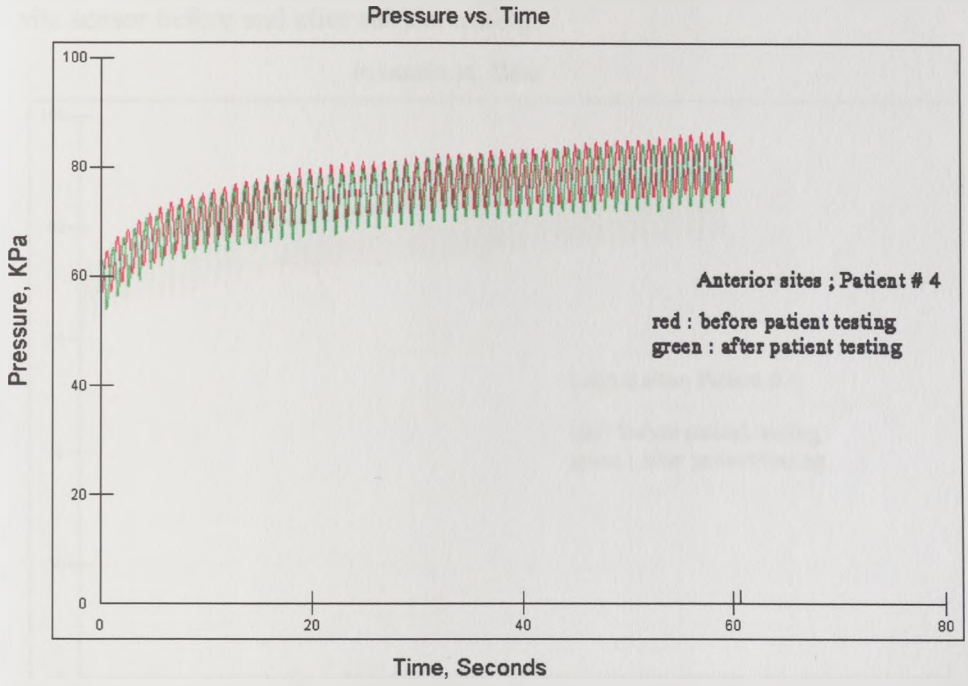

Figure 4.17: Sample subject no. 4; Average entire F-Socket™ sensor pressure at anterior site sensor before and after subject testing.

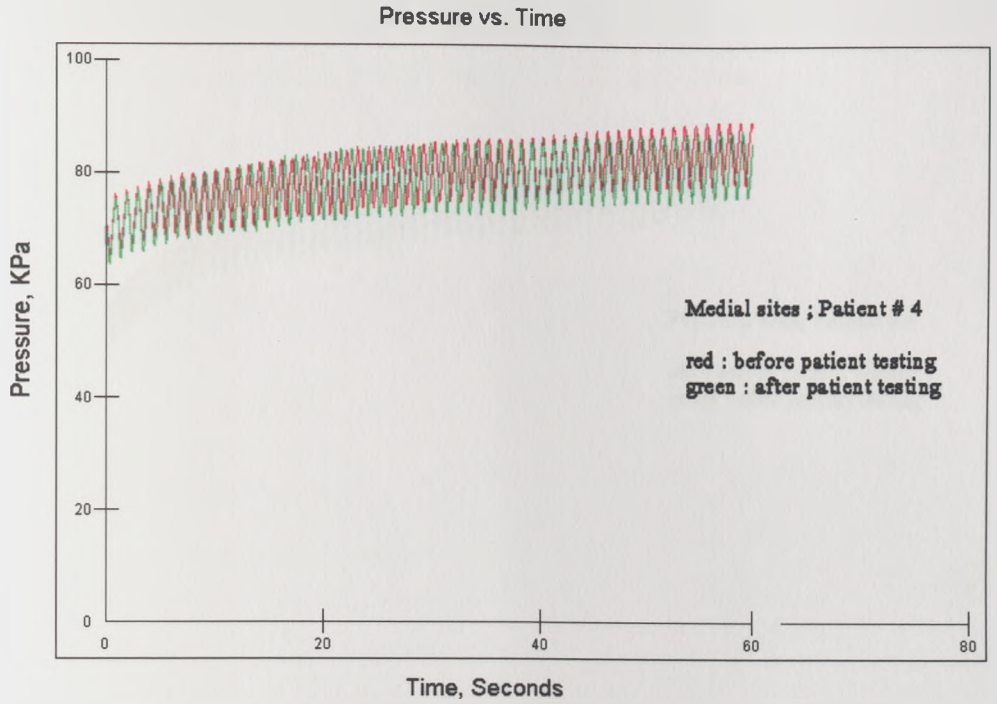

Figure 4.18: Sample subject no. 4; Average entire F-Socket™ sensor pressure at medial site sensor before and after subject testing.

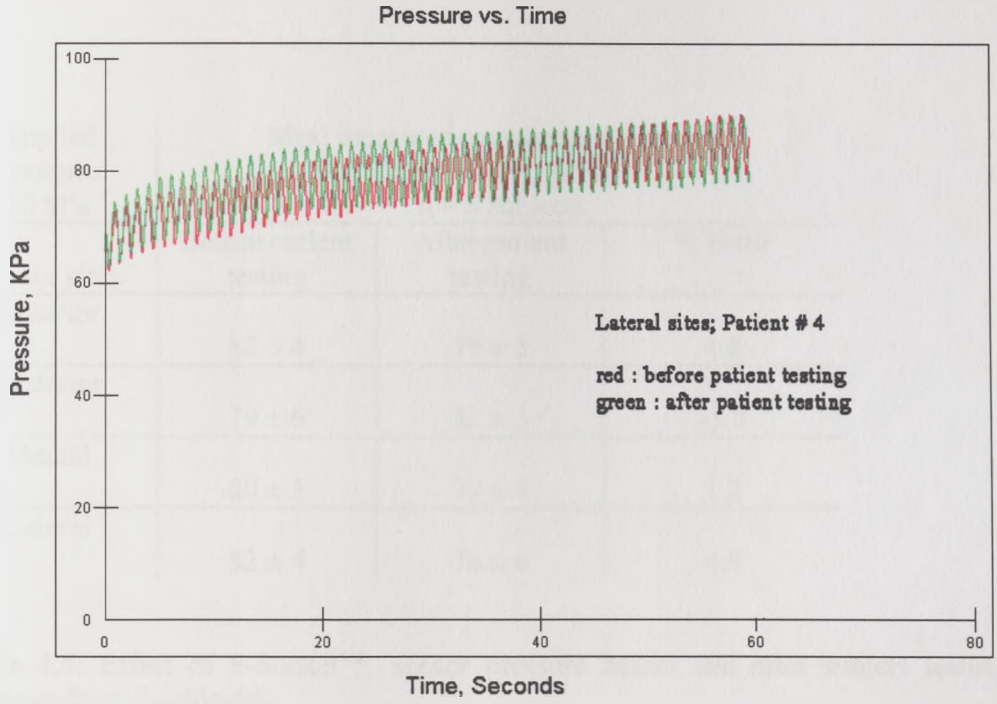

Figure 4.19: Sample subject no. 4; Average entire F-Socket™ sensor pressure at lateral site sensor before and after subject testing.

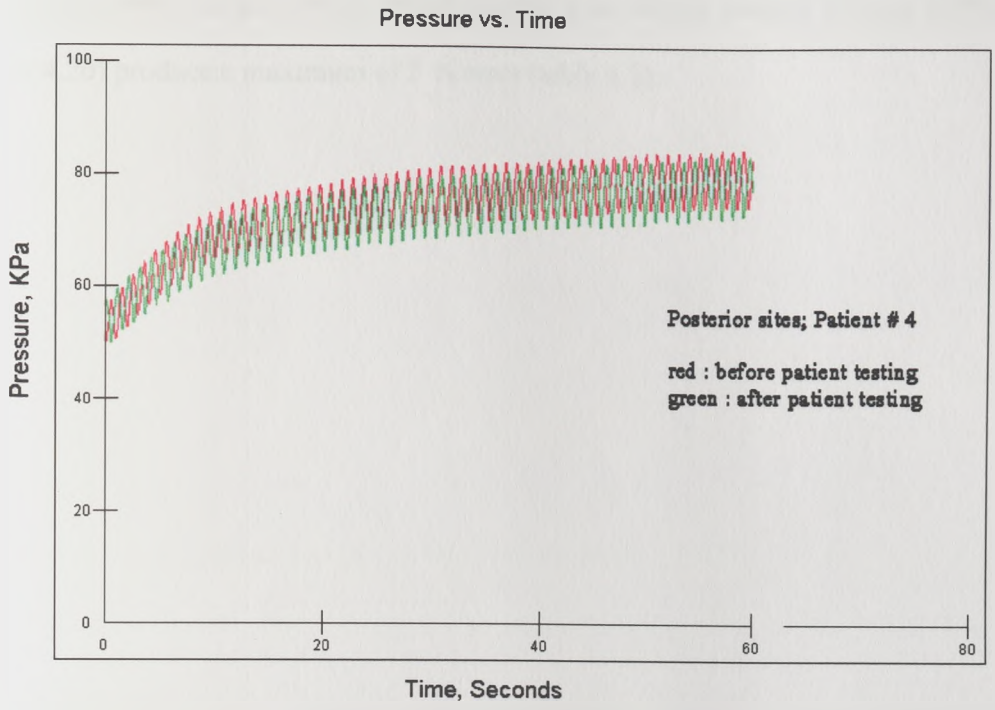

Figure 4.20: Sample subject no. 4; Average entire F-Socket™ sensor pressure at posterior site sensor before and after subject testing.

Applied pressure 80 kPa	Max. measured pressure at 60 seconds mean ± 1 SD (kPa) n = 5 subjects		
Sensor sites	Before patient testing	After patient testing	% Error
Anterior	83 ± 4	79 ± 5	4.8
Posterior	79 ± 6	82 ± 3	-3.8
Medial	80 ± 3	79 ± 4	1.2
Lateral	82 ± 4	78 ± 6	4.9

Table 4.5: Effect of F-Socket™ sensor pressure before and after subject testing. (average from 5 subjects).

The sample sensor output results tested pre and post subject testing, (Figure 4.17 to Figure 4.20) produce a maximum of 5 % error (table 4.5).

CHAPTER 5: TRANSDUCER PERFORMANCE

5.1 Introduction

The Bioengineering Shear transducer and Patellar Tendon transducer used throughout this study monitors all three orthogonal components of the applied load. The linear mathematical approach was used due to accuracy required for the particular application. (Bray et al, 1990).

Detailed discussion on these approaches follow in the sections 5.2 to 5.6.

5.2 Calibration Linear Approach

The approach described simply assumes that each signal can be expressed as a linear combination of the components of the applied load.

From the data, a 3 x 3 column matrix was generated, using the following methods; the output signal, S_i (i=1,2,3), i.e. the output voltage that was measured, is a direct function of the input signal, F_j (j=1,2,3), i.e. an applied load. In this study each signal can be expressed mathematically as a combination of the components of the applied load :

$$S_i = \sum_{i=1}^{3} M_{ij} F_j$$ ----------equation (5. 1)

where M_{ij} are relating the output to the input signals. When i = j the coefficient corresponds to a main effect and in all other cases the coefficients correspond to the two cross-talk and ideally should be zero.

In matrix form this can be expressed as:

$$[S] = [M][F]$$ ---------- equation (5. 2)

where

$$[S] = \begin{bmatrix} SFx \\ SFy \\ SFz \end{bmatrix}$$; A column matrix (3 x 1) of output signal voltages

equation (5.3)

$$[M] = \begin{bmatrix} M_{11} & M_{12} & M_{13} \\ M_{21} & M_{22} & M_{23} \\ M_{31} & M_{32} & M_{33} \end{bmatrix}$$; Square matrix (3 x 3) containing calibration factors M_{ij} determined from calibration data

equation (5.4)

The output signals are recorded in volts (V), after the amplification performed by the strain gauge amplifiers, and the applied loads are measured in Newtons (N), therefore M_{ij} have units of $\left[\frac{V}{N}\right]$

$$[F] = \begin{bmatrix} Fx \\ Fy \\ Fz \end{bmatrix} ; \quad \text{A column matrix (3 x 1) of input applied loads}$$

equation (5.5)

This can be written as;

$$\begin{bmatrix} SFx \\ SFy \\ SFz \end{bmatrix} = \begin{bmatrix} M_{11} & M_{12} & M_{13} \\ M_{21} & M_{22} & M_{23} \\ M_{31} & M_{32} & M_{33} \end{bmatrix} \begin{bmatrix} Fx \\ Fy \\ Fz \end{bmatrix}$$

equation (5.6)

Therefore the matrix can be expressed as ;

$$SFx = M_{11}Fx + M_{12}Fy + M_{13}Fz$$

$$SFy = M_{21}Fx + M_{22}Fy + M_{23}Fz$$

$$SFx = M_{31}Fx + M_{32}Fy + M_{33}Fz$$

equation (5.7)

These equations state that each output signal will in general contain components corresponding to the forces Fx,Fy and Fz.

M_{11}, M_{22}, M_{33} are the principal sensitivity coefficients. All other coefficients are referred as cross-talk coefficients are due to slight inaccuracies in the manufacture of the transducers and in slight misalignments in the positioning of the strain gauges.

When a pure shear force, Fx, is applied to the transducer, the element M_{11} of matrix [M] representing the principal sensitivity coefficient and the two cross-talk M_{21}, M_{31} calibration factors of the channel can be determined. This is repeated for Fy and Fz to obtain the other calibration coeficients.

These can be arranged as;

$$[F] = [M]^{-1}[S] \quad \text{---------- equation(5.8)}$$

where $[M]^{-1}$ is the inverse of the calibration matrix [M]

which is a more convenient equation during subject testing, where the output signals are recorded and the loads are to be determined.

Say $[M]^{-1} = [N]$, then this matrix

$$[N] = \begin{bmatrix} N_{11} & N_{12} & N_{13} \\ N_{21} & N_{22} & N_{23} \\ N_{31} & N_{32} & N_{33} \end{bmatrix} \qquad \text{equation (5.9)}$$

The elements of equation 5.9 have the units of matrix [M] inverted. The units of [M] were $\left[\frac{V}{N}\right]$, then the units of element [N] are $\left[\frac{N}{V}\right]$

Previous investigators who calibrated pylon transducers (Berme et al, 1976; Jones, 1976; Grant-Thompson, 1977; Lawes, 1982; Pashalides, 1989; and Magnissalis, 1992) have all followed the linear approach i.e. the above outlined method for the calibration of the devices.

5.3 Theoretical analysis of the transducers

The Bioengineering Shear Transducer and Patellar Tendon transducer are instrumented with three full bridges of strain gauges, whereby each bridge is responsible for measuring one of the three components of a load acting upon the transducer.

5.3.1 The mechanical properties of the material used and cross-sectional geometries of the transducers

- Mechanical properties

Made of: Aluminium Alloy, 6082 T4 (BS1474:1987)

Modulus of elasticity, $E = 68.9$ GPa

Poissons ratio, $\nu = 0.26$

Shear Modulus, $G = \left(\frac{E}{2(1+\nu)}\right) = 27.3$ GPa

- Various geometries of a cross-section of the transducers

B.E.S.T. transducer , Outer radius, Ro =5.5mm and Inner radius, Ri = 4.5mm. (See figure 4.8).

PT transducer, Ro = 6.0mm and Ri = 5.5mm.

Area, $A = \pi (Ro^2 - Ri^2)$; B.E.S.T. $= 3.1416 \times 10^{-5}$ m^2
PT transducer $= 1.806 \times 10^{-5}$ m^2

Second moment of inertia, $I = \pi (Ro^4 - Ri^4) / 4$; B.E.S.T. $= 3.966 \times 10^{-10}$ m^4
PT transducer $= 2.992 \times 10^{-10}$ m^4

The shear stress, τ is given by the following equations, which are derived in appendix A (originally derivation by Magnissalis, 1992):

$$\tau_{max} = \left(\frac{F.(Ro^3 - Ri^3)}{3.J(Ro - Ri)} \right) \qquad \text{.....equation (5.10)}$$

Strain ε is related to the shear stress τ by the following equation :

$$\text{Strain, } \varepsilon = \left(\frac{\tau}{2G} \right) \qquad \text{..... equation (5.11)}$$

output signal, V_o written as :

$$V_o = V_s \,.\, K \,.\, \varepsilon \qquad \text{..... equation.(5.12)}$$

where nominal gauge factor, K = 2

Normal force , Fy : Strain, ε is related to the applied load Fy by equation (5.13):

$$\text{Strain, } \varepsilon = \left(\frac{\sigma}{E} \right) = \left(\frac{Fy}{AE} \right) \qquad \text{.....equation (5.13)}$$

and output signal, V_o written as

$$V_o = V_s \,.\, (1 + \nu) \,.\, \left(\frac{K}{2} \right) . \varepsilon \qquad \text{..... equation (5.14)}$$

5.3.2 Quantitative results of the analysis

Equations (5.10) to (5.14) will be used here to quantify the effect of the loads and to determine the sensitivity of the bridges to the applied loads.

5.3.2.1 Applied shear force, F (along x or z axes)

Figure 5.1 shows the loading configuration for which shear force, F is applied through a cross-section of the custom-made transducers. Section A-A is only subjected to the shear force, F.

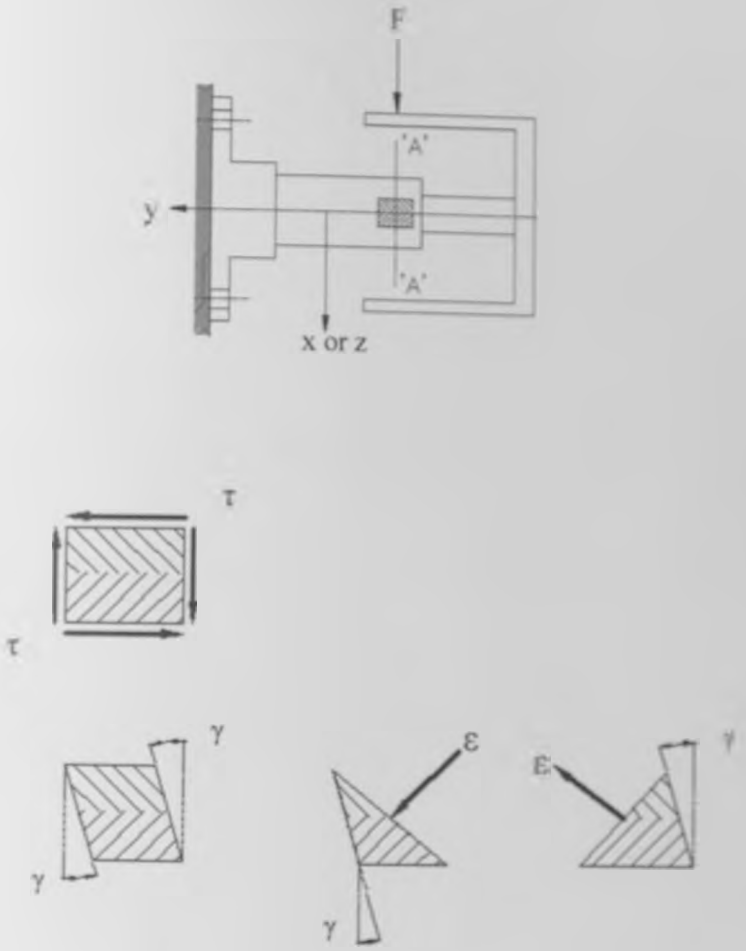

Figure 5.1: Application of shear stress due to shear force and direction of linear strain (the change for unit length due to shear force in an original linear dimension of an element).

e.g.

B.E.S.T. transducer ; stress, σ = 100 kPa @ 3.142 N

PT transducer ; stress, σ = 100 kPa @ 1.806 N

$$\tau_{max} = \left(\frac{F.(Ro^3 - Ri^3)}{3.I(Ro - Ri)}\right) ; \quad \tau_{max\ (B.E.S.T.)} = 198.72 \text{ kPa}$$

$$\tau_{max\ (PT\ transd.)} = 199.69 \text{ kPa}$$

$$\text{Strain, } \varepsilon = \left(\frac{\tau}{2G}\right) ; \quad \varepsilon_{max\ (B.E.S.T.)} = 3.64 \times 10^{-6}$$

$$\varepsilon_{max\ (PT\ transd.)} = 3.66 \times 10^{-6}$$

therefore; sensitivity of output signal, V_o

$$V_o = V_s \,.\, K \,.\, \varepsilon \quad ; \quad V_{o\ (B.E.S.T.)} = 2.184 \times 10^{-5} \text{ V or } 6.951 \times 10^{-6} \left(\frac{V}{N}\right)$$

$$V_{o\ (PT\ transd.)} = 2.194 \times 10^{-5} \text{ V or } 1.215 \times 10^{-5} \left(\frac{V}{N}\right)$$

Using an amplifier gain of 5000: therefore the sensitivity of output signal V_o:

$$V_{o\ theoretical\ (B.E.S.T.)} = 0.0347 \left(\frac{V}{N}\right)$$

$$V_{o\ theoretical\ (PT\ transd.)} = 0.0607 \left(\frac{V}{N}\right)$$

5.3.2.2 Applied normal force, Fy

Figure 5.2 show the loading configuration for which normal force, Fy is applied to the transducer.

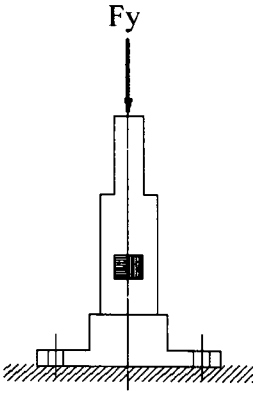

Figure 5.2: Application of normal force

e.g.

B.E.S.T. transducer; stress, $\sigma = 100$ kPa @ 3.142 N

PT transducer; stress, $\sigma = 100$ kPa @ 1.806 N

Strain, $\varepsilon = \left(\frac{\sigma}{E}\right) = \left(\frac{Fy}{AE}\right)$; Strain, $\varepsilon_{\text{max (B.E.S.T.)}} = 1.451 \times 10^{-6}$

Strain, $\varepsilon_{\text{max (PT transducer)}} = 1.451 \times 10^{-6}$

$V_o = V_s(1+\nu)\left(\frac{K}{2}\right)\varepsilon$; $V_{o\,(B.E.S.T.)} = 1.097 \times 10^{-5}$ V or $3.491 \times 10^{-6}\left(\frac{V}{N}\right)$

$V_{o\,(PT\ transd.)} = 1.097 \times 10^{-5}$ V or $6.074 \times 10^{-6}\left(\frac{V}{N}\right)$

Using an amplifier gain of 5000: therefore the sensitivity of output signal V_o:

$V_{o\ theoretical\ (B.E.S.T.)} = 0.0175\left(\frac{V}{N}\right)$

$V_{o\ theoretical\ (PT\ transd.)} = 0.0304\left(\frac{V}{N}\right)$

As a theoretical analysis in section 5.3, sensitivity values for three channels have been calculated and these values could be compared with the actual calibration using the dead weight method.

5.4 Calibration of Bioengineering Shear Transducer and Patellar Tendon transducer.

The performance of the assembled transducers was assessed by dead weight calibration methods. Calibration is the process whereby an accepted standard is compared against an unknown quantity and used to determine the value of the unknown quantity. Calibration devices were developed for both normal and shear directions.

5.4.1 Set-up for normal force calibration.

To calibrate the normal direction (Fy) the PT and the B.E.S.T. transducers were fixed to a specially designed calibration jig incorporating an axial loader. (Figure 5.3). This device enabled the normal force channel to be loaded accurately. Loads were applied by means of weights on the top disc resulting in compression of the transducer. Ball bearings were situated at both ends of the transducer to achieve point loading and loading was only applied in the compressive direction up to 400 kPa in 10 equal steps. This was repeated 10 times. Unloading to zero load was achieved

by removing the known loads in the reverse sequence. The signal outputs from all three channels were recorded simultaneously.

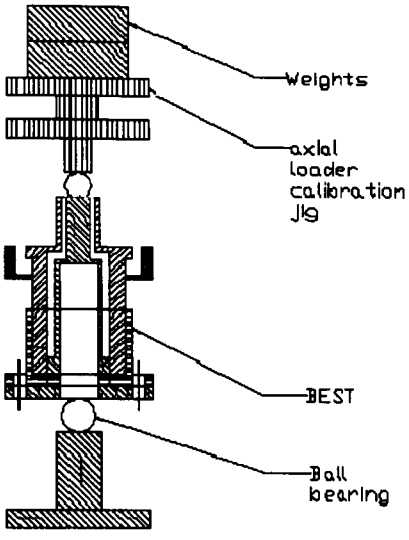

Figure 5.3: Calibration arrangement : Normal direction set-up.

5.4.2 Set-up for shear force calibration.

For the shear force calibration (Fx and Fz), a specially designed shear force adaptor was used. The transducer was positioned in a bench jig that held it rigidly in a horizontal position. The transducer was statically loaded using weights hung from a string around the shear calibration jig cap. (Figure 5.4). Thus forces would be applied directly over the row of shear strain gauges in the transducers, therefore eliminating any bending moment that the strain gauge piston would have experienced. Known loads were then applied in 5 steps up to 4.9N (200 kPa) for B.E.S.T and up to 98 N (200 kPa) for PT transducer and then unloaded to zero load whilst the signal outputs from all three channels were recorded simultaneously. This calibration procedure was repeated 10 times. On completion of the calibration procedure for the positive Fz

channel, the transducer was rotated through 90 degrees and the positive Fx channel was then calibrated. Two further rotations of 90° enabled – Fx and –Fz force to be calculated.

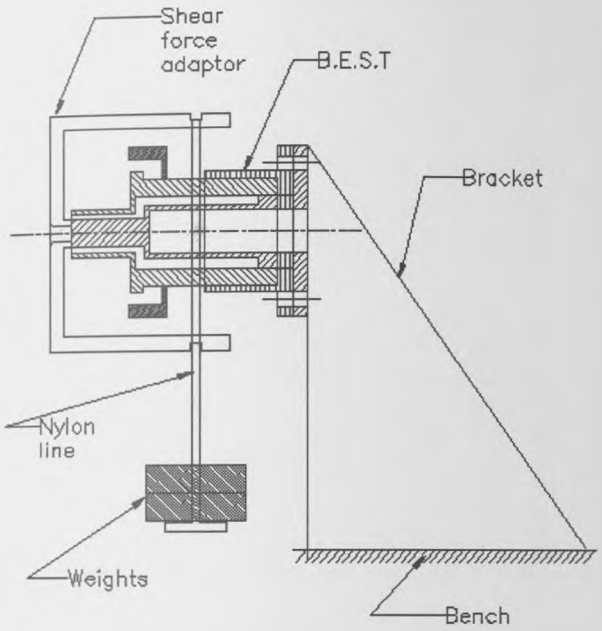

Figure 5.4: Calibration arrangement: Shear direction set-up.

To evaluate any cross-talk effects on the transducers outputs due to the small bending moment arising from the presence of shear force at the interface, additional calibration tests were undertaken. In these tests loads were applied on the transducers to simulate longitudinal and tangential shear force. The results of these tests showed that cross-talks due to these bending effects are negligible.

5.5 Actual calibration – results.

All loads were purely applied in one direction and output signals recorded from the strain gauge amplifiers during each test corresponded to one main effect and two cross-talks, caused by the particular load applied. These signals were recorded in volts (V), against the load in Newton (N) and were averaged using the values obtained during the ascent and descent loading cycles. Sample data of the results of the calibration tests from one Bioengineering Shear transducer of calibration tests are presented in this section together with the calibration graphs, whilst others are presented in appendix B1.

The results of the calibration test for B.E.S.T.2 are presented in tables 5.1, 5.2, 5.3 and figures 5.5, 5.6, 5.7 and consist of mean values of the coefficients and the coefficient of r-square values from the fitted lines. The results of these data are shown in table 5.4.

Load		Under shear load, Fx Averaged output signal, volts (V)		
		B.E.S.T.2-Fx	B.E.S.T.2-Fy	B.E.S.T.2-Fz
τ_x (kPa)	(N)			
0	0	0.00010	-0.00010	0.00010
40	0.981	0.03469	-0.00040	0.00046
80	1.962	0.06926	-0.00080	0.00087
119	2.943	0.10121	-0.00129	0.00129
159	3.924	0.13515	-0.00164	0.00170
199	4.905	0.17286	-0.00205	0.00215

Table 5.1: Calibration values for B.E.S.T. 2 under shear load Fx.

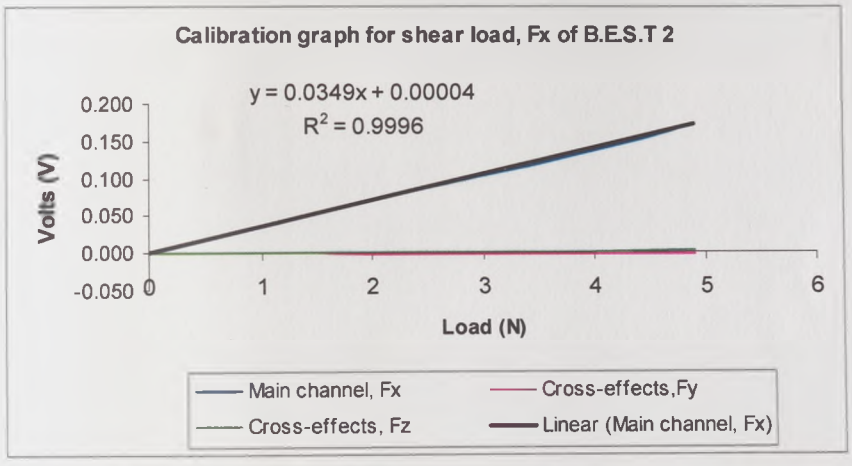

Figure 5.5: Calibration curve for B.E.S.T. 2 under shear load Fx.

Load		Under normal load, Fy Averaged output signal, volts (V)		
		B.E.S.T.2-Fx	B.E.S.T.2-Fy	B.E.S.T.2-Fz
σ_y (kPa)	(N)			
0	0	0.00015	0.00100	0.00009
40	0.981	0.00063	0.01743	0.00057
80	1.962	0.00122	0.03477	0.00120
119	2.943	0.00189	0.05229	0.00184
159	3.924	0.00253	0.06988	0.00247
199	4.905	0.00300	0.08675	0.00313
239	5.886	0.00370	0.10490	0.00383
279	6.867	0.00440	0.12285	0.00455
319	7.848	0.00490	0.14140	0.00513
358	8.829	0.00550	0.15760	0.00585
398	9.81	0.00590	0.17612	0.00643

Table 5.2: Calibration values for B.E.S.T. 2 under normal load Fy.

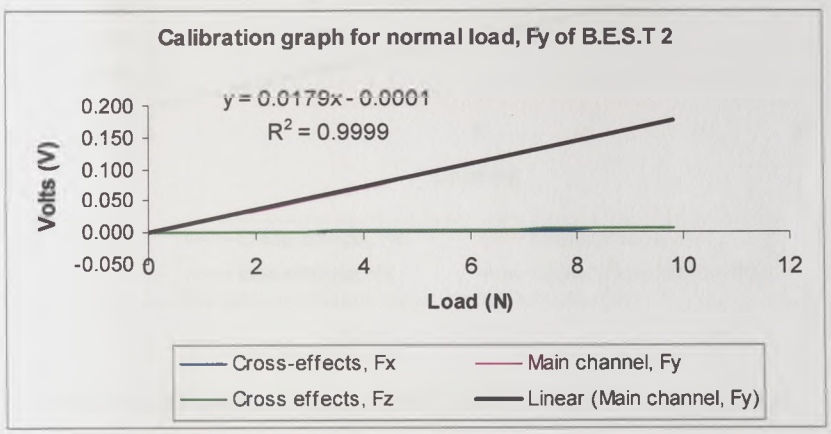

Figure 5.6: Calibration curve for B.E.S.T. 2 under normal load Fy.

Load		Under load shear, Fz Averaged output signal, volts (V)		
		B.E.S.T.2-Fx	B.E.S.T.2-Fy	B.E.S.T.2-Fz
τ_x (kPa)	(N)			
0	0	0.00010	0.00010	0.00090
40	0.981	0.00045	0.00041	0.03467
80	1.962	0.00086	0.00081	0.06931
119	2.943	0.00128	0.00128	0.10123
159	3.924	0.00171	0.00165	0.13519
199	4.905	0.00216	0.00202	0.17321

Table 5.3: Calibration values for B.E.S.T. 2 under shear load Fz.

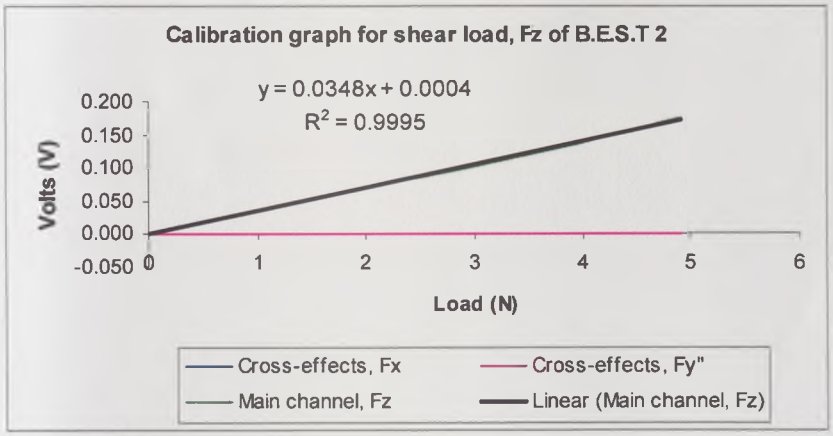

Figure 5.7: Calibration curve for B.E.S.T. 2 under shear load Fz.

Coef.	Mean (V/N)	r-square (%)
M_{11}	0.0349	99.96
M_{12}	-0.0004	99.65
M_{13}	0.0004	99.89
M_{21}	0.0006	99.83
M_{22}	0.0179	99.99
M_{23}	0.0007	99.91
M_{31}	0.0004	99.86
M_{32}	0.0004	99.76
M_{33}	0.0348	99.95

Table 5.4: B.E.S.T. 2 coefficient of r-square values from the fitted lines of B.E.S.T. 2 calibration curve.

The matrix [M] derived by using dead weights in this study was used throughout the study. This matrix [M] is shown in table 5.5 and the calibration matrix $[M]^{-1}$ or [N] in table 5.6.

0.0349	-0.0004	0.0004
0.0006	0.0179	0.0007
0.0004	0.0004	0.0348

Table 5.5 : Matrix [M] derived for B.E.S.T.2

28.646082	0.647785	-0.342295
-0.947754	55.869613	-1.112920
-0.318372	-0.649625	28.752359

Table 5.6 : The calibration Matrix $[M]^{-1}$ or [N] derived for B.E.S.T.2

As expected, there are differences between the coefficients of the main diagonal and the cross-talks. The coefficients of the main diagonal can now be compared with the theoretical values derived in section 5.3. The sensitivities derived in that section for the three channels, when multiplied by the gain settings can be compared to the experimentally derived main effects as in table 5.5.

Experimental sensitivity calibration results for B.E.S.T.2 (table 5.5) were very close to those predicted theoretically (section 5.3). Summaries of the theoretical values compared with the experimental derived value for the B.E.S.T. and PT transducer are shown in table 5.7 and 5.8 respectively.

Sensitivity channel	Exp. B.E.S.T.1	Exp. B.E.S.T.2	Exp. B.E.S.T.3	Exp. B.E.S.T.4	Exp. B.E.S.T.5	Theoretical B.E.S.T.
Fx	0.0348	0.0349	0.0348	0.0346	0.0348	0.0347
Fy	0.0173	0.0175	0.0174	0.0173	0.0174	0.0175
Fz	0.0349	0.0348	0.0347	0.0346	0.0348	0.0347

Table 5.7: B.E.S.T. sensitivity comparison, between experimental and theoretical values

Sensitivity channel	Exp. PT transd.	Theoretical PT transd.
Fx	0.0608	0.0607
Fy	0.0306	0.0304
Fz	0.0609	0.0607

Table 5.8: PT transducer sensitivity comparison, between experimental and theoretical values

Five BEST transducers and one PT transducer were evaluated for hysteresis error. *Hysteresis error* - The maximum difference between output readings for the same measured point, one point obtained while increasing from zero and the other while decreasing from full scale output (FSO). The deviation is expressed as a percent of full scale. In this study hysteresis was investigated during calibration by increasing and decreasing the stresses applied to the transducers. Average hysteresis error from the five BEST transducers was found to be 2.03 % FSO, for 200 kPa shear stress directions and 1.65 % FSO, for 400 kPa normal pressure direction while the hysteresis error from the PT transducer was found to be 1.53 % FSO, 200kPa for the shear directions and 1.85 % FSO, 400kPa for the normal direction. The hysteresis error obtained from this study falls within the range reported by Appoldt et al (1967),

Williams et al (1992) and Sanders et al (1993). A summary of transducer hysteresis performance from this and previous studies is shown in table 5.9.

Hysteresis error / Investigators		Normal direction					Shear direction				
Appoldt et al, (1967)		3 % FSO					Not reported				
Williams et al, (1992)		2 % FSO					8% FSO				
Sanders et. al, (1993)		3 % FSO					0.3 % FSO				
Current study	PT Transd.	1.85 % FSO					1.53 % FSO				
		BEST1	BEST2	BEST3	BEST4	BEST5	BEST1	BEST2	BEST3	BEST4	BEST5
	B.E.S.T	1.71% FSO	1.65% FSO	1.63% FSO	1.62% FSO	1.63% FSO	2.05% FSO	2.03% FSO	2.10% FSO	2.01% FSO	1.98% FSO
	B.E.S.T (average)	1.65 % FSO					2.03 % FSO				

Table 5.9: Comparison of reported hysteresis error from four studies.

CHAPTER 6: METHODS

6.1 Subjects

Ten trans-tibial amputees participated in this study on a voluntary basis, and gave written informed consent. All were male and had undergone amputation at least 5 years prior to this study. Safety and Ethical approval was granted from the relevant committees of the University of Strathclyde and the Southern General Hospital NHS Trust UK. (See appendix C).

The subjects ranged in age from 34 to 77 years, with a mean of 57 and a standard deviation of 12 years (Table 6.1). Subject mass and height ranged from 67 to 133 kg (88 ± 21 kg) and 1.68 to 1.91 m (1.78 ± 0.07 m), respectively. Body Mass Index ranged from 21.88 to 38.86 kg / m^2 (27.75 ± 5.74 kg / m^2). Body Mass Index diagram (Figure 6.1), which is a number calculated from an individual's weight and height, which is used to determine whether a person is within, or outside of, a normal weight range is also presented. Anterior views of the stumps of the subjects who participated in the testing programme can be viewed in appendix D.

Subject no.	Age	Height	Mass	**Body Mass Index (BMI)	Reason for amputation	Amputation side	Current prosthesis	Stump length (mm)	Mobility grade*
		(m)	(kg)	(kg / m^2)					
1	77	1.78	95	29.98	Trauma	Right	PTB	177	4a
2	73	1.91	80	21.93	PVD	Right	PTB	125	4c
3	58	1.69	72	25.21	Trauma	Left	PTB	145	6
4	53	1.74	95	31.38	PVD	Left	PTB	123	4a
5	56	1.78	76	23.99	PVD	Left	PTB	150	6
6	61	1.78	108	34.09	PVD	Left	PTB	120	5
7	49	1.85	133	38.86	Trauma	Right	PTB	145	4a
8	34	1.75	67	21.88	Trauma	Right	PTB	130	4c
9	47	1.8	89	27.47	*Others*	Left	PTB	148	4b
10	61	1.68	64	22.68	PVD	Right	PTB	130	5
aver. ± SD	56.90 ± 12.47	1.78 ± 0.07	87.90 ± 21.09	27.75 ± 5.74					
					PVD/Trauma	Left/Right	PTB		4 to 6
Mean	56.90	1.78	87.90	27.75				139.30	
Min.	34	1.68	64	21.93				120	
Max.	77	1.91	133	38.86				177	

* Mobility Grades in Prosthetic Rehabilitation. (Devised by Stanmore & Harold Wood Disability Service Centres)
** Kindly see Figure 6.1 to determine whether the subject is within, or outside of, a normal weight range.

Table 6.1: Summary and characteristics of ten male test subjects.

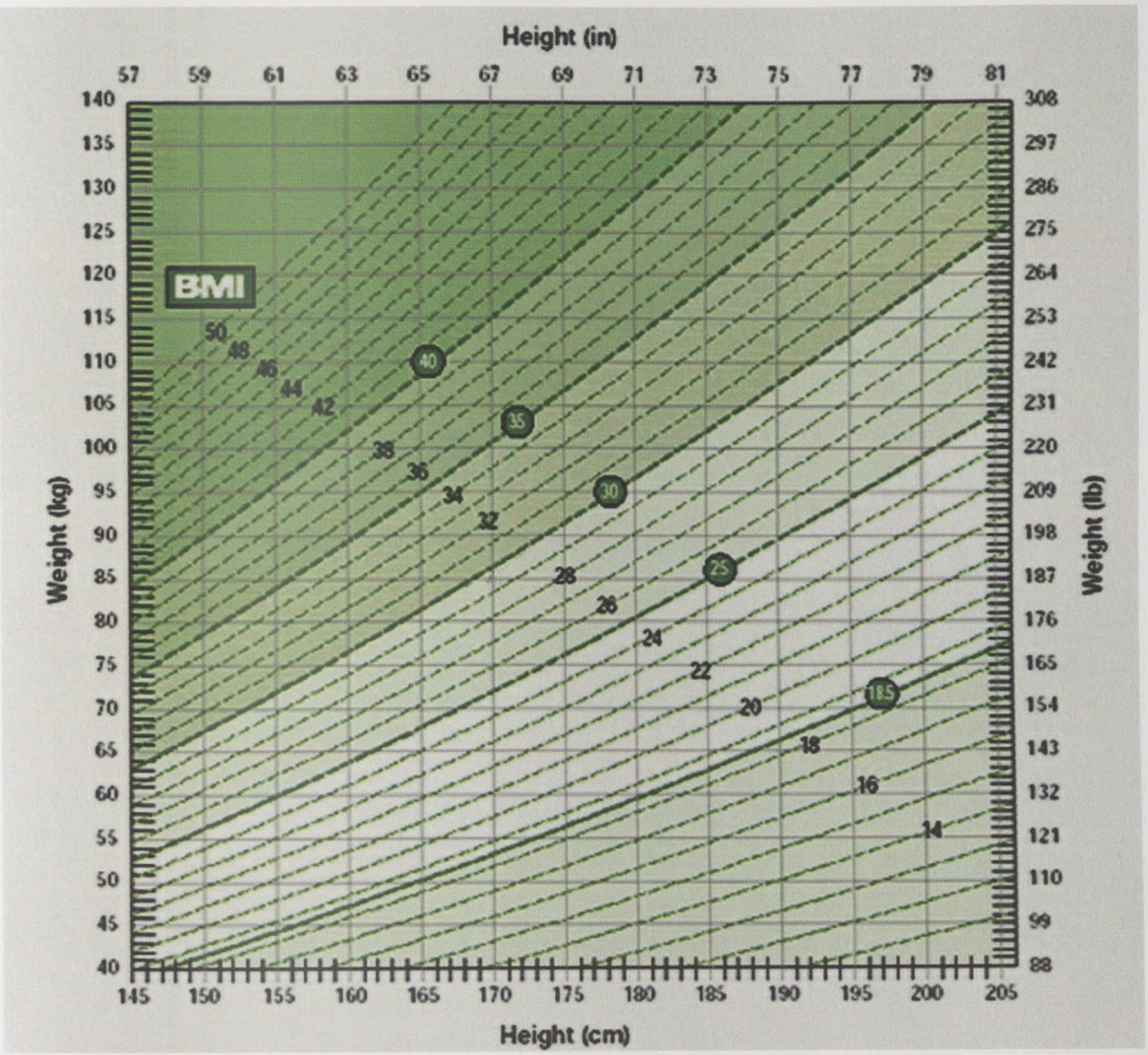

Body Mass Index is a number calculated from an individual's weight and height, which is used to determine whether a person is within, or outside of, a normal weight range.

BMI Less than 20 — Under Weight
BMI 20-25 — Normal Weight
BMI 25-30 — Over Weight
BMI 30-40 — Obese
BMI Over 40 — Severely Obese

Figure 6.1: Body Mass Index Chart. Adapted from website, 17 March 2005, 16.47 GMT (http://www.hc-sc.gc.ca/hpfb-dgpsa/onpp-bppn/bmi_chart_java_e.html)

6.2 Experimental sockets

'Hard' sockets, i.e. without soft liners, containing machined metal inserts were manufactured, using standard laminating techniques, for each subject. (Figure 6.2 and Figure 6.3). The cast was marked longitudinally at 45° segments using a 'dividing head' and the transducer sites were located on these lines at 50mm intervals. (Figure 6.4) All subjects were fitted with check sockets prior to production of the experimental socket to ensure that the experimental socket was a total contact socket and was comfortable. (Figure 6.5 and 6.6). (Check socket is made by forming a heated sheet of clear plastic over the model. Then, filling the "confirmed good fitting" check socket with a mixture of water and plaster of Paris to make a new positive model.) Each subject wore their experimental sockets with stump socks and no liner.

Figure 6.2 : Laminated socket with metal inserts.

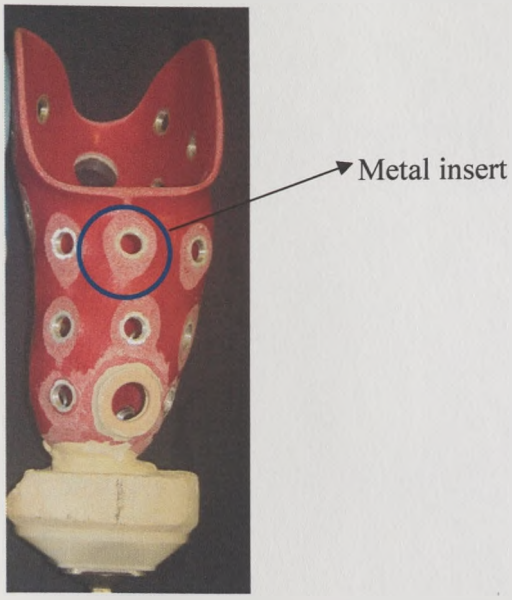

Figure 6.3 : Socket with metal insert exposed.

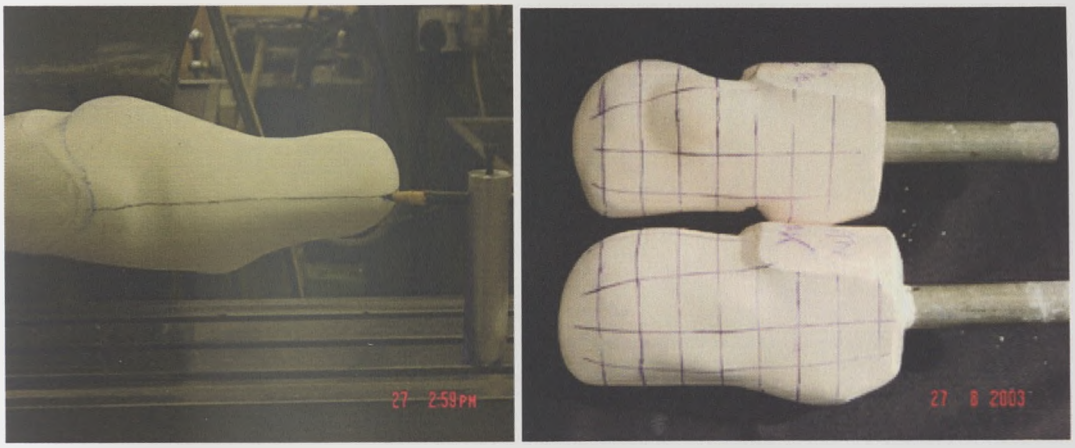

Figure 6.4 : Marking on the positive cast.

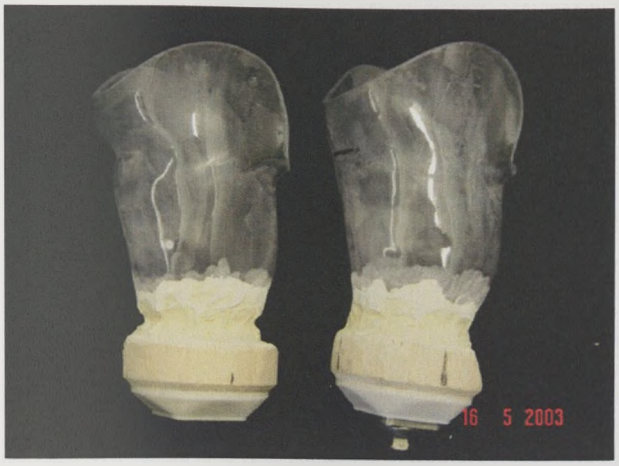

Figure 6.5: Check sockets; left - PTB socket, right - hydrocast socket.

Figure 6.6: Subject wearing experimental check socket with TEC Prolink (TEC Interface Systems, Minnesota, USA) suspension sleeve.

The shape of the PTB and Hydrocast sockets present different socket contours (Figure 6.7) and therefore different socket axes. The socket dimensions (volume and shape) are not identical. These differences occur because the soft tissues are rectified by applying localized pressure on pre-defined pressure areas during production of the PTB socket whilst no or minimal rectification is involved during the hydrocast casting procedure. These dissimilarities in casting procedures will result in a variety of differences such as volume, shape and dimension. The PTB method develops a shape which is triangular whereas a circular shape is developed for the hydrostatic method. The socket axis also changes accordingly. It was therefore difficult to establish an identical reference grid for sensor positioning in both sockets. In order to overcome the difficulty of establishing a central axes for an irregular shape such as a prosthetic socket, Szulc (1988) designed a centre-line positioner named the Szulc Socket Axis Locator (SSAL). (See Figure 6.8). This axis positioning tool consists of two separate sub-units placed on a central axis. Each unit has two pairs of independently operating legs allowing both pairs independent movement.

When the SSAL is placed inside a socket, the pairs of legs extend until they contact the walls of the socket. When all four legs of a sub-unit are in contact with the walls of the socket the centre of the central axis coincides with the centre of the socket in the plane defined by the point of the four legs. When both sub-units are so located then the central axis defines the axis of the socket. Therefore this device was utilised to determine the individual socket axis of each socket tested.

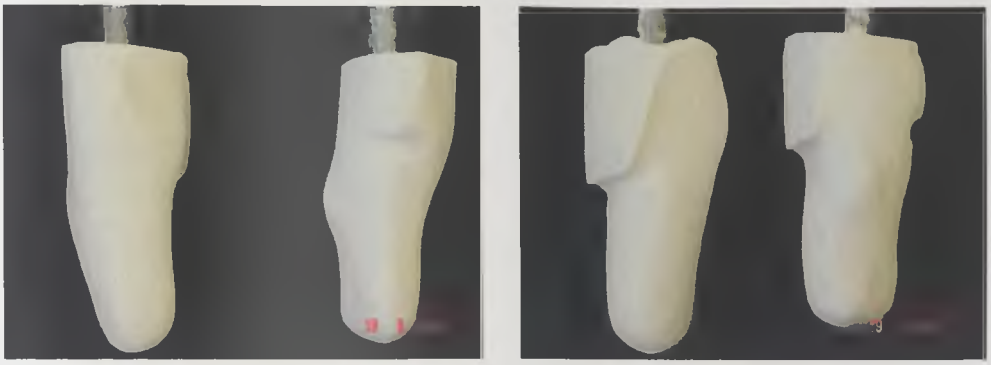

(a) (b)

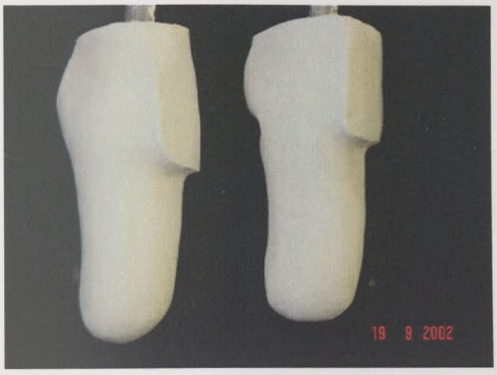

(c)

Figure 6.7 ; Contour of Hydrocast positive cast (left) and PTB positive cast (right) from different view orientation.

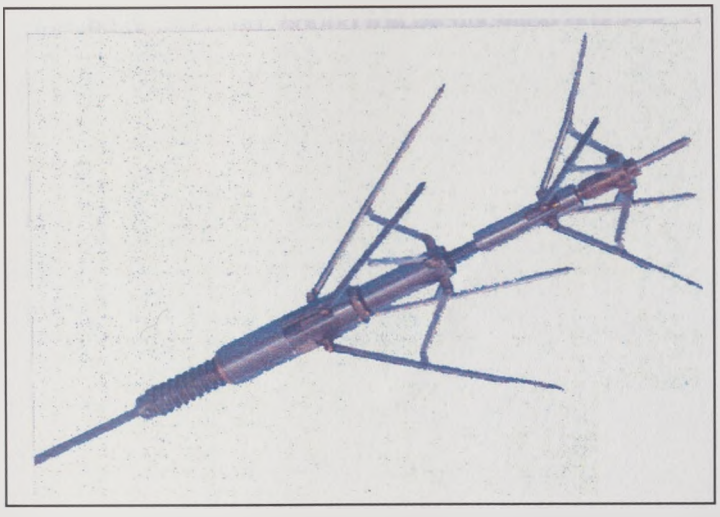

Figure 6.8 Szulc Socket Axis Locator (SSAL)

The SSAL device was designed to be self aligning. According to Szulc (1988) after 10 successive placements of the device in a uniform cylinder, the average centre line offset is ± 0.75 mm..

The metal inserts allowed the transducers to be placed within the socket wall such that the sensing surface was flush with the inside surface of the socket. The sites of transducer locations were the same for all experimental sockets for each individual subject with the centre of the patellar tendon acting as a datum. (Figure 6.9 and 6.10). A general flow diagram for manufacture of the experimental socket is shown in figure 6.11.

Figure 6.9: PTB socket (left) and Hydrocast socket (right); Transducer locations for the subject no. 4

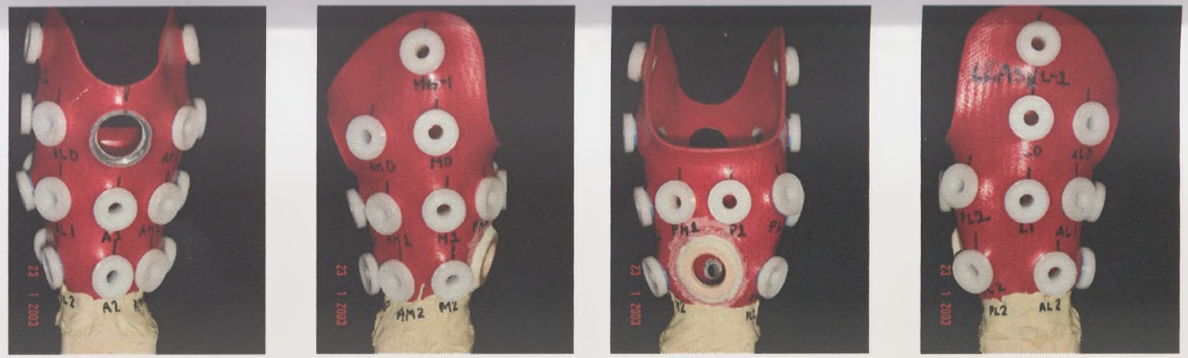

ANTERIOR MEDIAL POSTERIOR LATERAL

(a)

(b)

Figure 6.10: (a) Transducers location on a trans-tibial socket. (b) Reference used throughout the study for the trans-tibial socket. (The size of the socket dictates the number of possible transducer sites).

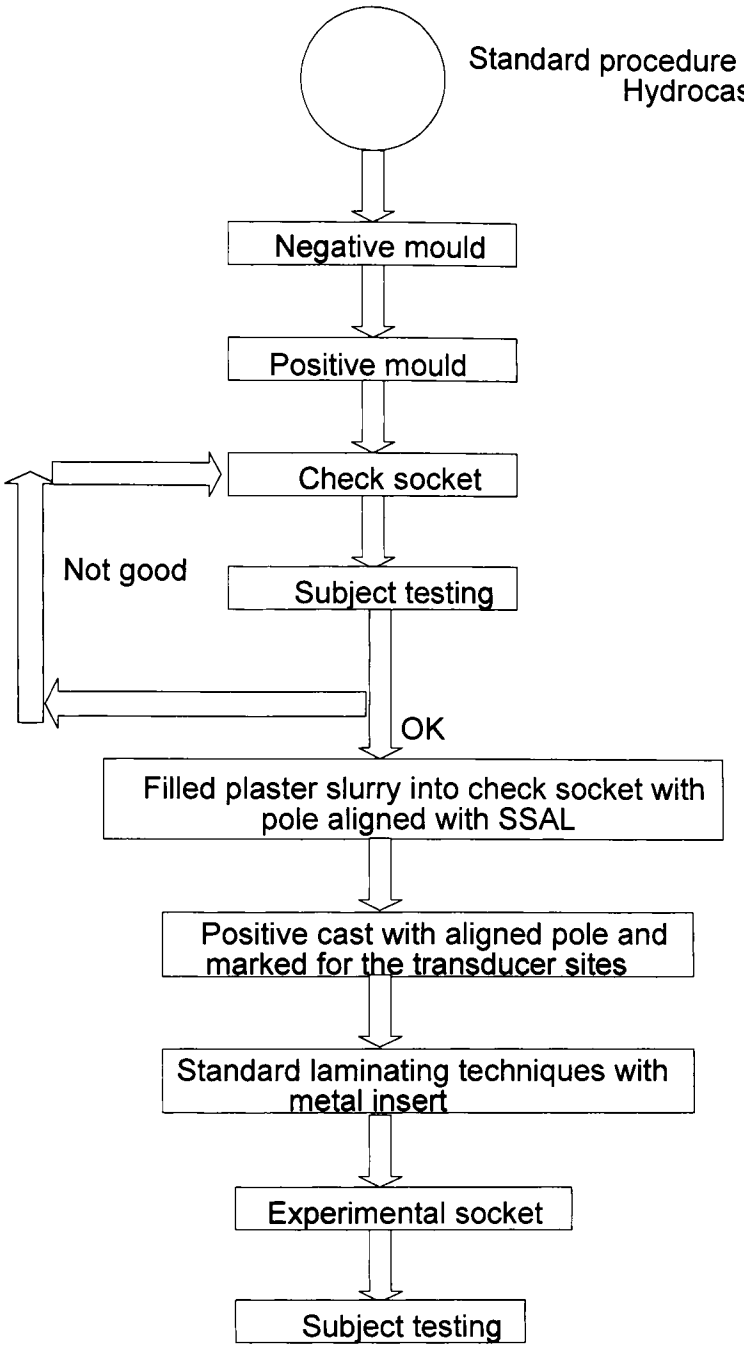

Figure 6.11: General production procedure for the experimental socket.

The total mass of each experimental prosthesis, with all transducers and blanking plugs in situ, was approximately 3.0kg. A TEC ProLink (TEC Interface Systems, Minnesota, USA) suspension sleeve in conjunction with a simple one-way valve was used for suspension. (Figure 6.12). This method of suspension was found to successfully eliminate the pistoning action between the stump and the socket during walking.

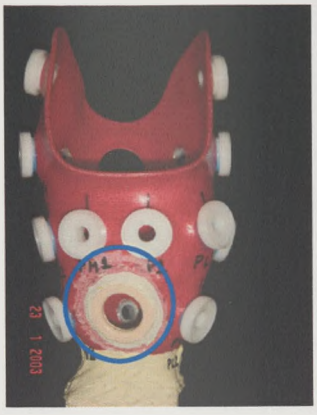
(a)

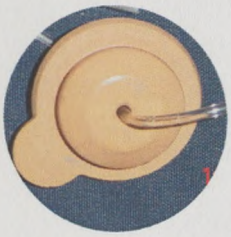
(b)

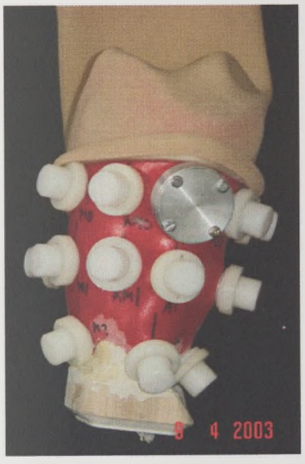

(c)

Figure 6.12: (a) Socket showing the position of a simple one way valve (highlighted with blue circle) (b) One way valve used (c) Socket with suspension sleeve.

Alignment was performed by one prosthetist until the subject's gait was agreed to be optimal by both subject and prosthetist. All data collection events for each experimental socket were performed on the same day with the amputee wearing the socket at all times.

6.3 Experimental procedure

In this study a two part experimental procedure was utilised. The first part involved the measurement of normal and shear stresses at discrete sites mapped out in the sockets using the Entran based transducers, PT transducer and B.E.S.T. transducers. The second part, attempted to measure the interface pressure using the Tekscan Inc., F-Scan (F-Socket™ sensors) model 9811. During the experiment the Entran, PT and B.E.S.T transducers were removed and replaced by blanking plugs.

6.3.1 Experiment 1

This experiment was designed to obtain (1) peak average stresses recorded throughout the walking gait, and (2) average stresses recorded during standing i.e. static. The number of transducer sites available without adjacent transducers impinging on each other was dependent on the physical size of the socket (stump), however over the ten subjects tested an average of 16 transducer sites were available for pressure measurement. The specific number of transducers used for each subject in shown in table 6.3. Owing to a limitation of the number of recording channels available with the data acquisition system a restriction of up to 11 'Entran' sites, 5 B.E.S.T. sites, 1 Electrohydraulic transducer site and 1 patellar tendon site was imposed for simultaneous recording, therefore sites that were not monitored were sealed with blank transducer plugs to ensure that the pressure

difference across the socket wall was maintained. By collecting data from all sites using the Entran transducer and then replacing then with B.E.S.T. and vice versa ensured that data were obtained from all sites by both types of transducer.

Subject no.		1	2	3	4	5	6	7	8	9	10	aver. (SD)
No. of transducer sites	PTB socket	31	19	15	14	15	18	14	13	12	15	16.6 (5.5)
	Hydrocast socket	30	19	14	15	15	19	14	14	12	14	16.4 (5.5)

Table 6.3: Number of transducer sites available for pressure measurement using Electrohydraulic, Entran, B.E.S.T. and PT transducer for each subject.

The sampling rate used was 50 Hz and data were recorded for approximately 15 seconds for each walking trial at the subject's self-selected walking speed. Data were collected simultaneously using a two 16 channel strain gauge amplifiers, model DAQN-Bridge (Dewetron, Austria) with PCMCIA Lab View DaqCard 700 (National Instruments, Austin, TX) for data acquisition and a Dell Inspiron PIII for data storage with Lab View version 6.1 as analyzing software.

For the locomotion test, the subject was asked to walk a distance of 7 metres on a level walk-way. At least 3 trials were recorded for each test. Data were obtained with the patellar tendon bar of the prosthesis in the neutral position (the original position as cast/rectified by the prosthetist), compressed by (+) 2 and 4mm and relieved by (-) 2mm. In addition to the measurement obtained from the patellar tendon bar, the other test sites containing transducers were sampled simultaneously i.e. Electrohydraulic, Entran, and B.E.S.T. transducer. In order to correlate the measured pressure and stresses with the

phases of the gait cycle, heel strike and toe off events were recorded. Two footswitches (Interlink Electronic Inc., CA, USA) were fitted separately at the heel and toe of the shoe subject in the gait cycle indicating heel strike, toe contact, heel off and toe off. Signals from the switches were passed on to the amplifier. Any change of the contact state of heel or toe will alter the output signal. The foot switches leads were secured in place by tape. The average (gait cycle) heel strike to heel strike on 8 subjects using foot switches were 1.201 ± 0.03 second. Sanders et al, (1998) on socket experiment, had shown step duration (heel strike to ensuing heel strike) of 1.26 ± 0.04 second by using an instrumented prosthetic shank. A pilot study was performed on one of the subjects one month in advance of the full testing programme to examine the effect of time on the repeatability of results.

6.3.2 Experiment 2

The small error centre line offset of ± 0.75 mm after placement of SSAL in a uniform cylinder was shown by Szulc (1988). (See section 6.2). Therefore, in this study, this error can be ignored in the establishment of a sensor reference. This is because of the relatively large active area of the F-Socket™ 96 cells sensor. The SSAL was placed inside the socket and one of the leg pointers from the proximal sub-unit was then positioned on the mark of the mid-patella tendon because of its clarity as a locatable landmark. (This position also acts as a datum in the experimental socket.) The legs were allowed to spring into place, thus the SSAL takes up its own position within the socket. Once this position had been attained, the socket was marked at each leg tip. The marks were then used to produce four axial reference lines at the anterior, posterior, medial and lateral aspects. The vertical reference lines were used as centre lines for the sensors and the horizontal reference line, situated just below the patellar tendon site, was used to position the proximal side of the transducers. F-Socket™ sensors were fixed with non aggressive spray

glue which allowed re-positioning. (Figure 6.13). All the proximal sensors of the anterior, posterior, medial and lateral aspects were positioned at a level just below the Patellar Tendon Bar. The nature of the experimental socket with a moveable patellar tendon bar prevented more proximal sensor measurement.

Figure 6.13: F-Socket™ sensor attached with non aggressive spray glue to the socket

Measurements of the socket interface pressure distribution during the second experimental procedure were made using F-Socket™ sensors in conjunction with a software program version 5.03 developed by Tekscan. Inc. Prior to each day of data collection, the sensors were calibrated according to the methods outlined in Chapter 4, section 4.4.5. The four F-Socket™ sensors were placed below the patellar tendon bar datum line such that one sensor covered the anterior side of the socket, one covered the

posterior side of the socket, and the other two sensors covered the medial and lateral sides of the socket (Figure 6.14).

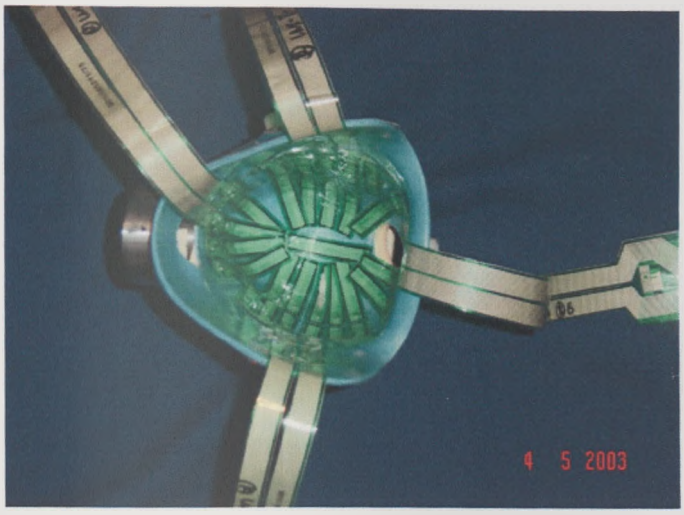

Figure 6.14: A test socket with F-Socket™ sensors on the anterior, posterior, medial and lateral aspects.

After the sensors were attached to the socket, the outlines of the regions of interest (the position of the custom made transducers) were traced directly onto the sensors via holes in the acetal mounts using a black marker before the holes were sealed with the blanking plugs. (Figure 6.15). This allowed local pressure measurements to be known. The subject donned the prosthesis in his usual fashion. The same ply of stump sock as was used in the previous test (experiment 1) was worn. The sensor leads, which emerged from the top of the socket, were directed upward and inserted into the data acquisition cuffs. These cuffs were firmly attached to the thigh of the subject using 'zap-on' strap. Data were recorded from the anterior and posterior sensors first and then, the same procedure was applied to the lateral and medial sites. The experimental set up could only be applied to

two positions at one time. These procedures were to minimize interference with the subject's gait. A TEC ProLink (TEC Interface Systems, Minnesota, USA) suspension sleeve was used to suspend the prosthesis (Figure 6.16). The cuffs were linked to the data acquisition computer via 10-metre long cables. These cables were looped through a belt on the subject's waist and were held by a co-worker so that they would trail behind as the subject walked and not interfere with locomotion.

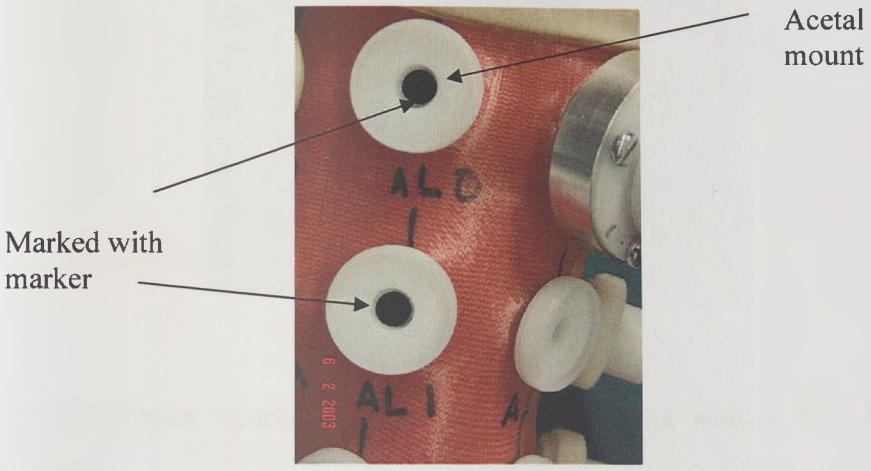

Figure 6.15: F-Socket™ sensors were attached inside the socket and the position of the Entran / B.E.S.T. transducer sites were marked via the hole in the acetal mount using a black marker pen.

Interface pressures from the F-Scan system were collected simultaneously from the anterior and posterior sensors. A second trial collected data simultaneously from the medial and lateral sensors. During the test, the subject walked at his self selected speed. All tests were conducted on the same day to minimize day-to-day variations due to sensor deterioration. It was assumed that the first trials collected each day would be affected least by sensor deterioration. For all walking trials, pressure data were collected for 120s at 50 Hz.

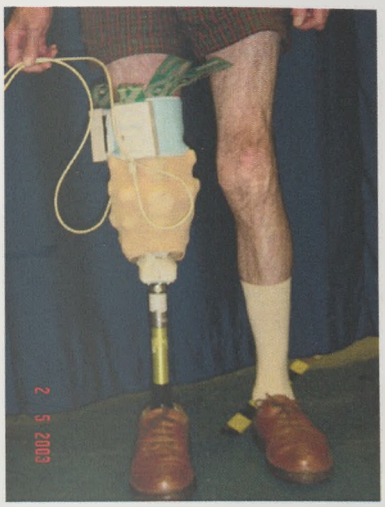

Figure 6.16: Subject wearing an experimental prosthesis with a TEC ProLink (TEC Interface Systems, Minnesota, USA) suspension sleeve to suspend the prosthesis. Complete set-up for F-Socket™ sensor testing.

Prior to each walking trial, the subjects were instructed to unload the prosthetic limb for one minute either by sitting or standing with all weight on the contralateral limb. The subject was then asked to walk for one minute before proceeding down the walkway.

6.3.2.1 Pressure Sensor Data Processing

After the pressure sensors were removed from the socket, the markings on the sensors were used to identify which individual cells corresponded with the Entran /

B.E.S.T. site. These same cells were then identified in each Tekscan recording and a box was drawn around each of these areas. The software program was used to calculate the average pressure within each region (box) over time and these data were exported to an ASCII file. (Figure 6.17). For each condition, pressure data from the trials were combined to calculate the mean pressure and standard deviation over the entire gait cycle. The pressure data were imported into Microsoft Excel 2000 for plotting and further analysis.

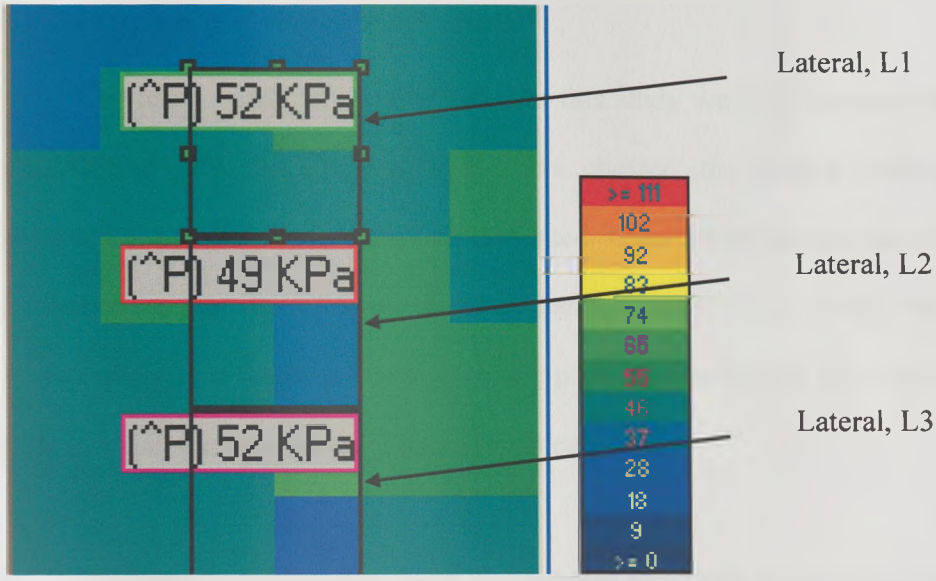

Figure 6.17: Example of F-Socket™ sensor recording with areas of interest identified.

CHAPTER 7: RESULTS

7.1 Overview

The ten subjects who participated in this study were all successfully fitted with both PTB and Hydrocast sockets. In this chapter, the results obtained from the experimental portion of the study are presented. Quantitative assessment of the pressure distribution at the stump/socket interface can be made. This should lead to a better understanding of the differences in interface pressure distribution with respect to the two types of socket design i.e. the PTB and Hydrocast socket.

The experimental results were divided into two main sections dealing with (a) the pressure and shear stress distribution and (b) the effect of load variation on the patellar tendon bar.

The first section is further subdivided to deal with the various transducers utilised:

- using strain gauge transducers. (PT bar transducer, BEST and Entran transducer).
- using commercial F-Socket™ sensor model 9811.

Whilst the second, deals with

- The correlation of the load on the patellar tendon bar with the pattern of pressure distribution at the stump/socket interface.

Abbreviations for transducer locations and for measurement directions are used in the text and in figure legends, their explanation follows: (see figure 7.1). Each transducer location is attributed an alphanumeric code to indicate its position in the socket. The letters identify the aspect (anterior, posterior, medial and lateral) and the number identifies the row from proximal -1 through 0 (the datum; (centre of patellar tendon bar)) to + 3, the distal row. The distal end being represented by D.E. The distance between each row being 50 mm. (See section 6.2, figures 6.9 and 6.10 for the location sites illustration).

Transducers sites

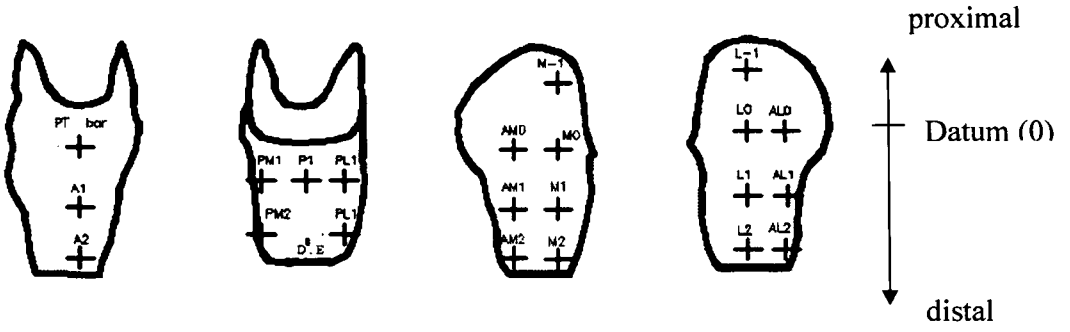

PT = Patellar Tendon bar
A = Anterior
P = Posterior
M = Medial
L = Lateral
D.E = Distal stump end

Examples of abbreviation used follow:

AM0 = Anterior-Medial on the same row as the datum line.
AM1 = Anterior-Medial, 50 mm distal from the datum line.
PM2 = Posterior-Medial, 100 mm distal from the datum line.

Figure 7.1: Example positioning of transducer locations on trans-tibial socket.

7.3 Coordinate system convention

A coordinate system was established, as described below, applied to the sensing surface of the transducer. Stresses reported are those applied to the stump/socket interface i.e. by the socket on the stump. The directions of the coordinate system convention are shown in Figure 7.2. The positive direction of the pressure, P (normal stress) is normal to the skin surface inwardly. Shear stress at any measured point is tangential to the socket surface, and divided into two orthogonal components: tangential (horizontal) and longitudinal (vertical). Longitudinal shear stress is positive if directed proximally by the socket on the stump. Tangential shear stress by the socket on the stump is positive if tending to produce outward rotation. The resultant shear stress is the resultant vector of the two shear stresses components of longitudinal and tangential. The shear angles, θ were calculated from $\theta = \tan^{-1}$ (tangential shear stress / longitudinal shear stress). All pressures and shear stresses values will be indicated in kPa and shear angles in degrees.

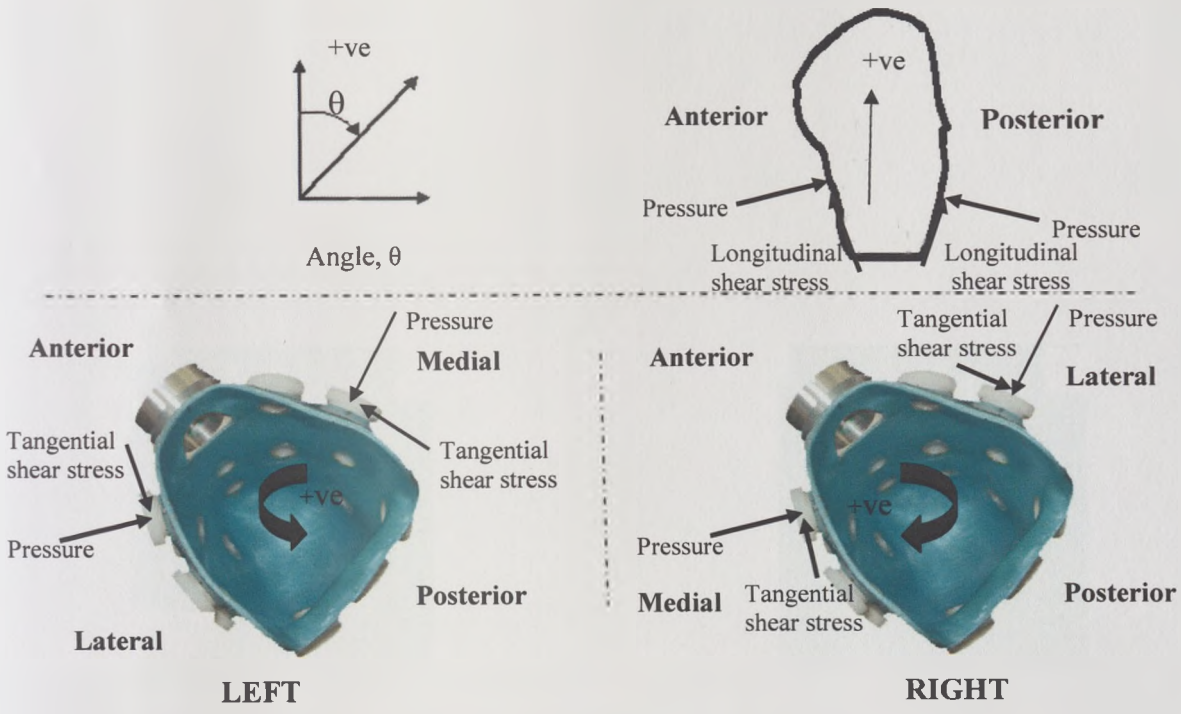

Figure 7.2: Coordinate system convention (+ve) used throughout. (By socket on stump).

7.4 Interface Stresses measurement

Interface pressure and shear stresses were recorded at all measurement sites except the distal end where only normal pressure was recorded for every subject. Table 7.1 (PTB sockets) and 7.2 (Hydrocast sockets) illustrates the measurement sites utilised for all subjects who participated in the experimental trials.

Subject no.	No. of sites	Transducer measurement sites																							
#1	31	PT	A1	A2	A3	AM-1	AM0	AM1	AM2	AM3	M0	M1	M2	M3	PM1	PM2	PM3	P1	P2	PL1	PL2	PL3		L0	
		L1	L2	L3	AL-1	AL0	AL1	AL2	AL3	DE															
#2	19	PT	A1	A2		AM0	AM1	AM2		M0	M1	M2	PM1	P1	PL1	PL2		L0	L1		AL-1	AL0	AL1		DE
#3	15	PT	A1	A2						M0	M1	M2	PM1	P1	PL1	PL2		L0	L1	L2	AL-1				DE
#4	14	PT	A1	A2						M0	M1	M2	PM1	P1	PL1	PL2		L0	L1	L2					DE
#5	15	PT	A1	A2		AM0				M0	M1	M2	PM1	P1	PL1			L0	L1	L2		AL0			DE
#6	18	PT	A1	A2		AM0	AM1	AM2		M0	M1	M2	PM1	P1	PL1			L0	L1			AL0	AL1	AL2	DE
#7	14	PT	A1			AM0	AM1			M0	M1		PM1	P1	PL1			L0	L1			AL0	AL1		DE
#8	13	PT	A1			AM0	AM1			M0	M1		PM1	P1	PL1			L0				AL0	AL1		DE
#9	12	PT	A1	A2		AM0	AM1			M0	M1		PM1		PL1			L0	L1						DE
#10	15	PT	A1	A2		AM0	AM1			M0	M1		PM1	P1	PL1	PL2		L0				AL0	AL1		DE

Table 7.1: Sites from which data were collected for all subject on PTB sockets.

Subject no.	No. of sites	Transducer measurement sites																						
#1	30	PT	A1	A2	A3	AM-1	AM0	AM1	AM2	AM3	M0	M1	M2	M3	PM1	PM2	PM3	P1	P2	PL1	PL2	PL3		
		L1	L2	L3	AL-1	AL0	AL1	AL2	AL3	DE														
#2	19	PT	A1	A2		AM0	AM1	AM2		M0	M1	M2	PM1	P1	PL1	PL2		L0	L1		AL-1	AL0	AL1		DE
#3	14	PT	A1	A2						M0	M1	M2	PM1	P1	PL1	PL2		L0	L1	L2					DE
#4	15	PT	A1	A2		AM0	AM1			M0	M1	M2	PM1	P1	PL1			L0	L1	L2					DE
#5	15	PT	A1	A2		AM0	AM1			M0	M1	M2	PM1	P1	PL1			L0	L1	L2					DE
#6	19	PT	A1	A2		AM0	AM1		M-1	M0	M1	M2	PM1	P1	PL1		L-1	L0	L1			AL0	AL1	AL2	DE
#7	14	PT	A1			AM0	AM1			M0	M1		PM1	P1	PL1			L0	L1			AL0	AL1		DE
#8	14	PT	A1			AM0	AM1			M0	M1		PM1	P1	PL1			L0	L1			AL0	AL1		DE
#9	12	PT	A1	A2		AM0	AM1			M0			PM1	P1	PL1			L0	L1						DE
#10	15	PT	A1	A2	AM-1	AM0	AM1			M0	M1		PM1	P1	PL1			L0	L1			AL0	AL1		DE

Table 7.2: Sites from which data were collected for all subject on hydrocast sockets

7.5 Pressure distribution at the stump socket interface – Standing trials

The purpose of conducting standing trials was to gain insight into standing interface stress patterns and compare them with dynamic interface stress patterns. There were two tests in a standing trial and they were conducted in the order listed in Table 7.3.

Test 1	Test name	Description
1	Single support (SS)	weight borne primarily on the prosthetic leg
2	Double support (DS)	weight borne equally on the prosthetic and sound legs

Table 7.3: Standing trials list of tests.

In the standing trial test, the sampled pressures were averaged during the period of data capture and then further grouped accordingly to the measurement sites and averaged for different trials. At the initial phase of data capture, the data collected were considered unstable; therefore only when the transducer output remained stable were the data collected and analysed. The results obtained from all 10 subjects from all sites measured in the PTB sockets and hydrocast sockets showed loading during single support and double support. These results imply that the sockets were total contact sockets. Figure 7.3 (PTB socket) and Figure 7.4 (Hydrocast socket) show examples of the magnitude of peak pressures at all measured sites from subject #2. Figures 7.5 and 7.6 show the magnitude and directions of the resultant shear stresses from the PTB and hydrocast sockets respectively during single support for subject #2. Resultant shear stresses were calculated from $\sqrt{(lon_{SS})^2 + (\tan_{SS})^2}$; where lon_{SS} = longitudinal shear stress and $\tan_{SS}$ = tangential shear stress. The results of the standing stresses all for the ten subjects of the standing stresses are listed in tables 7.4 and 7.5 (resultant shear stresses) for PTB sockets and tables 7.6 and 7.7 (resultant shear stresses) for hydrocast sockets.

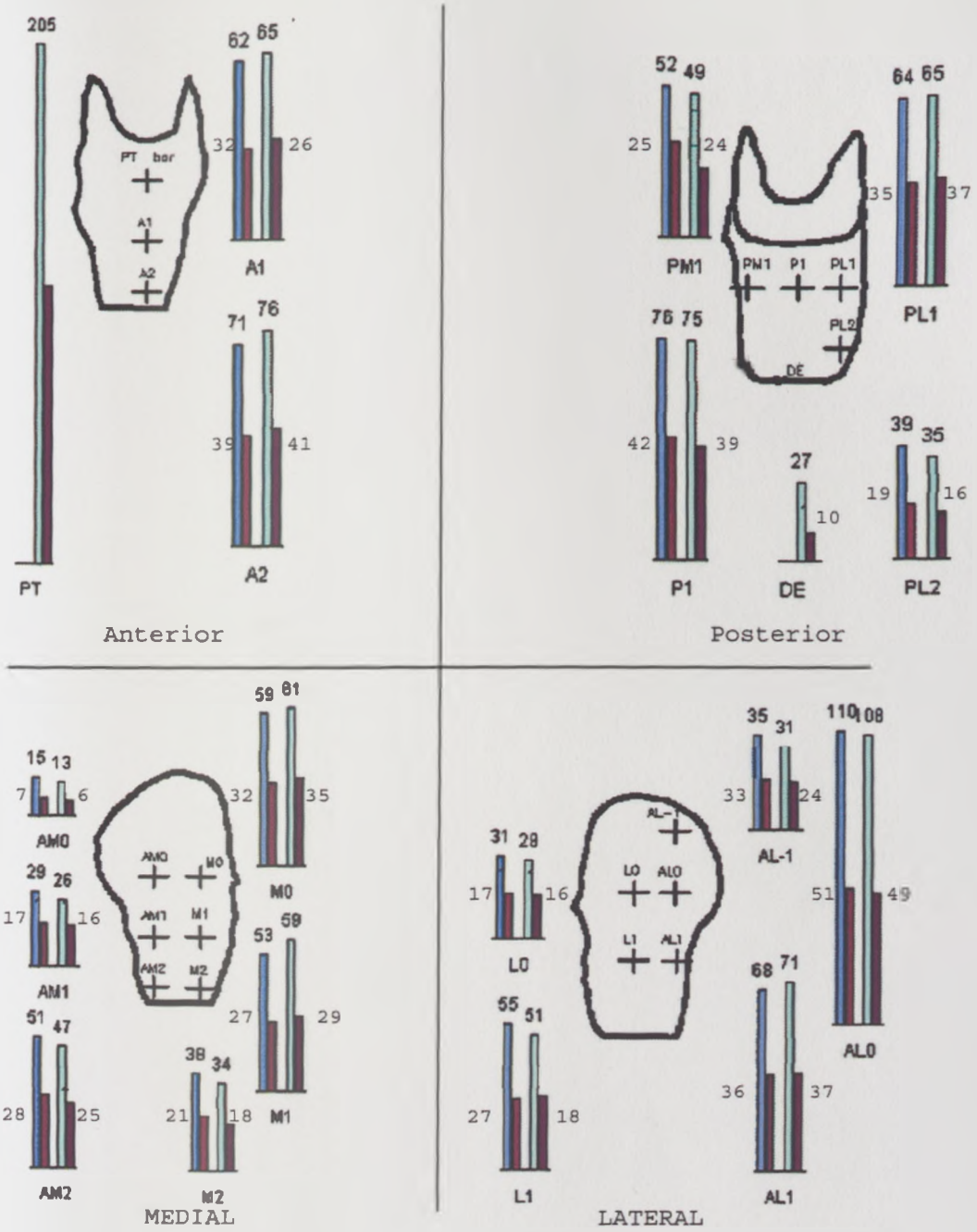

Pressure legend: from left to right for each site: (SS pressure result using Entran transducer, DS pressure result using Entran transducer , SS pressure result using B.E.S.T and DS pressure result using B.E.S.T).

Figure 7.3: The magnitude of single support (SS) and double support (DS) pressures for the PTB socket of subject #2 recorded from the Entran and BEST transducers. Note: No Entran transducer was used at the patellar tendon (PT) bar site. The (PT) bar pressure and distal end (DE) pressure were obtained using the PT and electrohydraulic transducers respectively. The bar diagrams of pressure are all to the same scale. All units in kPa.

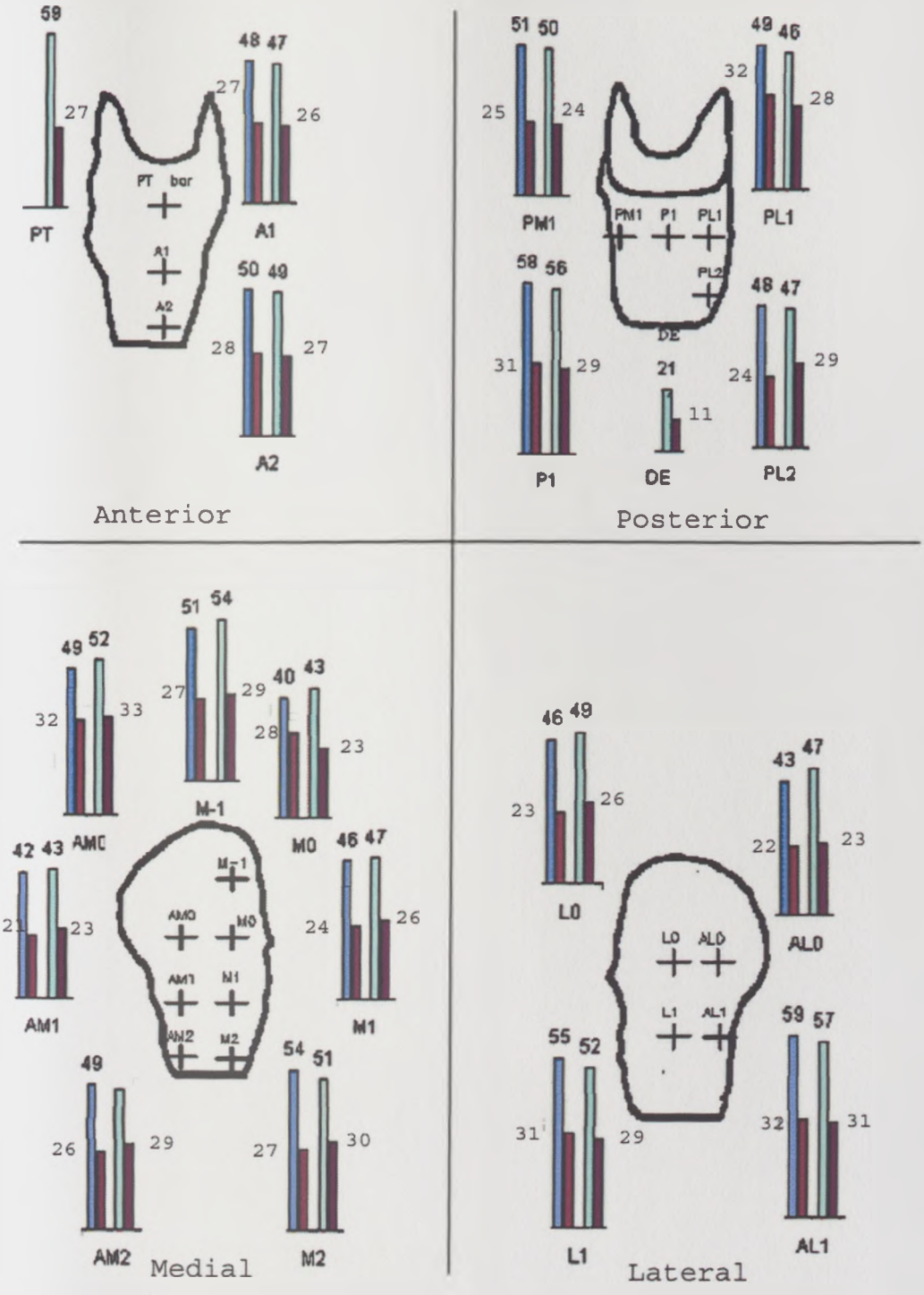

Pressure legend: from left to right for each site: (SS pressure result using Entran transducer, DS pressure result using Entran transducer , SS pressure result using B.E.S.T and DS pressure result using B.E.S.T).

Figure 7.4: The magnitude of single support (SS) and double support (DS) pressures for the Hydrocast socket of subject #2 recorded from the Entran and BEST transducers. Note: No Entran transducer was used at the patellar tendon (PT) bar site. The (PT) bar pressure and distal end (DE) pressure were obtained using the PT and electrohydraulic transducers respectively. The bar diagrams of pressure are all to the same scale. All units in kPa.

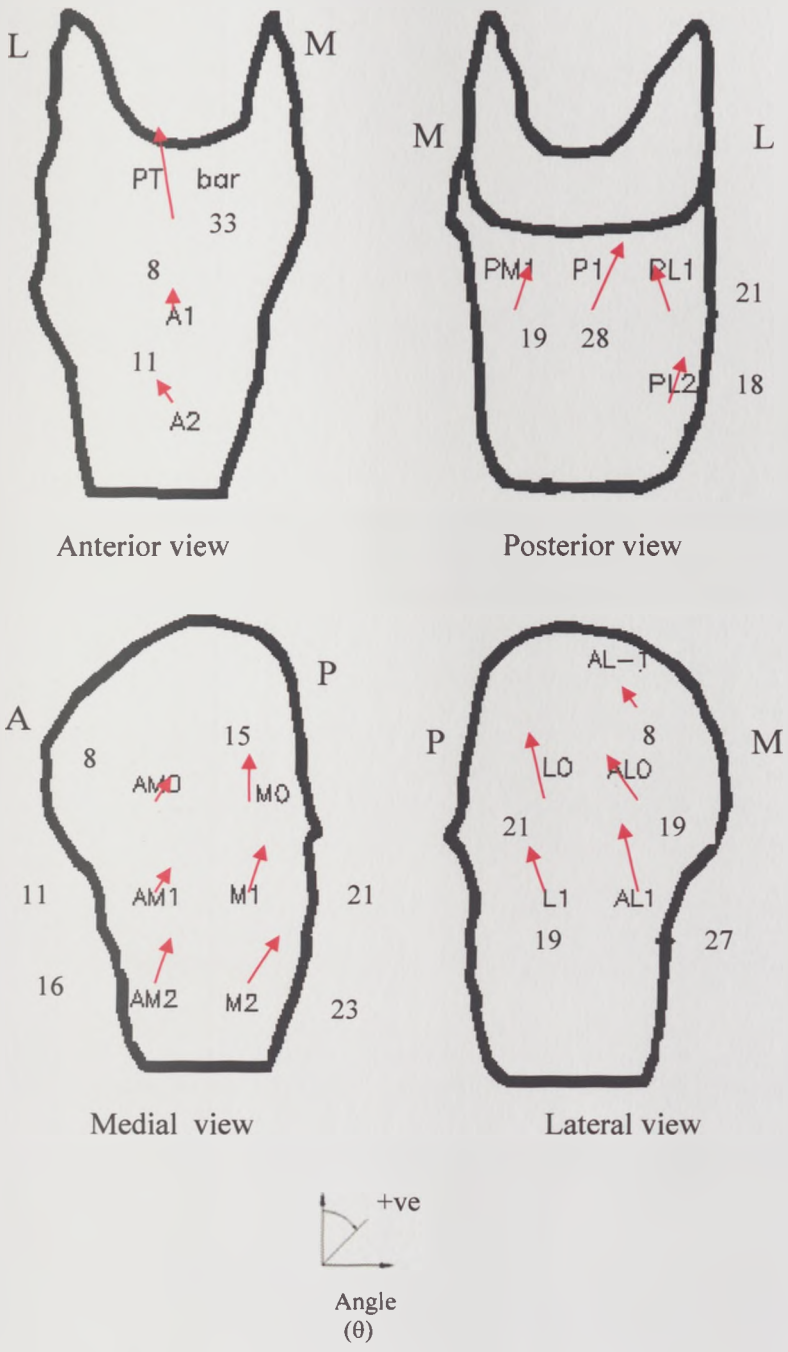

Figure 7.5: The magnitudes and directions of the resultant shear stresses by the socket on the stump during single support for the PTB socket of subject #2. The shear angles, θ were calculated from $\theta = \tan^{-1}(\tan_{ss}/lon_{ss})$. Note : A= anterior wall, P = posterior wall, M = medial wall and L = lateral wall. All units in kPa. Socket sketch and dimensions are not to scale.

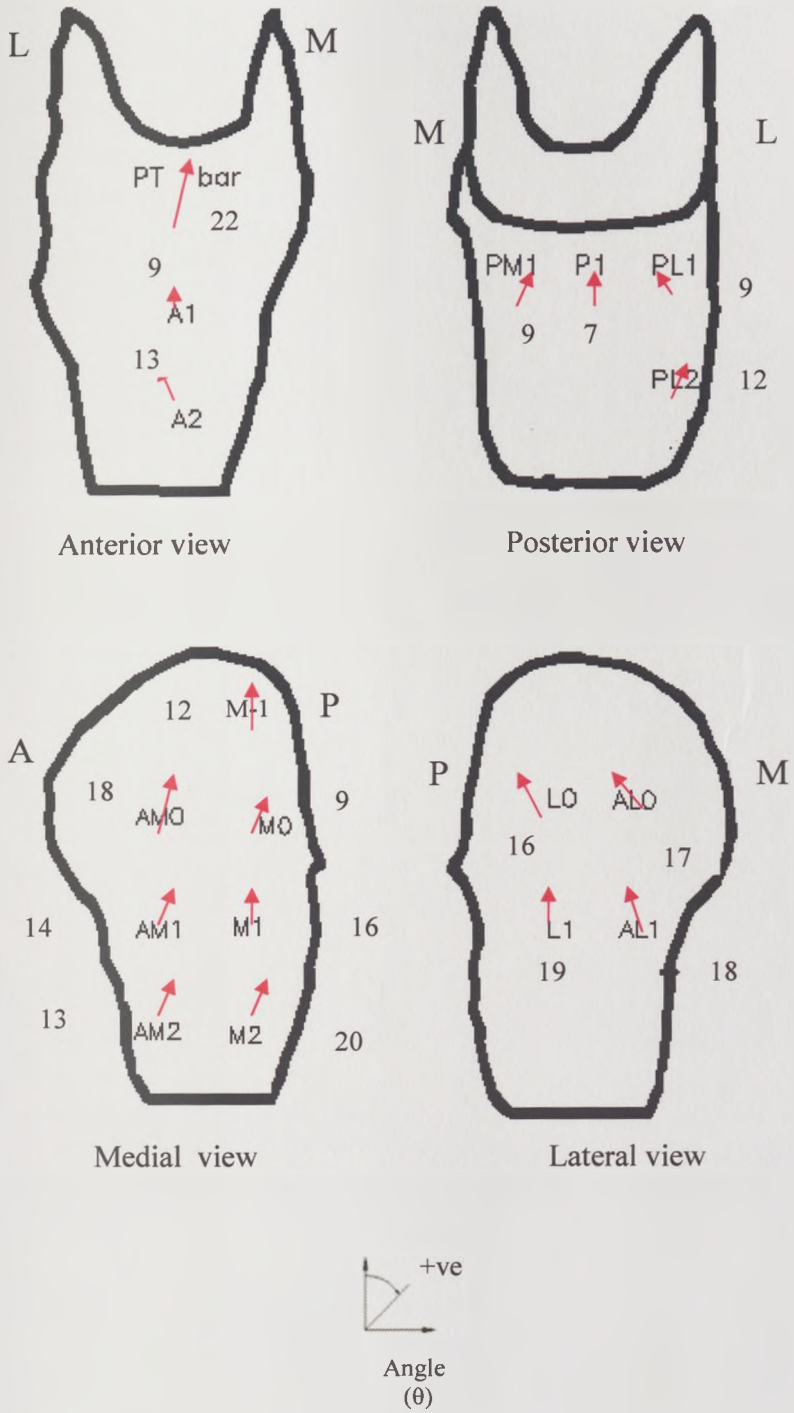

Figure 7.6: The magnitudes and directions of the resultant shear stresses by the socket on the stump during single support for the hydrocast socket of subject #2. The shear angles, θ were calculated from $\theta = \tan^{-1}(\tan_{ss} / lon_{ss})$. Note : A= anterior wall, P = posterior wall, M = medial wall and L = lateral wall. All units in kPa. Socket sketch and dimensions are not to scale.

		Transducer sites (Pressures in kPa)																							
		Trans. Type	**PT**	**A1**	**A2**	**A3**	**AM-1**	**AM0**	**AM1**	**AM2**	**AM3**	**M0**	**M1**	**M2**	**M3**	**PM1**	**PM2**	**PM3**	**P1**	**P2**	**PL1**	**PL2**	**PL3**	**L-1**	**L0**	
#1	SS Press.	Entran		46	71	61	10	6	41	28	12	61	65	29	18	61	43	17	71	43	54	30	38		29	
	DS Press.	Entran	N/A	23	33	41	6	4	29	15	8	31	32	16	10	32	21	10	35	26	32	19	14	N/A	11	
	SS Press.	B.E.S.T	180	44	69	64	12	4	45	22	8	66	62	25	13	56	40	12	75	40	52	32	37		25	
	DS Press.	B.E.S.T	85	21	37	39	9	3	27	13	5	34	30	13	8	29	22	7	39	22	29	17	18	N/A	13	

			L1	**L2**	**L3**	**AL-1**	**AL0**	**AL1**	**AL2**	**AL3**	**DE**
	SS Press.	Entran	58	44	47	6	33	61	88	20	
	DS Press.	Entran	24	23	24	4	14	33	27	8	N/A
	SS Press.	B.E.S.T	56	42	49	4	30	66	92	18	16
	DS Press.	B.E.S.T	27	20	22	3	16	39	49	10	9

N/A

			PT	**A1**	**A2**	**AM-1**	**AM0**	**AM1**	**AM2**	**M-1**	**M0**	**M1**	**M2**	**PM1**	**P1**	**PL1**	**PL2**	**L-1**	**L0**	**L1**	**L2**	**AL-1**	**AL0**	**AL1**	**AL2**	**DE**
#2	SS Press.	Entran		62	71		15	29	51		59	53	38	52	76	64	39		37	55		35	110	68		
	DS Press.	Entran	N/A	32	39	N/A	7	17	28	N/A	32	27	21	33	42	35	19	N/A	17	27	N/A	19	51	36	N/A	
	SS Press.	B.E.S.T	205	65	76		13	26	47		61	59	34	49	75	65	35		29	51		31	108	71		27
	DS Press.	B.E.S.T	110	35	41	N/A	6	6	25	N/A	34	29	18	24	39	37	16	N/A	16	28	N/A	18	49	37	N/A	10
#3	SS Press.	Entran		39	52						49	66	32	59	54	49	51		25	61	64	69				
	DS Press.	Entran	N/A	19	24			N/A			30	36	15	36	27	35	24	N/A	11	41	33	37		N/A		
	SS Press.	B.E.S.T	200	38	50						50	70	30	62	51	52	53		21	65	69	75				10
	DS Press.	B.E.S.T	95	18	23			N/A			28	38	17	38	29	30	29	N/A	13	39	34	39		N/A		7

Table 7.4 Pressures during standing in single support (SS) and double support (DS) for all ten subjects on PTB sockets. The patellar tendon (PT) bar pressure and the distal end (DE) pressure were measured using PT transducer and electrohydraulic transducer respectively. N/A = Not available. Peak pressure during SS.

Continued on page 134 and page 135

			PT	A1	A2	AM-1	AM0	AM1	AM2	M-1	M0	M1	M2	PM1	P1	PL1	PL2	L-1	L0	L1	L2	AL-1	AL0	AL1	AL2	DE
#4	SS Press.	Entran		52	64						59	64	43	51	67	52	30		19	47	66					
	DS Press.	Entran		19	29			N/A			34	30	21	20	29	34	16	N/A	11	24	35			N/A		
	SS Press.	B.E.S.T	185	49	68						62	68	40	57	62	56	32		21	49	68					25
	DS Press.	B.E.S.T	86	22	34			N/A			38	34	26	24	32	37	18	N/A	13	22	37			N/A		10
#5	SS Press.	Entran		51	53		19				51	64	31	56	49	47			21	51	58		32			
	DS Press.	Entran	N/A	29	33	N/A	17	N/A			29	21	20	22	20	29	N/A		16	31	27	N/A	20	N/A		
	SS Press.	B.E.S.T	175	49	56		21				49	62	34	54	51	49			23	54	56		30			11
	DS Press.	B.E.S.T	76	28	32	N/A	13	N/A			27	23	18	27	23	27	N/A		13	29	26	N/A	18	N/A		7
#6	SS Press.	Entran		51	63		13	37	33		49	73	30	75	64	59			41	57			34	92	93	
	DS Press.	Entran	N/A	29	32	N/A	10	20	18	N/A	24	41	16	40	33	35	N/A		21	27	N/A		18	46	46	N/A
	SS Press.	B.E.S.T	190	49	65		12	38	37		51	79	35	79	61	62			39	55			37	89	91	23
	DS Press.	B.E.S.T	85	26	30	N/A	7	18	20	N/A	27	43	18	43	35	37	N/A		23	29	N/A		20	48	51	10
#7	SS Press.	Entran		62			33	47			54	73		62	74	46			39	64			39	89		
	DS Press.	Entran	N/A	35	N/A		22	24	N/A		25	41	N/A	31	46	31	N/A		27	42	N/A		20	43	N/A	
	SS Press.	B.E.S.T	205	60			30	45			59	75		60	81	52			42	73			41	91		25
	DS Press.	B.E.S.T	75	33	N/A		20	26	N/A		27	39	N/A	29	43	29	N/A		24	39	N/A		25	47	N/A	13
#8	SS Press.	Entran		71			33	54			59	91		66	69	51			33				24	92		
	DS Press.	Entran	N/A	31	N/A		26	37	N/A		35	48	N/A	30	39	21	N/A		20	N/A			18	56	N/A	
	SS Press.	B.E.S.T	208	68			35	59			64	94		64	74	53			37				27	97		24
	DS Press.	B.E.S.T	102	33	N/A		24	35	N/A		34	46		33	34	27	N/A		18	N/A			15	49	N/A	10

.....contd....Table 7.4 Pressures during standing in single support (SS) and double support (DS) or all ten subjects on PTB sockets. The patellar tendon (PT) bar pressure and the distal end (DE) pressure were measured using PT transducer and electrohydraulic transducer respectively. N/A = Not available. Peak pressure during SS.

Continued from page 133 and on page 135

			PT	A1	A2	AM-1	AM0	AM1	AM2	M-1	M0	M1	M2	PM1	P1	PL1	PL2	L-1	L0	L1	L2	AL-1	AL0	AL1	AL2	DE
#9	SS Press.	Entran		67	59		22	31			72	93		56		51			30	57						
	DS Press.	Entran	N/A	30	36	N/A	15	20	N/A		37	52	N/A	38	N/A	31	N/A		32	39		N/A				
	SS Press.	B.E.S.T	195	65	62		20	35			69	91		62		55			33	62						15
	DS Press.	B.E.S.T	95	33	34	N/A	11	18	N/A		33	47	N/A	33	N/A	28	N/A		29	37		N/A				9
#10	SS Press.	Entran		52	76		25	44			51	80		52	52	70	21		51				30	88		
	DS Press.	Entran	N/A	24	36	N/A	15	18	N/A		22	43	N/A	31	33	41	18	N/A	22		N/A		26	51	N/A	
	SS Press.	B.E.S.T	199	50	74		20	48			55	86		55	57	75	25		57				40	92		20
	DS Press.	B.E.S.T	102	26	38	N/A	12	16	N/A		29	46	N/A	29	32	38	16	N/A	26		N/A		23	49	N/A	13

…..contd….Table 7.4 Pressures during standing in single support (SS) and double support (DS) or all ten subjects on PTB sockets. The patellar tendon (PT) bar pressure and the distal end (DE) pressure were measured using PT transducer and electrohydraulic transducer respectively. N/A = Not available. Peak pressure during SS.

Continued from page 133 and page 134

		Transducer sites (Resultant shear stresses in kPa)																							
Subject no.		Transducer type	PT	A1	A2	A3	AM-1	AM0	AM1	AM2	AM3	M0	M1	M2	M3	PM1	PM2	PM3	P1	P2	PL1	PL2	PL3	L-1	L0
#1	SS Resultant.	B.E.S.T	47	25	21	24	23	19	29	20	19	28	27	21	19	22	18	27	20	18	24	17	18		17
	DS Resultant.	B.E.S.T	21	12	13	15	14	9	14	13	11	13	14	10	9	10	9	14	12	11	10	9	7		9
			L1	L2	L3	AL-1	AL0	AL1	AL2	AL3															
	SS Resultant.	B.E.S.T	19	20	18	22	17	16	27	28															
	DS Resultant.	B.E.S.T	9	11	10	12	9	7	12	16															

			PT	A1	A2	AM-1	AM0	AM1	AM2	M-1	M0	M1	M2	PM1	P1	PL1	PL2	L-1	L0	L1	L2	AL-1	AL0	AL1	AL2
#2	SS Resultant.	B.E.S.T	33	8	11		8	11	16		15	21	23	19	28	21	18		21	19		8	19	27	
	DS Resultant.	B.E.S.T	14	5	6	N/A	5	6	9	N/A	8	10	11	9	17	13	12	N/A	13	11	N/A	5	10	16	N/A
#3	SS Resultant.	B.E.S.T	49	21	22						24	31	30	27	22	21	20		30	24	30	20			
	DS Resultant.	B.E.S.T	23	11	13			N/A			14	18	17	13	12	13	12	N/A	16	14	16	12		N/A	
#4	SS Resultant.	B.E.S.T	30	20	21						15	17	20	15	17	12	21		19	21	20				
	DS Resultant.	B.E.S.T	16	12	11			N/A			10	9	13	11	10	7	13	N/A	9	13	12			N/A	
#5	SS Resultant.	B.E.S.T	19	12	13		14				16	17	18	16	21	20			17	16	20		9		
	DS Resultant.	B.E.S.T	11	7	6	N/A	8		N/A		9	10	7	8	11	12	N/A		9	7	12	N/A	4	N/A	
#6	SS Resultant.	B.E.S.T	24	22	23		21	21	16		24	23	21	18	10	10			11	17			10	16	21
	DS Resultant.	B.E.S.T	13	14	11	N/A	11	10	12	N/A	10	11	10	11	6	4	N/A		6	9	N/A		6	8	11
#7	SS Resultant.	B.E.S.T	24	10			17	15			14	22		23	27	20			14	16			12	10	
	DS Resultant.	B.E.S.T	13	6	N/A		8	7	N/A		8	11	N/A	14	16	11	N/A		8	10	N/A		8	4	N/A
#8	SS Resultant.	B.E.S.T	28	14			20	11			21	17		16	13	21			10				15	20	
	DS Resultant.	B.E.S.T	16	9	N/A		11	8	N/A		12	9	N/A	7	6	12	N/A		6	N/A			8	13	N/A
#9	SS Resultant.	B.E.S.T	30	19	17		15	16			14	17		16		18			17	16					
	DS Resultant.	B.E.S.T	16	11	9	N/A	8	9	N/A		8	6	N/A	10	N/A	11	N/A		9	7		N/A			
#10	SS Resultant.	B.E.S.T	27	14	13		17	16			20	22		23	23	22	19		20				21	18	
	DS Resultant.	B.E.S.T	14	9	8	N/A	10	9	N/A		11	13	N/A	14	15	10	9	N/A	11	N/A			10	12	

Table 7.5 Resultant shear stresses during standing in single support (SS) and double support (DS) for or all ten subjects on PTB sockets. Note : The patellar tendon (PT) bar pressure was measured using PT transducer. N/A = Not available

			Transducer sites (Pressure in kPa)																						
		Trans. Type	**PT**	**A1**	**A2**	**A3**	**AM-1**	**AM0**	**AM1**	**AM2**	**AM3**	**M0**	**M1**	**M2**	**M3**	**PM1**	**PM2**	**PM3**	**P1**	**P2**	**PL1**	**PL2**	**PL3**	**L-1**	**L0**
#1	**SS Press.**	Entran		55	54	52	47	44	43	49	51	42	42	44	51	46	47	43	41	38	59	51	48		
	DS Press.	Entran	N/A	26	24	22	25	24	19	26	27	23	21	26	27	19	24	19	26	24	32	27	28	N/A	
	SS Press.	B.E.S.T	55	51	53	49	46	45	44	51	49	43	44	47	55	40	49	44	42	39	62	49	47		
	DS Press.	B.E.S.T	24	25	27	25	26	24	22	27	26	22	23	27	28	21	26	20	21	23	30	27	26	N/A	
			L1	**L2**	**L3**	**AL-1**	**AL0**	**AL1**	**AL2**	**AL3**	**DE**														
	SS Press.	Entran	57	52	49	52	49	62	55	45															
	DS Press.	Entran	23	26	27	26	24	26	27	23															
	SS Press.	B.E.S.T	56	49	47	50	50	61	59	47	30														
	DS Press.	B.E.S.T	24	25	24	27	23	30	28	22	17	N/A													

			PT	**A1**	**A2**	**AM-1**	**AM0**	**AM1**	**AM2**	**M-1**	**M0**	**M1**	**M2**	**PM1**	**P1**	**PL1**	**PL2**	**L-1**	**L0**	**L1**	**L2**	**AL-1**	**AL0**	**AL1**	**AL2**	**DE**
#2	**SS Press.**	Entran		48	50		49	42	49	51	40	46	54	51	58	49	48		46	55			43	59		
	DS Press.	Entran	N/A	27	28	N/A	32	21	26	27	28	24	27	25	31	32	24	N/A	23	31	N/A		22	32	N/A	
	SS Press.	B.E.S.T	59	47	49		52	43	47	54	43	47	51	50	56	46	47		49	52			47	57		21
	DS Press.	B.E.S.T	27	26	27	N/A	33	23	29	29	23	26	30	24	29	28	29	N/A	26	29	N/A		23	31	N/A	11
#3	**SS Press.**	Entran		53	47						44	51	53	47	42	57	44		43	46	42					
	DS Press.	Entran	N/A	22	20	N/A					19	24	31	24	25	30	27	N/A	22	24	22	N/A				
	SS Press.	B.E.S.T	65	51	49						46	42	51	42	44	59	43		42	44	43					27
	DS Press.	B.E.S.T	32	19	18	N/A					22	21	29	21	27	28	26	N/A	24	21	20	N/A				19

Table 7.6 Pressures during standing in single support (SS) and double support (DS) or all ten subjects on hydrocast sockets. The patellar tendon (PT) bar pressure and the distal end (DE) pressure were measured using PT transducer and electrohydraulic transducer respectively. N/A = Not available. Peak pressure during SS.

Continued on page 138 and page 139

			PT	A1	A2	AM-1	AM0	AM1	AM2	M-1	M0	M1	M2	PM1	P1	PL1	PL2	L-1	L0	L1	L2	AL-1	AL0	AL1	AL2	DE
#4	**SS Press.**	Entran		43	46		47	41			39	48	49	47	41	49			51	44	43					
	DS Press.	Entran	N/A	18	21	N/A	22	19	N/A		18	14	24	26	21	28	N/A		27	21	28	N/A				
	SS Press.	B.E.S.T	50	45	44		46	45			41	47	51	50	43	51			53	49	42					34
	DS Press.	B.E.S.T	24	23	20	N/A	21	22	N/A		19	28	23	24	21	27	N/A		26	27	29	N/A				20
#5	**SS Press.**	Entran		42	43		44	41			47	39	38	44	45	47			44	43	45					
	DS Press.	Entran	N/A	18	19	N/A	22	17	N/A		24	15	23	21	27	23	N/A		24	21	22	N/A				
	SS Press.	B.E.S.T	47	48	44		43	40			49	42	41	46	58	55			52	59	55					27
	DS Press.	B.E.S.T	23	20	21	N/A	24	18	N/A		24	18	20	19	22	24	N/A		27	22	24	N/A				23
#6	**SS Press.**	Entran		50	49		44	43		47	49	50	39	45	49	56		49	51	56		48	49	51		
	DS Press.	Entran	N/A	22	24	N/A	19	22	N/A	26	27	24	19	22	27	25	N/A	26	21	20	N/A	21	25	20	N/A	
	SS Press.	B.E.S.T	53	54	52		46	51		51	55	53	41	50	55	59		51	54	53		50	51	48	35	
	DS Press.	B.E.S.T	19	25	24	N/A	21	23	N/A	24	28	25	21	20	25	24	N/A	25	20	21	N/A	23	24	22	17	
#7	**SS Press.**	Entran		54			55	61			53	59		61	49	54			55	47		57	62			
	DS Press.	Entran	N/A	28	N/A		24	30	N/A		27	24	N/A	30	27	28	N/A		24	22	N/A	20	30	N/A		
	SS Press.	B.E.S.T	65	56			57	59			55	58		59	51	58			56	49		59	60			35
	DS Press.	B.E.S.T	29	27	N/A		26	28	N/A		24	25	N/A	29	24	27	N/A		25	20	N/A	21	32	N/A		16
#8	**SS Press.**	Entran		47			46	43			37	39		45	41	52			47	44		47	46			
	DS Press.	Entran	N/A	20	N/A		28	28	N/A		24	26	N/A	24	19	25	N/A		27	26	N/A	20	21	N/A		
	SS Press.	B.E.S.T	60	49			45	44			39	41		47	42	49			45	46		49	45			37
	DS Press.	B.E.S.T	17	13	N/A		17	14	N/A		16	15	N/A	13	11	13	N/A		17	14	N/A	11	15	N/A		17

....contd.....Table 7.6 Pressures during standing in single support (SS) and double support (DS) or all ten subjects on hydrocast sockets. The patellar tendon (PT) bar pressure and the distal end (DE) pressure were measured using PT transducer and electrohydraulic transducer respectively. N/A = Not available. Peak pressure during SS.

Continued from page 137 and on page 139

			PT	A1	A2	AM-1	AM0	AM1	AM2	M-1	M0	M1	M2	PM1	P1	PL1	PL2	L-1	L0	L1	L2	AL-1	AL0	AL1	AL2	DE
#9	SS Press.	Entran		45	41		49	42			47			43	49	44			48	53						
	DS Press.	Entran	N/A	23	21	N/A	25	22	N/A		23	N/A		24	25	22	N/A		23	26			N/A			
	SS Press.	B.E.S.T	54	47	45		51	43			49			45	51	46			50	56						29
	DS Press.	B.E.S.T	26	25	24	N/A	26	24	N/A		27	N/A		26	26	24	N/A		25	27			N/A			16
#10	SS Press.	Entran		48	50	44	43				41	46		44	49	44			47	49			47	39		
	DS Press.	Entran	N/A	22	26	20	21	N/A			20	27	N/A	22	26	20	N/A		27	26	N/A		25	19	N/A	
	SS Press.	B.E.S.T	49	47	49	46	44				43	47		46	50	47			48	50			45	41		27
	DS Press.	B.E.S.T	23	24	24	21	23	N/A			24	26	N/A	21	24	22	N/A		26	24	N/A		27	21	N/A	14

...contd....Table 7.6 Pressures during standing in single support (SS) and double support (DS) for all ten subjects on hydrocast sockets. The patellar tendon (PT) bar pressure and the distal end (DE) pressure were measured using PT transducer and electrohydraulic transducer respectively. N/A = Not available. Peak pressure during SS.

Continued from page 137 and page 138

Subject no.		Transducer type	Transducer sites (Resultant shear stresses in kPa)																						
			PT	**A1**	**A2**	**A3**	**AM-1**	**AM0**	**AM1**	**AM2**	**AM3**	**M0**	**M1**	**M2**	**M3**	**PM1**	**PM2**	**PM3**	**P1**	**P2**	**PL1**	**PL2**	**PL3**	**L-1**	**L0**
#1	SS Resultant.	B.E.S.T	35	30	31	28	26	24	25	23	20	24	23	21	19	20	27	26	30	31	28	29	27		
	DS Resultant.	B.E.S.T	18	15	14	17	21	13	15	11	9	10	11	10	9	11	17	16	10	16	14	18	16	N/A	
			L1	**L2**	**L3**	**AL-1**	**AL0**	**AL1**	**AL2**	**AL3**															
	SS Resultant.	B.E.S.T	21	20	20	19	28	24	26	25															
	DS Resultant.	B.E.S.T	10	11	11	17	15	14	17	16	N/A														
			PT	**A1**	**A2**	**AM-1**	**AM0**	**AM1**	**AM2**	**M-1**	**M0**	**M1**	**M2**	**PM1**	**P1**	**PL1**	**PL2**	**L-1**	**L0**	**L1**	**L2**	**AL-1**	**AL0**	**AL1**	**AL2**
#2	SS Resultant.	B.E.S.T	22	9	13		18	14	13	12	9	16	20	9	7	9	12		16	19			17	18	
	DS Resultant.	B.E.S.T	13	4	6	N/A	9	9	11	9	6	8	9	6	4	5	6	N/A	6	8	N/A		8	7	N/A
#3	SS Resultant.	B.E.S.T	22	18	18						17	16	22	19	16	21	22		22	25	26				
	DS Resultant.	B.E.S.T	10	12	10		N/A				9	8	12	9	10	9	15	N/A	16	15	13	N/A			
#4	SS Resultant.	B.E.S.T	31	26	21		30	33			34	33	32	26	21	29			34	29	26				
	DS Resultant.	B.E.S.T	20	13	8	N/A	15	17	N/A		18	15	22	21	11	15	N/A		19	20	23	N/A			
#5	SS Resultant.	B.E.S.T	18	17	19		21	25			21	13	18	14	24	24			20	19	18				
	DS Resultant.	B.E.S.T	14	8	16	N/A	10	11	N/A		10	10	12	13	9	12	N/A		10	15	12	N/A			
#6	SS Resultant.	B.E.S.T	31	28	27		28	29		30	28	24	19	25	27	25		24	26	21			20	25	23
	DS Resultant.	B.E.S.T	16	19	21	N/A	18	16	N/A	17	17	16	12	16	15	16	N/A	14	15	12	N/A		11	17	15
#7	SS Resultant.	B.E.S.T	31	27			30	33			27	26		24	21	19			28	24			25	24	
	DS Resultant.	B.E.S.T	15	15	N/A		16	17	N/A		13	14	N/A	11	15	17	N/A		15	11	N/A		17	13	N/A
#8	SS Resultant.	B.E.S.T	37	31			24	24			19	24		27	30	27			26	21			25	27	
	DS Resultant.	B.E.S.T	16	17	N/A		16	17	N/A		10	13	N/A	15	16	16	N/A		14	12	N/A		10	14	N/A
#9	SS Resultant.	B.E.S.T	25	21	23		21	17			16			20	21	26			27	24					
	DS Resultant.	B.E.S.T	12	11	10	N/A	11	8	N/A		7	N/A		9	10	11	N/A		10	9	N/A				
#10	SS Resultant.	B.E.S.T	24	21	20	18	16				20	16		17	21	19			17	21			19	17	
	DS Resultant.	B.E.S.T	13	11	12	11	10	N/A			11	9	N/A	10	11	11	N/A		10	11	N/A		10	11	N/A

Table 7.7 Resultant shear stresses during standing in single support (SS) and double support (DS) for all ten subjects on hydrocast sockets. Note : The patellar tendon (PT) bar pressure was measured using PT transducer. N/A = Not available

Generally, the results for the double support showed the same pattern as the single support results. The values of the pressures on the PTB socket are much higher compared to the hydrocast socket. The highest was found at patellar tendon bar of the PTB socket, 208 kPa for subject # 8 for single support and 102 kPa for the double support. Excluding the pressures at the patellar tendon bar in the PTB socket, the highest peak pressures among 10 subjects was found at site AL1, subject no. 8, 97 kPa for single support and 49 kPa with double support (table 7.4 and table 7.8), whilst for the hydrocast socket the peak pressures were up to 65 kPa for single support and 32 kPa for double support for subject no.3 (table 7.5 and table 7.8). At most points the peak pressures and the peak shear stresses with single support were larger than during double support, with the exception of the PTB socket for subjects # 1 and # 6 at the AM0 and AL-1(only subject no.1) where peak pressures at double support were nearly equivalent to single support. (i.e. subject # 1, AM0 and AL-1, SS = 4 kPa and DS = 3 kPa; subject # 6, AM0, SS = 13 kPa and DS = 10 kPa. (table 7.4). A possible explanation is that the pre-stresses existed at this point to assure the suspension function and the pressures were maintained with the tilt of the body or as the limb moved down into the socket. The other results are as expected whereby almost all the stresses were approximately half the value of the single support stresses due to the load being equally distributed between both legs. The results for the PTB and hydrocast sockets show a similar trend i.e. stresses during double support were approximately half of the single support values.

Socket type	Subject no.	Peak pressure (kPa)	Location on socket
PTB**	1	92	AL2
	2	95	AL0
	3	75	AL-1
	4	68	A2, M1, L2
	5	64	M1
	6	93	AL2
	7	91	AL1
	8	97	AL1
	9	93	M1
	10	92	AL1
Hydrocast	1	62	PL1
	2	59	AL1
	3	65	PT
	4	53	L0
	5	59	L1
	6	59	PL1
	7	65	PT
	8	60	PT
	9	56	L1
	10	50	L1

Table 7.8: Summary of peak pressures in single support (SS) for PTB and hydrocast sockets. Note : ** Peak pressures at Patellar tendon in PTB socket is not included since the patellar tendon bar in PTB socket is known as a high pressure point.

Inter subject comparison of these tests is highly dependent on the subjects' shape, biomechanical properties and physiology of the stump. However comparing ten subjects using PTB and hydrocast sockets, it was noted during standing trial tests that the pressure values around the hydrocast were about the same unlike the PTB which showed greater variation in magnitude.

7.6 Pressure distribution correlation between PT bar and stump socket interface

This section presents the results of the investigation into the effect varying the load on the patellar tendon bar has on the pattern of pressure distribution at the stump/socket interface.

The results presented in this section are focused on the correlation of the pressure at the patellar tendon bar with the other measurement sites in the PTB socket and Hydrocast socket. All average peak pressures and standard deviations were in kPa units. Average peak pressures mean the average value of the peak pressures from different steps.

7.6.1 Correlation in the socket

The range of average peak pressures recorded at the patellar tendon bar with the bar in the neutral position, for all subjects, during walking was from 203kPa to 230kPa for PTB sockets and the range of peak pressure at the patellar tendon bar recorded for the same situation in hydrocast sockets was 57 kPa to 80 kPa. (Figure 7.8 to Figure 7.17). Percentage increase /decrease of pressure, for each 2 mm bar translation, at the patellar tendon for subject #1 to #10 with the PTB and hydrocast sockets are also shown in figures 7.18, 7.19, table 7.9 and table 7.10.

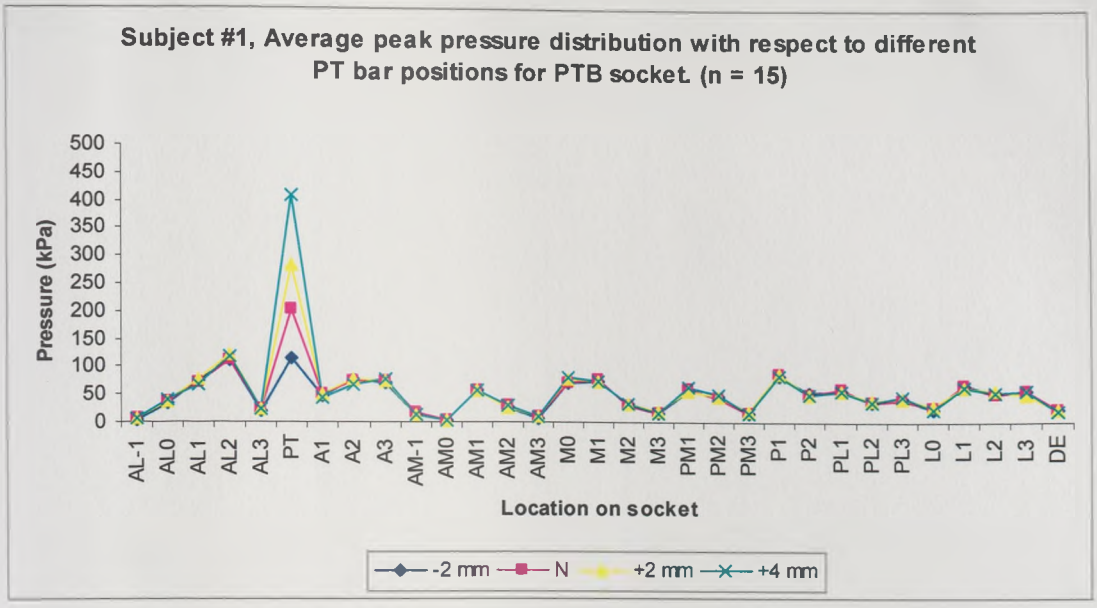

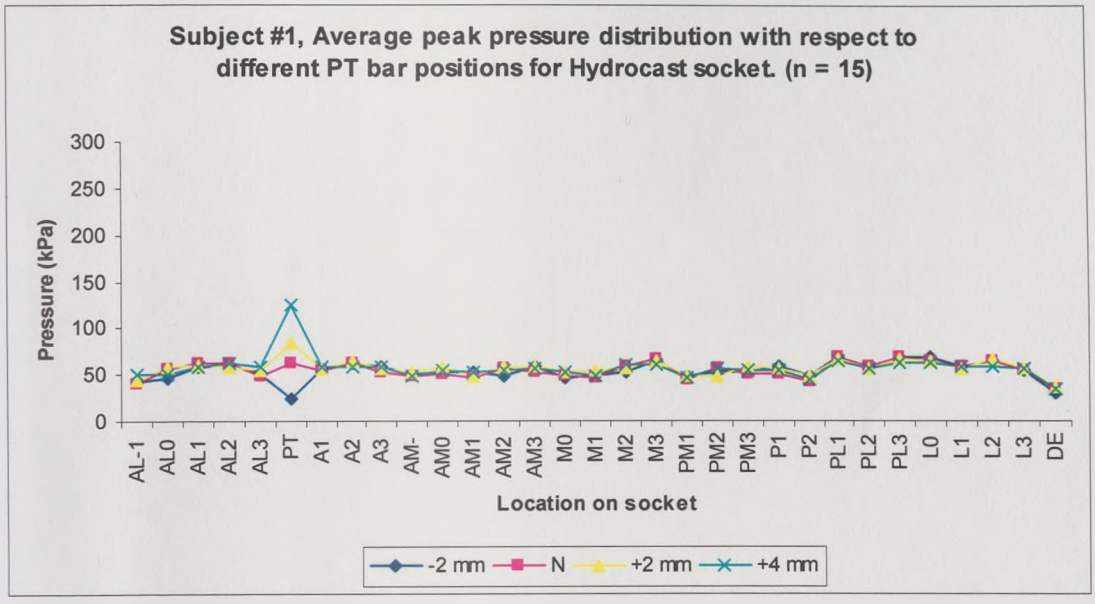

Figure 7.8: Average peak pressures for PTB and Hydrocast sockets on subject #1. Variation in pattern on the other areas of the socket when the patellar tendon bar was compressed (+) or relieved (-). Note : n = numbers of tests represented in each peak pressure and the insert shows the change in PT bar location from the neutral position (N).

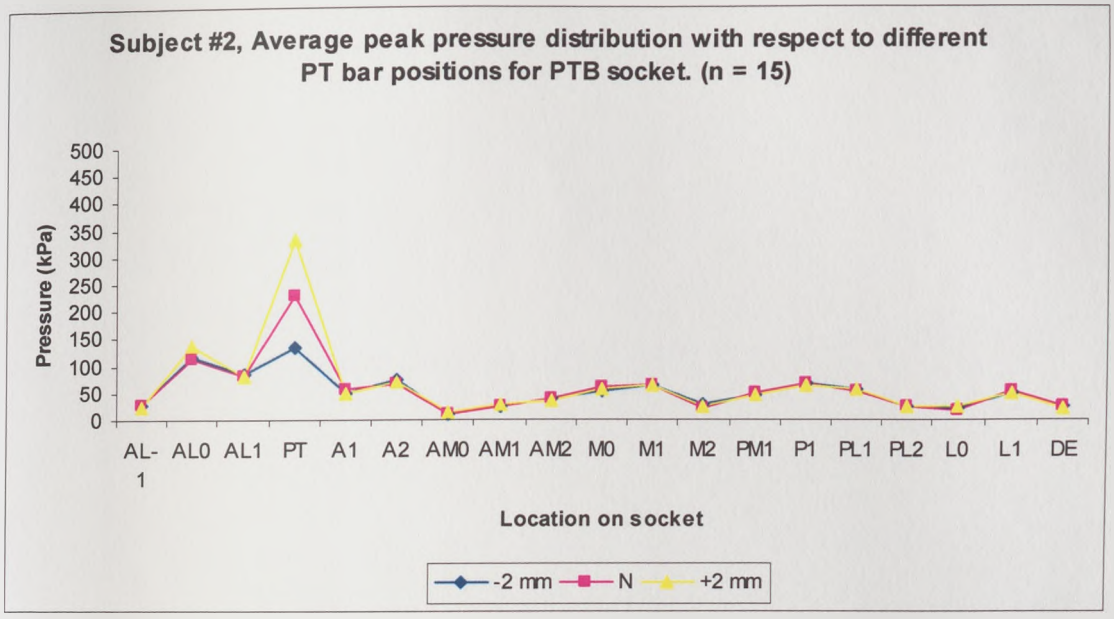

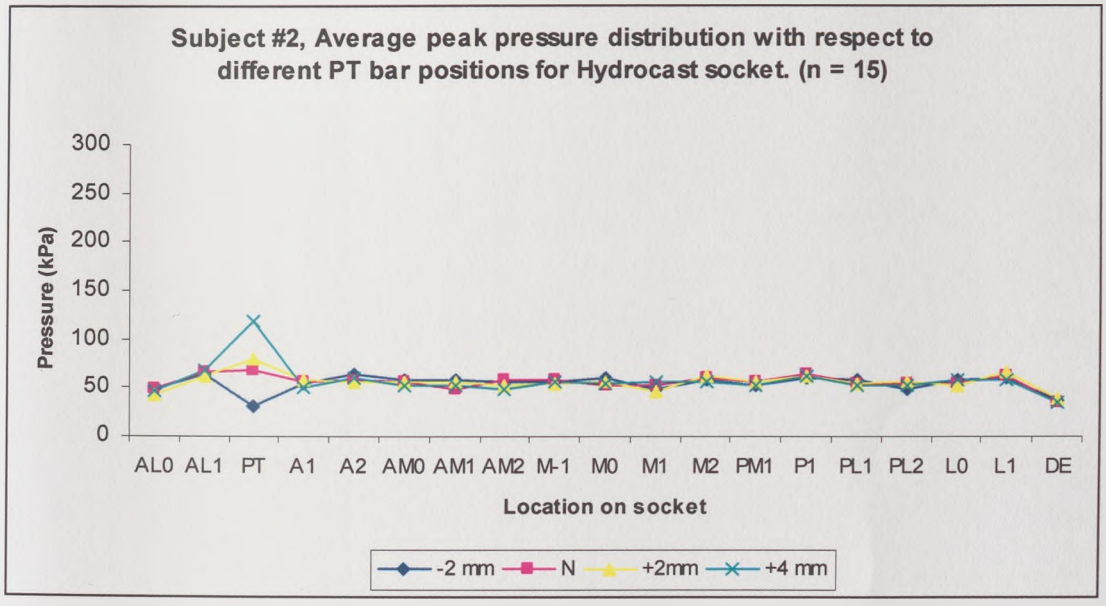

Figure 7.9: Average peak pressures for PTB and Hydrocast sockets on subject #2. Variation in pattern on the other areas of the socket when the patellar tendon bar was compressed (+) or relieved (-). Note : n = numbers of tests represented in each peak pressure and the insert shows the change in PT bar location from the neutral position (N).

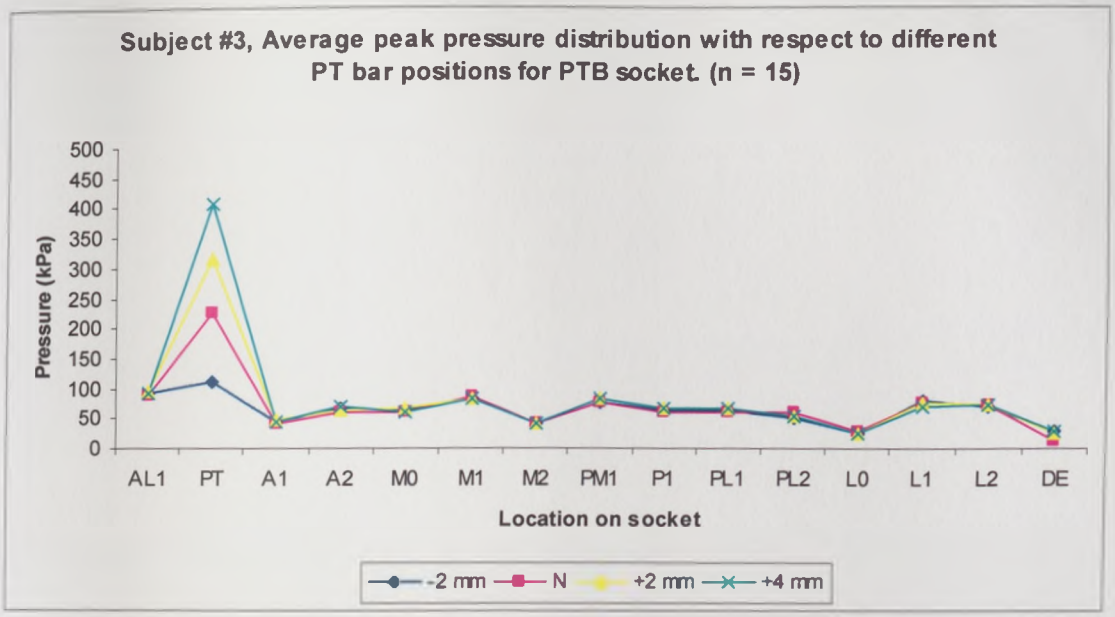

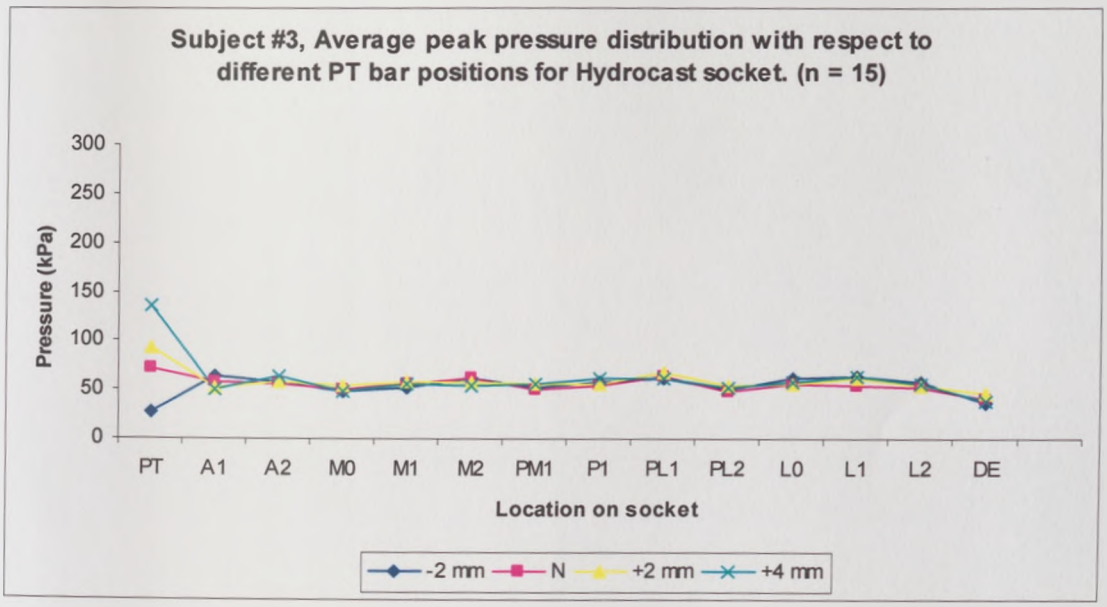

Figure 7.10: Average peak pressures for PTB and Hydrocast sockets on subject #3. Variation in pattern on the other areas of the socket when the patellar tendon bar was compressed (+) or relieved (-). Note : n = numbers of tests represented in each peak pressure and the insert shows the change in PT bar location from the neutral position (N).

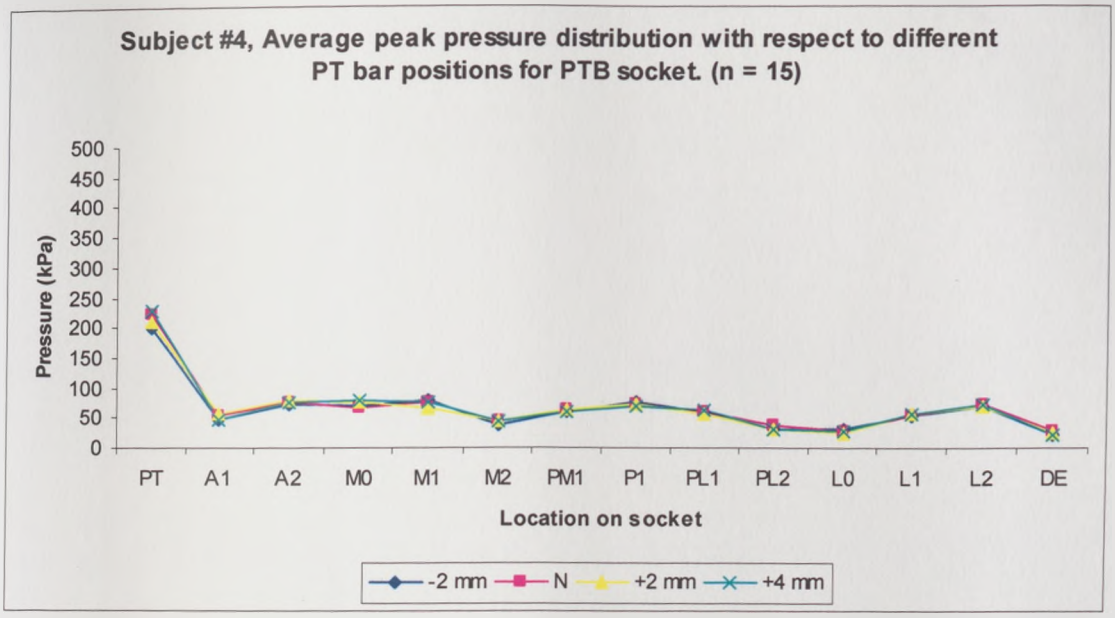

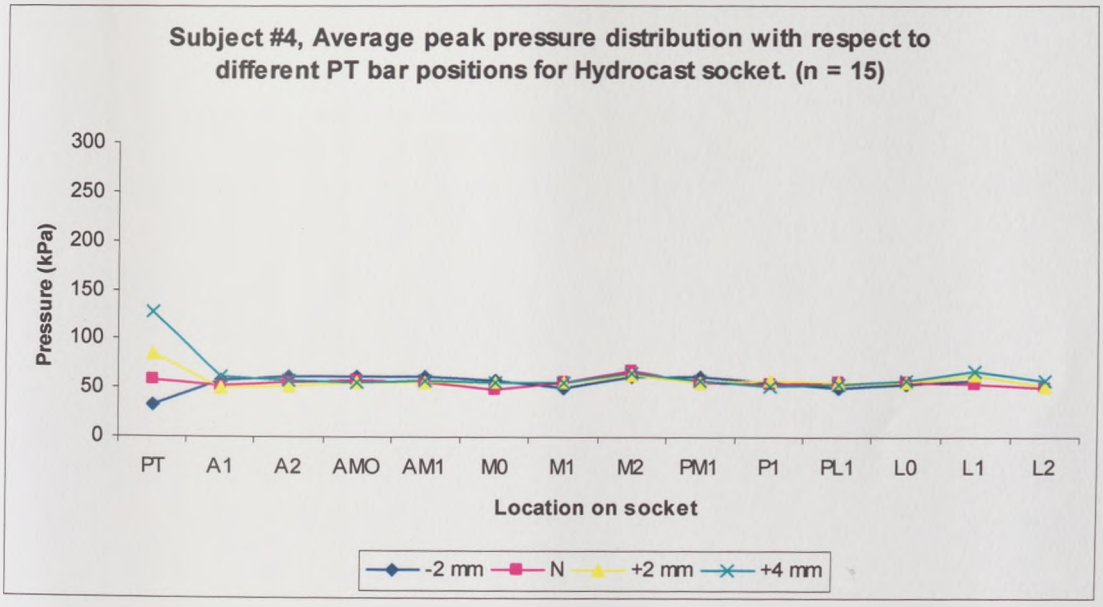

Figure 7.11: Average peak pressures for PTB and Hydrocast sockets on subject #4. Variation in pattern on the other areas of the socket when the patellar tendon bar was compressed (+) or relieved (-). Note : n = numbers of tests represented in each peak pressure and the insert shows the change in PT bar location from the neutral position (N).

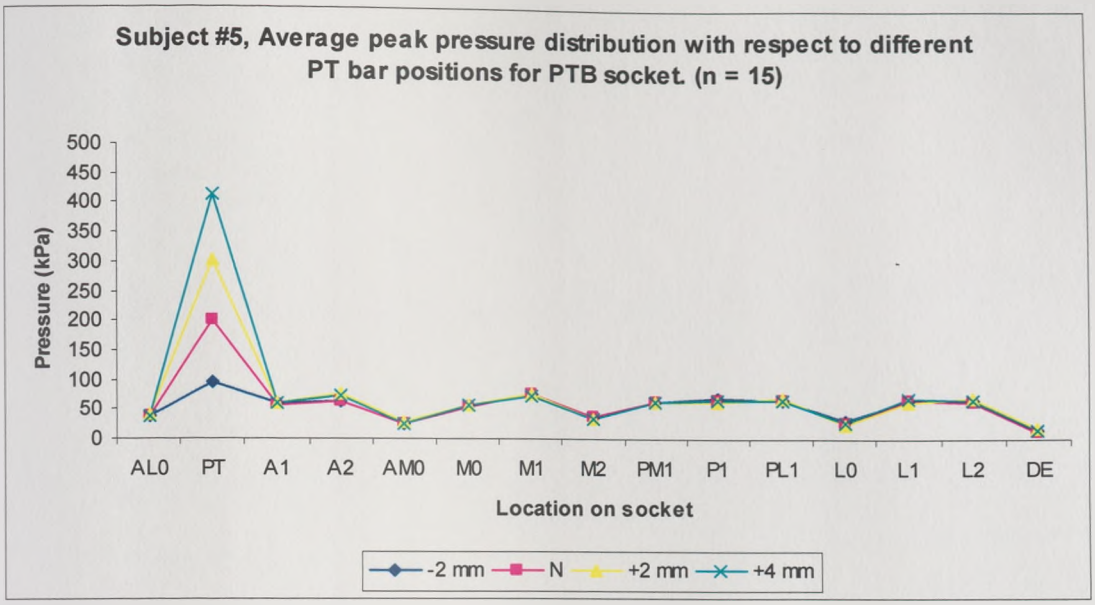

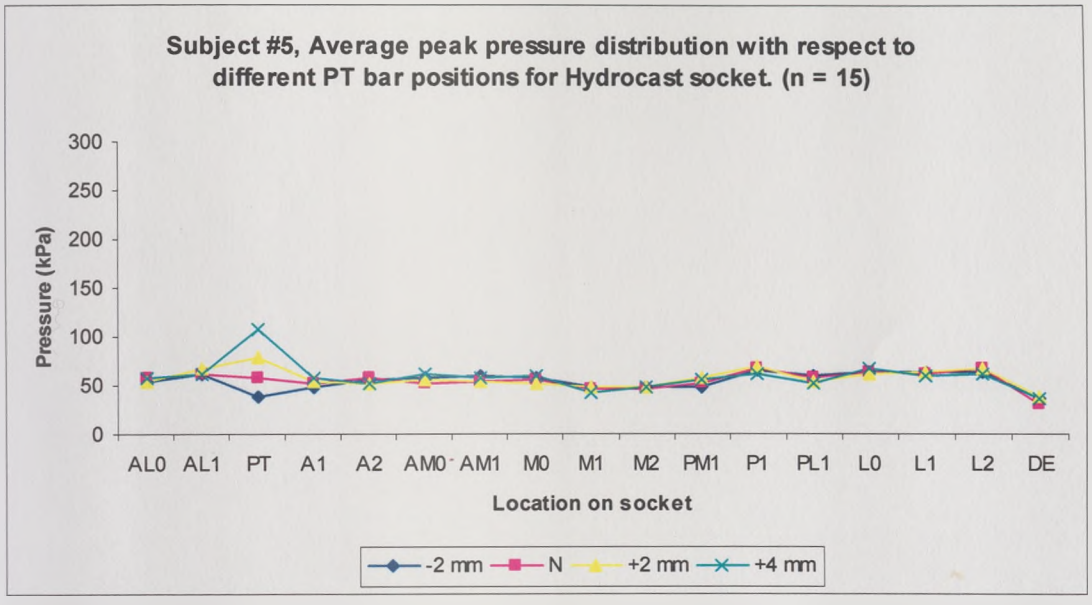

Figure 7.12: Average peak pressures for PTB and Hydrocast sockets on subject #5. Variation in pattern on the other areas of the socket when the patellar tendon bar was compressed (+) or relieved (-). Note : n = numbers of tests represented in each peak pressure and the insert shows the change in PT bar location from the neutral position (N).

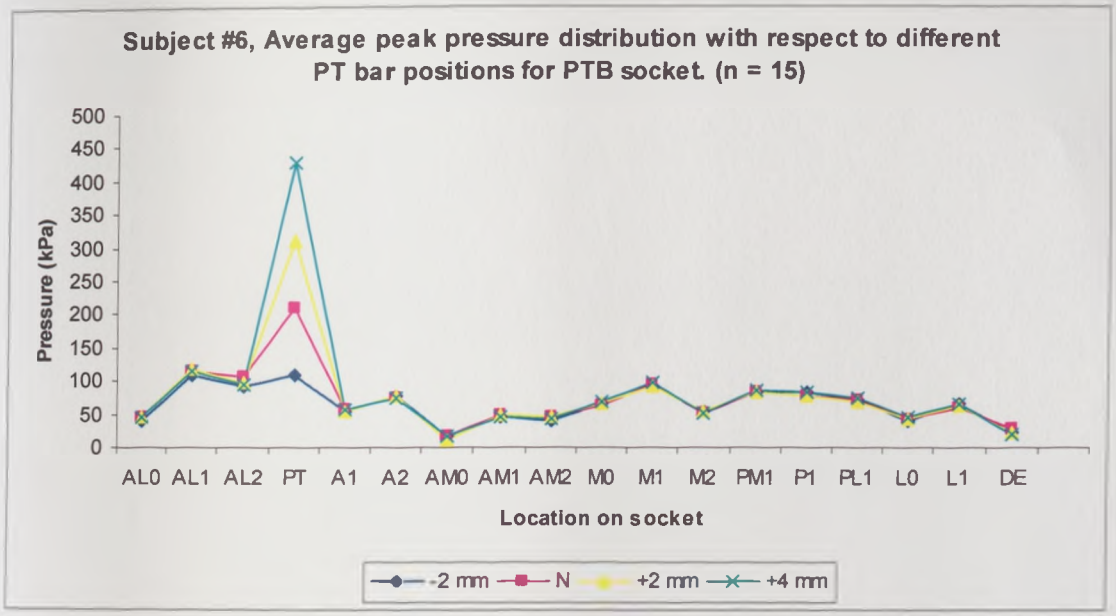

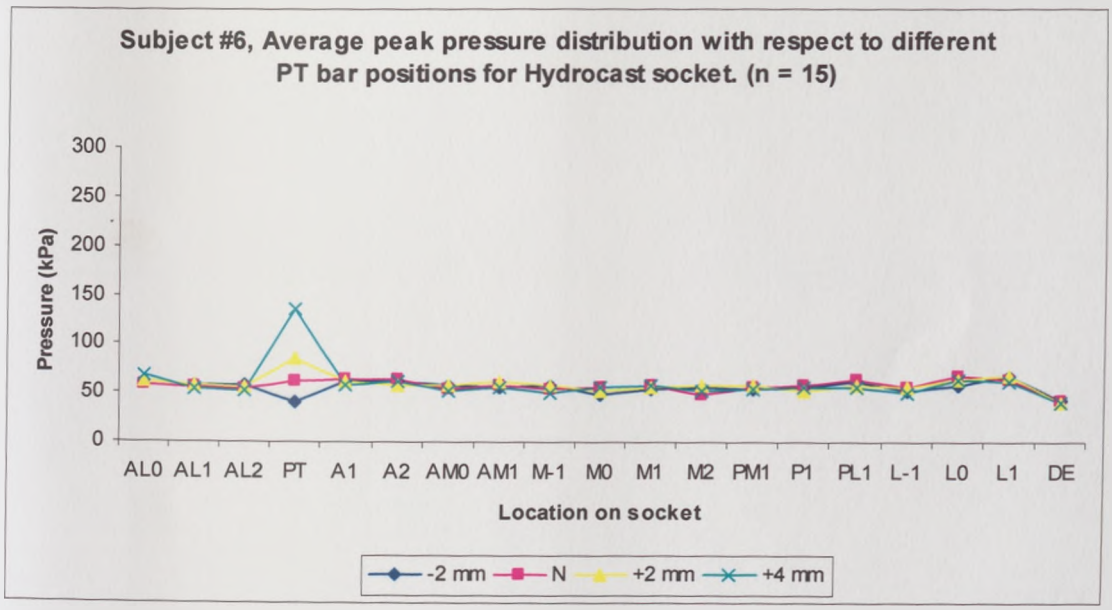

Figure 7.13: Average peak pressures for PTB and Hydrocast sockets on subject #6. Variation in pattern on the other areas of the socket when the patellar tendon bar was compressed (+) or relieved (-). Note : n = numbers of tests represented in each peak pressure and the insert shows the change in PT bar location from the neutral position (N).

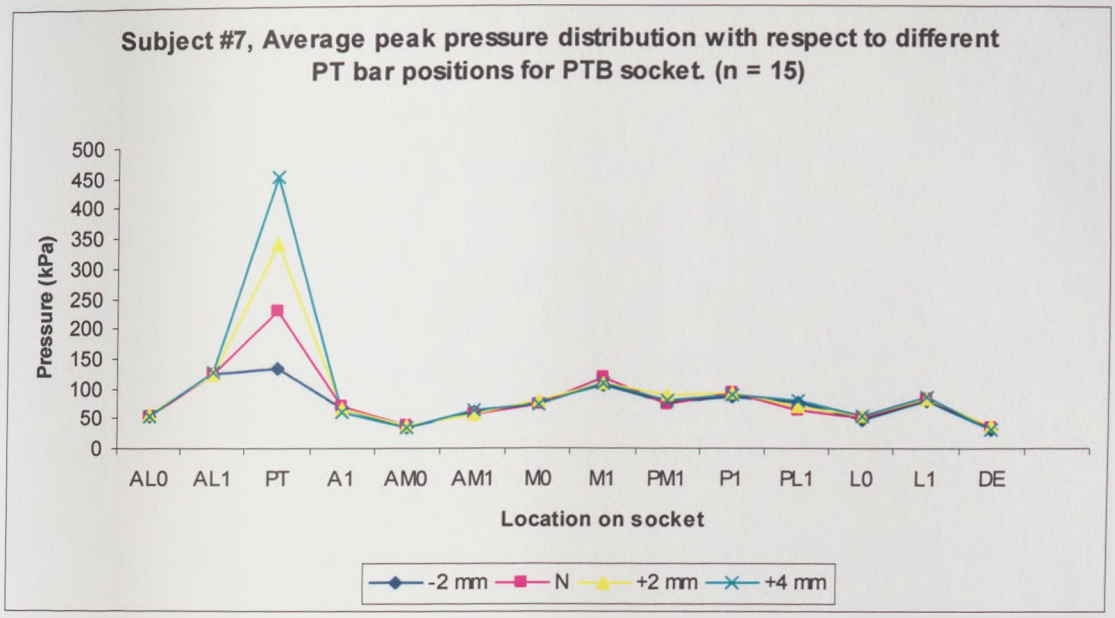

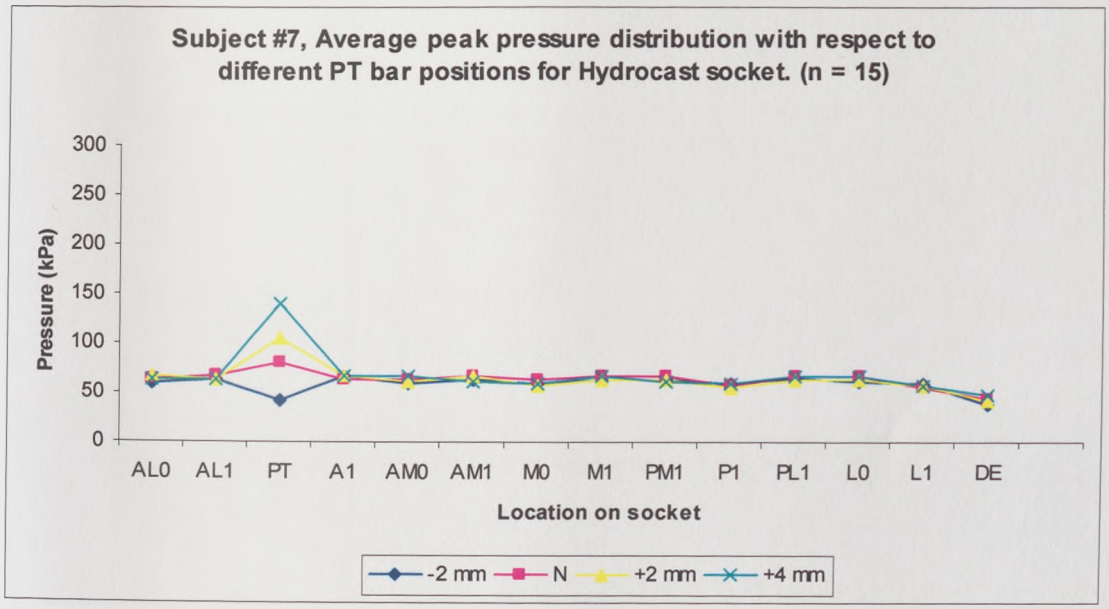

Figure 7.14: Average peak pressures for PTB and Hydrocast sockets on subject #7. Variation in pattern on the other areas of the socket when the patellar tendon bar was compressed (+) or relieved (-). Note : n = numbers of tests represented in each peak pressure and the insert shows the change in PT bar location from the neutral position (N).

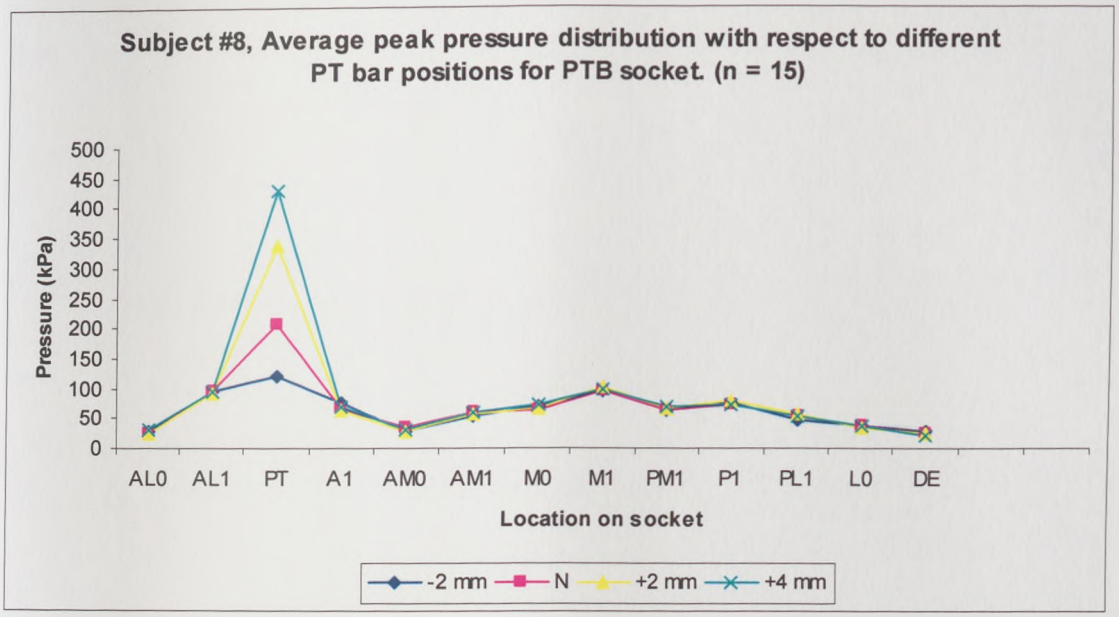

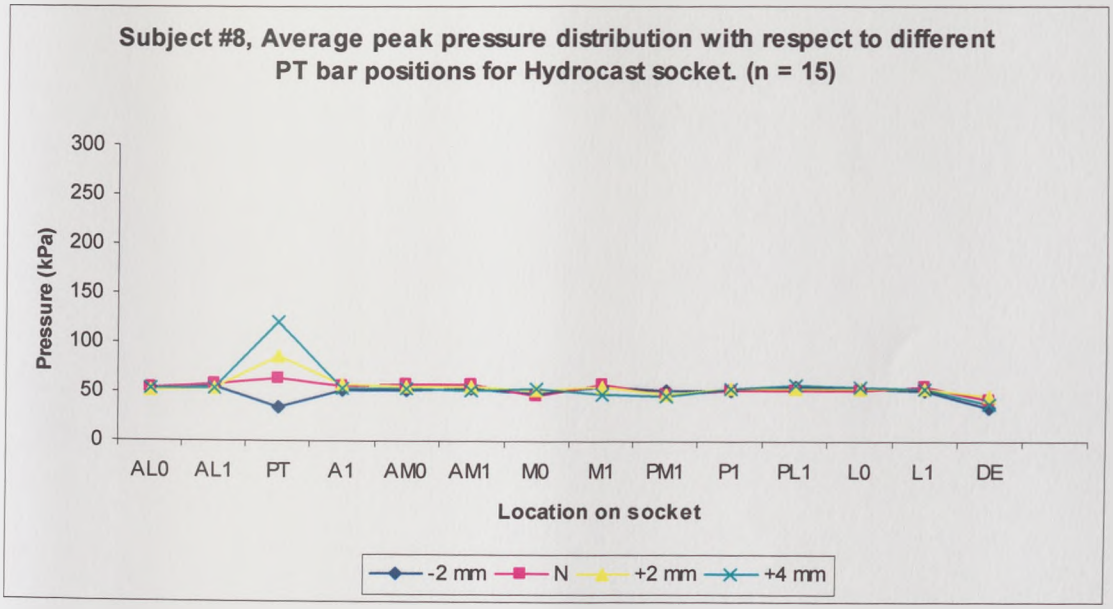

Figure 7.15: Average peak pressures for PTB and Hydrocast sockets on subject #8. Variation in pattern on the other areas of the socket when the patellar tendon bar was compressed (+) or relieved (-). Note : n = numbers of tests represented in each peak pressure and the insert shows the change in PT bar location from the neutral position (N).

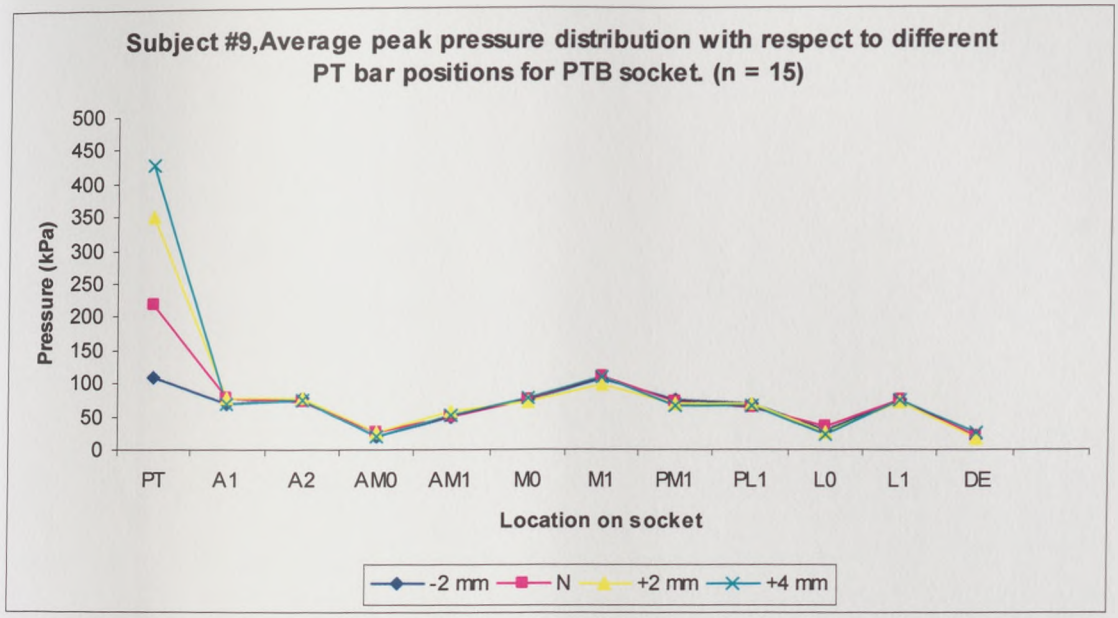

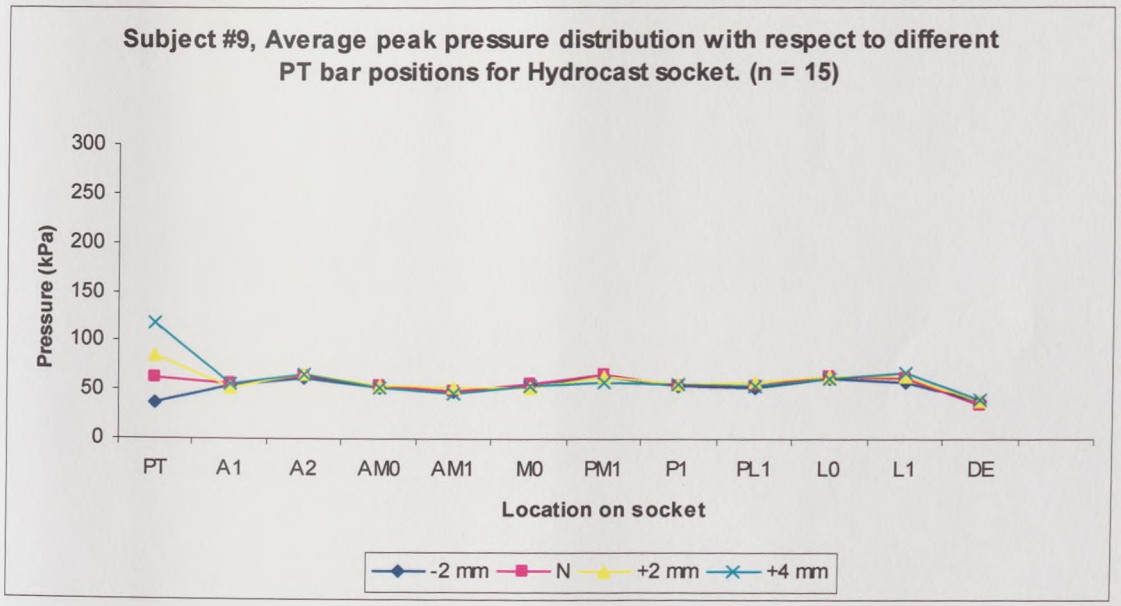

Figure 7.16: Average peak pressures for PTB and Hydrocast sockets on subject #9. Variation in pattern on the other areas of the socket when the patellar tendon bar was compressed (+) or relieved (-). Note : n = numbers of tests represented in each peak pressure and the insert shows the change in PT bar location from the neutral position (N).

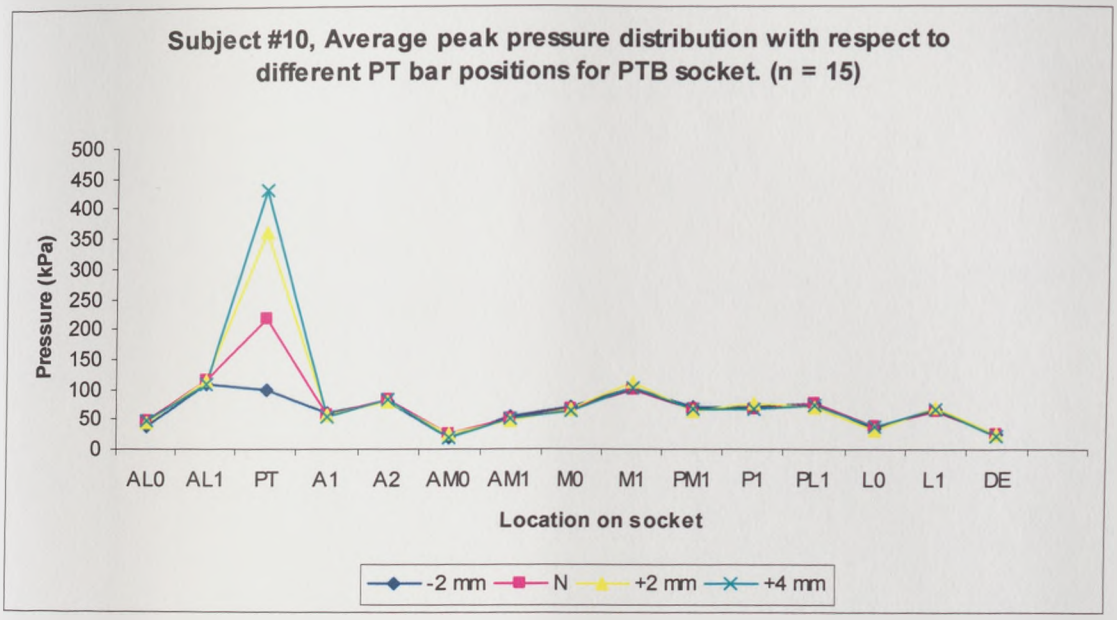

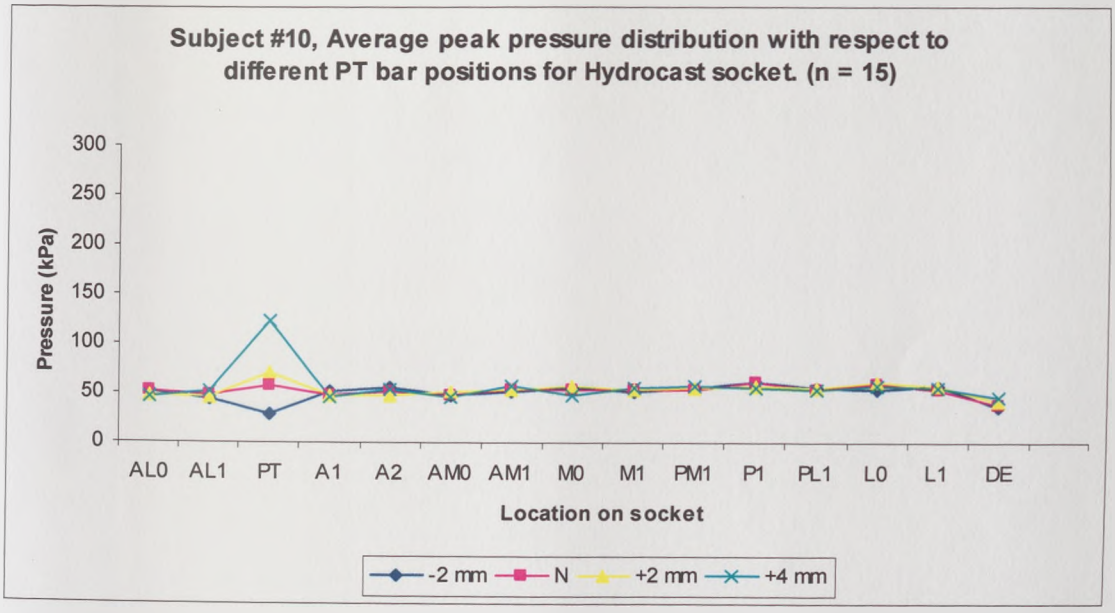

Figure 7.17: Average peak pressures for PTB and Hydrocast sockets on subject #10. Variation in pattern on the other areas of the socket when the patellar tendon bar was compressed (+) or relieved (-). Note : n = numbers of tests represented in each peak pressure and the insert shows the change in PT bar location from the neutral position (N).

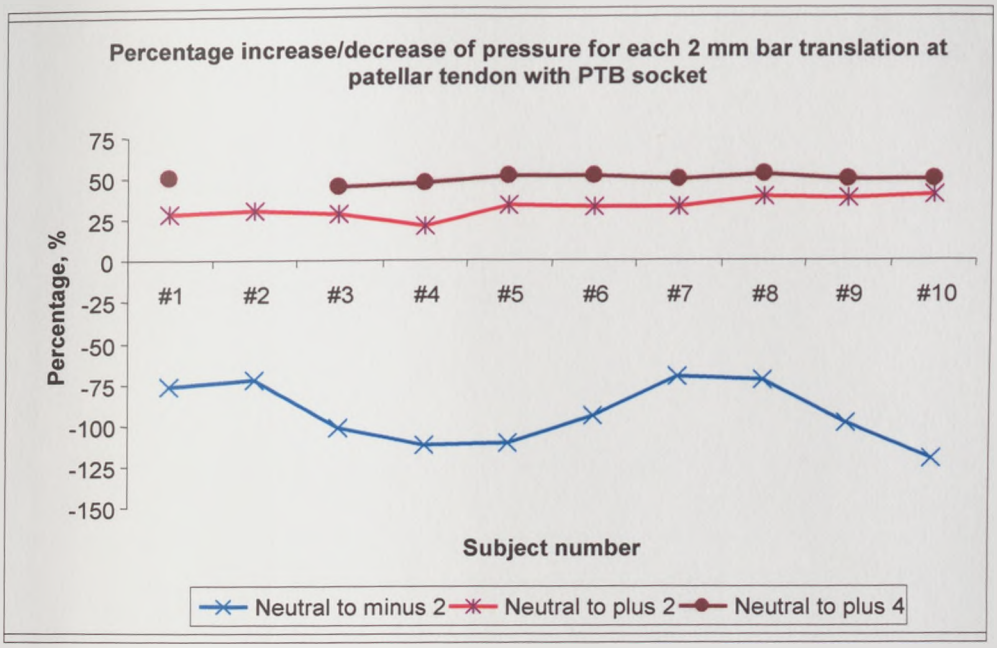

Figure 7.18: Percentage increase (+) or decrease(-) of pressure for each 2mm of bar translation for subject # 1 to #10 with the PTB socket.

	Subject no.										
	#1	#2	#3	#4	#5	#6	#7	#8	#9	#10	aver.
Bar translation	Percentage (%)										
Neutral to minus 2	-77	-73	-102	-111	-110	-94	-70	-72	-98	-120	-93
Neutral to plus 2	29	31	28	21	34	32	33	39	38	40	32
Neutral to plus 4	50	N/A	45	47	51	51	49	52	49	49	44

(-) = decrease of pressure and (+) = increase of pressure

Table 7.9: The value of pressure resulting from each 2 mm of bar translation for subject # 1 to #10 with the PTB socket is shown as a percentage change from the neutral position. N/A = not available due to error.

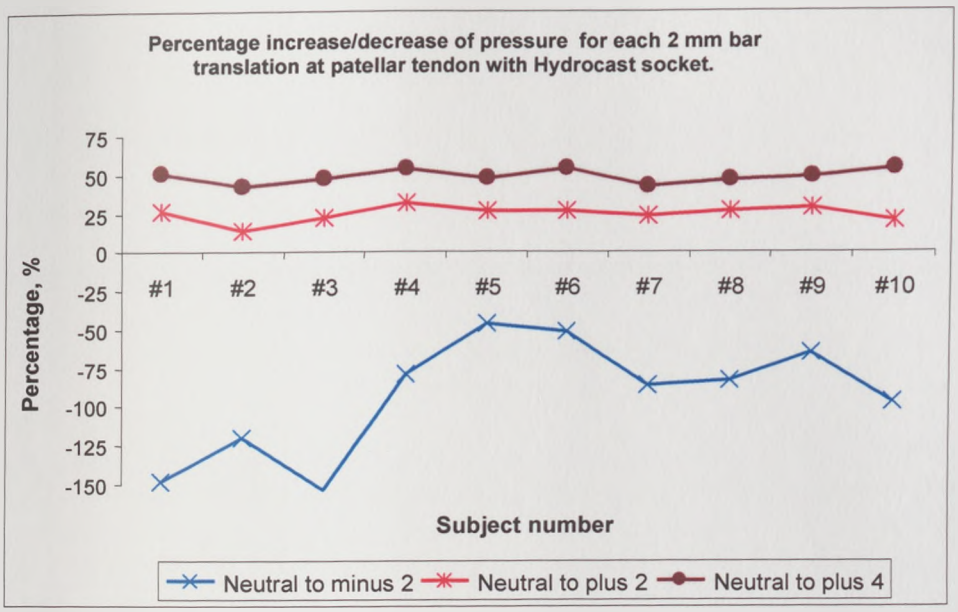

Figure 7.19: Values of increase/decrease pressure for each 2mm of bar translation for subject # 1 to #10 with the Hydrocast socket.

	Subject no.										
	#1	#2	#3	#4	#5	#6	#7	#8	#9	#10	aver.
Bar translation	Percentage (%)										
Neutral to minus 2	-148	-119	-154	-79	-46	-51	-86	-83	-65	-97	-93
Neutral to plus 2	27	14	23	31	27	27	24	26	29	21	25
Neutral to plus 4	50	43	47	54	47	54	43	47	49	54	49

(-) = decrease of pressure and (+) = increase of pressure

Table 7.10: The value of pressure resulting from each 2 mm of bar translation for subject # 1 to #10 with the Hydrocast socket is shown as a percentage change from the neutral position..

The peak values of the pressures determined at the patellar tendon bar area of a PTB socket are in agreement with those published in the literature, with a maximum value reported as 304 kPa. (Isherwood, 1978). The percentage change in pressure as a result of varying the indentation of the patellar tendon bar is shown in figure 7.18 and table 7.9 for the PTB socket and figure 7.19 and table 7.10 for the hydrocast socket. The percentage change was found to be subject dependent and not socket type dependent.

The average percentage increases in pressure values, from the neutral position to + 2 mm indentation and to + 4 mm indentation, in all ten subjects, were 25 % and 49 % for the PTB and 24 % and 48 % for the hydrocast sockets. Whilst the average percentage decreases in pressure values from the neutral position of the patellar tendon bar to -2 mm were 92 % for the PTB and 93 % for the hydrocast socket.

Looking at the interface pressures, repeatable characteristics were evident in the data from different steps at all sites. Excluding the patellar tendon site, the results from the PTB socket from 10 subjects showed that M1 sites (mid medial between proximal and distal of the medial aspect) and anterior distal sites yielded greater pressures than other sites. These were in the range of 65 kPa to 72.3 kPa and 63 kPa to 110 kPa respectively. Pearson et al (1973) reported anterior distal sites averaged 289 ± 194kPa, lateral tibial condyle site pressures averaged 122 ± 100kPa, and medial tibial condyle site pressures averaged 50 ± 40Pa. Sanders et al (1992) found pressure maxima at the anterior proximal sites (including patellar tendon) and anterior medial sites ranged from 52.2 kPa to 223.8 kPa. Whilst for the hydrocast sockets, generally results showed the pressures were evenly distributed and of about the same value unlike the distribution in the PTB socket. In this

section, with socket wall location defined as i.e. anterior as A1,A2,A3; posterior PL1, PL2, P1, P2, PM1, PM2; medial M-1, M0, M1, M2, AM-1, AM0, AM1, AM2 and lateral L-1, L0, L1, L2, AL-1, AL0, AL1, AL2 the overall results from ten subjects of the pressures for the PTB and hydrocast sockets are shown in table 7.11.

Socket type	Patellar Tendon bar			Anterior			Posterior			Medial			Lateral			Distal end		
	Aver. (±1SD)	Min.	Max.	Aver. (±1SD)	Min.	Max.	Aver. (±1SD)	Min.	Max.	Aver. (±1SD)	Min.	Max.	Aver. (±1SD)	Min.	Max.	Aver. (±1SD)	Min.	Max.
	(kPa)			(kPa)			(kPa)			(kPa)			(kPa)			(kPa)		
Hydrocast socket	77 (34)	25	140	57 (9)	46	68	56 (9)	43	69	55 (9)	42	68	55 (9)	40	68	40 (12)	31	48
PTB socket	265 (117)	96	451	69 (16)	41	83	51 (22)	16	92	40 (30)	3	112	55 (37)	4	139	30 (16)	12	39

Table 7.11: Values of pressure with PTB and hydrocast sockets during bar translation from -2 mm to + 4 mm for ten subjects.

7.7 Results of pressure and shear stresses measurements in the PTB and Hydrocast sockets.

The same technique of 'ensemble averaging' , (Fleming, 1997) was used to present a mean value, normalised over the gait cycle heel strike to heel strike, 0 – 100% of the gait cycle. Prior to the process of averaging, all the data obtained had to be normalised to 100% of the gait cycle. Since stresses is a function of area and force, and each subject was to be compared only with data collected from the same subject, at self-selected velocity, but on a different socket (PTB or hydrocast sockets), no further normalisation (height or weight or others) was performed. For each subject all the data on one socket have been averaged and compared to the corresponding data from the other socket. The mean results for the PTB and Hydrocast socket for each subject of the ten subjects are presented in figures 7.20 to 7.69. The peak mean values of the result for the ten subjects during dynamic tests including standard deviations are listed in table 7.12 for PTB sockets and table 7.13 for hydrocast sockets. The average peak stresses and standard deviation were obtained from the statistical analysis of the fifteen step data.

7.7 Results of pressure and shear stresses measurement on the PTB and Hydrocast sockets

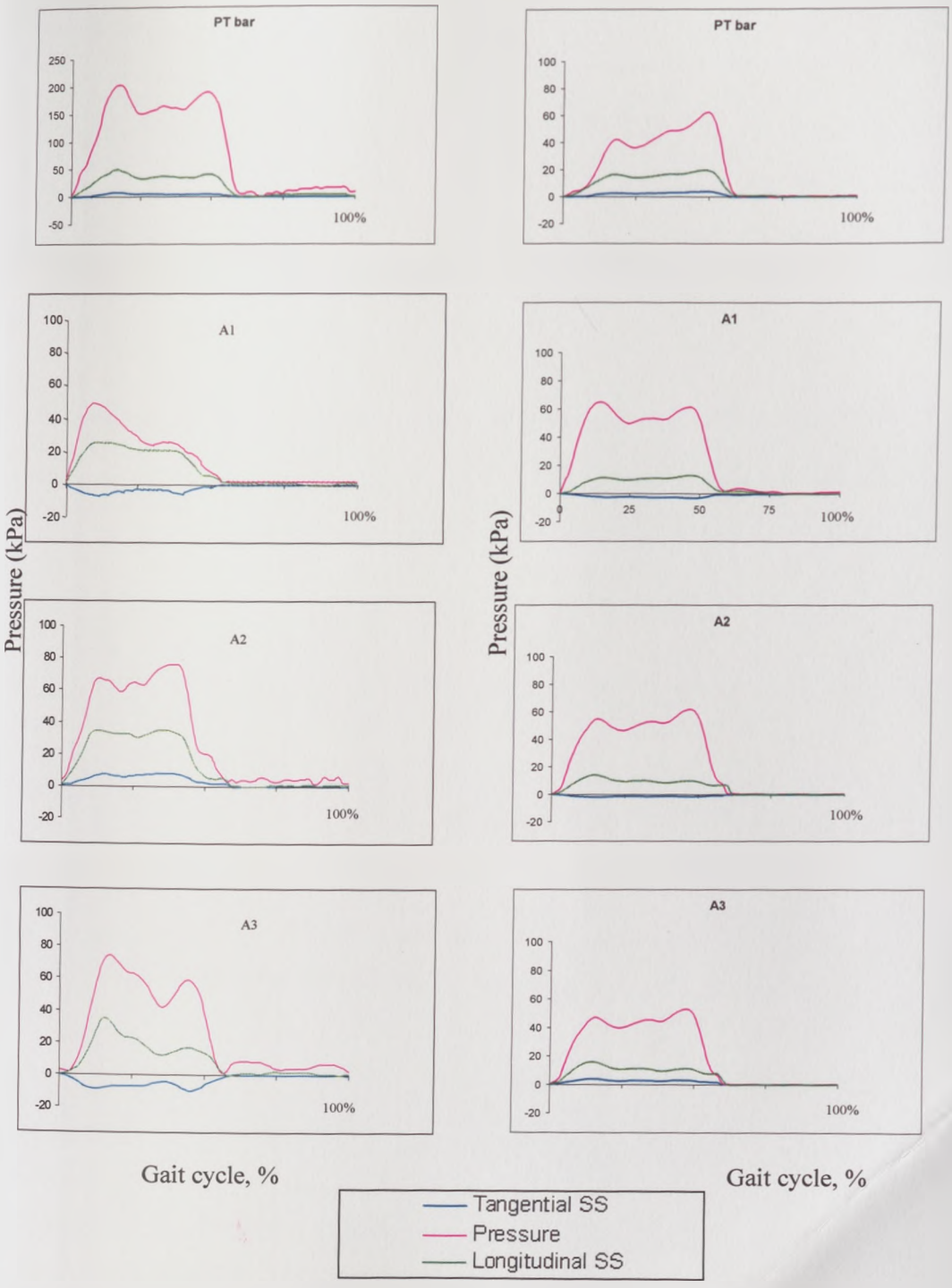

Figure 7.20: Interface pressure and shear stresses results (kPa) versus percentage of the gait cycle (one division = 25%), heel strike to heel strike of prosthetic leg for subject 1 on PTB socket (left) and Hydrocast socket (right) measured using B.E.S.T transducers at anterior sites.
n = number of tests represented in each summary curve.

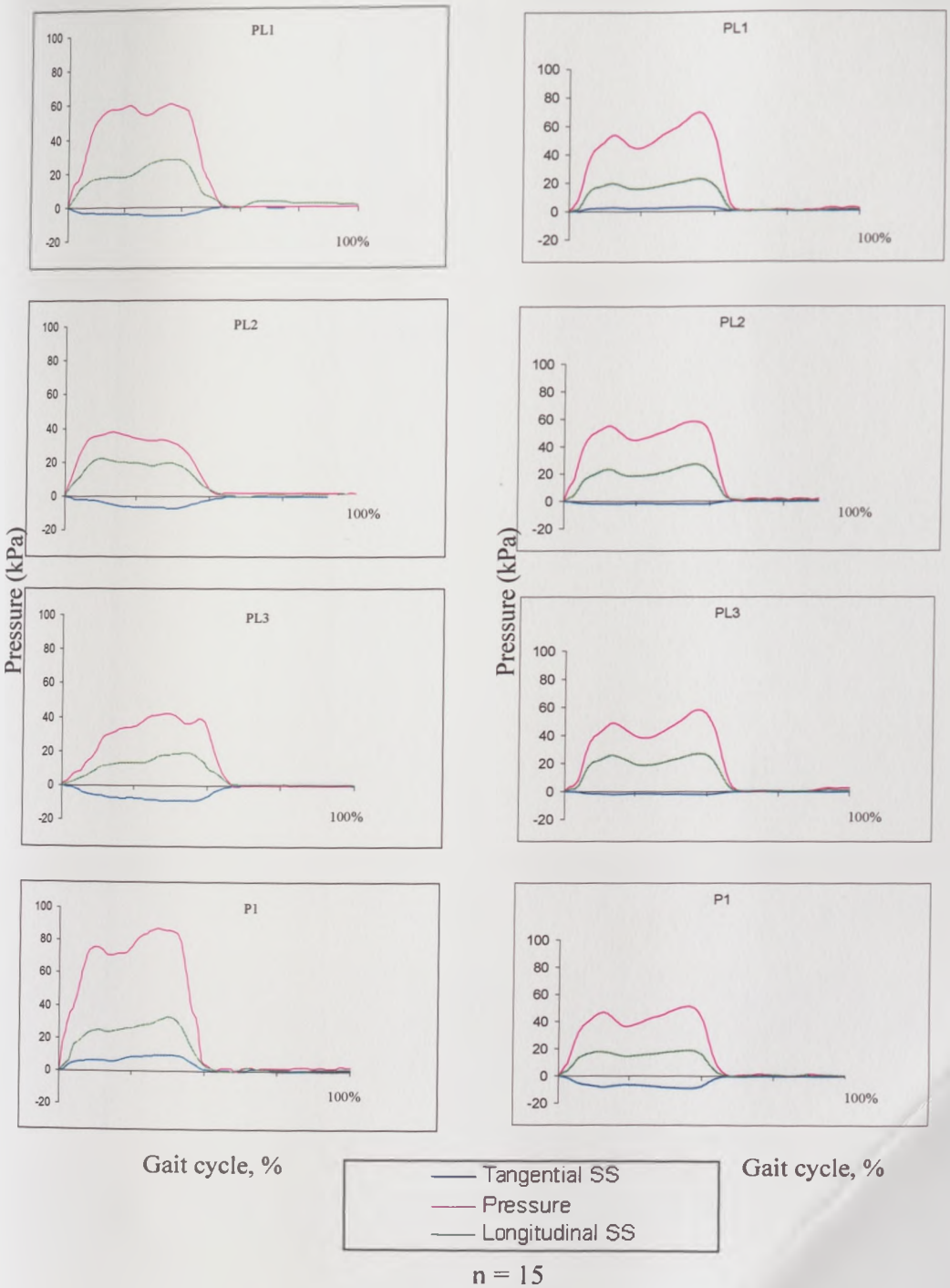

Figure 7.21: Interface pressure and shear stresses results (kPa) versus percentage of the gait cycle (one division = 25%), heel strike to heel strike of prosthetic leg for subject 1 on PTB socket (left) and Hydrocast socket (right) measured using B.E.S.T transducers at posterior sites.
n = number of tests represented in each summary curve.

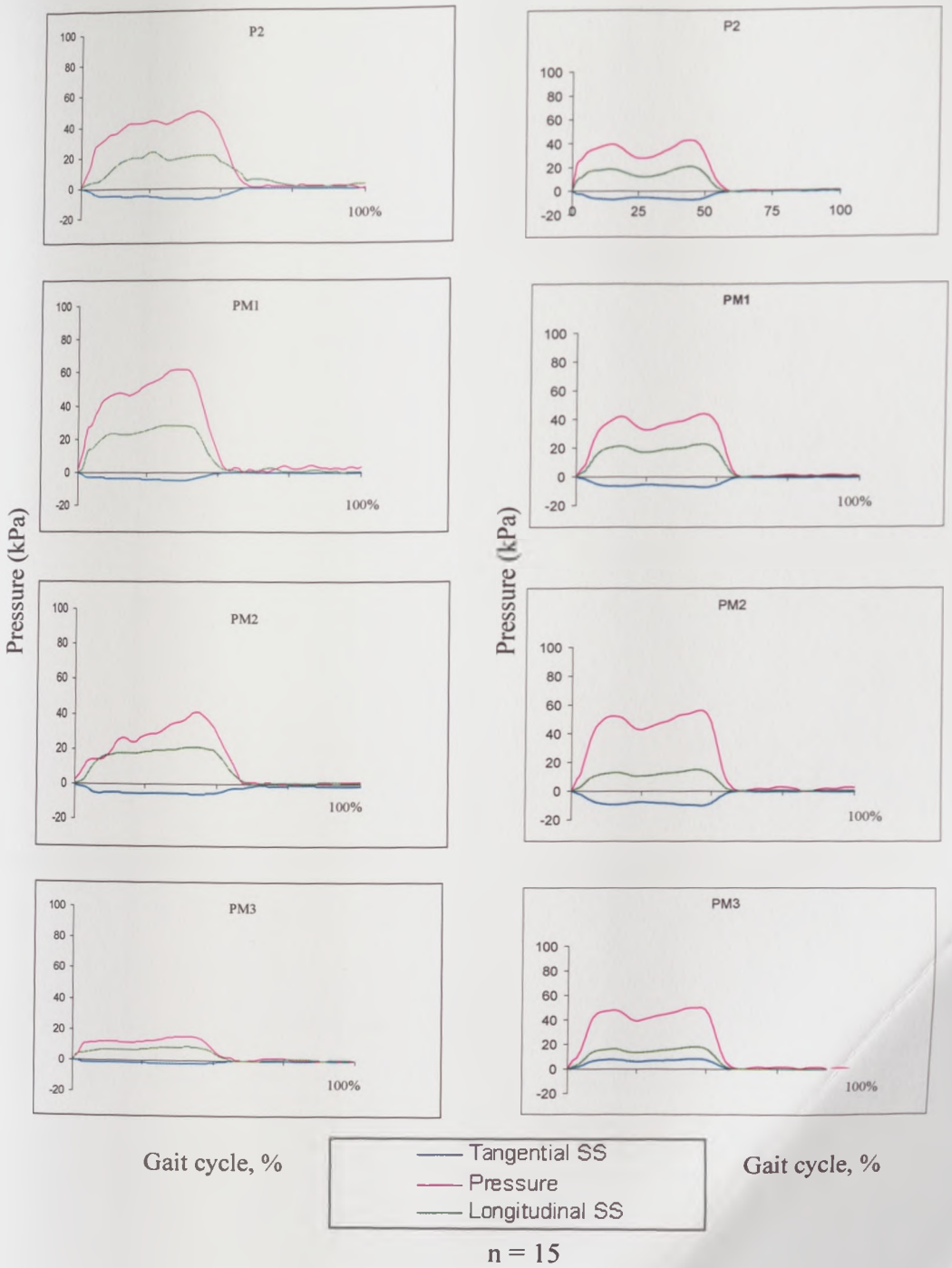

... Contd....Figure 7.21: Interface pressure and shear stresses results (kPa) versus percentage of the gait cycle (one division = 25%), heel strike to heel strike of prosthetic leg for subject 1 on PTB socket (left) and Hydrocast socket (right) measured using B.E.S.T transducers at posterior sites.
n = number of tests represented in each summary curve.

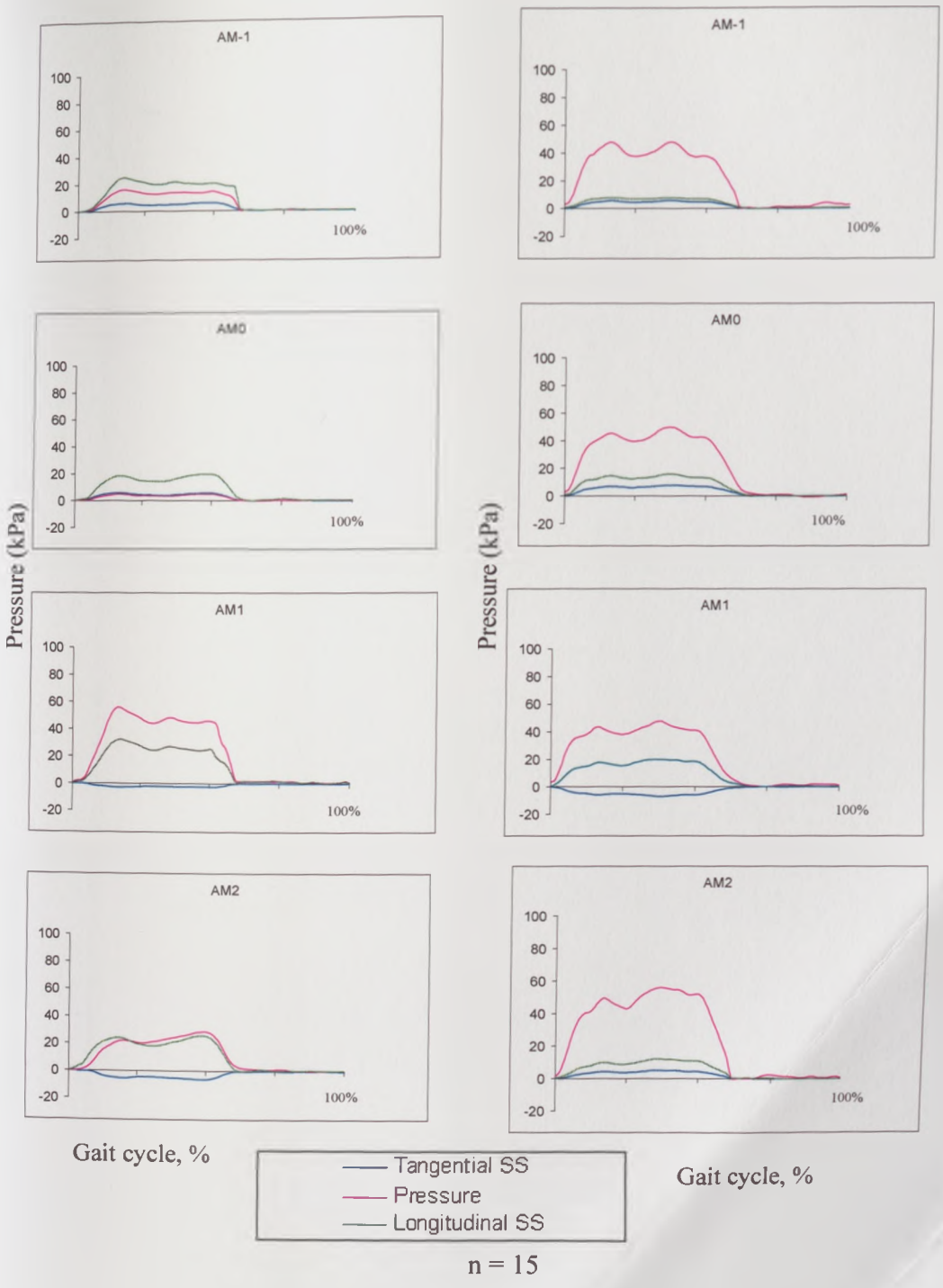

Figure 7.22: Interface pressure and shear stresses results (kPa) versus percentage of the gait cycle (one division = 25%), heel strike to heel strike of prosthetic leg for subject 1 on PTB socket (left) and Hydrocast socket (right) measured using B.E.S.T transducers at medial sites.
n = number of tests represented in each summary curve.

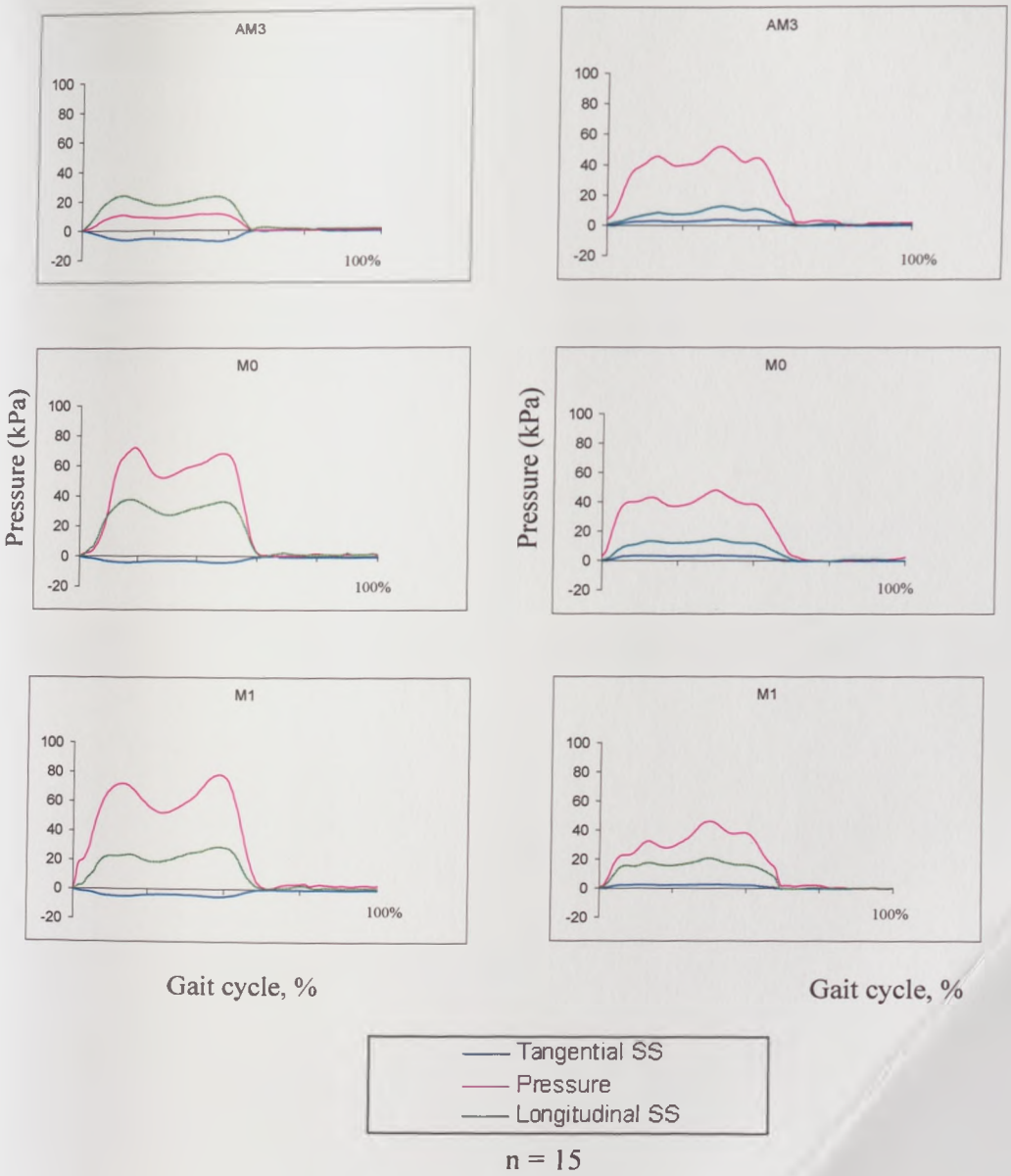

...Contd...Figure 7.22: Interface pressure and shear stresses results (kPa) versus percentage of the gait cycle (one division = 25%), heel strike to heel strike of prosthetic leg for subject 1 on PTB socket (left) and Hydrocast socket (right) measured using B.E.S.T transducers at medial sites.
n = number of tests represented in each summary curve.

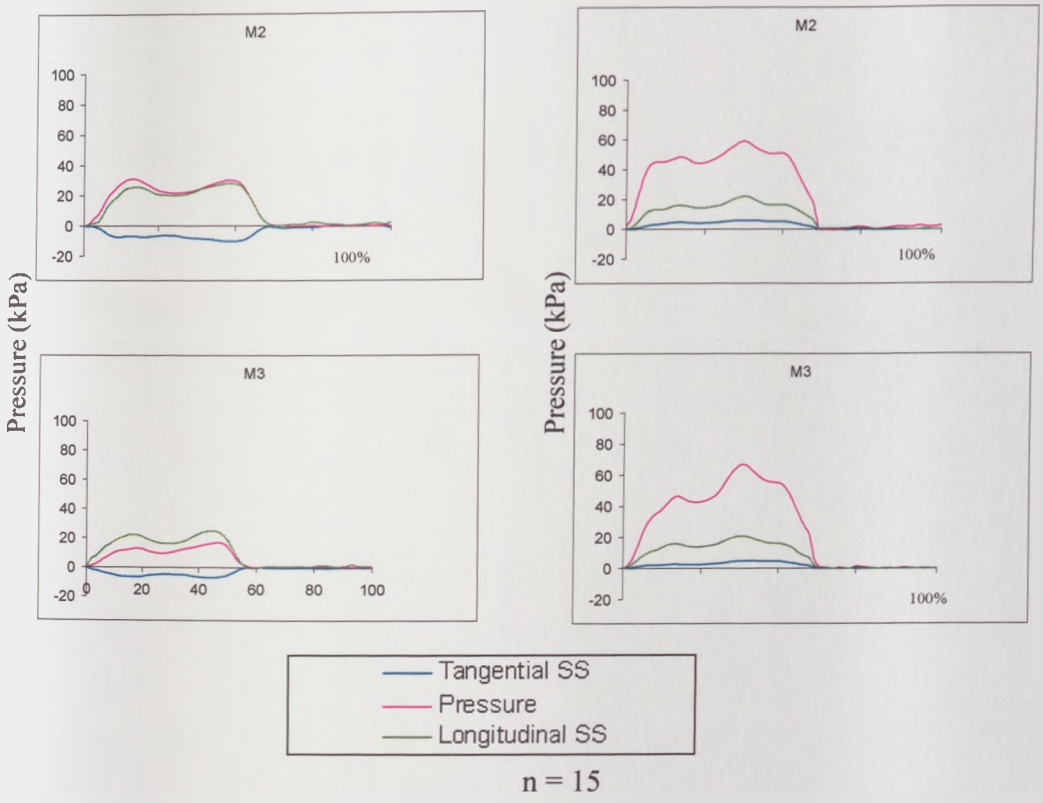

...Contd...Figure 7.22: Interface pressure and shear stresses results (kPa) versus percentage of the gait cycle (one division = 25%), heel strike to heel strike of prosthetic leg for subject 1 on PTB socket (left) and Hydrocast socket (right) measured using B.E.S.T transducers at medial sites.
n = number of tests represented in each summary curve.

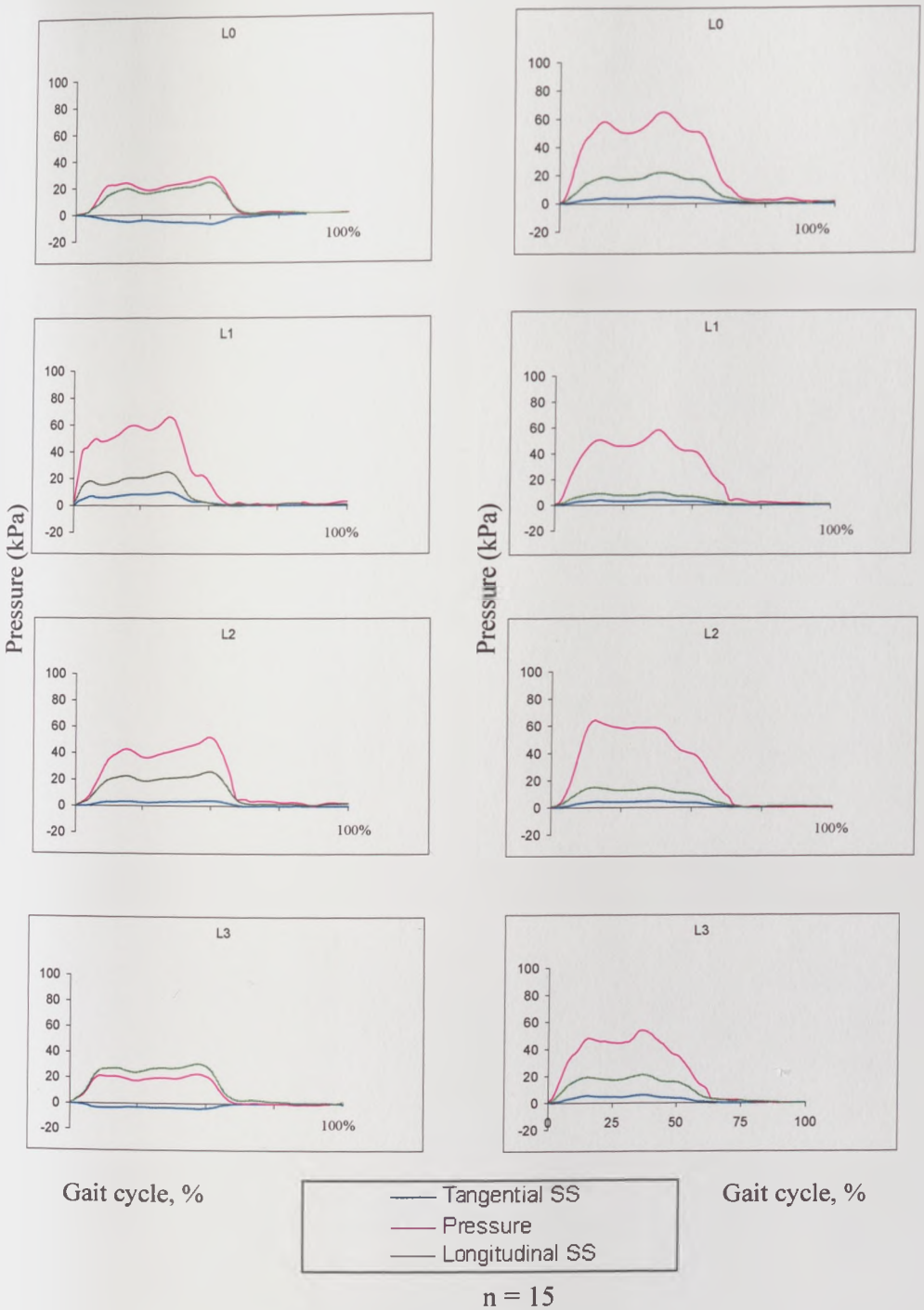

Figure 7.23: Interface pressure and shear stresses results (kPa) versus percentage of the gait cycle (one division = 25%), heel strike to heel strike of prosthetic leg for subject 1 on PTB socket (left) and Hydrocast socket (right) measured using B.E.S.T transducers at lateral sites.
n = number of tests represented in each summary curve.

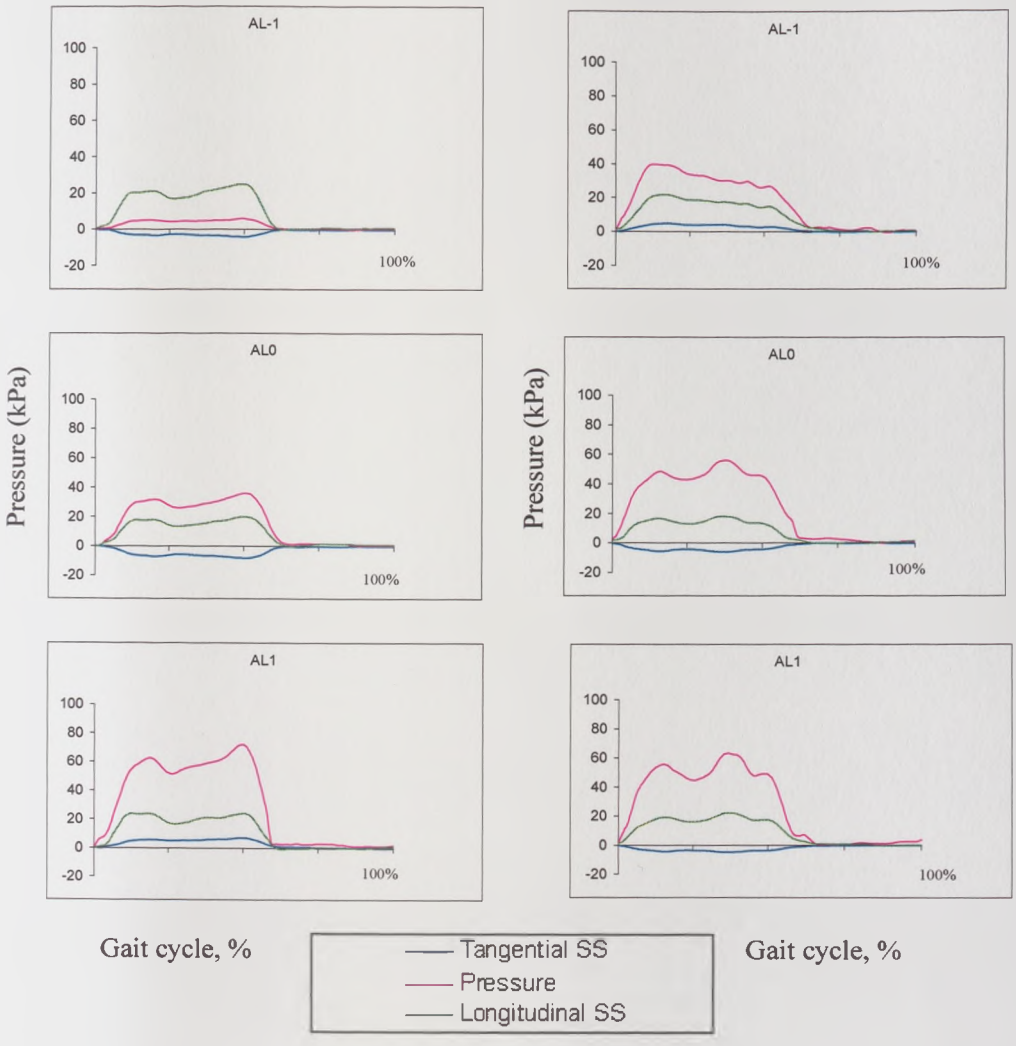

..Contd...Figure 7.23: Interface pressure and shear stresses results (kPa) versus percentage of the gait cycle (one division = 25%), heel strike to heel strike of prosthetic leg for subject 1 on PTB socket (left) and Hydrocast socket (right) measured using B.E.S.T transducers at lateral sites.
n = number of tests represented in each summary curve.

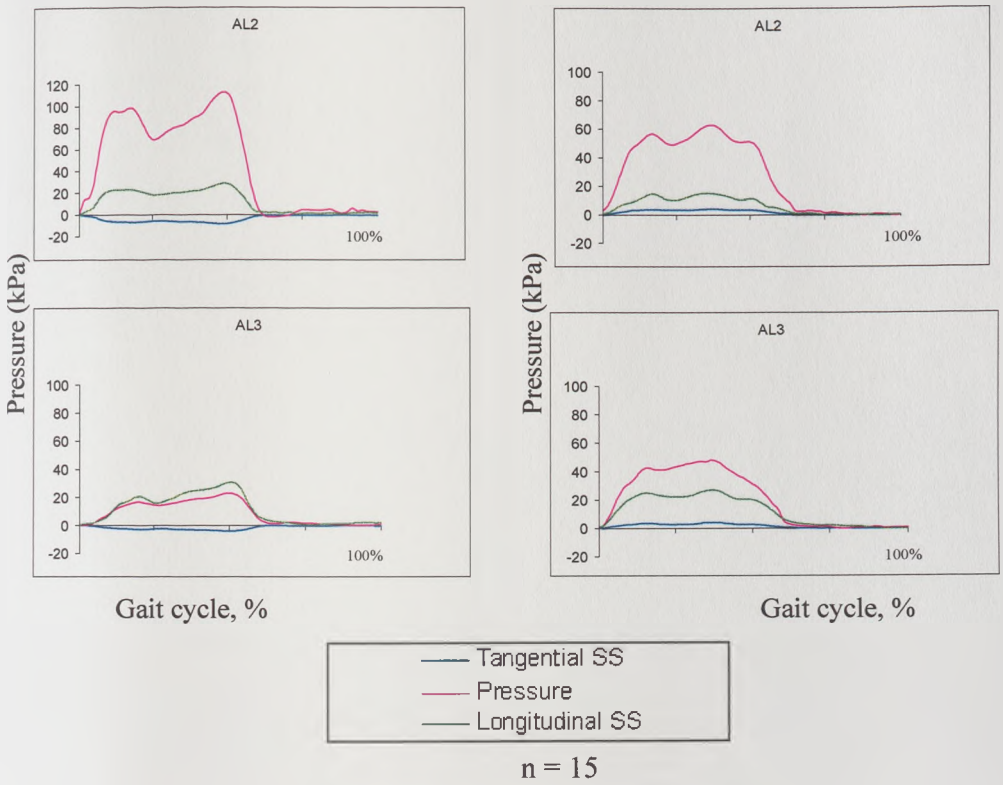

..Contd…Figure 7.23: Interface pressure and shear stresses results (kPa) versus percentage of the gait cycle (one division = 25%), heel strike to heel strike of the prosthetic leg for subject 1 on the PTB socket (left) and the Hydrocast socket (right) measured using B.E.S.T transducers at the lateral sites.
n = number of tests represented in each summary curve.

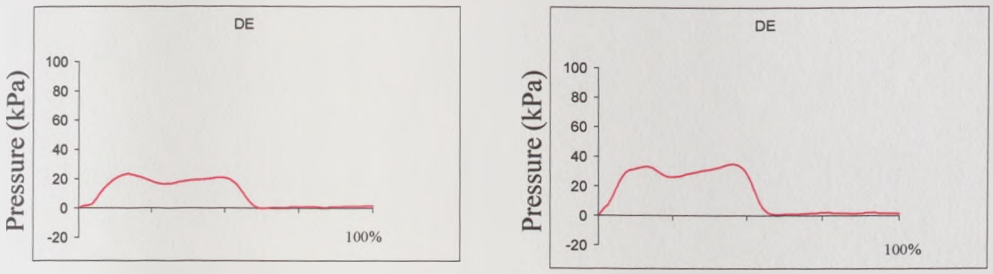

Figure 7.24: Interface pressure (kPa) versus percentage of the gait cycle (one division = 25%), heel strike to heel strike of the prosthetic leg for subject 1 on the PTB socket (left) and the Hydrocast socket (right) measured using electrohydraulic transducer at the distal end site.
n = number of tests represented in each summary curve.

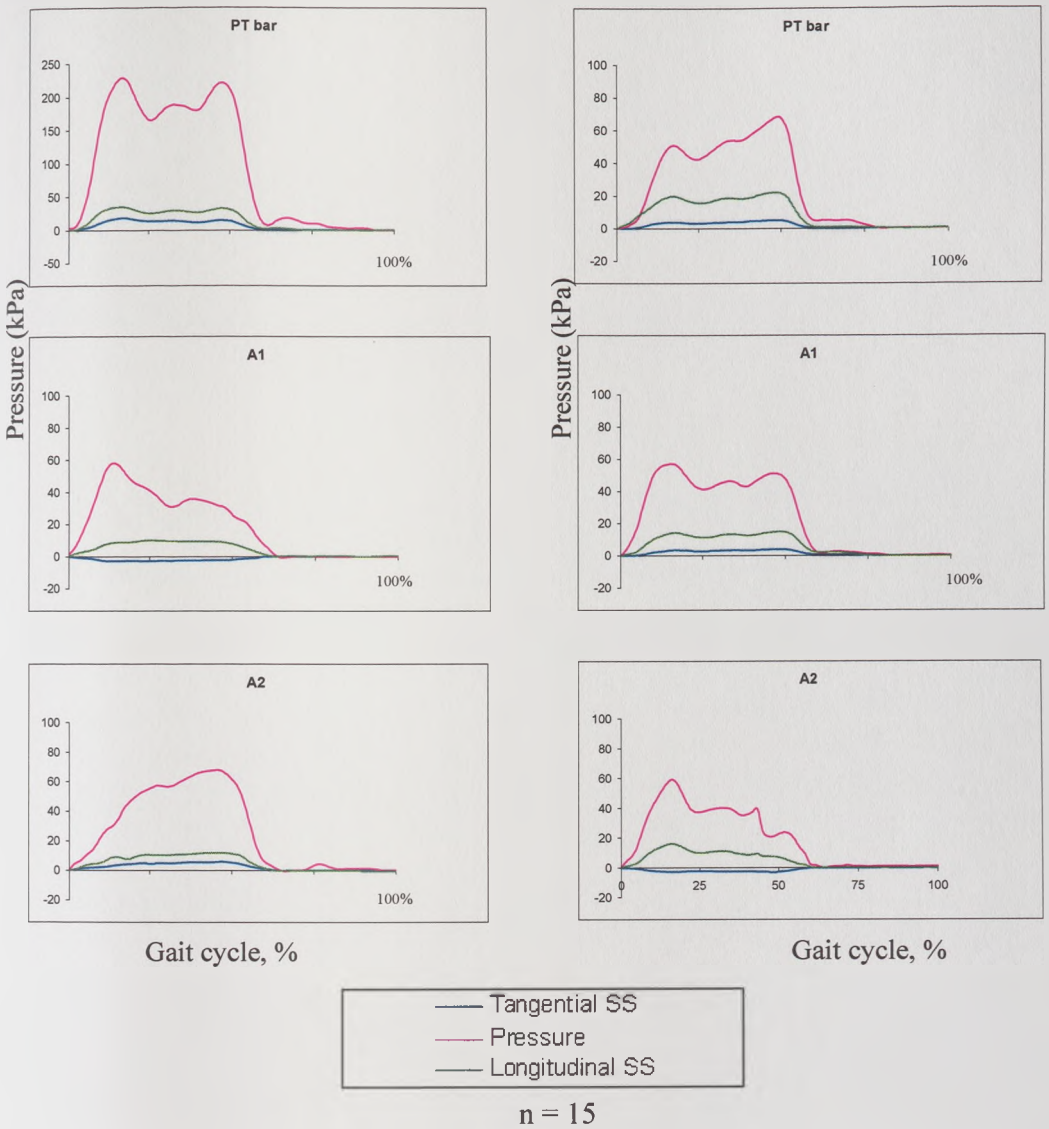

Figure 7.25: Interface pressure and shear stresses results (kPa) versus percentage of the gait cycle (one division = 25%), heel strike to heel strike of the prosthetic leg for subject 2 on the PTB socket (left) and the Hydrocast socket (right) measured using B.E.S.T transducers at the anterior sites.
n = number of tests represented in each summary curve.

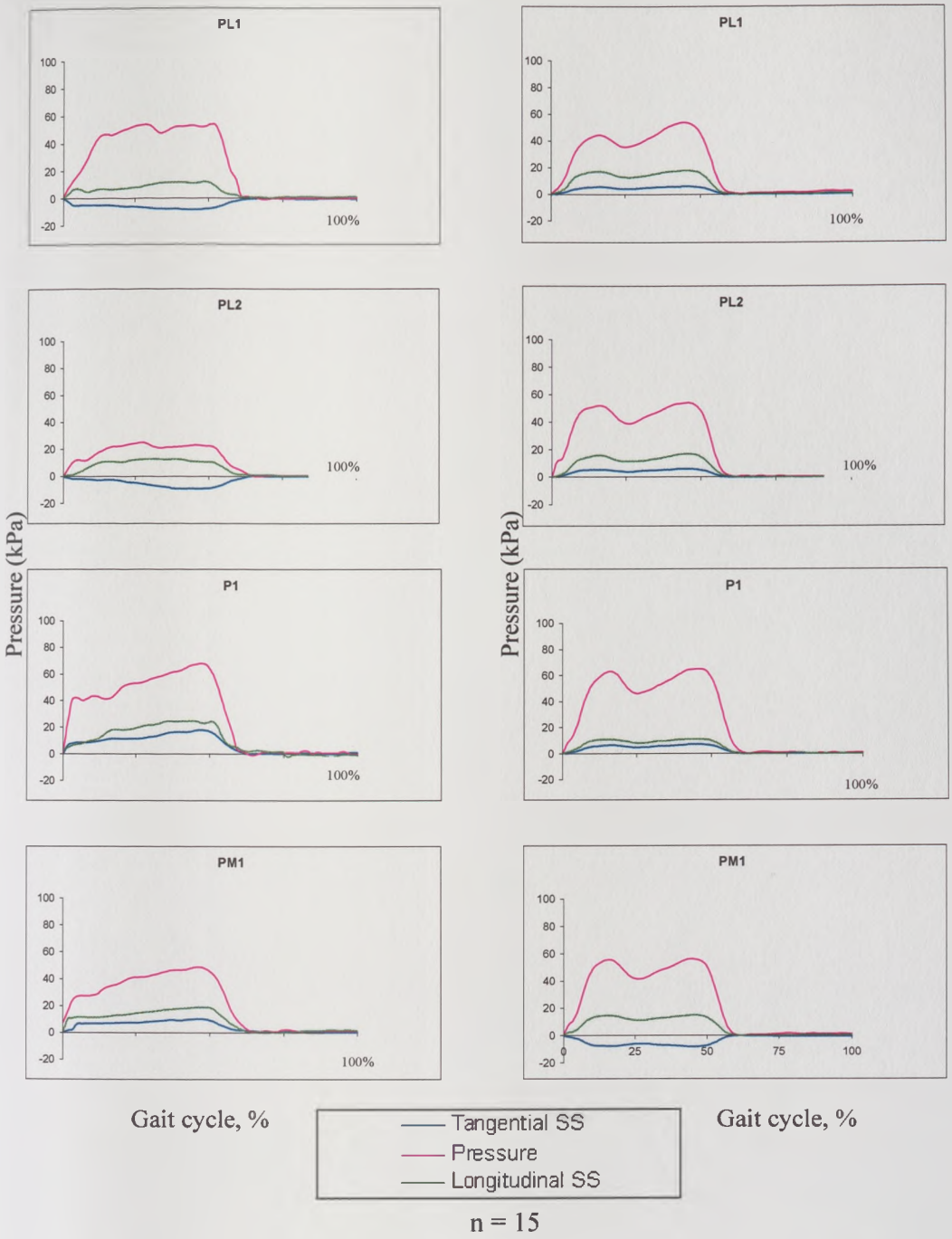

Figure 7.26: Interface pressure and shear stresses results (kPa) versus percentage of the gait cycle (one division = 25%), heel strike to heel strike of the prosthetic leg for subject 2 on the PTB socket (left) and the Hydrocast socket (right) measured using B.E.S.T transducers at the posterior sites.
n = number of tests represented in each summary curve.

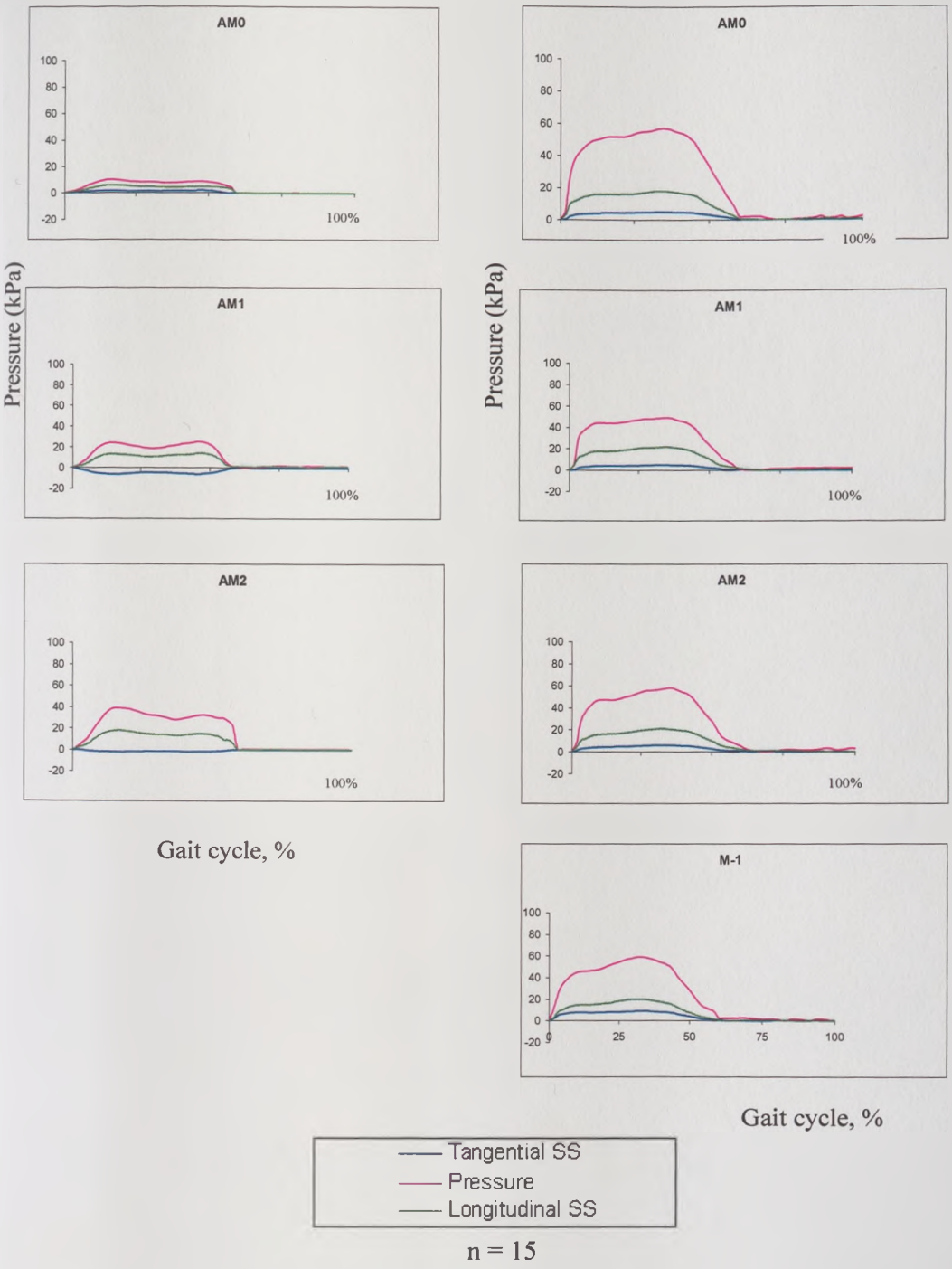

Figure 7.27: Interface pressure and shear stresses results (kPa) versus percentage of the gait cycle (one division = 25%), heel strike to heel strike of the prosthetic leg for subject 2 on the PTB socket (left) and the Hydrocast socket (right) measured using B.E.S.T transducers at the medial sites.
n = number of tests represented in each summary curve.

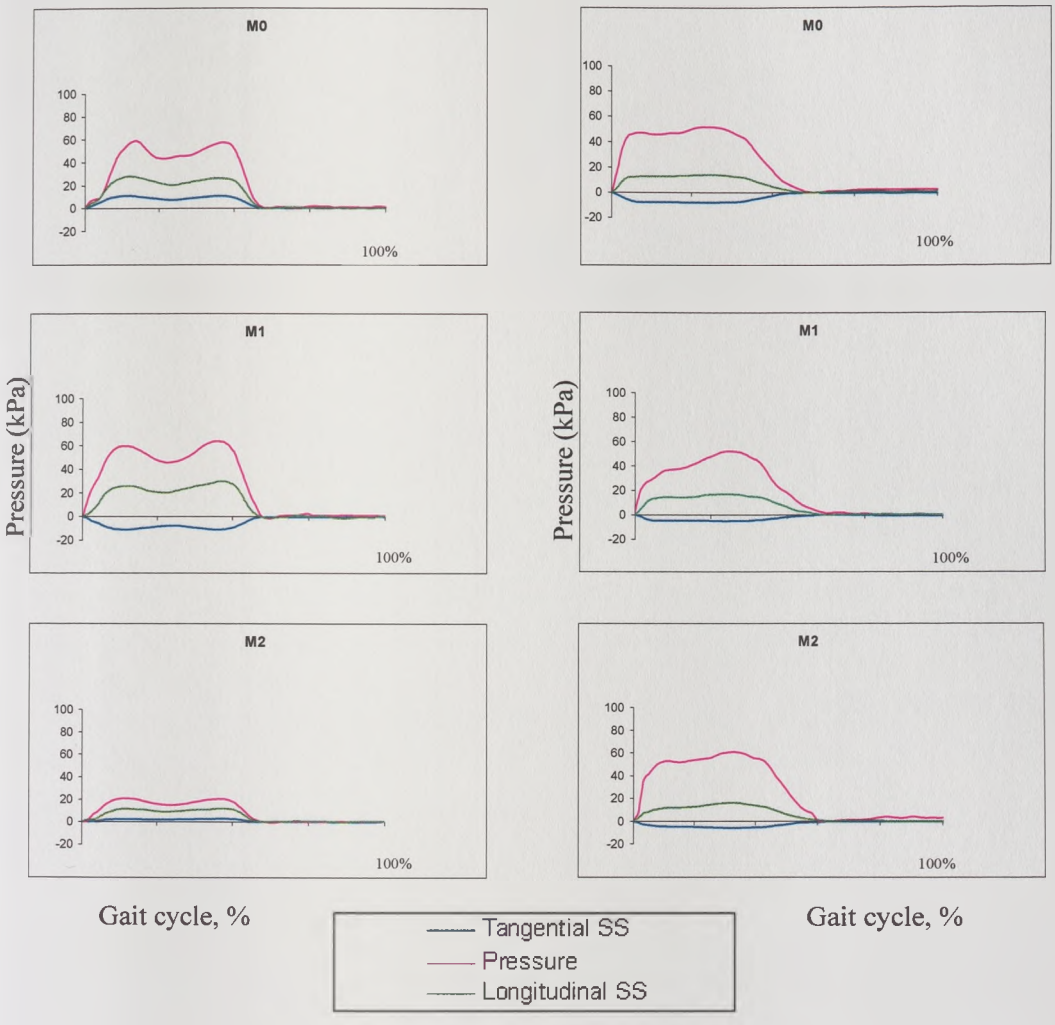

..Contd...Figure 7.27: Interface pressure and shear stresses results (kPa) versus percentage of the gait cycle (one division = 25%), heel strike to heel strike of the prosthetic leg for subject 2 on the PTB socket (left) and the Hydrocast socket (right) measured using B.E.S.T transducers at the medial sites.
n = number of tests represented in each summary curve.

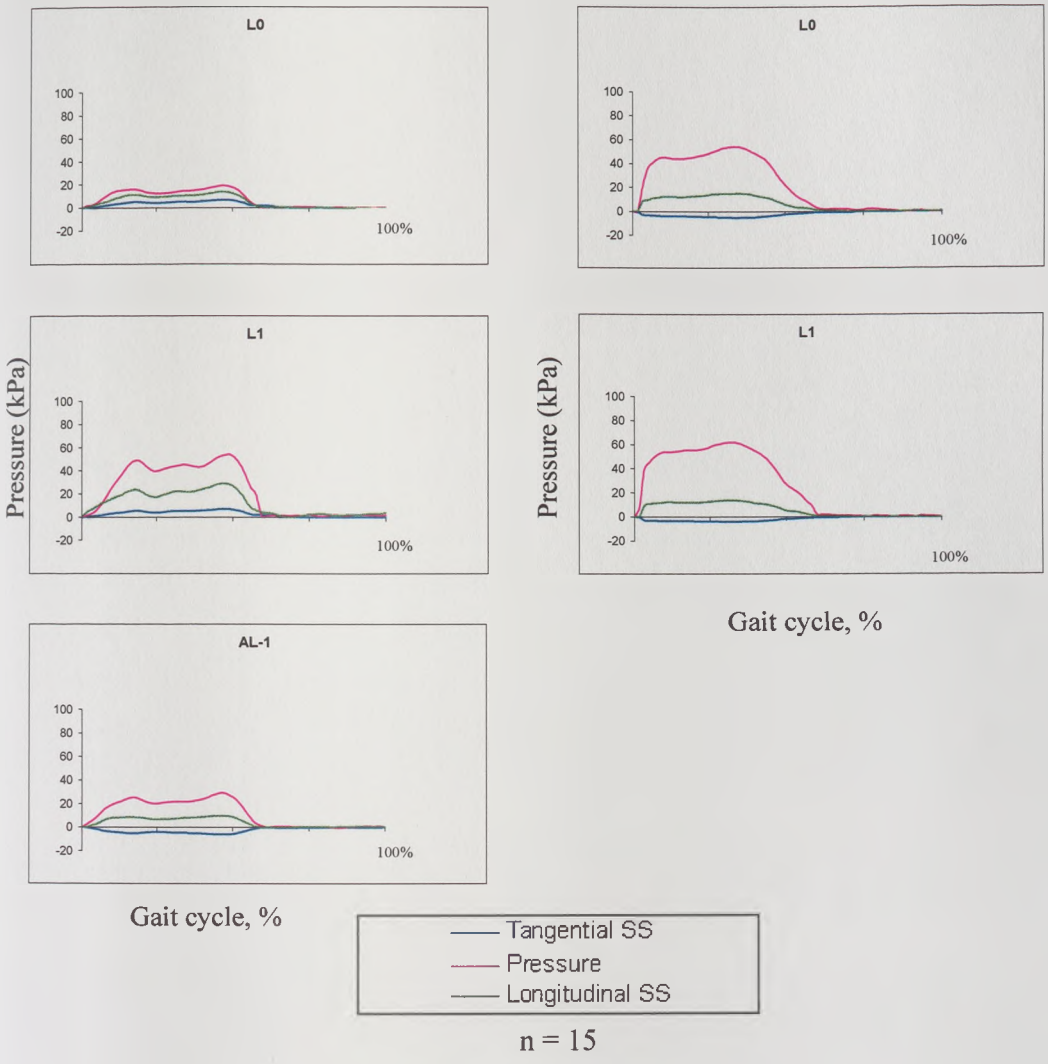

Figure 7.28: Interface pressure and shear stresses results (kPa) versus percentage of the gait cycle (one division = 25%), heel strike to heel strike of the prosthetic leg for subject 2 on the PTB socket (left) and the Hydrocast socket (right) measured using B.E.S.T transducers at the lateral sites.
n = number of tests represented in each summary curve.

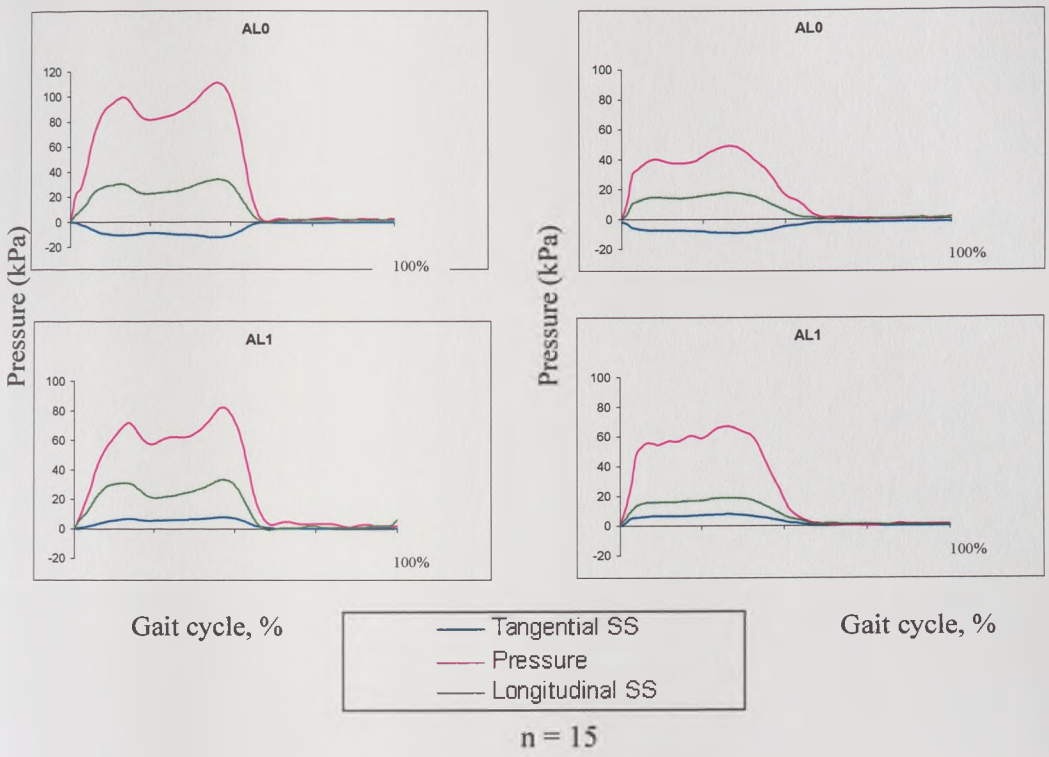

..Contd…Figure 7.28: Interface pressure and shear stresses results (kPa) versus percentage of the gait cycle (one division = 25%), heel strike to heel strike of the prosthetic leg for subject 2 on the PTB socket (left) and the Hydrocast socket (right) measured using B.E.S.T transducers at the lateral sites.
n = number of tests represented in each summary curve.

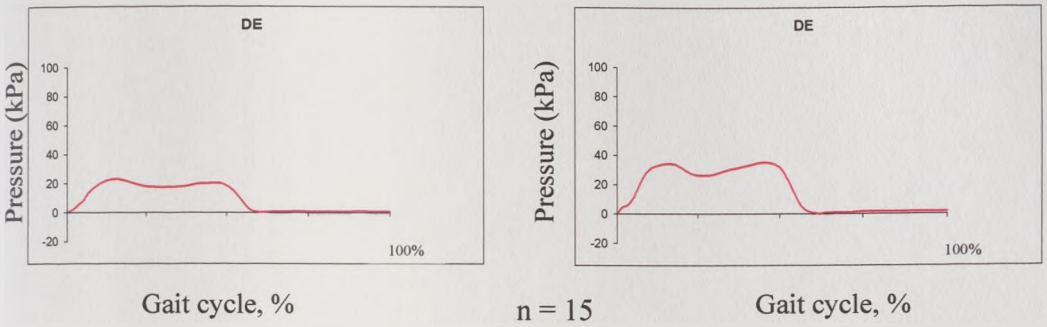

Figure 7.29: Interface pressure (kPa) versus percentage of the gait cycle (one division = 25%), heel strike to heel strike of the prosthetic leg for subject 2 on the PTB socket (left) and the Hydrocast socket (right) measured using electrohydraulic transducer at the distal end site.
n = number of tests represented in each summary curve.

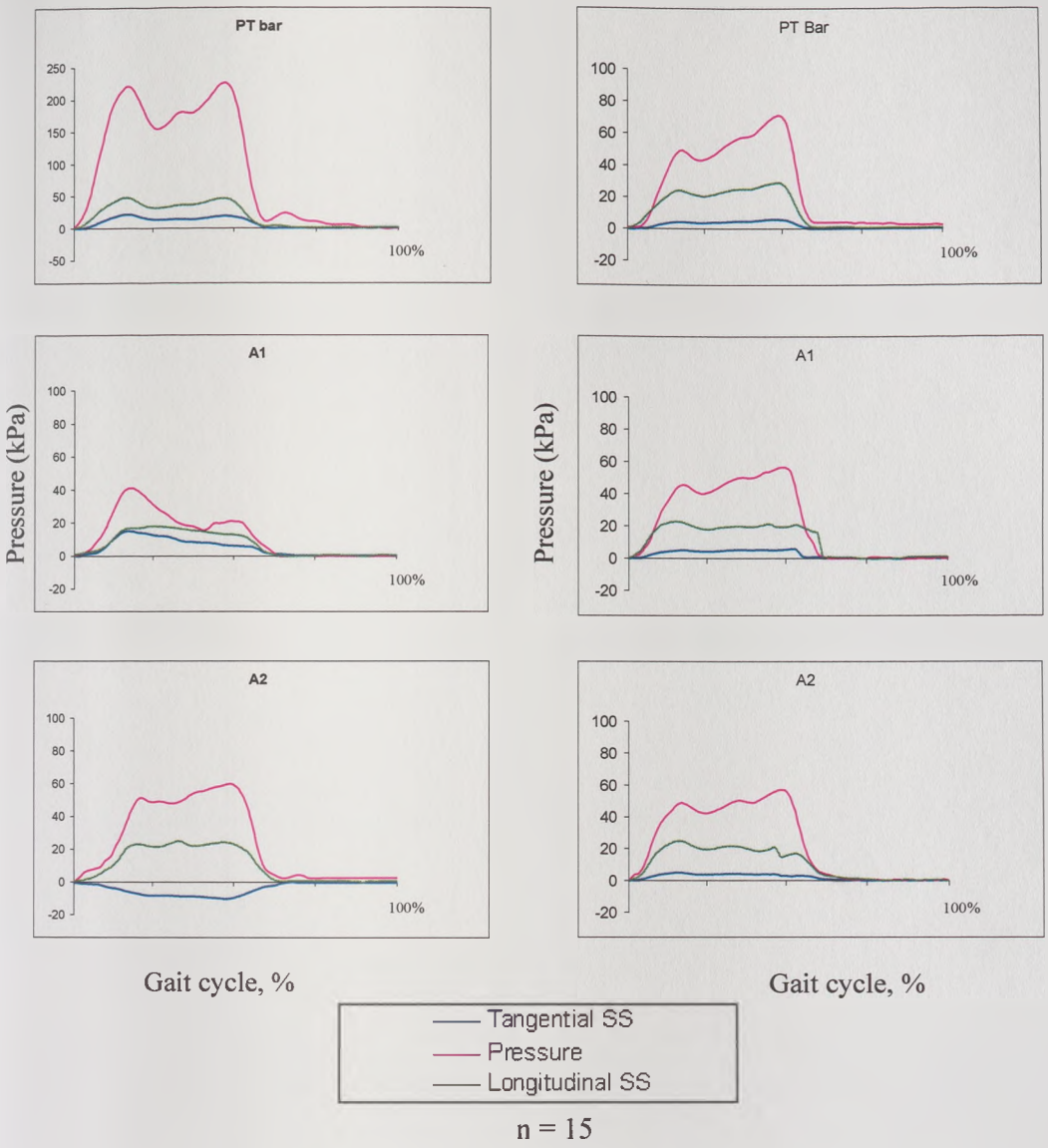

Figure 7.30: Interface pressure and shear stresses results (kPa) versus percentage of the gait cycle (one division = 25%), heel strike to heel strike of the prosthetic leg for subject 3 on the PTB socket (left) and the Hydrocast socket (right) measured using B.E.S.T transducers at the anterior sites.
n = number of tests represented in each summary curve.

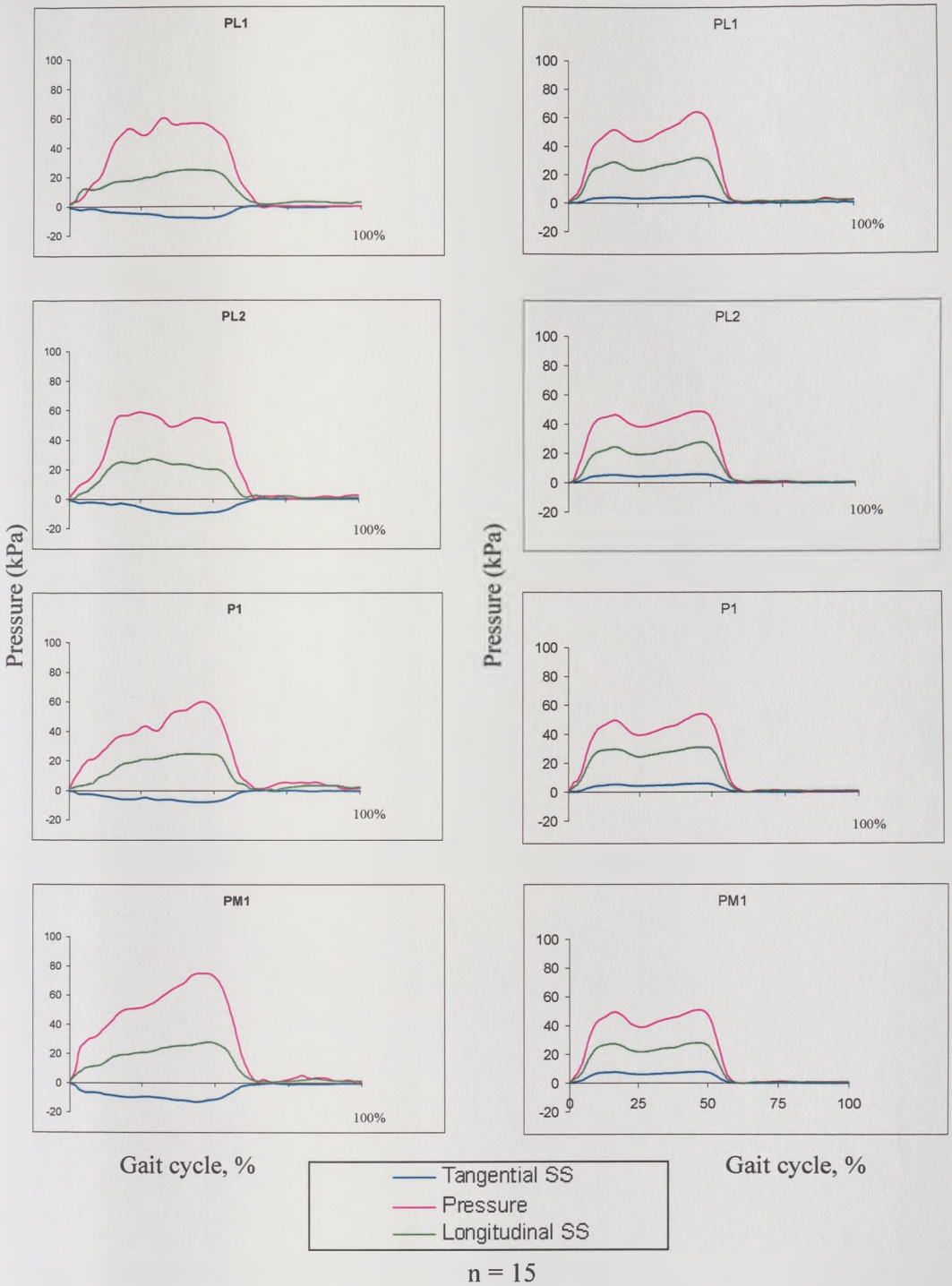

Figure 7.31: Interface pressure and shear stresses results (kPa) versus percentage of the gait cycle (one division = 25%), heel strike to heel strike of the prosthetic leg for subject 3 on the PTB socket (left) and the Hydrocast socket (right) measured using B.E.S.T transducers at the posterior sites.
n = number of tests represented in each summary curve.

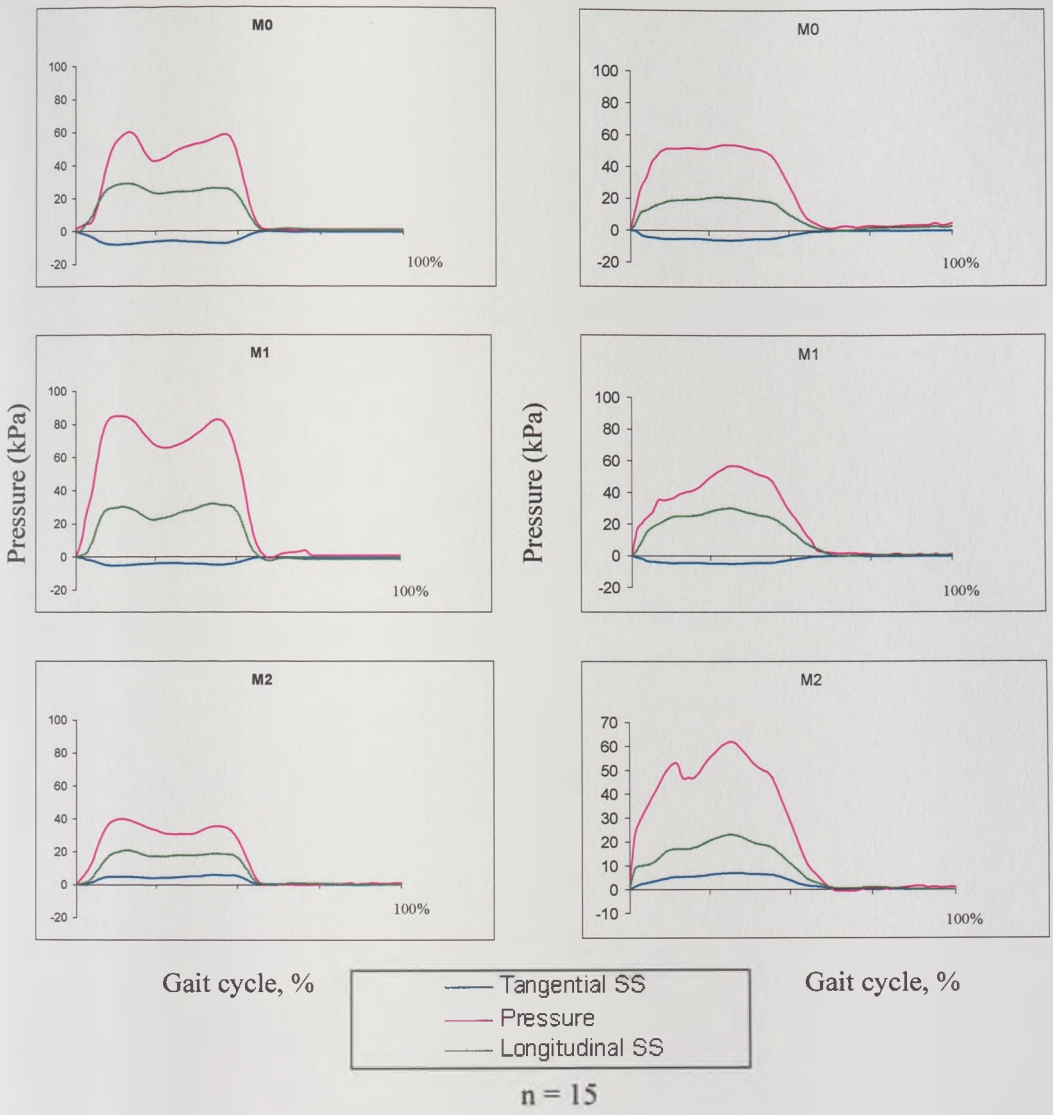

Figure 7.32: Interface pressure and shear stresses results (kPa) versus percentage of the gait cycle (one division = 25%), heel strike to heel strike of the prosthetic leg for subject 3 on the PTB socket (left) and the Hydrocast socket (right) measured using B.E.S.T transducers at the medial sites.
n = number of tests represented in each summary curve.

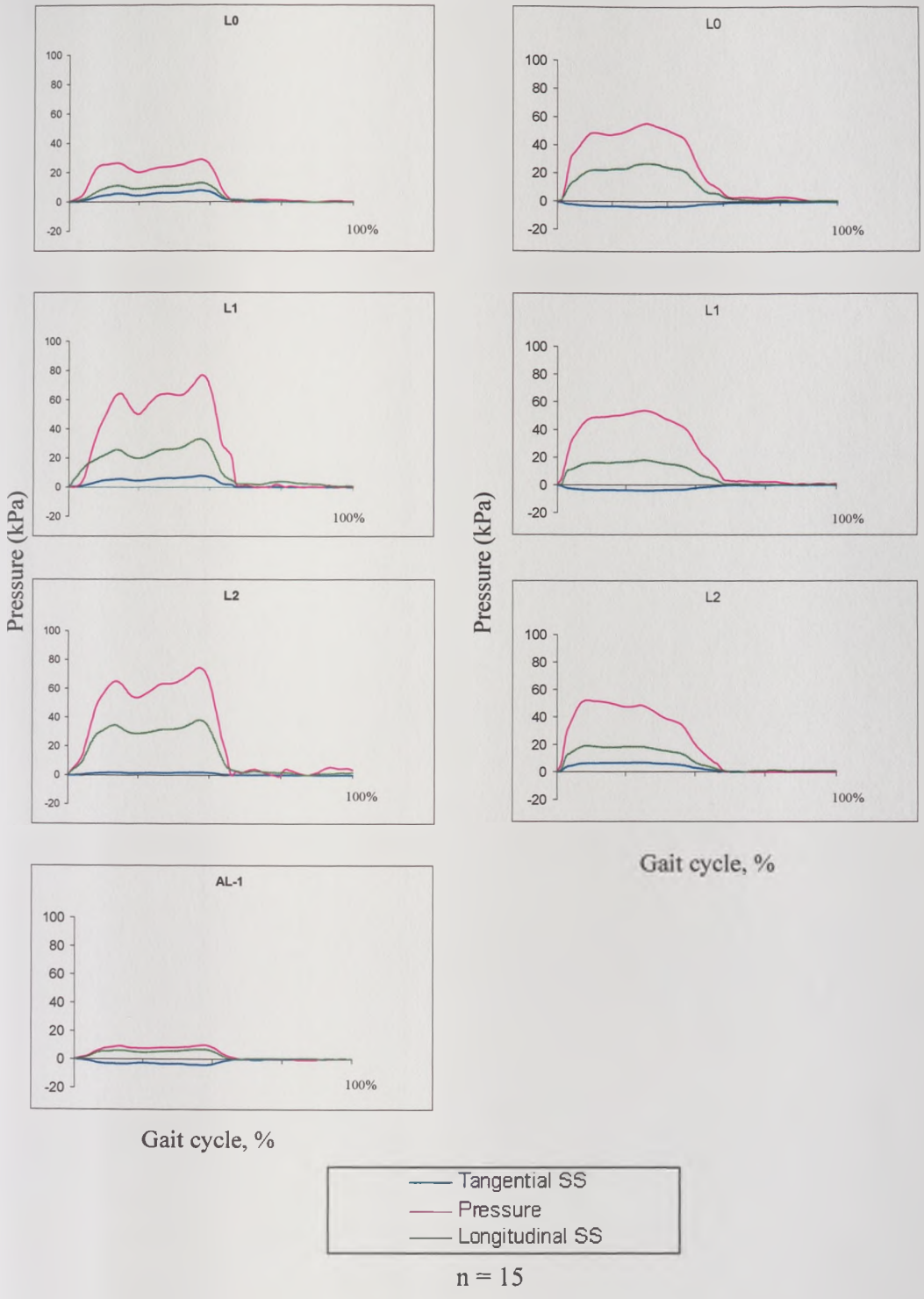

Figure 7.33: Interface pressure and shear stresses results (kPa) versus percentage of the gait cycle (one division = 25%), heel strike to heel strike of the prosthetic leg for subject 3 on the PTB socket (left) and the Hydrocast socket (right) measured using B.E.S.T transducers at the lateral sites.
n = number of tests represented in each summary curve.

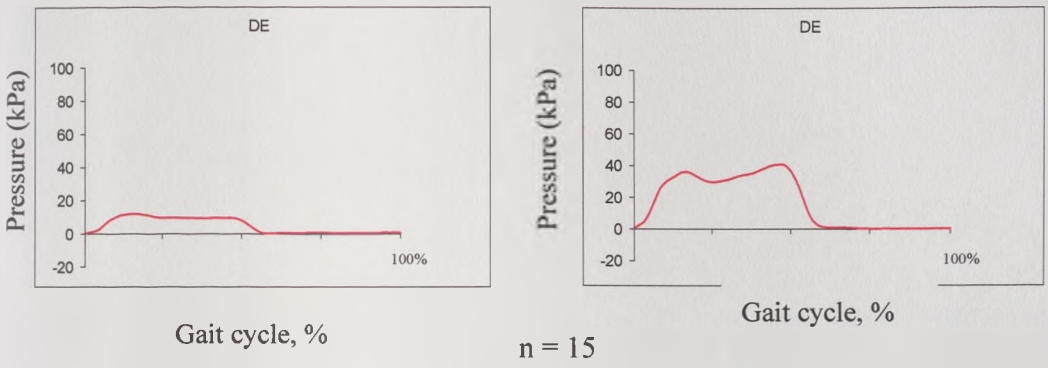

n = 15

Figure 7.34: Interface pressure (kPa) versus percentage of the gait cycle (one division = 25%), heel strike to heel strike of the prosthetic leg for subject 3 on the PTB socket (left) and the Hydrocast socket (right) measured using electrohydraulic transducers at the distal end site.
n = number of tests represented in each summary curve.

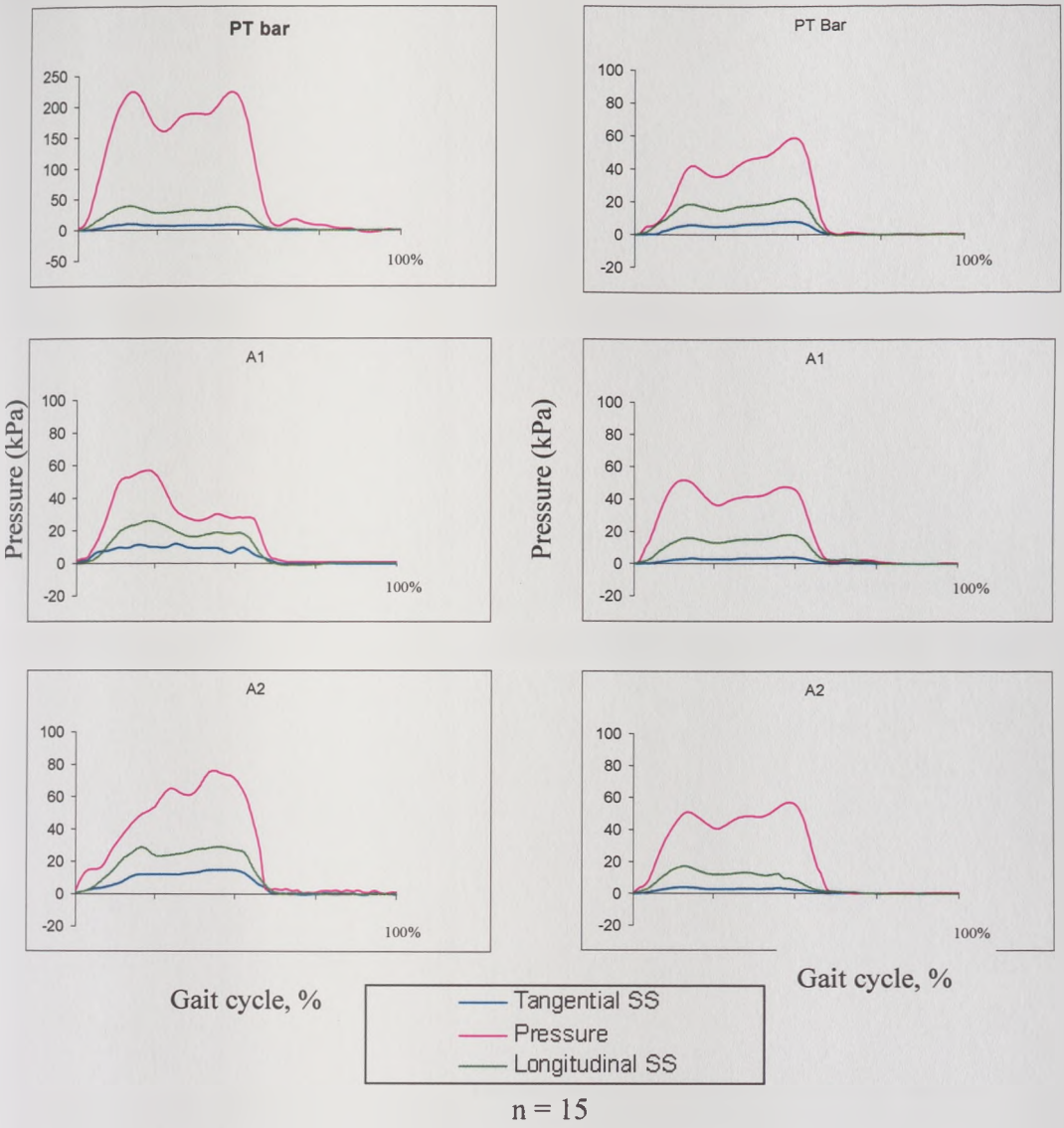

Figure 7.35:Interface pressure and shear stresses results (kPa) versus percentage of the gait cycle (one division = 25%), heel strike to heel strike of the prosthetic leg for subject 4 on the PTB socket (left) and the Hydrocast socket (right) measured using B.E.S.T transducers at the anterior sites.
n = number of tests represented in each summary curve.

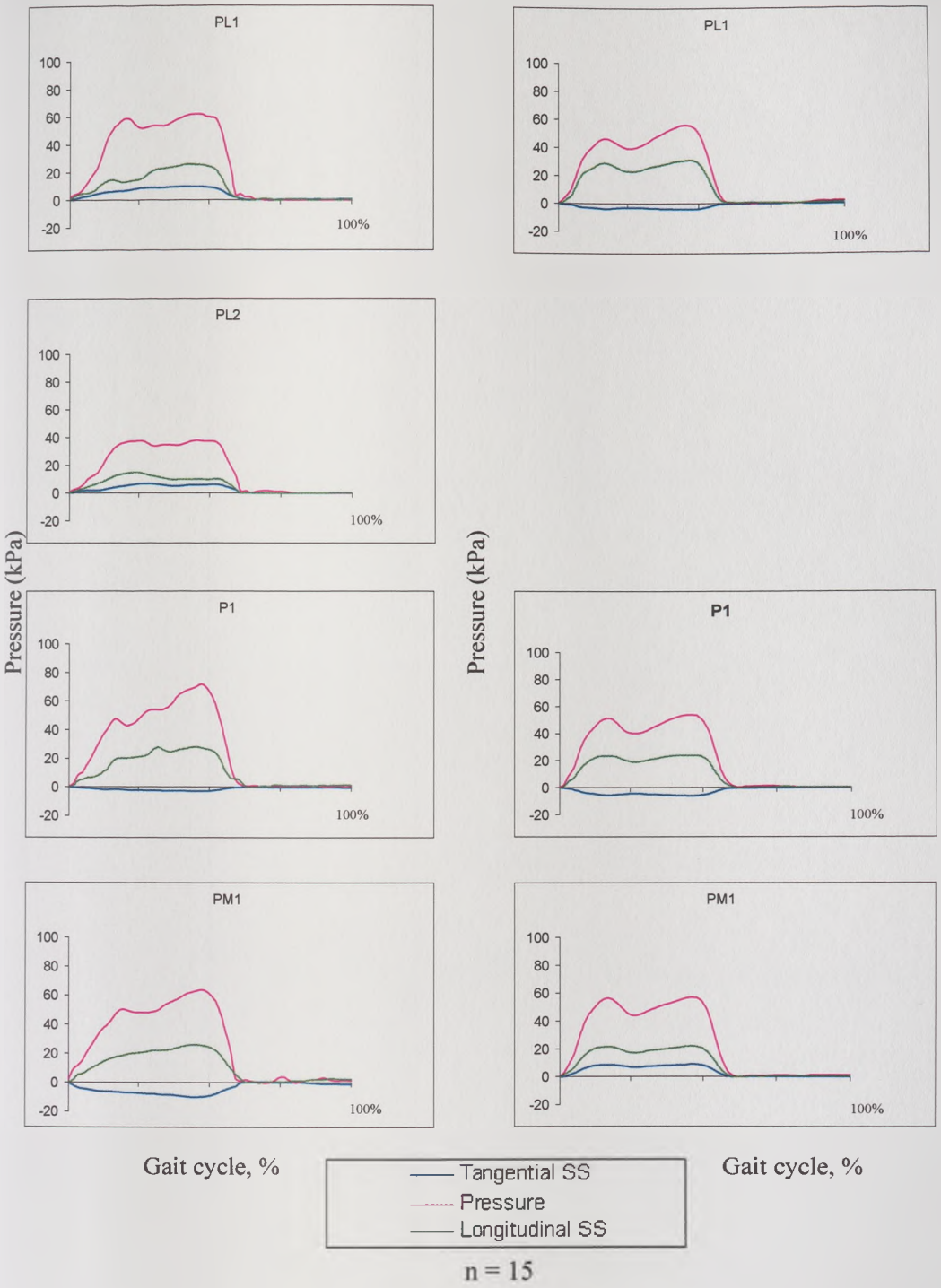

Figure 7.36: Interface pressure and shear stresses results (kPa) versus percentage of the gait cycle (one division = 25%), heel strike to heel strike of the prosthetic leg for subject 4 on the PTB socket (left) and the Hydrocast socket (right) measured using B.E.S.T transducers at the posterior sites.
n = number of tests represented in each summary curve.

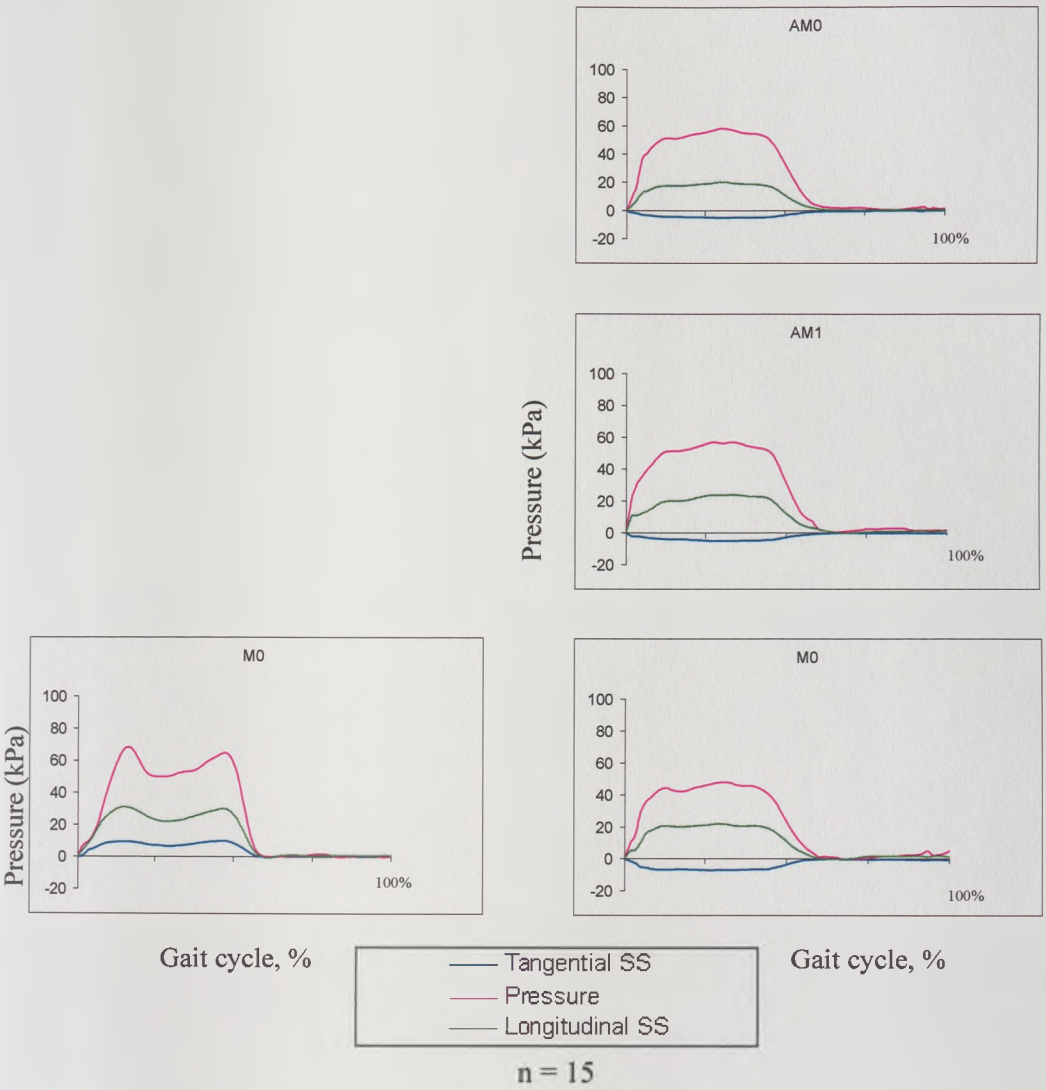

Figure 7.37: Interface pressure and shear stresses results (kPa) versus percentage of the gait cycle (one division = 25%), heel strike to heel strike of the prosthetic leg for subject 4 on the PTB socket (left) and the Hydrocast socket (right) measured using B.E.S.T transducers at the medial sites.
n = number of tests represented in each summary curve.

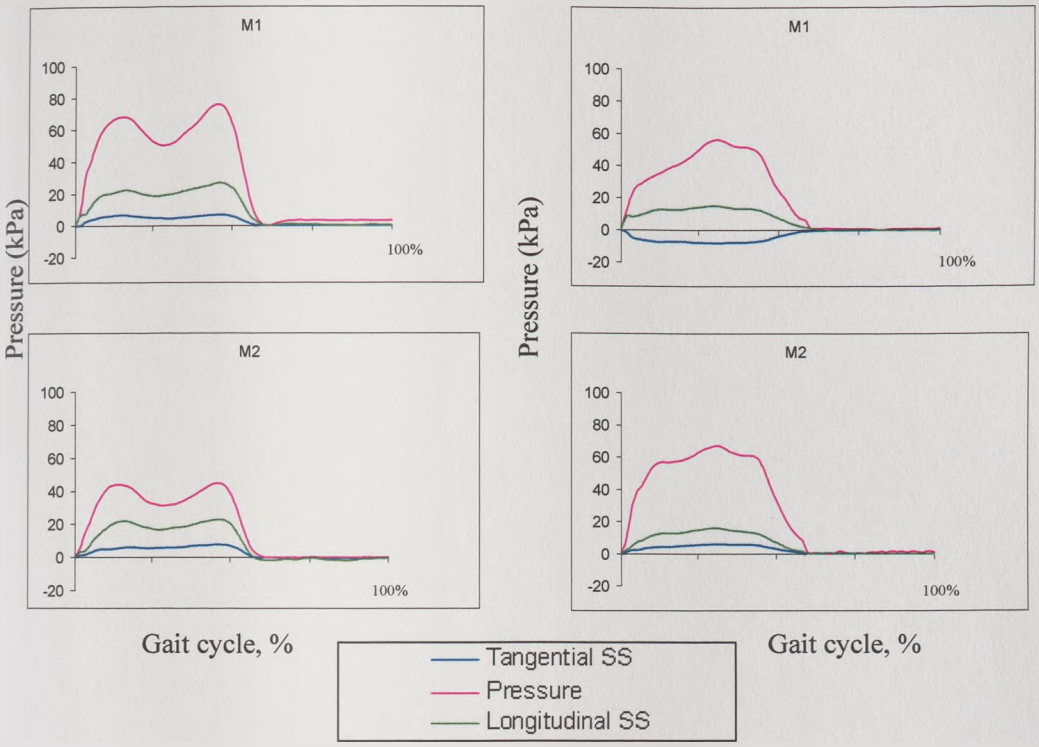

n = 15

...Contd....Figure 7.37: Interface pressure and shear stresses results (kPa) versus percentage of the gait cycle (one division = 25%), heel strike to heel strike of the prosthetic leg for subject 4 on the PTB socket (left) and the Hydrocast socket (right) measured using B.E.S.T transducers at the medial sites.
n = number of tests represented in each summary curve.

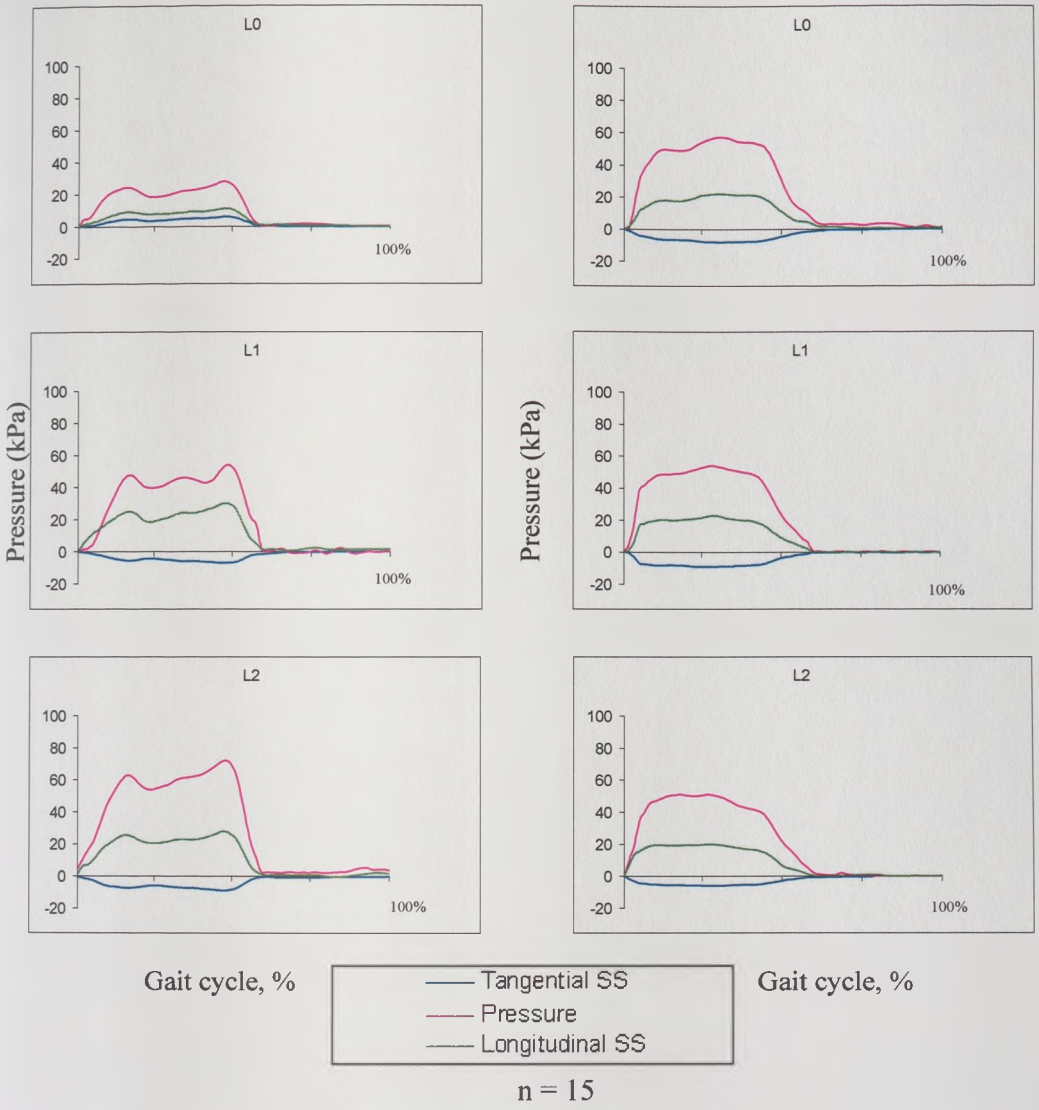

Figure 7.38: Interface pressure and shear stresses results (kPa) versus percentage of the gait cycle (one division = 25%), heel strike to heel strike of the prosthetic leg for subject 4 on the PTB socket (left) and the Hydrocast socket (right) measured using B.E.S.T transducers at the lateral sites.
n = number of tests represented in each summary curve.

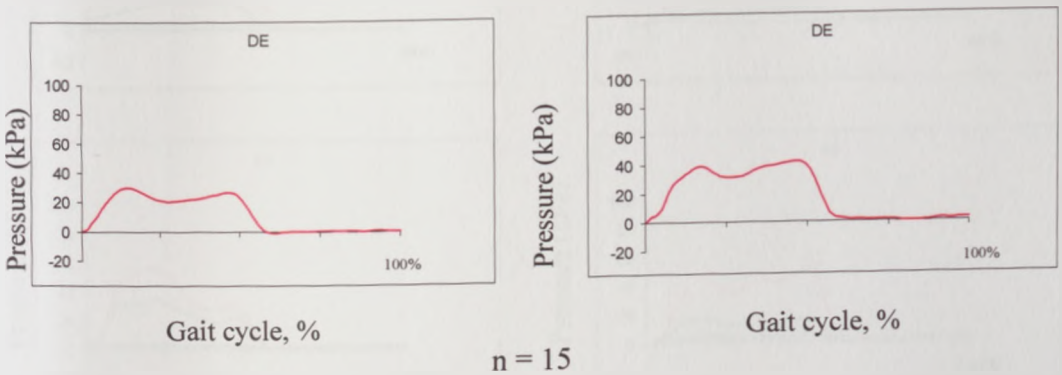

n = 15

Figure 7.39: Interface pressure (kPa) versus percentage of the gait cycle (one division = 25%), heel strike to heel strike of the prosthetic leg for subject 4 on the PTB socket (left) and the Hydrocast socket (right) measured using electrohydraulic transducers at the distal end site.
n = number of tests represented in each summary curve.

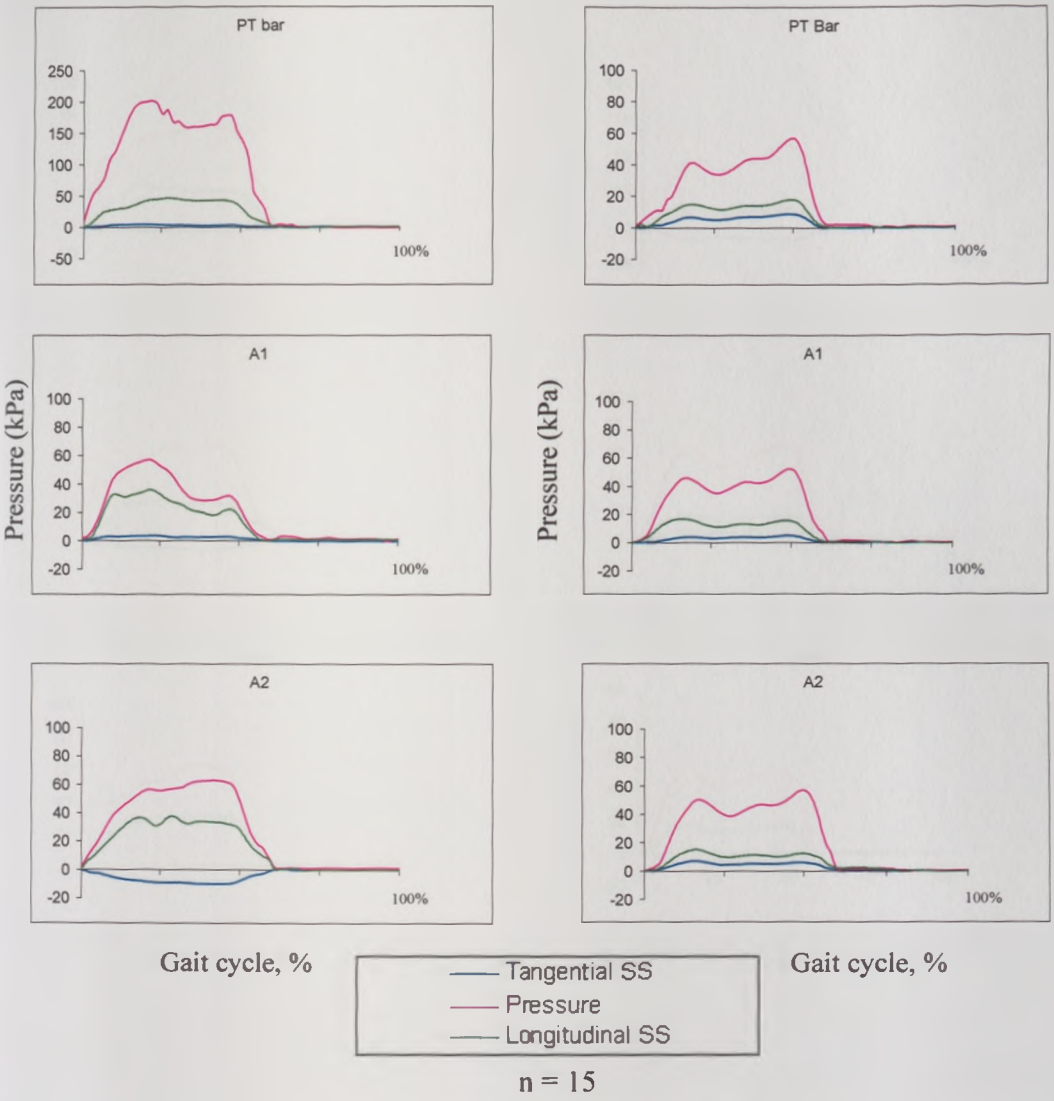

Figure 7.40: Interface pressure and shear stresses results (kPa) versus percentage of the gait cycle (one division = 25%), heel strike to heel strike of the prosthetic leg for subject 5 on the PTB socket (left) and the Hydrocast socket (right) measured using B.E.S.T transducers at the anterior sites.
n = number of tests represented in each summary curve.

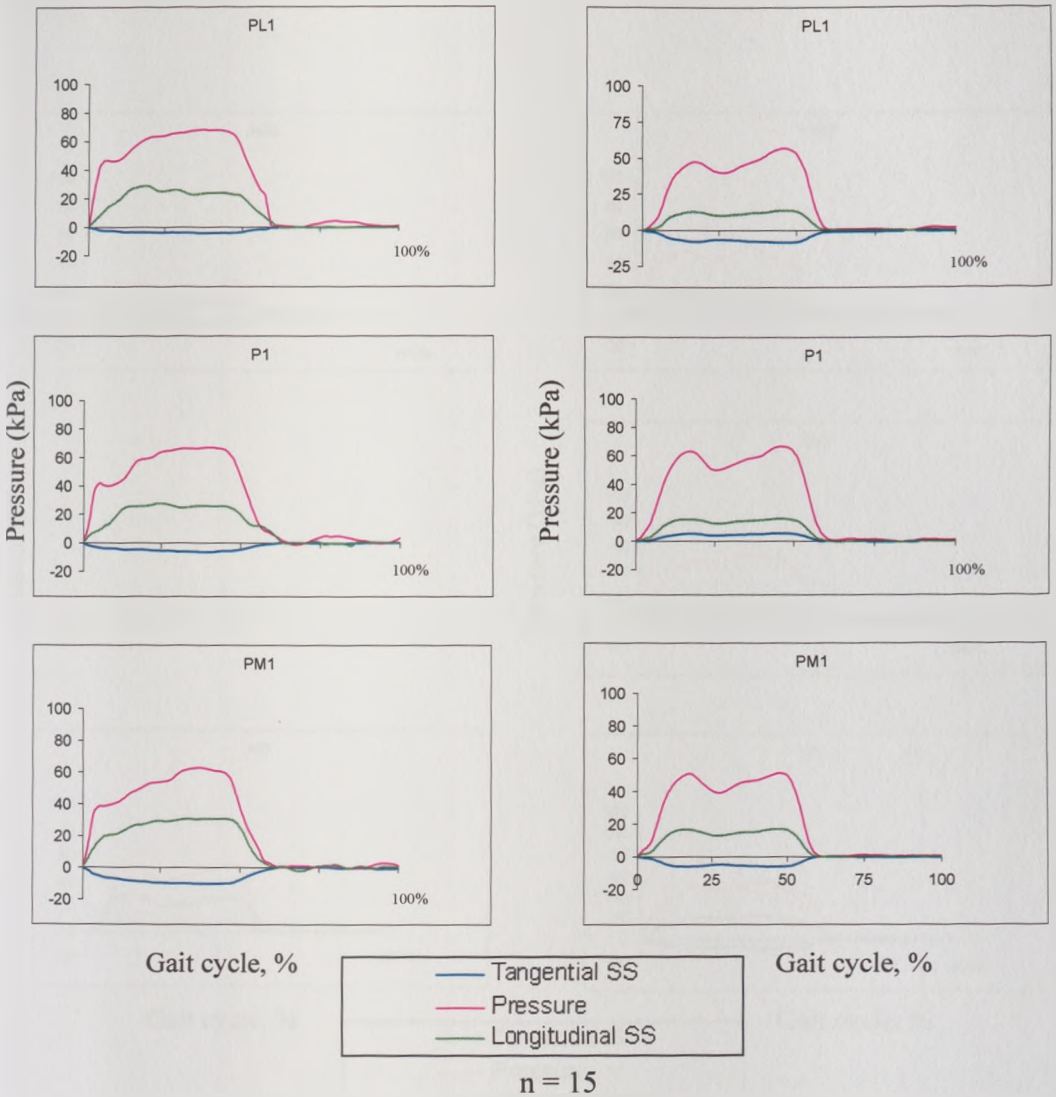

Figure 7.41: Interface pressure and shear stresses results (kPa) versus percentage of the gait cycle (one division = 25%), heel strike to heel strike of the prosthetic leg for subject 5 on the PTB socket (left) and the Hydrocast socket (right) measured using B.E.S.T transducers at the posterior sites.
n = number of tests represented in each summary curve.

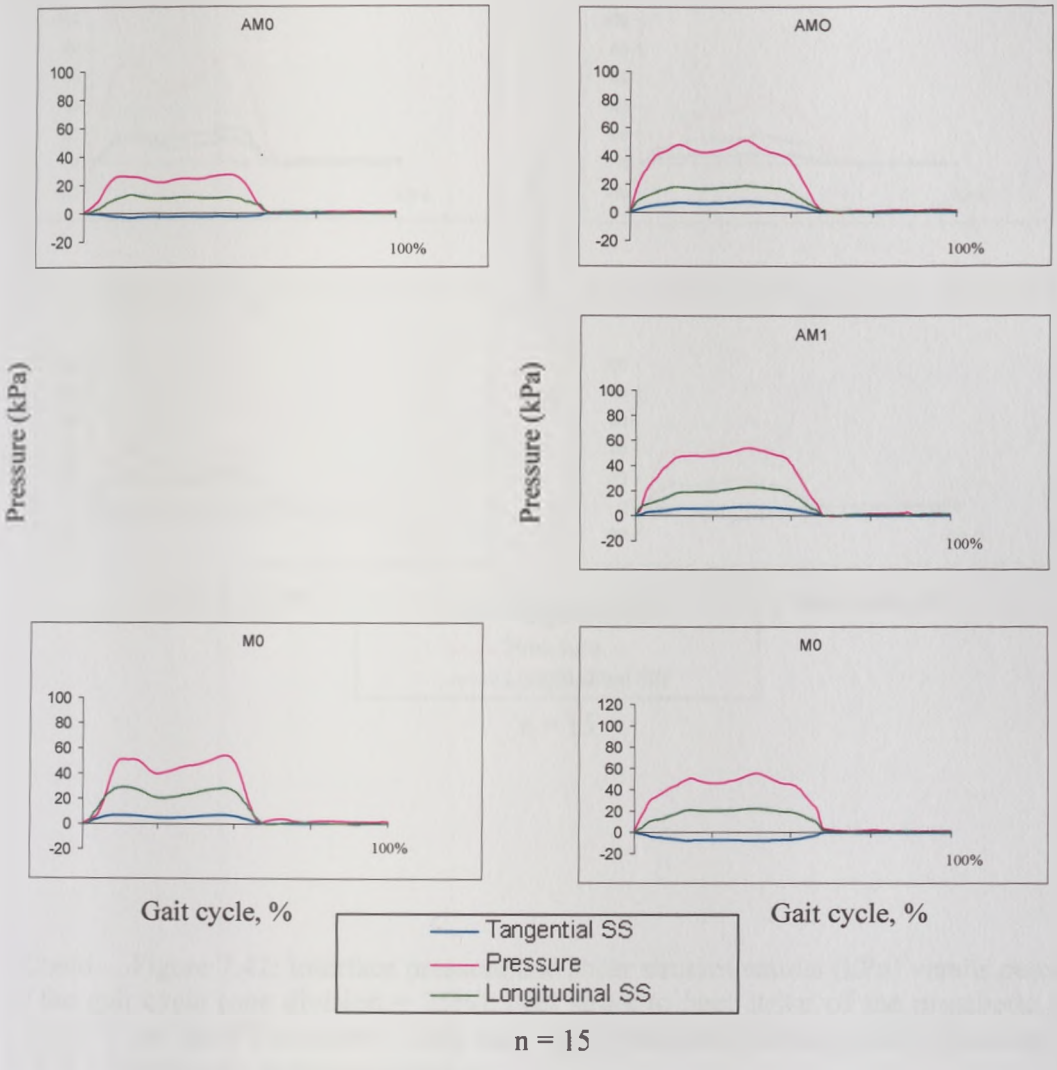

Figure 7.42: Interface pressure and shear stresses results (kPa) versus percentage of the gait cycle (one division = 25%), heel strike to heel strike of the prosthetic leg for subject 5 on the PTB socket (left) and the Hydrocast socket (right) measured using B.E.S.T transducers at the medial sites.
n = number of tests represented in each summary curve.

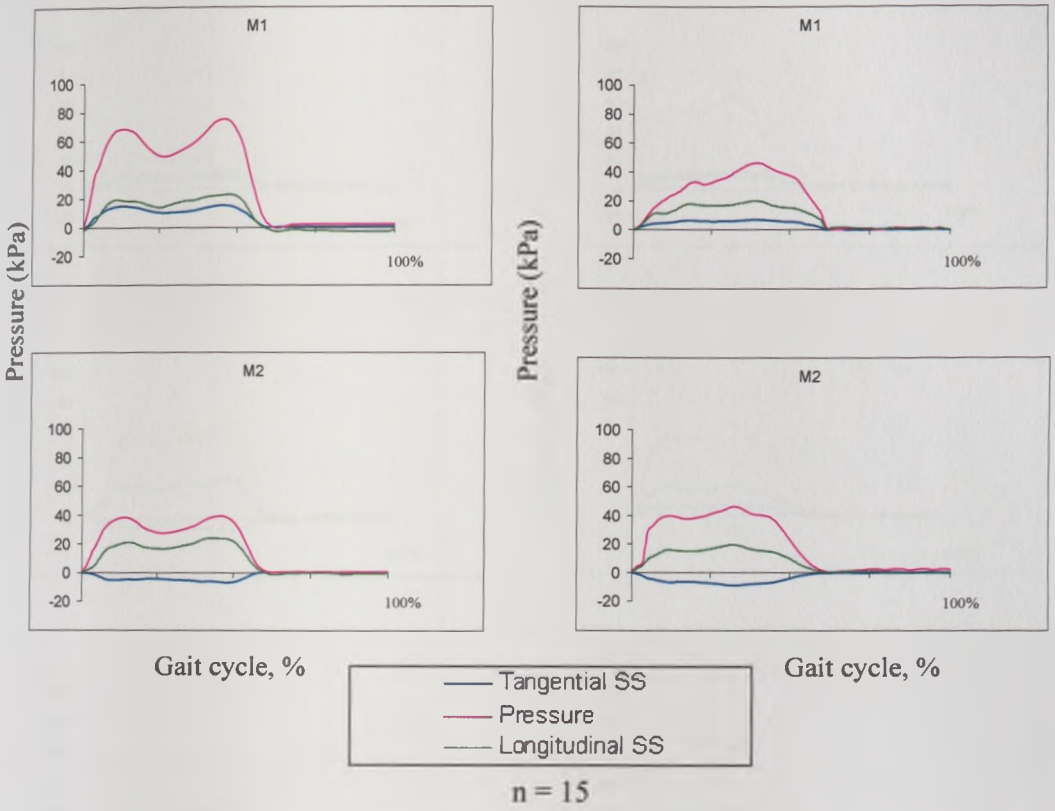

..Contd....Figure 7.42: Interface pressure and shear stresses results (kPa) versus percentage of the gait cycle (one division = 25%), heel strike to heel strike of the prosthetic leg for subject 5 on the PTB socket (left) and the Hydrocast socket (right) measured using B.E.S.T transducers at the medial sites.
n = number of tests represented in each summary curve.

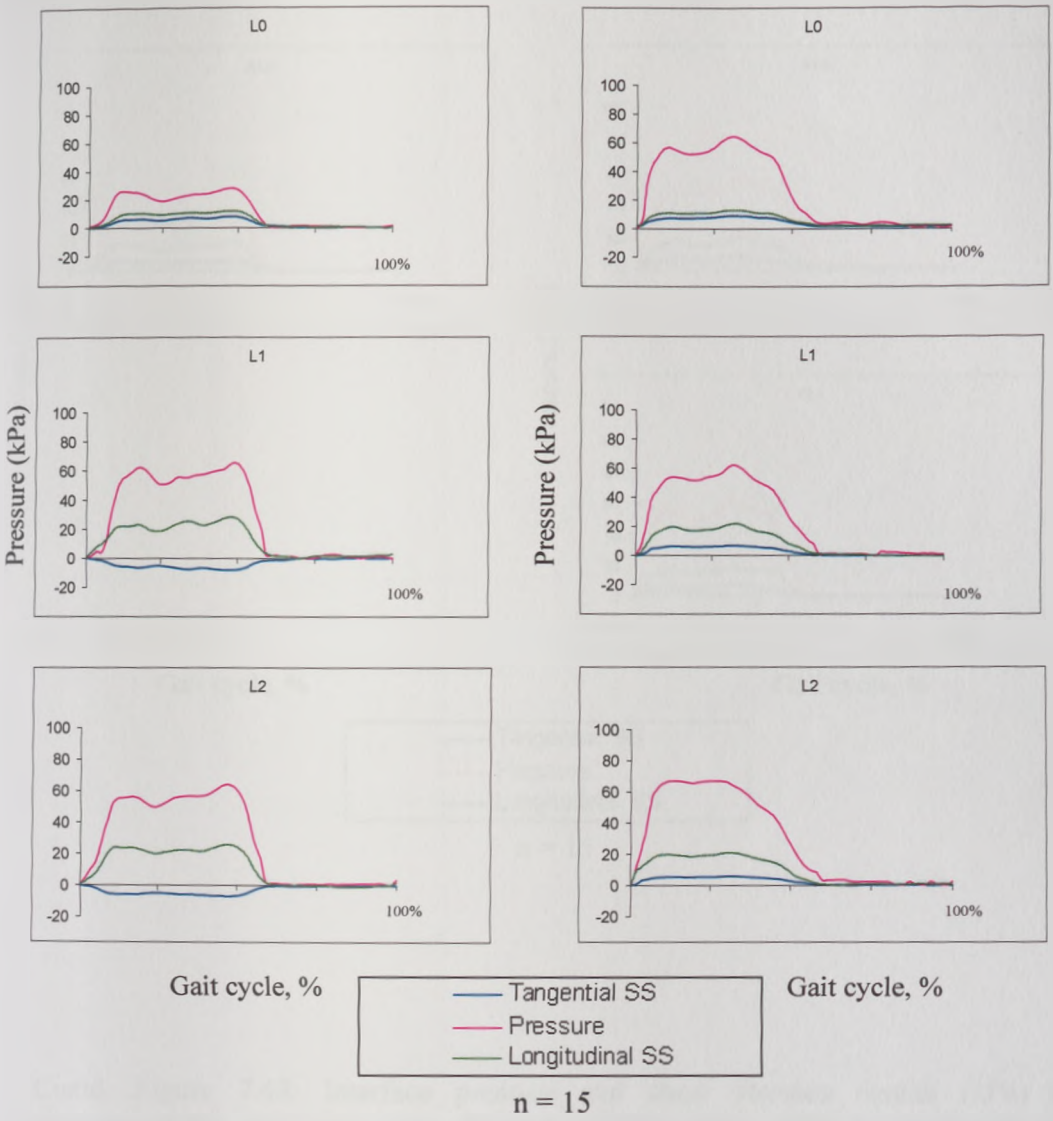

Figure 7.43: Interface pressure and shear stresses results (kPa) versus percentage of the gait cycle (one division = 25%), heel strike to heel strike of the prosthetic leg for subject 5 on the PTB socket (left) and the Hydrocast socket (right) measured using B.E.S.T transducers at the lateral sites.
n = number of tests represented in each summary curve.

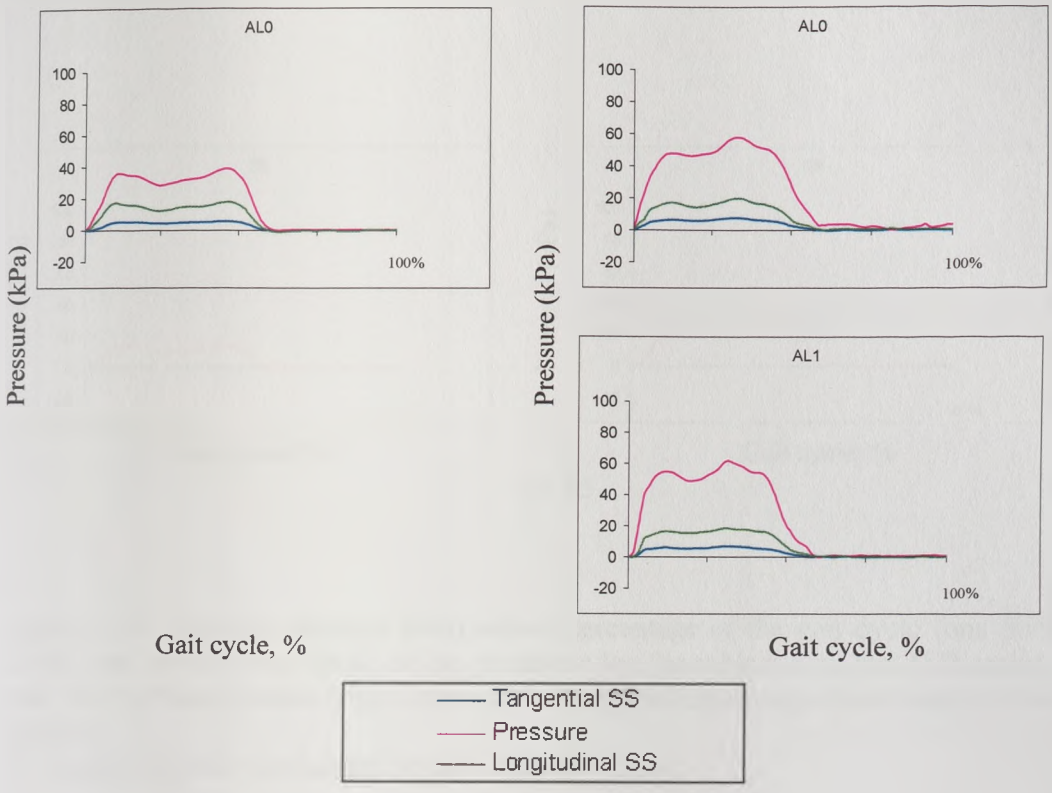

...Contd...Figure 7.43: Interface pressure and shear stresses results (kPa) versus percentage of the gait cycle (one division = 25%), heel strike to heel strike of the prosthetic leg for subject 5 on the PTB socket (left) and the Hydrocast socket (right) measured using B.E.S.T transducers at the lateral sites.
n = number of tests represented in each summary curve.

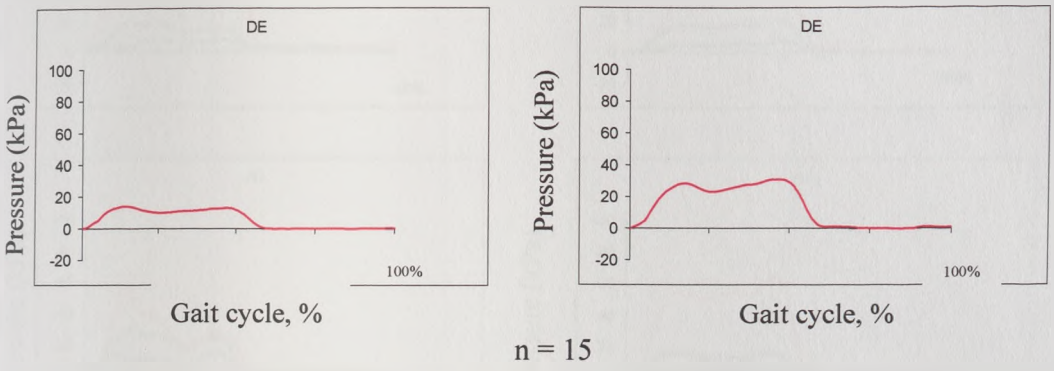

Figure 7.44: Interface pressure (kPa) versus percentage of the gait cycle (one division = 25%), heel strike to heel strike of the prosthetic leg for subject 5 on the PTB socket (left) and the Hydrocast socket (right) measured using electrohydraulic transducers at the distal end site.
n = number of tests represented in each summary curve.

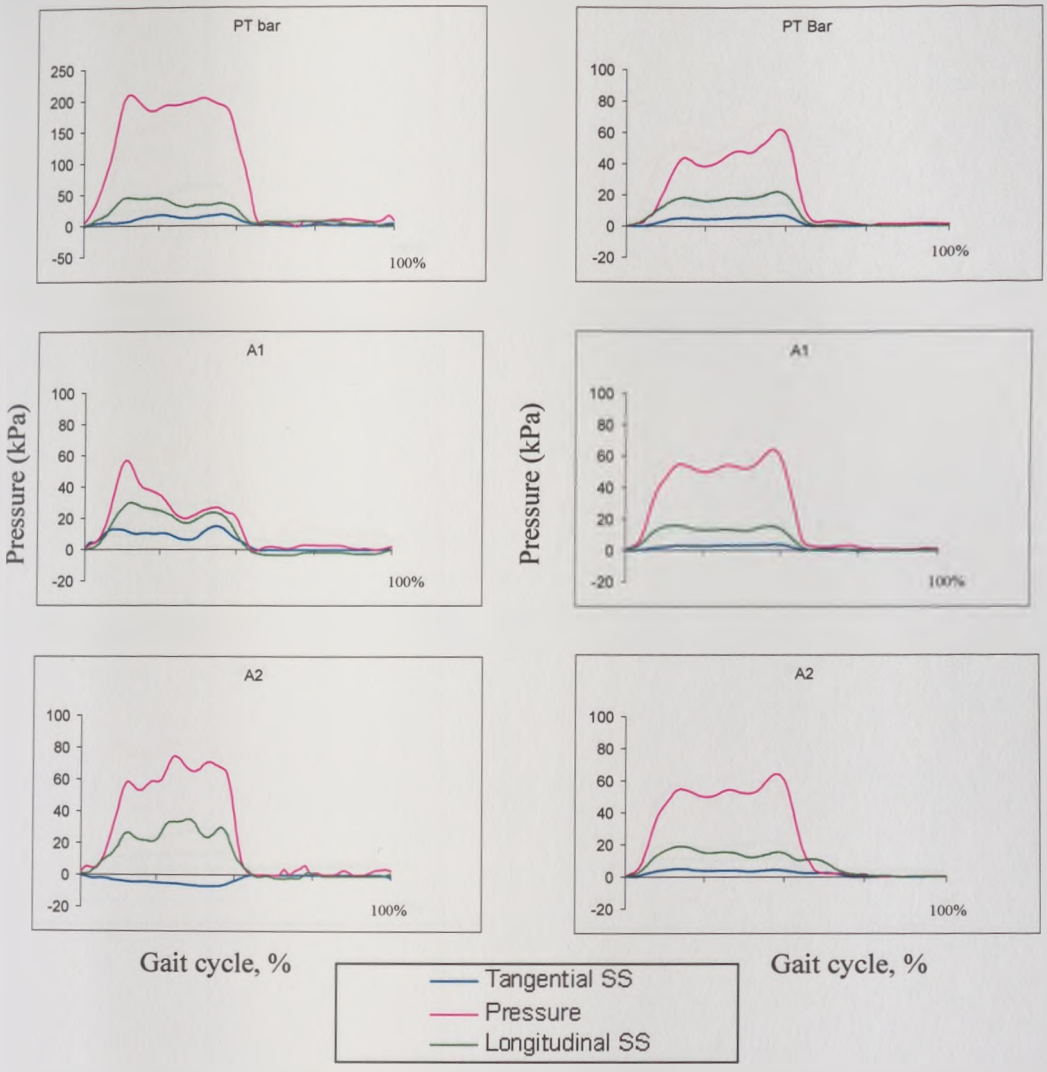

Figure 7.45 : Interface pressure and shear stresses results (kPa) versus percentage of the gait cycle (one division = 25%), heel strike to heel strike of the prosthetic leg for subject 6 on the PTB socket (left) and the Hydrocast socket (right) measured using B.E.S.T transducers at the anterior sites.
n = number of tests represented in each summary curve.

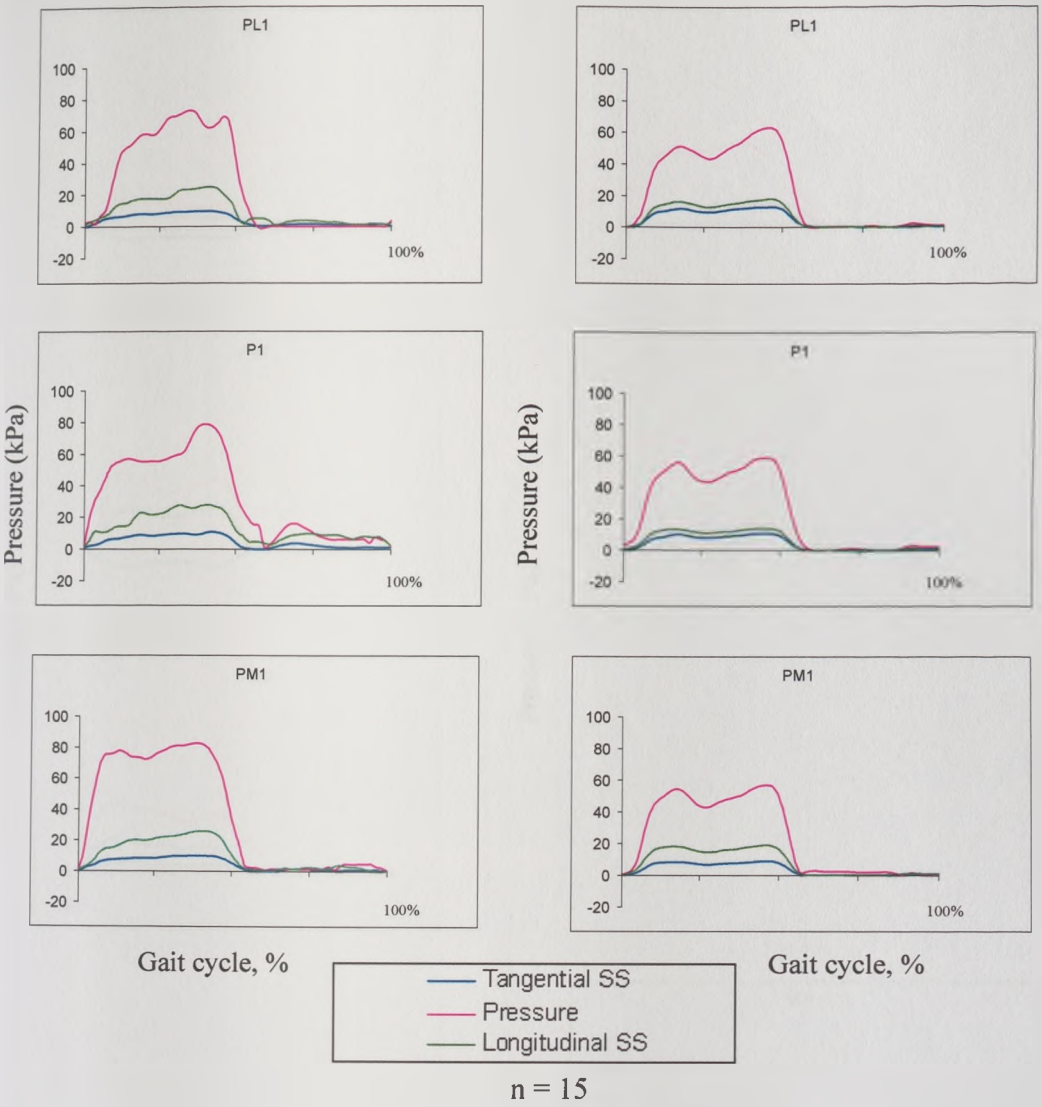

Figure 7.46 : Interface pressure and shear stresses results (kPa) versus percentage of the gait cycle (one division = 25%), heel strike to heel strike of the prosthetic leg for subject 6 on the PTB socket (left) and the Hydrocast socket (right) measured using B.E.S.T transducers at the posterior sites.
n = number of tests represented in each summary curve.

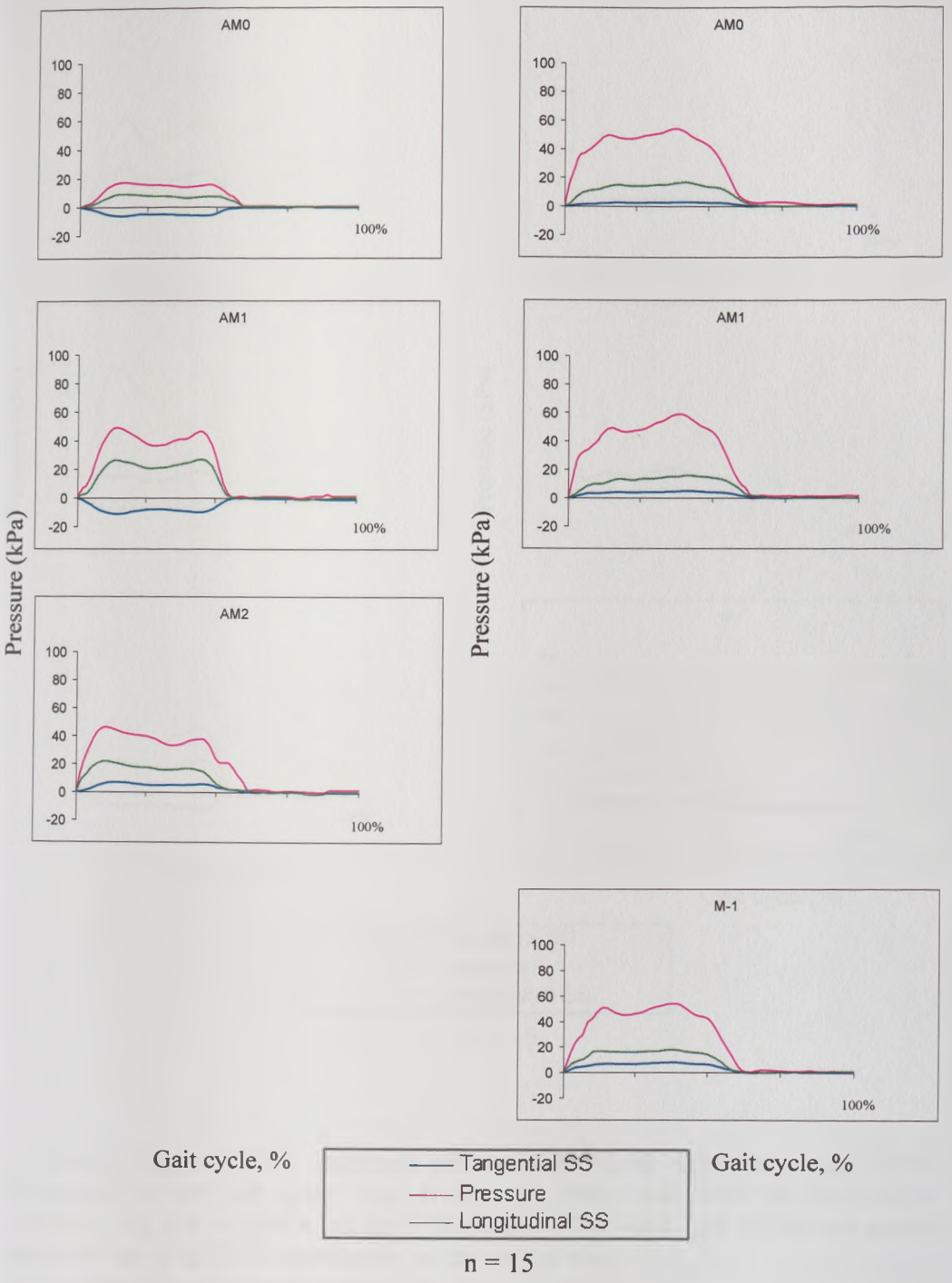

Figure 7.47 : Interface pressure and shear stresses results (kPa) versus percentage of the gait cycle (one division = 25%), heel strike to heel strike of the prosthetic leg for subject 6 on the PTB socket (left) and the Hydrocast socket (right) measured using B.E.S.T transducers at the medial sites.
n = number of tests represented in each summary curve.

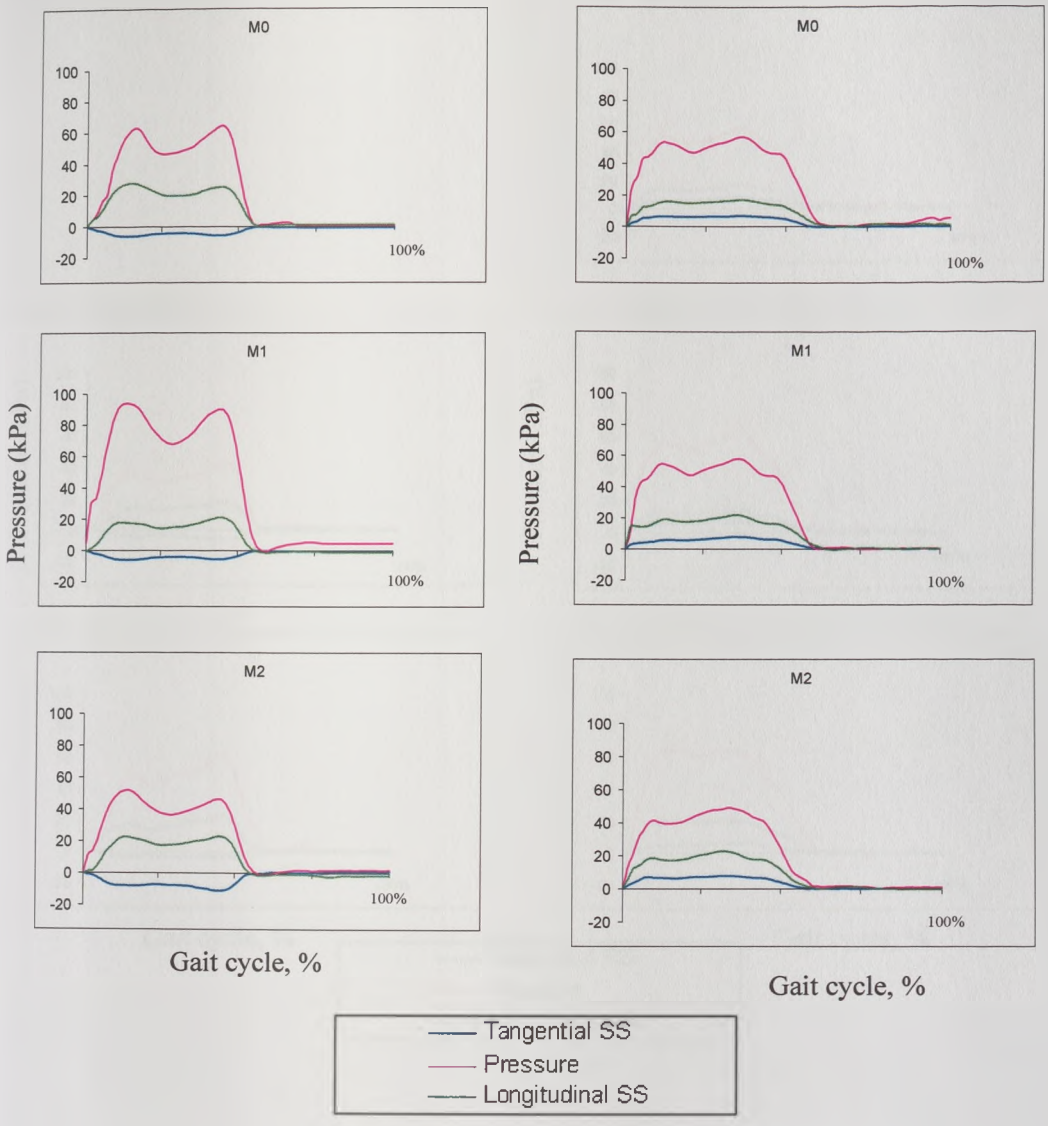

.. Contd....Figure 7.47 : Interface pressure and shear stresses results (kPa) versus percentage of the gait cycle (one division = 25%), heel strike to heel strike of the prosthetic leg for subject 6 on the PTB socket (left) and the Hydrocast socket (right) measured using B.E.S.T transducers at the medial sites.
n = number of tests represented in each summary curve.

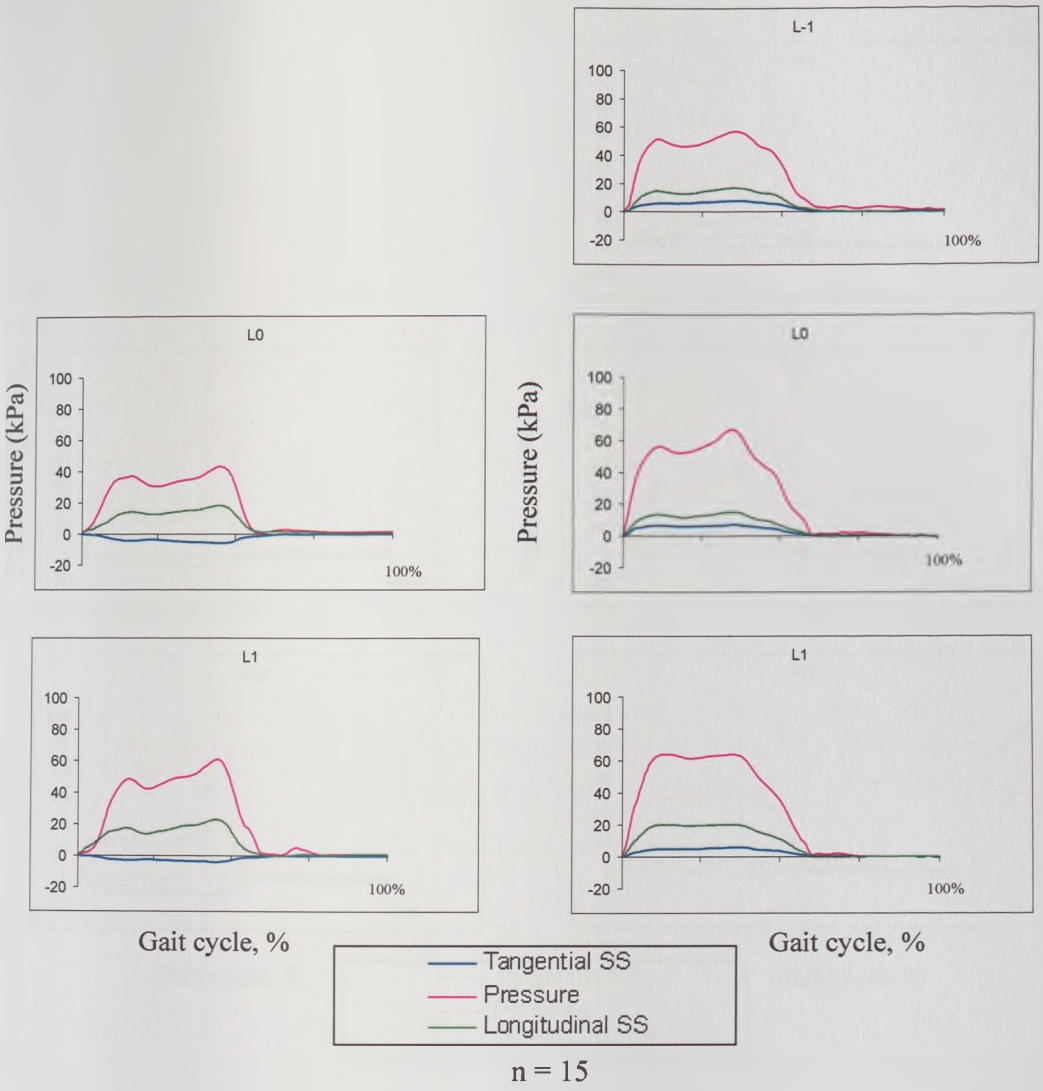

Figure 7.48 : Interface pressure and shear stresses results (kPa) versus percentage of the gait cycle (one division = 25%), heel strike to heel strike of the prosthetic leg for subject 6 on the PTB socket (left) and the Hydrocast socket (right) measured using B.E.S.T transducers at the lateral sites.
n = number of tests represented in each summary curve.

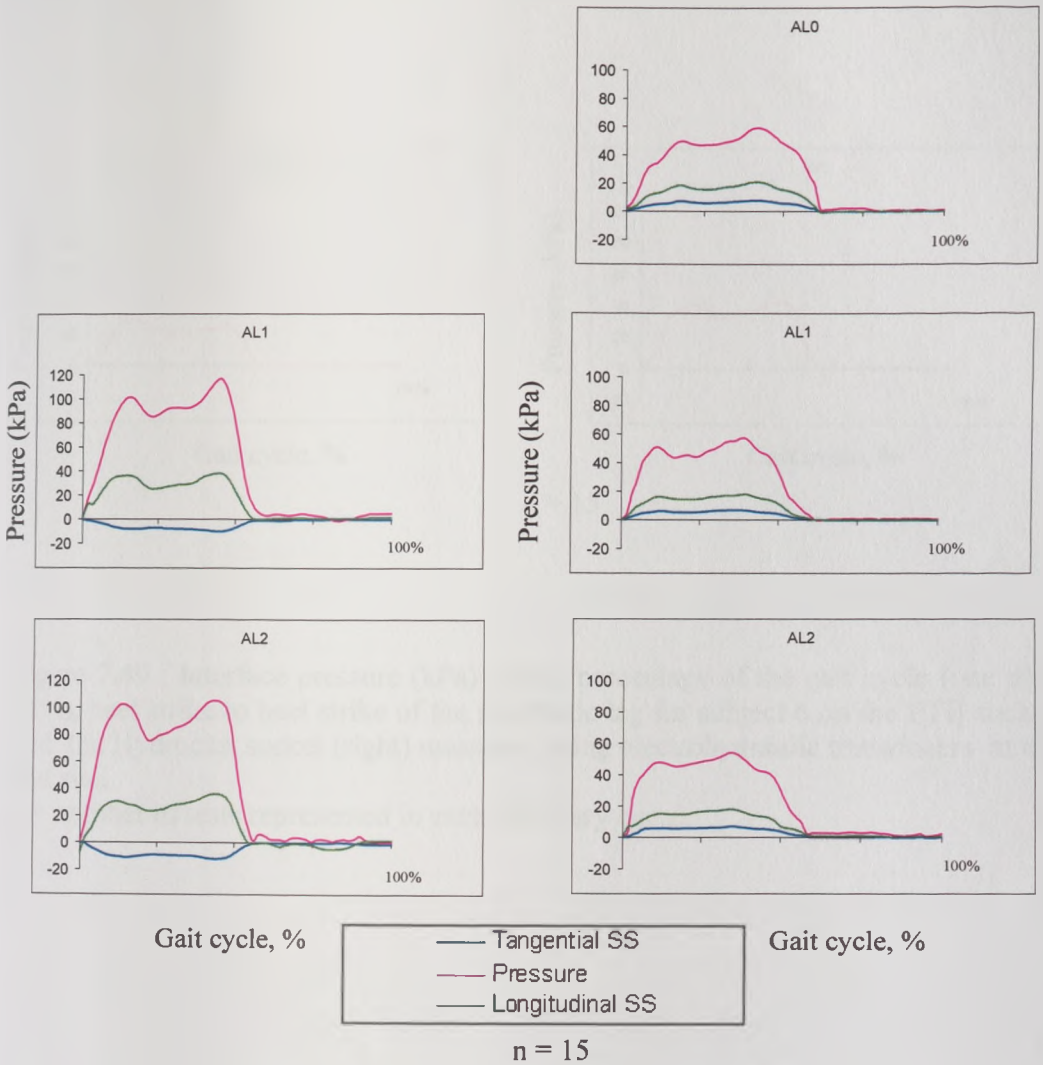

..Contd....Figure 7.48 : Interface pressure and shear stresses results (kPa) versus percentage of the gait cycle (one division = 25%), heel strike to heel strike of the prosthetic leg for subject 6 on the PTB socket (left) and the Hydrocast socket (right) measured using B.E.S.T transducers at the lateral sites.
n = number of tests represented in each summary curve.

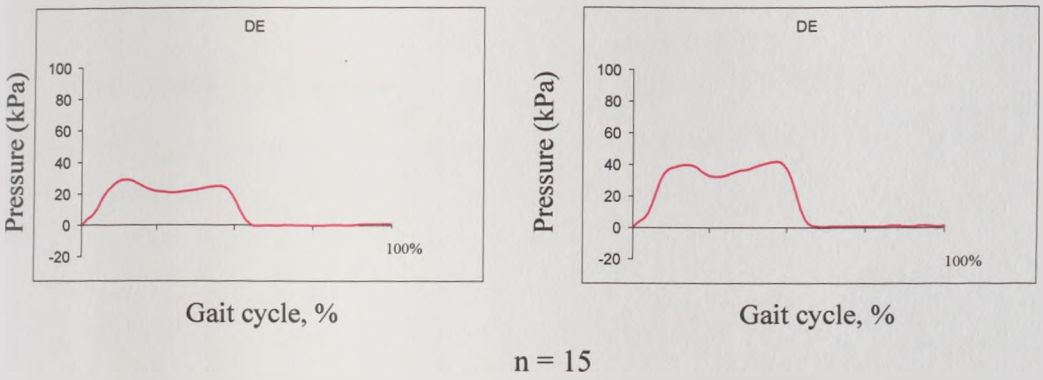

Figure 7.49 : Interface pressure (kPa) versus percentage of the gait cycle (one division = 25%), heel strike to heel strike of the prosthetic leg for subject 6 on the PTB socket (left) and the Hydrocast socket (right) measured using electrohydraulic transducers at the distal end site.
n = number of tests represented in each summary curve.

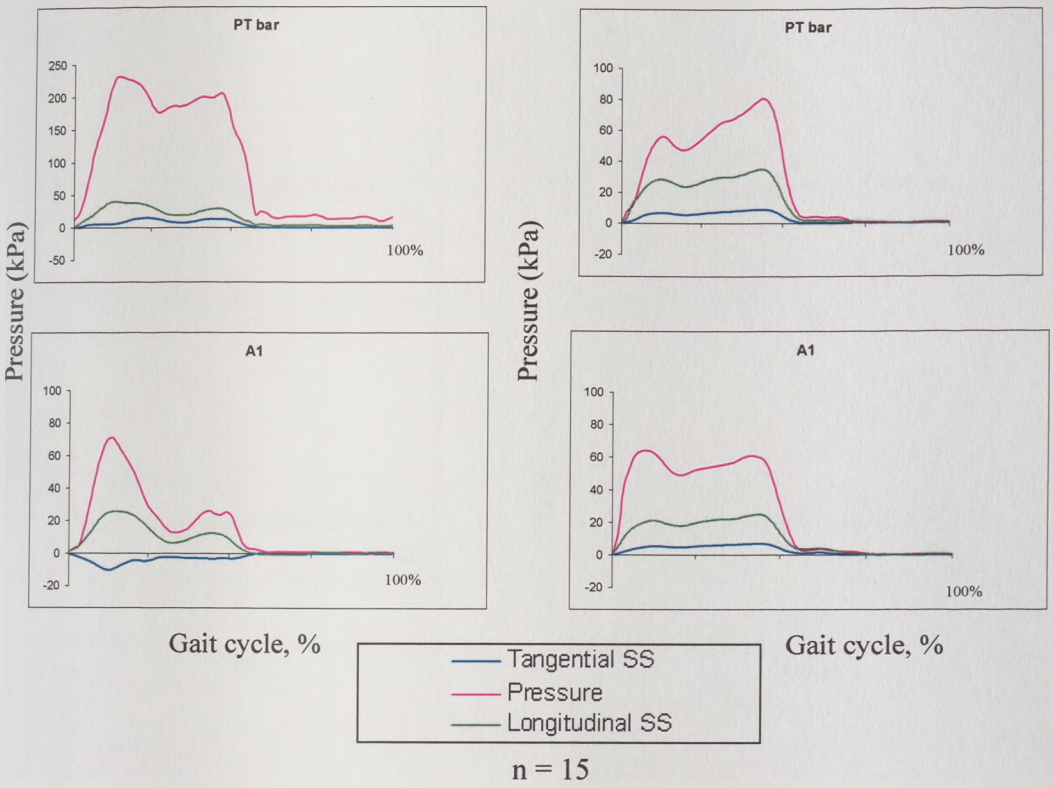

Figure 7.50 : Interface pressure and shear stresses results (kPa) versus percentage of the gait cycle (one division = 25%), heel strike to heel strike of the prosthetic leg for subject 7 on the PTB socket (left) and the Hydrocast socket (right) measured using B.E.S.T transducers at the anterior sites.
n = number of tests represented in each summary curve.

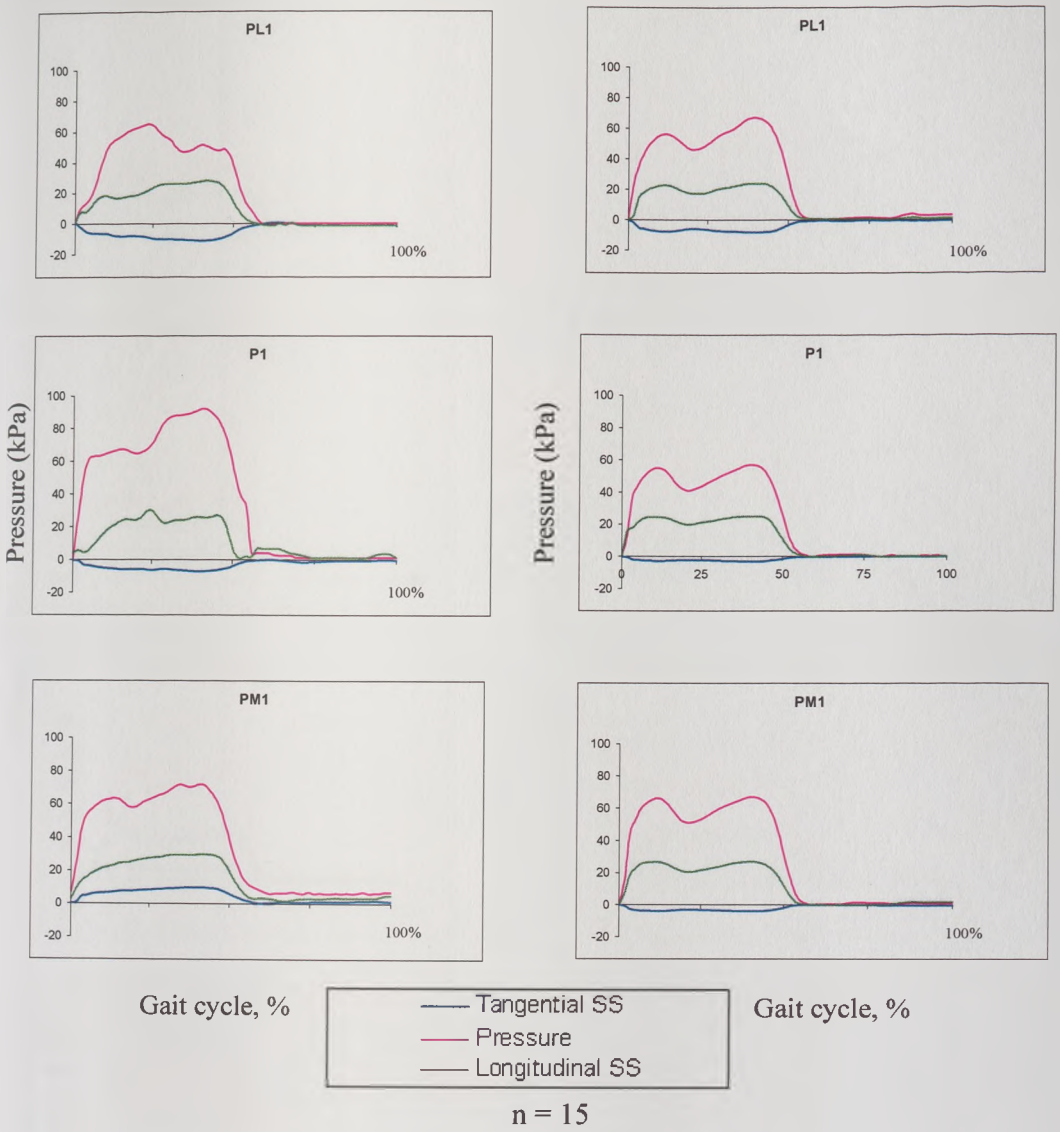

Figure 7.51 : Interface pressure and shear stresses results (kPa) versus percentage of the gait cycle (one division = 25%), heel strike to heel strike of the prosthetic leg for subject 7 on the PTB socket (left) and the Hydrocast socket (right) measured using B.E.S.T transducers at the posterior sites.
n = number of tests represented in each summary curve.

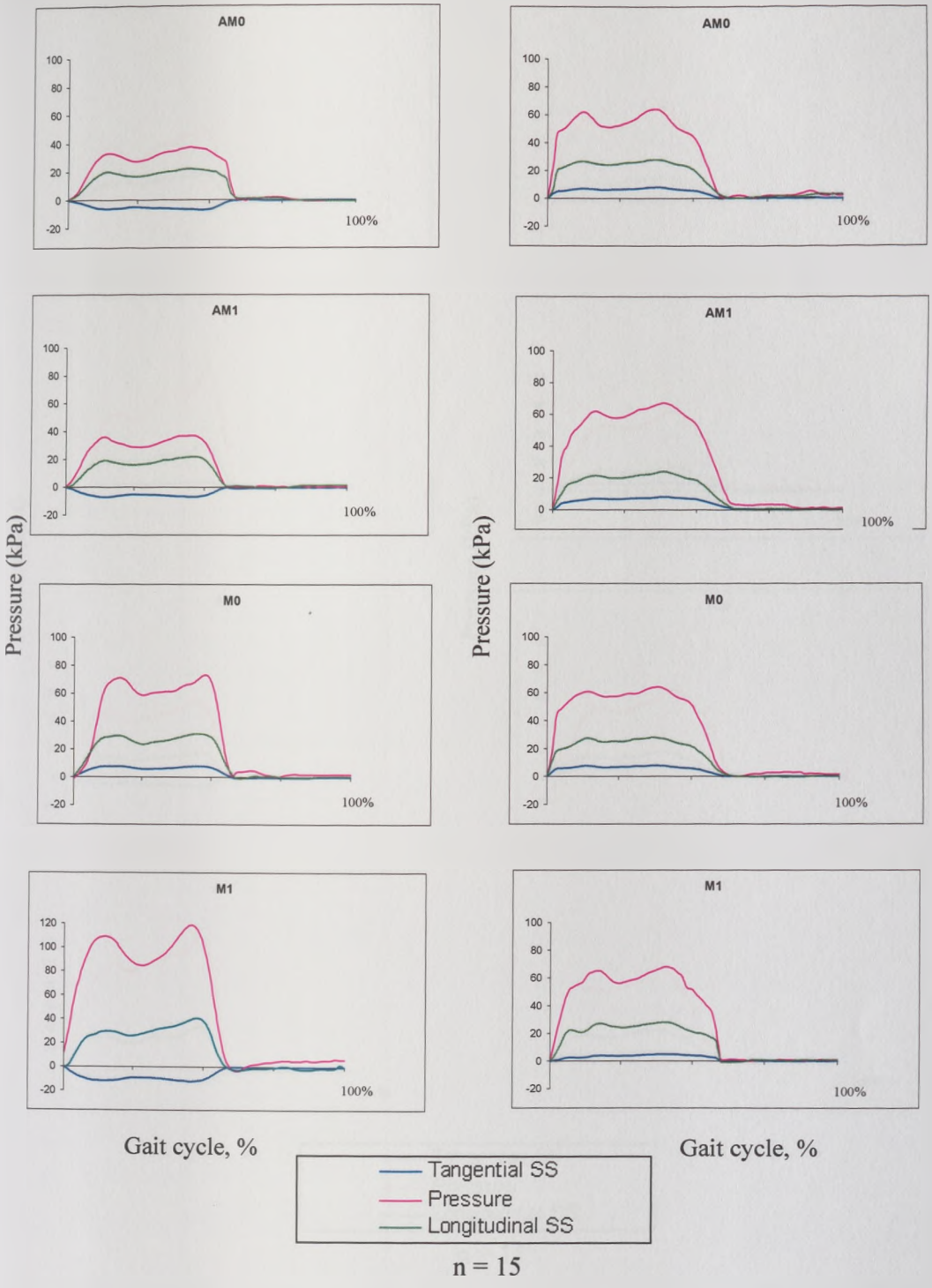

Figure 7.52 : Interface pressure and shear stresses results (kPa) versus percentage of the gait cycle (one division = 25%), heel strike to heel strike of the prosthetic leg for subject 7 on the PTB socket (left) and the Hydrocast socket (right) measured using B.E.S.T transducers at the medial sites.
n = number of tests represented in each summary curve.

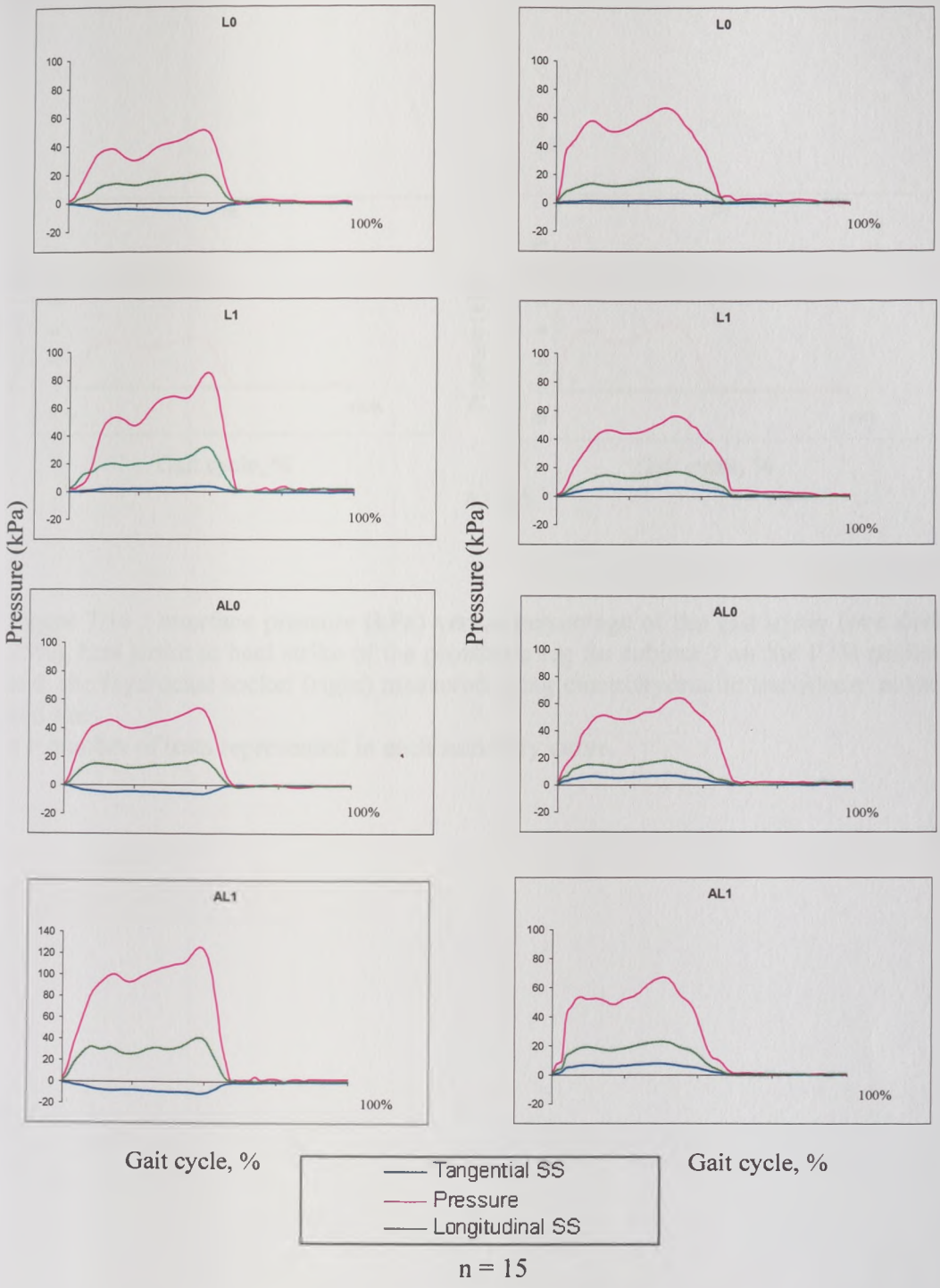

Figure 7.53: Interface pressure and shear stresses results (kPa) versus percentage of the gait cycle (one division = 25%), heel strike to heel strike of the prosthetic leg for subject 7 on the PTB socket (left) and the Hydrocast socket (right) measured using B.E.S.T transducers at the posterior sites.
n = number of tests represented in each summary curve.

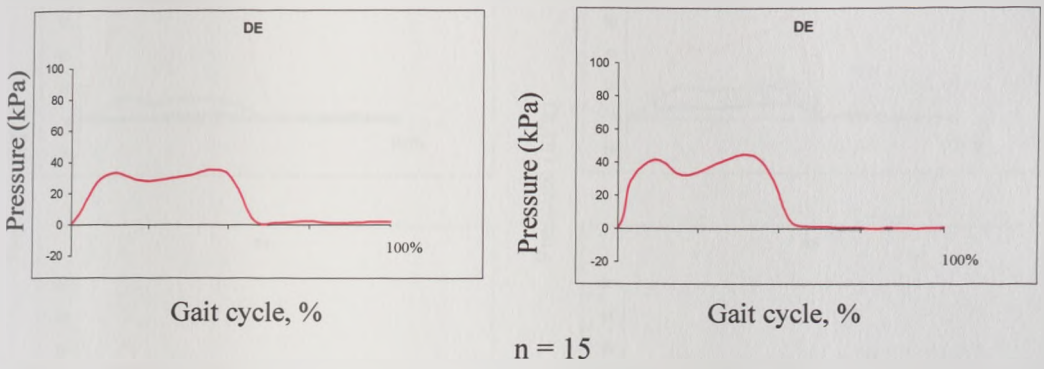

Figure 7.54 : Interface pressure (kPa) versus percentage of the gait cycle (one division = 25%), heel strike to heel strike of the prosthetic leg for subject 7 on the PTB socket (left) and the Hydrocast socket (right) measured using electrohydraulic transducer at the distal end site .
n = number of tests represented in each summary curve.

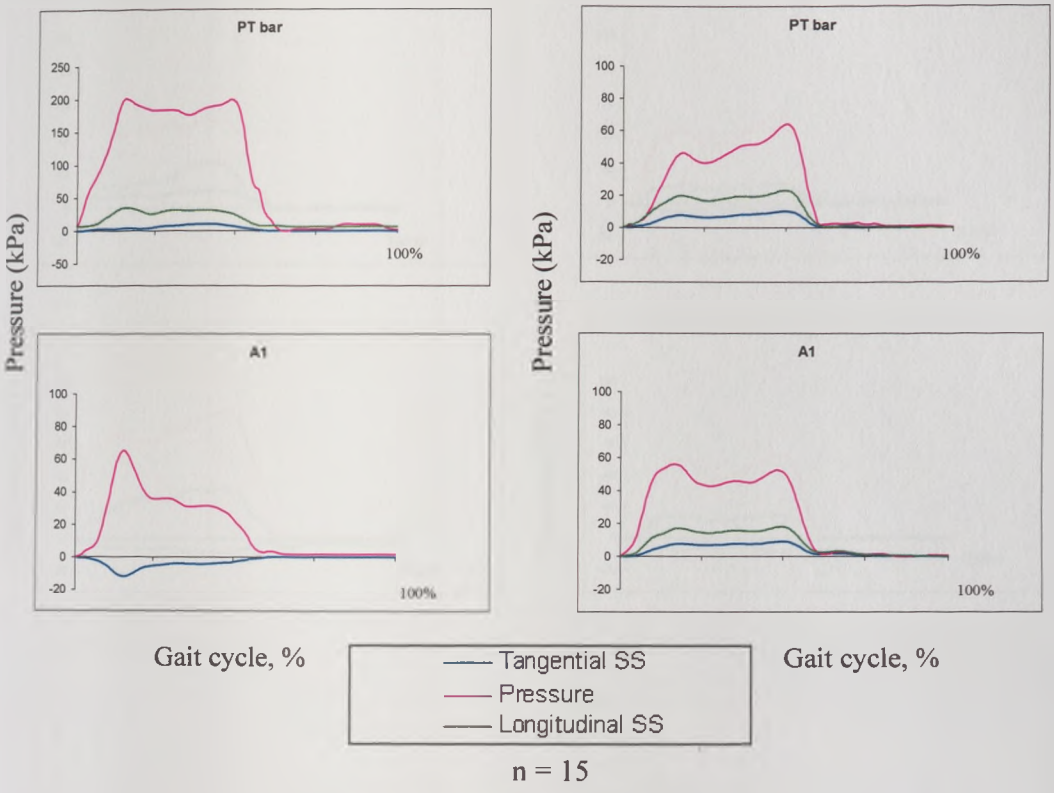

Figure 7.55 : Interface pressure and shear stresses results (kPa) versus percentage of the gait cycle (one division = 25%), heel strike to heel strike of the prosthetic leg for subject 8 on the PTB socket (left) and the Hydrocast socket (right) measured using B.E.S.T transducers at the anterior sites.
n = number of tests represented in each summary curve.

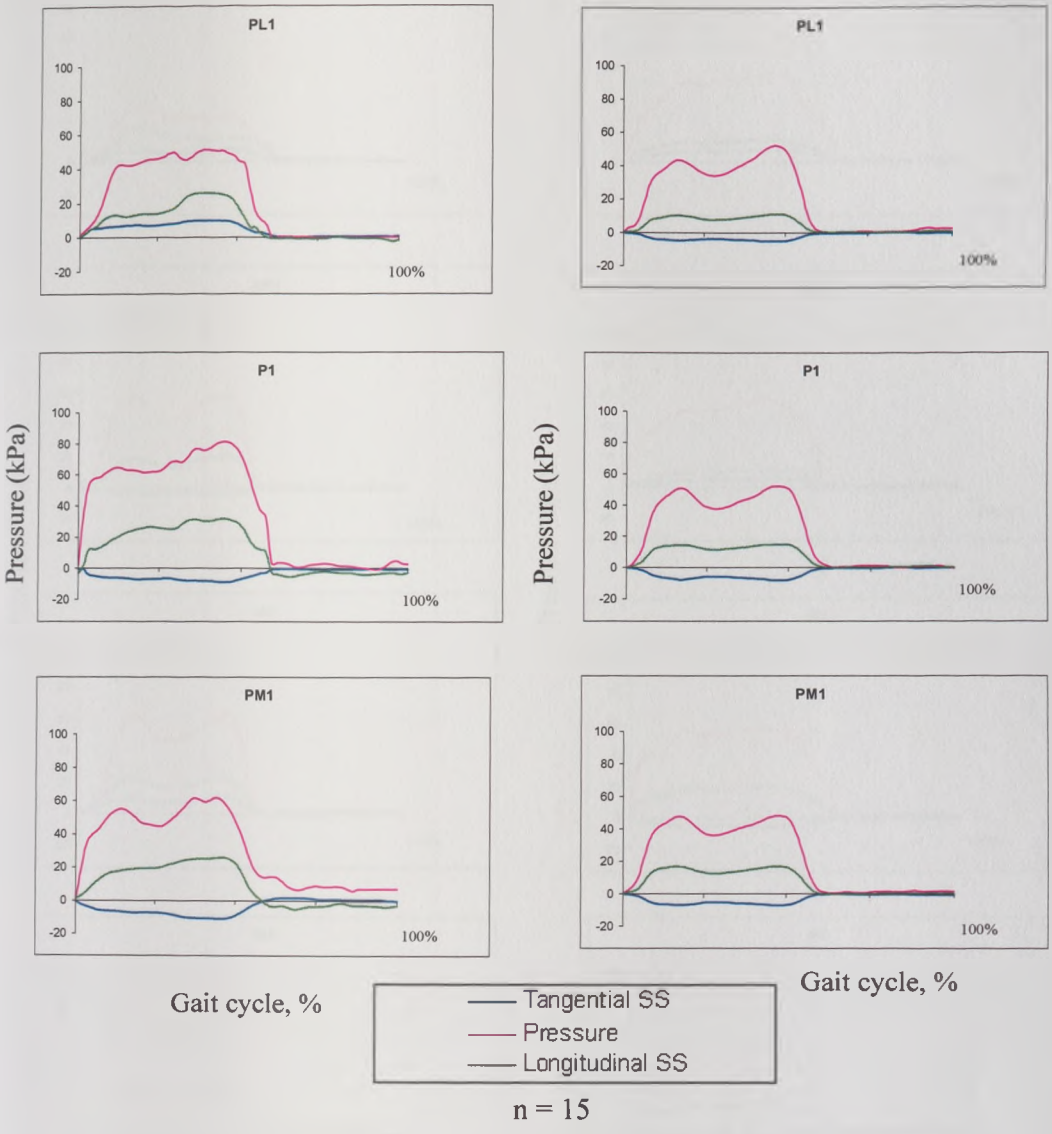

Figure 7.56 : Interface pressure and shear stresses results (kPa) versus percentage of the gait cycle (one division = 25%), heel strike to heel strike of the prosthetic leg for subject 8 on the PTB socket (left) and the Hydrocast socket (right) measured using B.E.S.T transducers at the posterior sites.
n = number of tests represented in each summary curve.

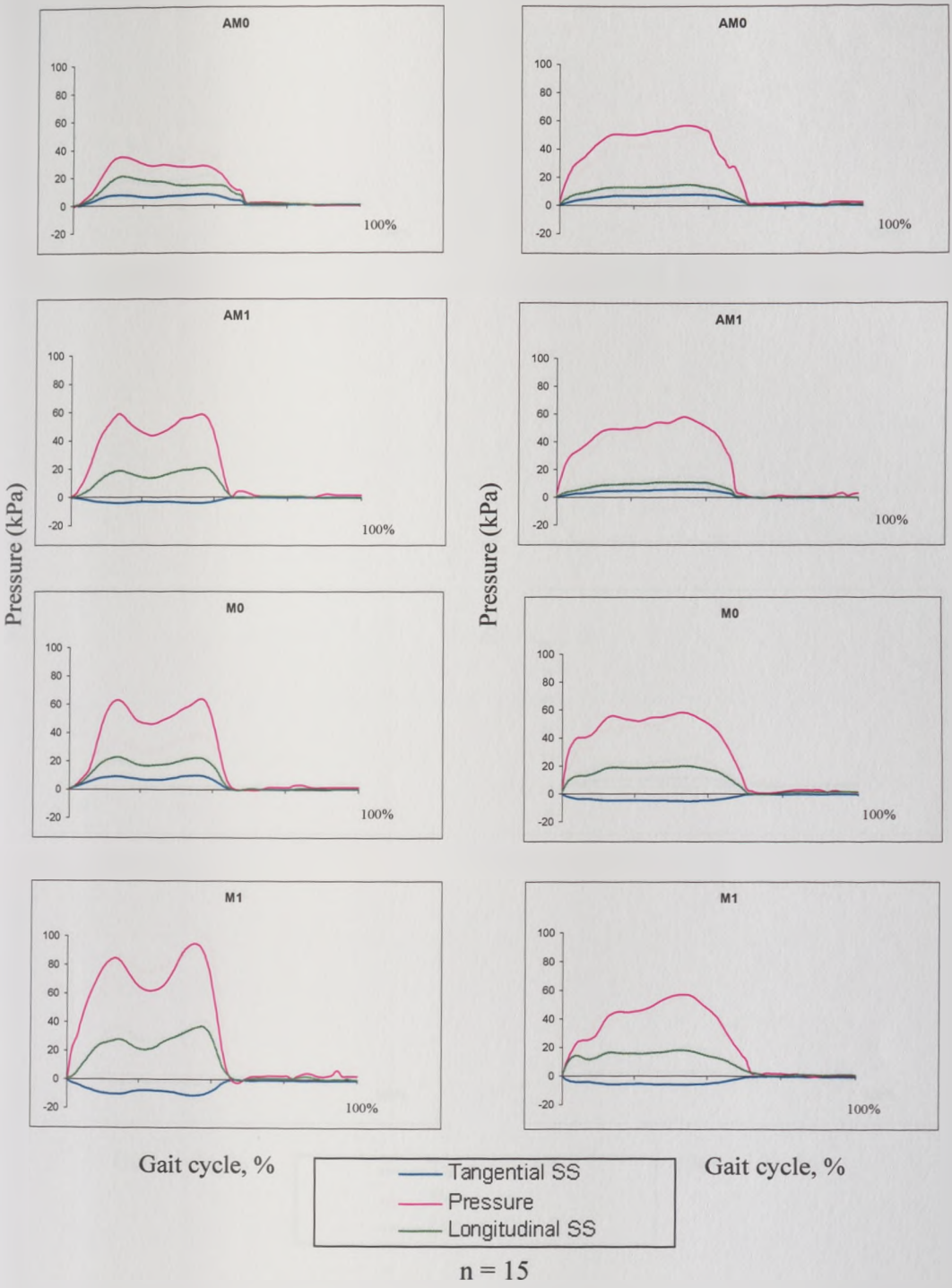

Figure 7.57 : Interface pressure and shear stresses results (kPa) versus percentage of the gait cycle (one division = 25%), heel strike to heel strike of the prosthetic leg for subject 8 on the PTB socket (left) and the Hydrocast socket (right) measured using B.E.S.T transducers at the medial sites.
n = number of tests represented in each summary curve.

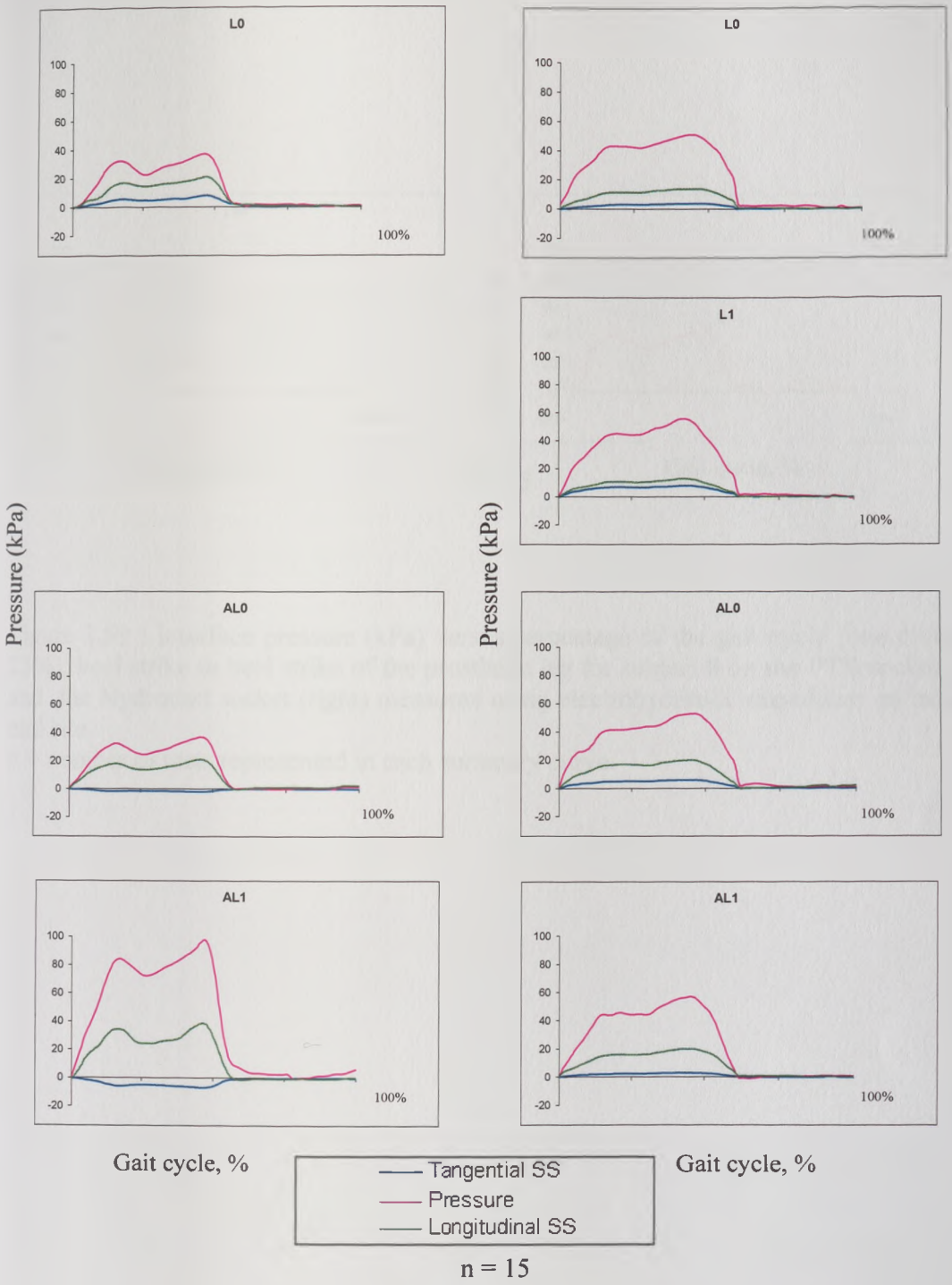

Figure 7.58 : Interface pressure and shear stresses results (kPa) versus percentage of the gait cycle (one division = 25%), heel strike to heel strike of the prosthetic leg for subject 8 on the PTB socket (left) and the Hydrocast socket (right) measured using B.E.S.T transducers at the lateral sites.
n = number of tests represented in each summary curve.

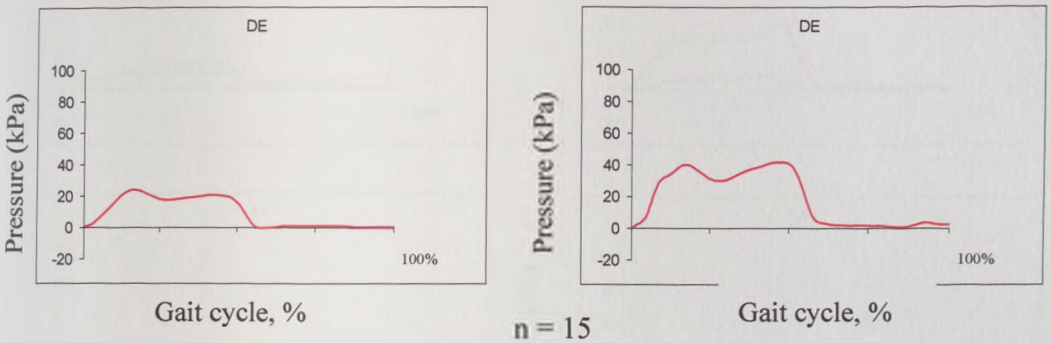

n = 15

Figure 7.59 : Interface pressure (kPa) versus percentage of the gait cycle (one division = 25%), heel strike to heel strike of the prosthetic leg for subject 8 on the PTB socket (left) and the Hydrocast socket (right) measured using electrohydraulic transducer at the distal end site.
n = number of tests represented in each summary curve.

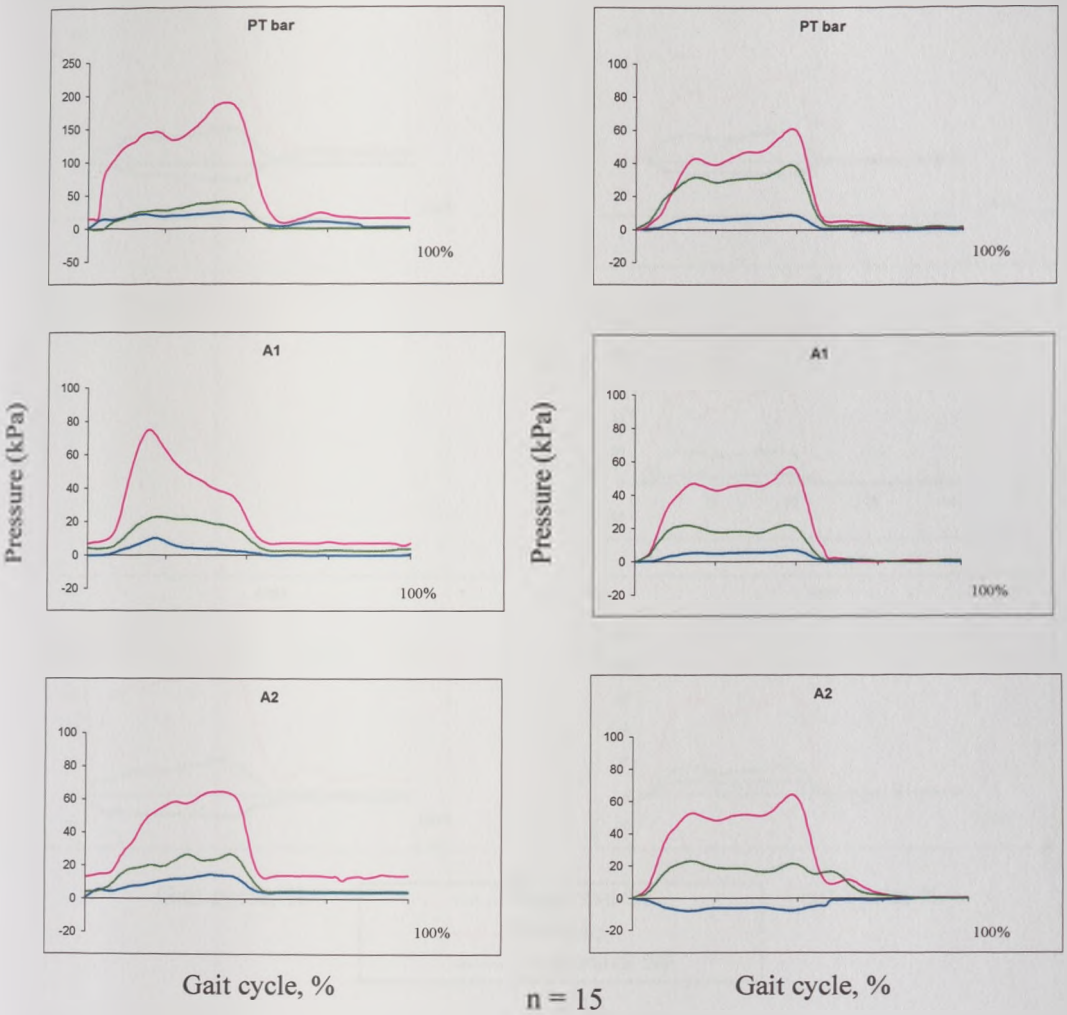

Figure 7.60 : Interface pressure and shear stresses results (kPa) versus percentage of the gait cycle (one division = 25%), heel strike to heel strike of the prosthetic leg for subject 9 on the PTB socket (left) and the Hydrocast socket (right) measured using B.E.S.T transducers at the anterior sites.
n = number of tests represented in each summary curve.

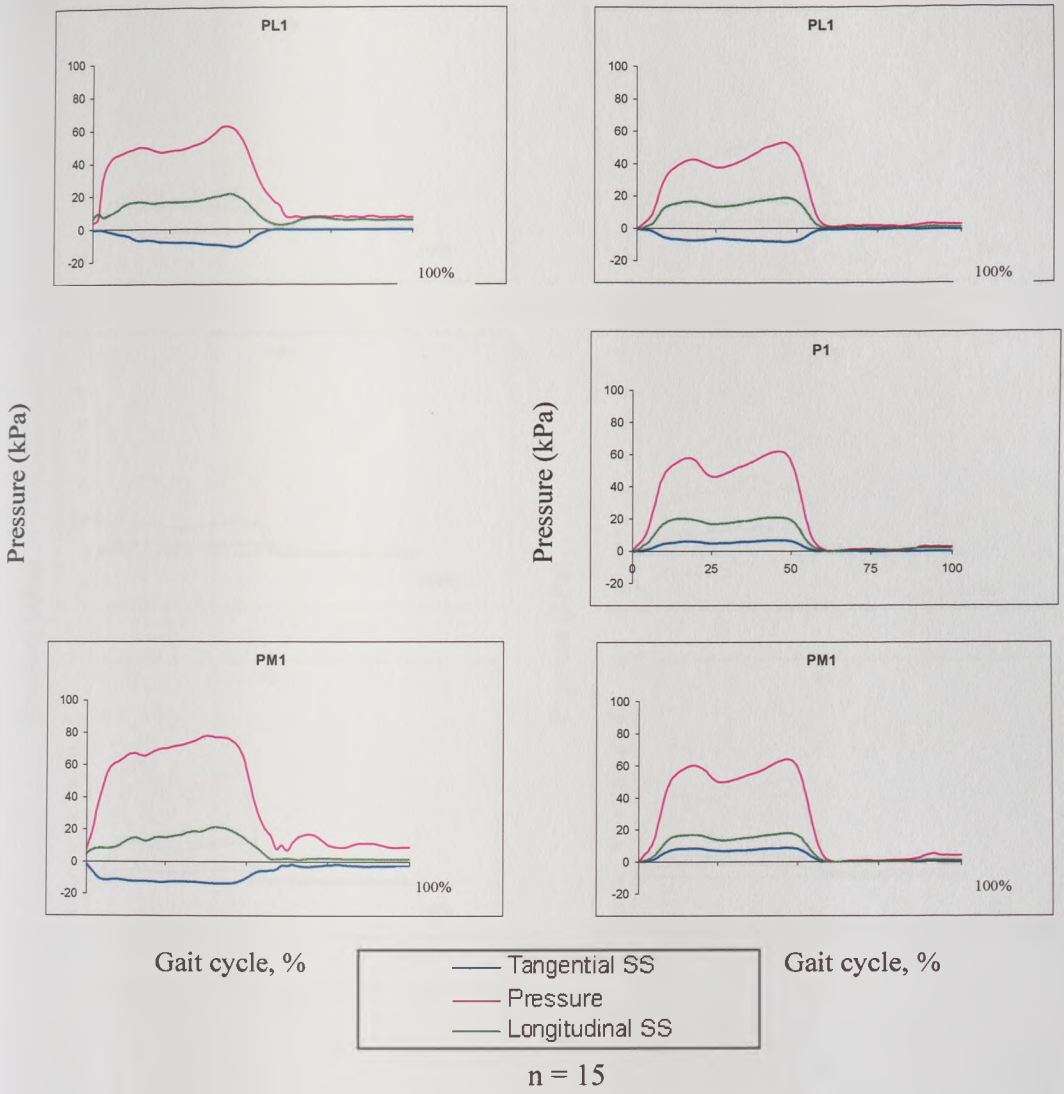

Figure 7.61 : Interface pressure and shear stresses results (kPa) versus percentage of the gait cycle (one division = 25%), heel strike to heel strike of the prosthetic leg for subject 9 on the PTB socket (left) and the Hydrocast socket (right) measured using B.E.S.T transducers at the posterior sites.
n = number of tests represented in each summary curve.

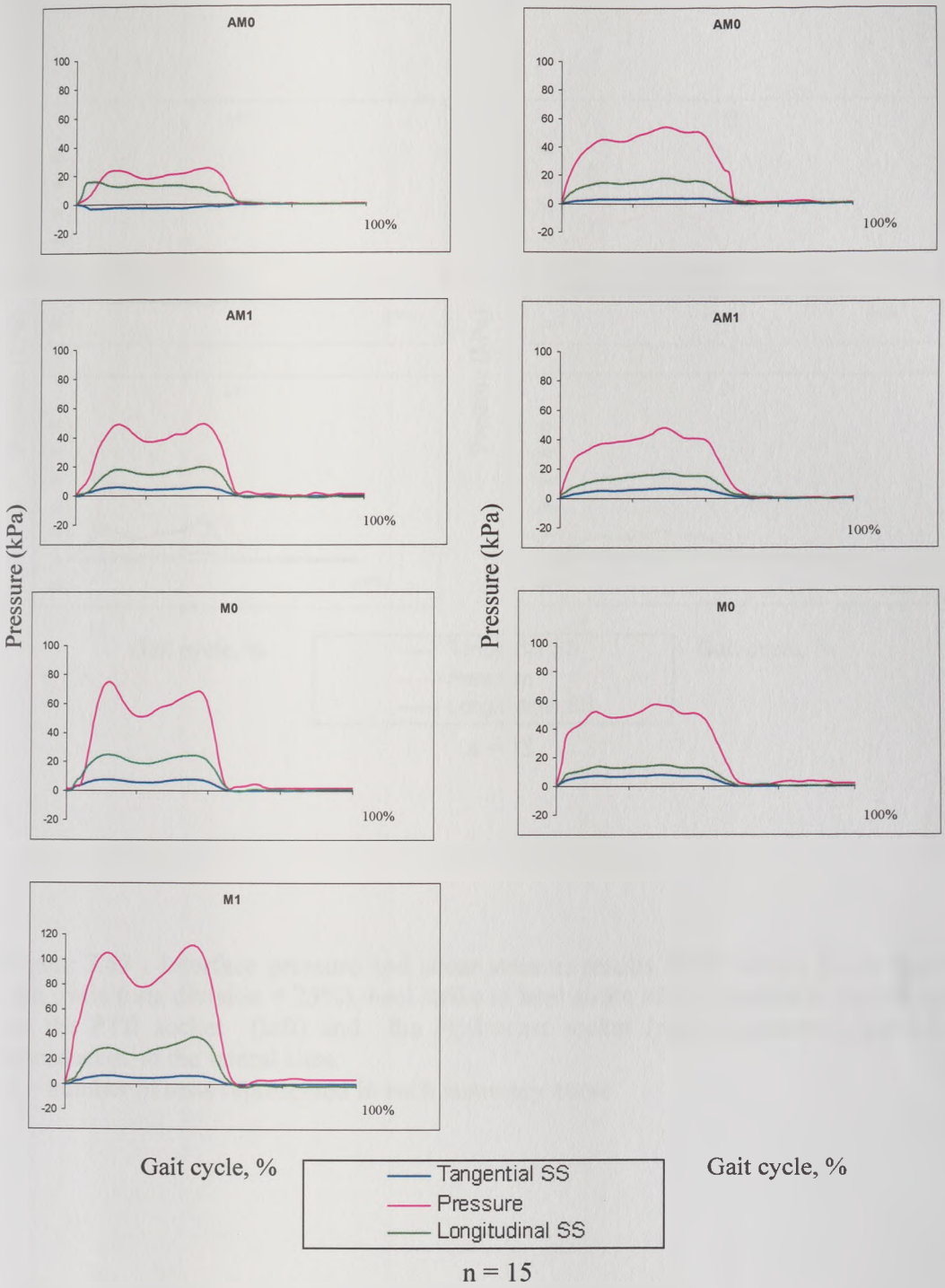

Figure 7.62 : Interface pressure and shear stresses results (kPa) versus percentage of the gait cycle (one division = 25%), heel strike to heel strike of the prosthetic leg for subject 9 on the PTB socket (left) and the Hydrocast socket (right) measured using B.E.S.T transducers at the medial sites.
n = number of tests represented in each summary curve.

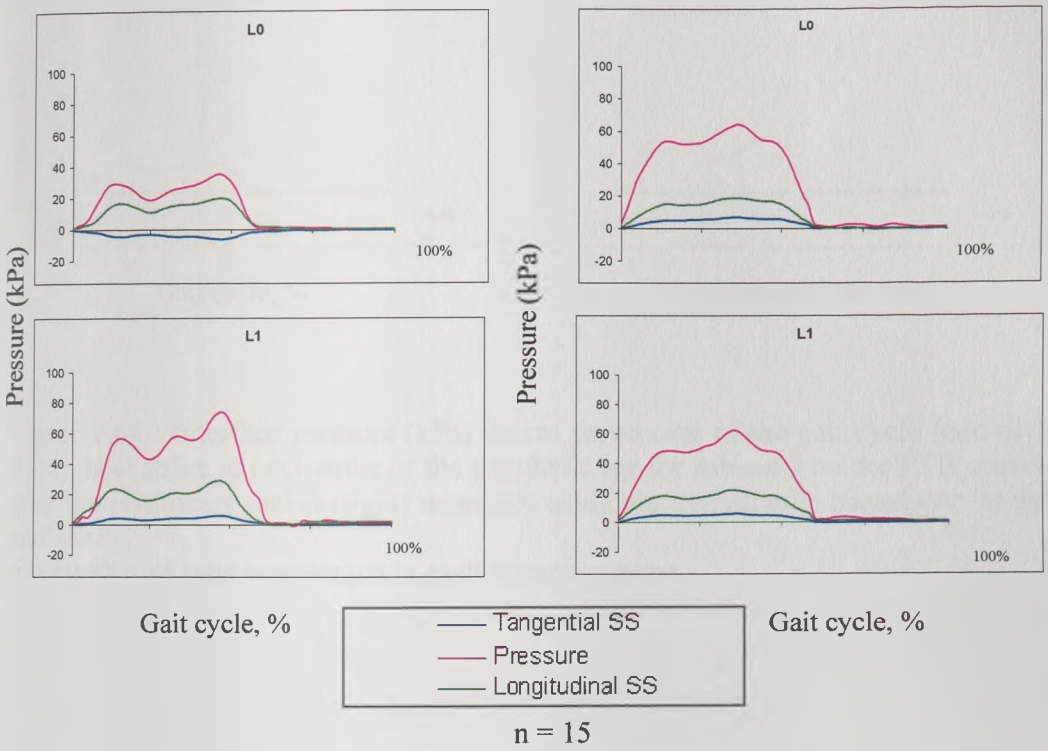

Figure 7.63 : Interface pressure and shear stresses results (kPa) versus percentage of the gait cycle (one division = 25%), heel strike to heel strike of the prosthetic leg for subject 9 on the PTB socket (left) and the Hydrocast socket (right) measured using B.E.S.T transducers at the lateral sites.
n = number of tests represented in each summary curve.

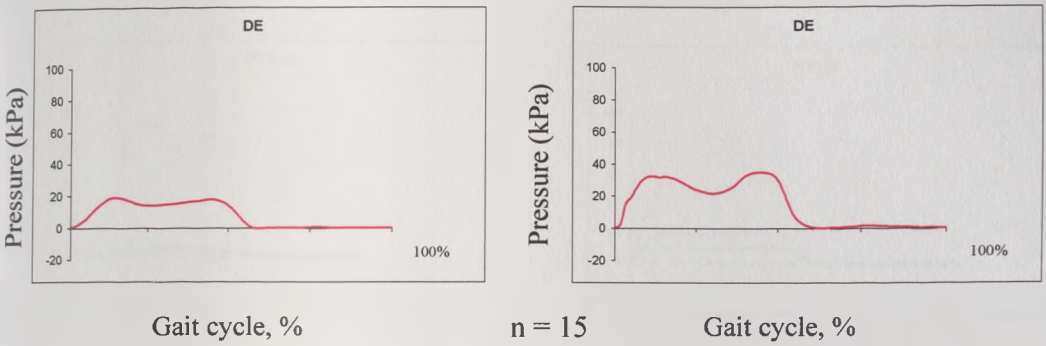

Figure 7.64 : Interface pressure (kPa) versus percentage of the gait cycle (one division = 25%), heel strike to heel strike of the prosthetic leg for subject 9 on the PTB socket (left) and the Hydrocast socket (right) measured using electrohydraulic transducer at the distal end site.
n = number of tests represented in each summary curve.

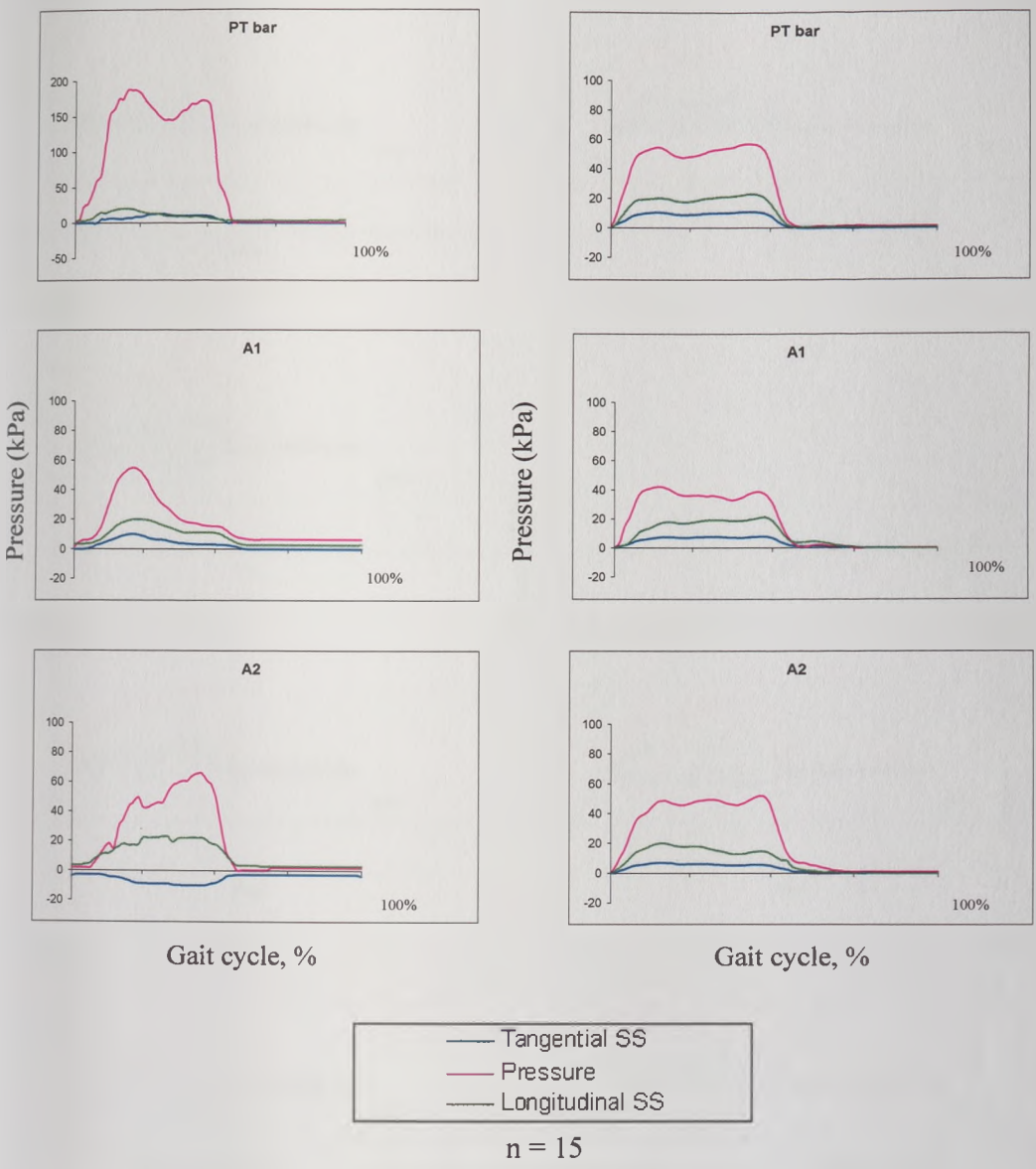

Figure 7.65 : Interface pressure and shear stresses results (kPa) versus percentage of the gait cycle (one division = 25%), heel strike to heel strike of the prosthetic leg for subject 10 on the PTB socket (left) and the Hydrocast socket (right) measured using B.E.S.T transducers at the anterior sites.
n = number of tests represented in each summary curve.

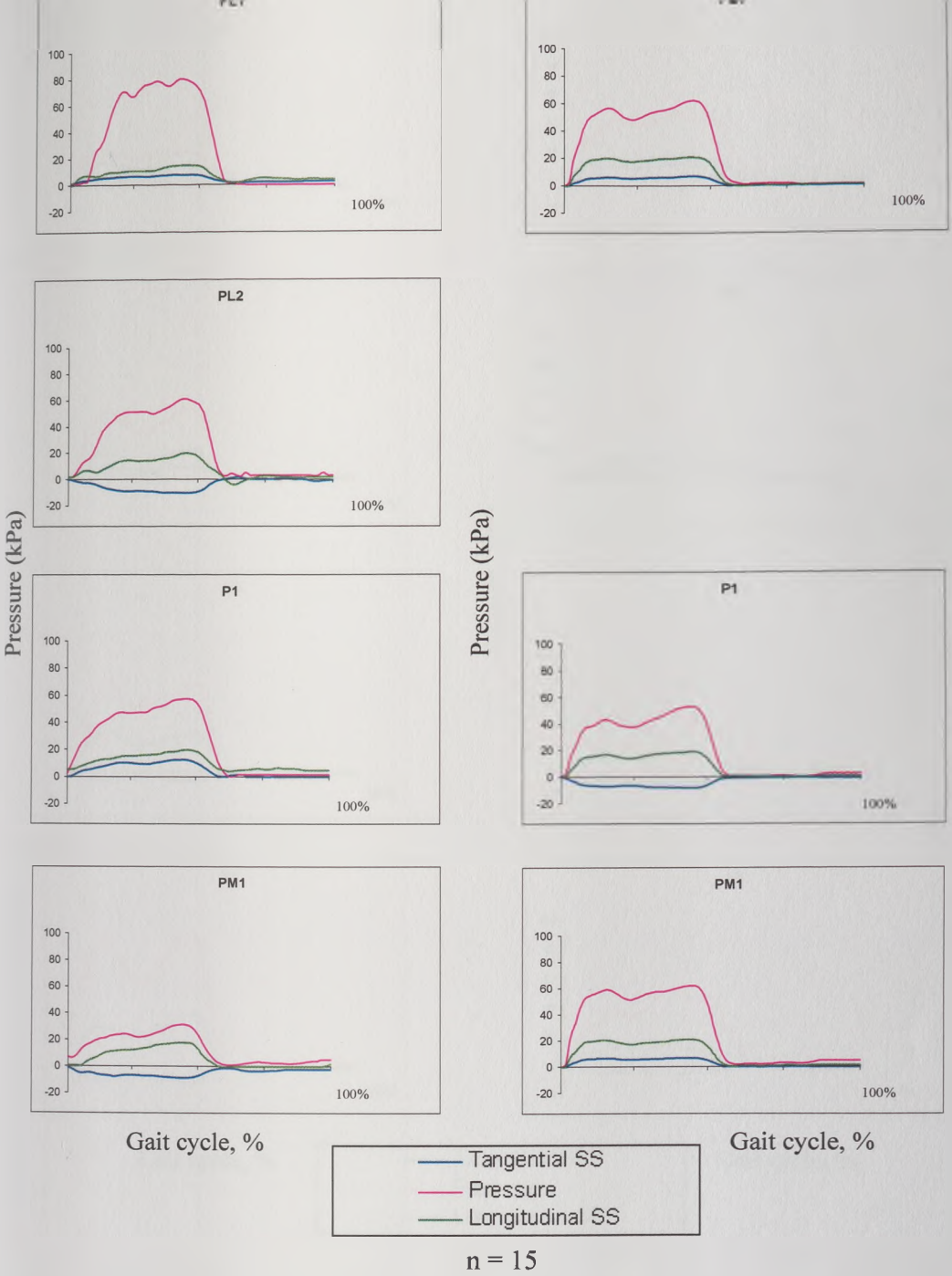

Figure 7.66 : Interface pressure and shear stresses results (kPa) versus percentage of the gait cycle (one division = 25%), heel strike to heel strike of the prosthetic leg for subject 10 on the PTB socket (left) and the Hydrocast socket (right) measured using B.E.S.T transducers at the posterior sites .
n = number of tests represented in each summary curve.

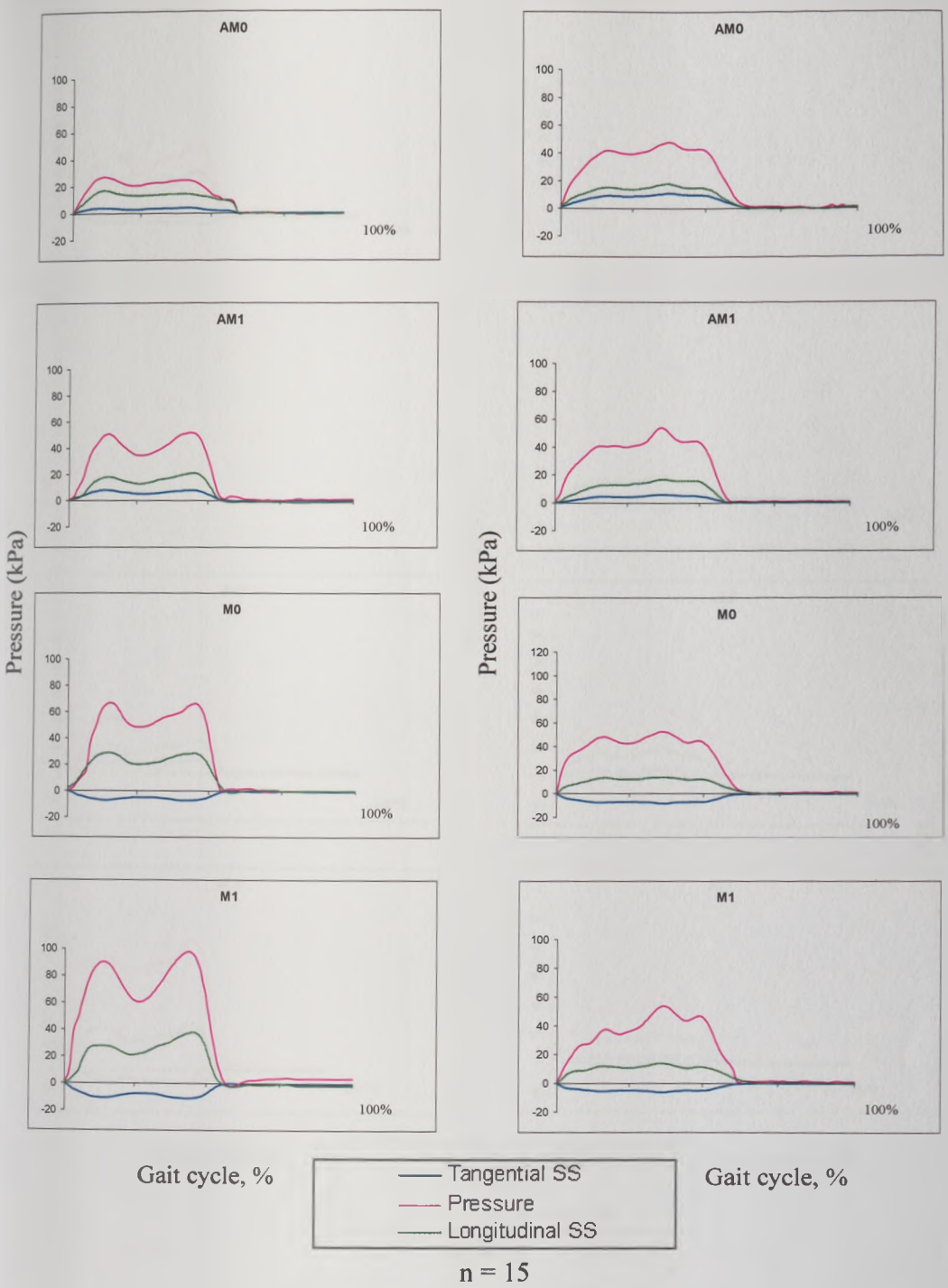

Figure 7.67: Interface pressure and shear stresses results (kPa) versus percentage of the gait cycle (one division = 25%), heel strike to heel strike of the prosthetic leg for subject 10 on the PTB socket (left) and the Hydrocast socket (right) measured using B.E.S.T transducers at the medial sites .
n = number of tests represented in each summary curve.

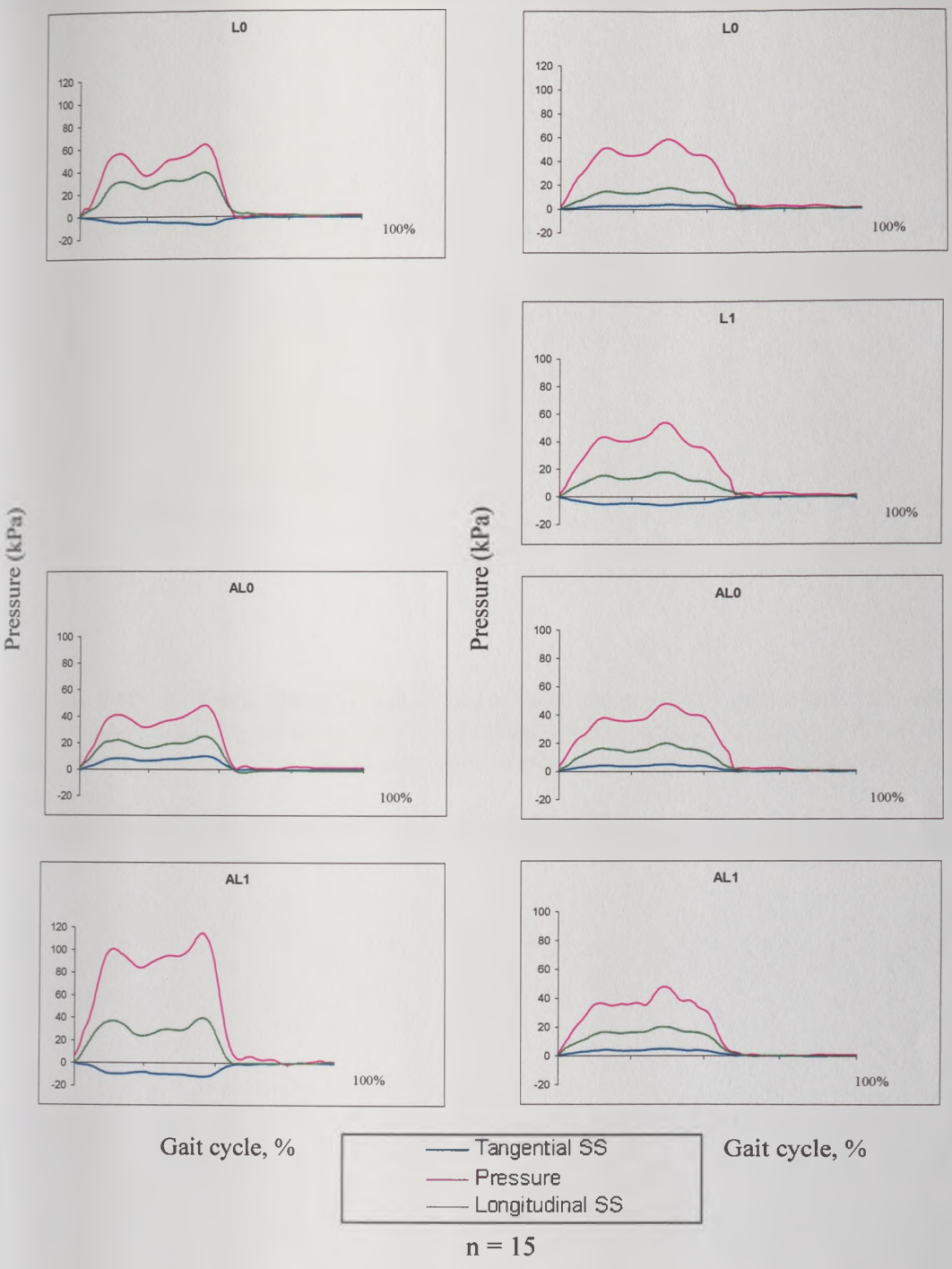

Figure 7.68: Interface pressure and shear stresses results (kPa) versus percentage of the gait cycle (one division = 25%), heel strike to heel strike of the prosthetic leg for subject 10 on the PTB socket (left) and the Hydrocast socket (right) measured using B.E.S.T transducers at the lateral sites .
n = number of tests represented in each summary curve.

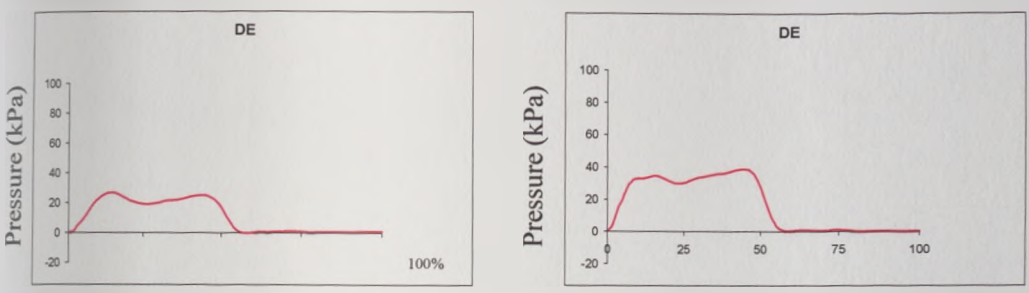

Gait cycle, %

Gait cycle, %

n = 15

Figure 7.69: Interface pressure (kPa) versus percentage of the gait cycle (one division = 25%), heel strike to heel strike of the prosthetic leg for subject 10 on the PTB socket (left) and the Hydrocast socket (right) measured using electrohydraulic transducer at the distal end site .
n = number of tests represented in each summary curve.

		PT	A1	A2	A3	AM-1	AM0	AM1	AM2	AM3	M0	M1	M2	M3	PM1	PM2	PM3	P1	P2	PL1	PL2	PL3	L-1	L0
#1	Tan $_{SS}$	8(2)	-7(2)	8(1)	-10(3)	6(2)	6(2)	-3(1)	-6(1)	-7(2)	-4(3)	-5(1)	-10(2)	-7(1)	15(3)	-6(2)	-2(1)	10(3)	-7(3)	-5(3)	-7(2)	-9(4)		-7(3)
	Press.	203(10)	49(5)	76(6)	74(8)	16(7)	5(2)	56(5)	29(3)	11(4)	72(9)	78(6)	31(5)	17(8)	62(9)	45(3)	16(4)	87(5)	50(6)	60(3)	38(8)	42(7)		28(6)
	Lon $_{SS}$	50(3)	25(3)	35(3)	35(2)	25(5)	20(6)	30(1)	26(4)	24(3)	38(3)	29(2)	28(2)	25(3)	28(2)	21(4)	9(5)	33(2)	24(2)	28(1)	22(3)	19(4)		24(5)
	Resultant SS	51(4)	26(4)	36(3)	36(4)	26(5)	21(6)	30(1)	27(4)	25(4)	38(4)	29(2)	30(3)	26(3)	32(4)	22(4)	9(5)	34(4)	25(4)	28(3)	23(4)	21(6)		25(6)
	Shear angle,θ	9	-16	13	-16	13	17	-6	-13	-16	-6	-10	-20	-16	28	-16	-13	17	-16	-10	-18	-25		-16

		L1	L2	L3	AL-1	AL0	AL1	AL2	AL3	DE
#1	Tan $_{SS}$	10(3)	4(1)	3(2)	-4(1)	-8(3)	7(2)	-8(1)	-4(1)	
	Press.	66(5)	52(8)	58(6)	6(4)	36(3)	72(7)	113(10)	23(6)	23(4)
	Lon $_{SS}$	25(1)	26(3)	20(2)	25(2)	20(2)	24(2)	27(3)	31(1)	
	Resultant SS	27(3)	26(3)	20(3)	25(2)	22(4)	25(3)	28(3)	31(1)	
	Shear angle,θ	22	9	9	-9	-22	16	-16	-7	

		PT	A1	A2	AM-1	AM0	AM1	AM2	M-1	M0	M1	M2	PM1	P1	PL1	PL2	L-1	L0	L1	L2	AL-1	AL0	AL1	AL2	DE
#2	Tan $_{SS}$	18(2)	-3(1)	6(1)		2(1)	-9(2)	-2(1)		11(2)	-11(2)	-3(1)	10(2)	18(2)	-8(3)	-9(3)		7(3)	-7(3)		-6(4)	-12(2)	8(2)		
	Press.	229(14)	58(2)	68(2)		10(1)	25(2)	39(2)		59(4)	64(2)	21(3)	49(3)	68(6)	54(5)	25(10)		19(6)	54(7)		29(8)	111(15)	82(5)		23(3)
	Lon $_{SS}$	35(3)	10(3)	12(2)		6(2)	14(2)	18(3)		28(3)	30(2)	12(1)	19(4)	25(2)	12(2)	13(2)		14(3)	29(1)		10(1)	34(2)	33(3)		
	Resultant SS	39(4)	10(3)	13(2)		6(2)	17(3)	18(3)		30(4)	32(3)	12(1)	21(4)	31(3)	14(4)	16(4)		16(4)	30(3)		12(4)	36(3)	34(4)		
	Shear angle,θ	27	-17	27		18	-33	-6		21	-20	-14	28	36	-34	-35		27	-14		-31	-19	14		
#3	Tan $_{SS}$	22(5)	15(6)	-10(2)						-8(1)	-5(1)	6(1)	-13(3)	-8(2)	-8(2)	-10(2)		8(2)	8(3)	-2(1)	-4(1)				
	Press.	226(15)	41(3)	60(4)						60(4)	85(6)	40(7)	75(3)	60(5)	60(4)	59(3)		29(2)	77(3)	74(4)	10(3)				12(2)
	Lon $_{SS}$	48(3)	18(2)	25(4)						29(1)	32(1)	21(3)	28(2)	30(3)	25(3)	27(2)		13(3)	33(4)	38(3)	7(2)				
	Resultant SS	53(6)	23(6)	27(4)						30(1)	32(1)	22(3)	31(4)	31(4)	26(4)	29(3)		15(4)	34(5)	38(3)	8(2)				
	Shear angle,θ	25	40	-22						-15	-9	16	-25	-15	-18	-20		32	14	-3	-30				

Table7.12: Average pressures ± (1SD) across all sites for PTB sockets during gait measured using B.E.S.T. Note; Tan $_{SS}$ = Tangential shear stress, Press. = Pressure and Lon $_{SS}$ = Longitudinal shear stress. Stress units all in kPa and shear angle in degree. The patellar tendon (PT) bar pressure and shear stresses were measured using PT transducer and distal end pressure was measured using electrohydraulic transducer.

		PT	A1	A2	AM-1	AM0	AM1	AM2	M-1	M0	M1	M2	PM1	P1	PL1	PL2	L-1	L0	L1	L2	AL-1	AL0	AL1	AL2	DE
#4	Tan $_{SS}$	10(2)	12(3)	15(1)						10(2)	7(1)	8(2)	-10(2)	-3(2)	10(3)	7(1)		6(2)	-7(2)	-9(2)					
	Press.	224(10)	57(4)	76(6)						68(4)	76(8)	45(6)	64(7)	72(6)	62(6)	38(8)		28(3)	54(4)	72(5)					30(4)
	Lon $_{SS}$	39(5)	26(4)	29(5)						31(3)	27(2)	23(2)	26(2)	28(1)	26(3)	15(1)		11(4)	30(2)	28(3)					
	Resultant SS	40(5)	29(5)	33(5)						33(4)	28(2)	24(3)	28(3)	28(2)	28(4)	17(1)		13(4)	31(3)	29(4)					
	Shear angle,θ	14	25	27						18	15	19	-21	-6	21	25		29	-13	-18					
#5	Tan $_{SS}$	5(1)	4(1)	-10(2)		-3(1)				-7(1)	8(1)	-7(3)	-10(2)	-6(3)	-4(3)			8(2)	-8(2)	-7(2)		6(2)			
	Press.	202(10)	57(6)	63(8)		27(4)				54(7)	75(7)	39(6)	63(8)	67(3)	68(3)			28(4)	66(5)	64(2)		39(4)			14(3)
	Lon $_{SS}$	47(2)	26(2)	38(3)		13(1)				29(2)	23(2)	24(2)	31(3)	27(3)	29(2)			12(1)	29(1)	26(3)		18(1)			
	Resultant SS	47(2)	26(2)	39(4)		13(1)				30(2)	24(2)	25(4)	33(4)	28(4)	29(4)			14(2)	30(2)	27(4)		19(2)			
	Shear angle,θ	6	9	-15		-13				-14	19	-16	-18	-13	-8			34	-15	-15		18			
#6	Tan $_{SS}$	18(3)	-15(2)	-7(2)		-6(1)	-11(2)	7(2)		-6(1)	-6(3)	-11(3)	10(2)	11(2)	10(2)			-6(3)	-4(2)			7(1)	-10(2)	-12(2)	
	Press.	210(16)	57(3)	74(2)		17(2)	49(1)	46(2)		64(7)	94(8)	52(8)	83(3)	79(4)	73(6)			43(6)	61(2)			45(3)	116(5)	105(4)	29(4)
	Lon $_{SS}$	45(3)	30(2)	35(3)		9(1)	27(2)	22(2)		28(4)	21(3)	23(3)	26(1)	28(1)	25(1)			18(2)	23(2)			19(3)	38(2)	36(1)	
	Resultant SS	48(4)	34(3)	36(4)		11(1)	29(3)	23(3)		29(4)	22(4)	25(4)	28(2)	30(2)	27(2)			19(4)	23(3)			20(3)	39(3)	38(2)	
	Shear angle,θ	22	-27	-11		-34	-22	18		-12	-16	-26	21	21	22			-18	-10			20	-15	-18	
#7	Tan $_{SS}$	15(1)	-10(2)			-7(2)	-9(2)			8(1)	-12(1)		10(2)	-7(2)	-11(3)			-7(2)	4(2)			-6(3)	-11(3)		
	Press.	230(17)	71(8)			37(6)	58(6)			73(3)	118(3)		72(8)	92(9)	65(11)			51(7)	83(6)			54(4)	124(13)		35(4)
	Lon $_{SS}$	40(3)	26(6)			22(1)	25(1)			31(2)	41(2)		30(3)	30(3)	28(4)			20(2)	32(2)			18(3)	41(3)		
	Resultant SS	43(3)	28(6)			23(2)	27(2)			32(2)	43(2)		32(4)	31(4)	30(5)			21(3)	32(3)			19(4)	42(4)		
	Shear angle,θ	21	-21			-18	-20			14	-16		18	-13	-21			-19	7			-18	-15		

...Contd... Table7.12 : Average pressures ± (1SD) across all sites for PTB sockets during gait measured using B.E.S.T. Note; Tan $_{SS}$ = Tangential shear stress, Press. = Pressure and Lon $_{SS}$ = Longitudinal shear stress. Stress units all in kPa and shear angle in degree. The patellar tendon (PT) bar pressure and shear stresses were measured using PT transducer and distal end pressure was measured using electrohydraulic transducer.

		PT	A1	A2	AM-1	AM0	AM1	AM2	M-1	M0	M1	M2	PM1	P1	PL1	PL2	L-1	L0	L1	L2	AL-1	AL0	AL1	AL2	DE
#8	Tan $_{ss}$	10(2)	-12(2)			8(4)	-4(3)			10(3)	-11(3)		-11(4)	-10(2)	10(2)			8(3)				-2(3)	-7(3)		
	Press.	200(9)	65(8)			35(10)	59(11)			64(3)	94(8)		62(7)	70(6)	51(9)			37(8)				27(3)	97(10)		24(5)
	Lon $_{ss}$	35(4)	28(3)			21(2)	21(2)			23(2)	37(2)		26(3)	32(3)	26(1)			21(2)				17(2)	39(2)		
	Resultant SS	36(4)	30(4)			22(4)	21(4)			25(4)	39(4)		28(5)	34(4)	28(2)			22(4)				17(4)	40(4)		
	Shear angle,θ	16	-23			21	-11			23	-17		-23	-17	21			21				-7	-10		
#9	Tan $_{ss}$	25(6)	-10(3)	15(2)		-3(2)	6(2)			8(3)	7(3)		-11(3)		-12(3)			-6(1)	6(1)						
	Press.	190(9)	75(10)	65(11)		25(9)	49(3)			75(3)	110(4)		70(13)		64(5)			35(6)	74(8)						19(3)
	Lon $_{ss}$	40(2)	23(2)	28(2)		16(4)	20(3)			25(2)	38(2)		30(3)		20(5)			20(2)	29(2)						
	Resultant SS	47(6)	25(4)	32(3)		16(4)	21(4)			26(4)	39(4)		32(4)		23(6)			21(2)	30(2)						
	Shear angle,θ	32	-23	28		-11	17			18	10		-20		-31			-17	12						
#10	Tan $_{ss}$	13(2)	10(3)	-10(3)		4(1)	8(2)			-7(3)	-11(3)		13(2)	-10(2)	8(3)	-10(4)		-7(2)				10(5)	-12(1)		
	Press.	187(10)	55(8)	80(7)		27(6)	52(5)			67(5)	98(5)		67(5)	63(8)	70(7)	35(6)		64(8)				48(3)	115(12)		27(4)
	Lon $_{ss}$	30(4)	20(5)	23(1)		17(1)	21(1)			29(3)	38(2)		25(2)	20(2)	15(4)	18(4)		39(3)				25(2)	40(1)		
	Resultant SS	33(4)	22(6)	25(3)		17(1)	22(2)			30(4)	40(4)		28(3)	22(3)	17(5)	21(6)		40(4)				27(5)	42(1)		
	Shear angle,θ	23	27	-23		13	21			-14	-16		27	-27	28	-29		-10				22	-17		

...Contd... Table 7.12: Average pressures ± (1SD) across all sites for PTB sockets during gait measured using B.E.S.T. Note; Tan $_{ss}$ = Tangential shear stress, Press. = Pressure and Lon $_{ss}$ = Longitudinal shear stress. Stress units all in kPa and shear angle in degree. The patellar tendon (PT) bar pressure and shear stresses were measured using PT transducer and distal end pressure was measured using electrohydraulic transducer.

		PT	A1	A2	A3	AM-1	AM0	AM1	AM2	AM3	M0	M1	M2	M3	PM1	PM2	PM3	P1	P2	PL1	PL2	PL3	L-1	L0
#1	Tan $_{ss}$	4(2)	-3(2)	-2(2)	4(3)	6(2)	8(3)	-7(2)	5(4)	4(3)	4(2)	3(2)	6(4)	5(2)	-7(3)	-10(6)	8(3)	9(2)	-7(1)	3(1)	-2(7)	4(2)		5(3)
	Press.	62 (8)	55(6)	62(3)	53(3)	48(8)	50(4)	47(5)	56(6)	52(7)	48(8)	46(3)	59(8)	67(7)	44(8)	56(8)	50(8)	51(4)	43(6)	69(8)	58(8)	68(6)		65(4)
	Lon $_{ss}$	20(3)	13(4)	14(3)	16(3)	8(2)	16(2)	20(2)	12(4)	13(3)	15(2)	21(2)	22(5)	21(2)	23(2)	15(7)	18(2)	19(2)	21(2)	23(1)	27(3)	24(2)		22(2)
	Resultant SS	20(4)	13(4)	14(4)	16(4)	10(3)	18(4)	21(3)	13(6)	14(4)	16(3)	21(3)	23(6)	22(3)	24(4)	18(9)	20(4)	21(3)	22(2)	23(1)	27(8)	24(3)		23(4)
	Shear angle,θ	11	-13	-8	14	37	27	-19	23	17	15	8	15	13	-17	-34	24	25	-18	7	-4	9		13

		L1	L2	L3	AL-1	AL0	AL1	AL2	AL3	DE
#1	Tan $_{ss}$	4(2)	5(2)	6(4)	5(3)	-6(1)	-5(3)	4(2)	4(3)	
	Press.	58(7)	64(3)	54(8)	40(6)	56(8)	63(7)	63(6)	48(8)	35(4)
	Lon $_{ss}$	10(2)	15(1)	21(3)	22(2)	18(2)	22(1)	15(4)	27(1)	
	Resultant SS	11(3)	16(2)	22(5)	23(4)	19(2)	23(3)	16(4)	27(3)	
	Shear angle,θ	22	18	16	13	-18	-13	15	8	

		PT	A1	A2	AM-1	AM0	AM1	AM2	M-1	M0	M1	M2	PM1	P1	PL1	PL2	L-1	L0	L1	L2	AL-1	AL0	AL1	AL2	DE
#2	Tan $_{ss}$	5(5)	4(2)	-3(1)		5(3)	5(1)	6(1)	9(2)	-8(3)	-5(2)	-6(1)	-8(2)	7(1)	6(2)	6(2)		-5(2)	-4(1)			-9(2)	82)		
	Press.	68(7)	57(8)	59(7)		57(8)	49(7)	58(6)	59(4)	52(5)	52(5)	61(1)	56(6)	65(7)	54(3)	54(3)		54(4)	62(3)			49(6)	67(3)		35(3)
	Lon $_{ss}$	22(2)	15(2)	16(4)		18(2)	22(1)	21(1)	20(1)	14(2)	17(3)	16(4)	15(2)	11(2)	18(1)	17(1)		15(1)	14(2)			18(1)	19(2)		
	Resultant SS	23(5)	16(2)	16(4)		19(4)	23(1)	22(1)	22(2)	16(4)	18(4)	17(4)	17(3)	13(2)	19(2)	18(2)		16(2)	15(2)			20(2)	21(3)		
	Shear angle,θ	13	15	-11		16	13	16	24	-30	-16	-21	-28	32	18	19		-18	-16			-27	23		

#3	Tan $_{ss}$	6(2)	6(3)	-5(2)						-6(1)	-5(1)	7(2)	8(3)	6(1)	5(1)	6(1)		-4(2)	-4(1)	7(1)					
	Press.	71(8)	59(7)	57(6)						51(2)	57(3)	62(2)	51(3)	54(4)	64(5)	49(6)		56(7)	54(8)	53(9)					41(5)
	Lon $_{ss}$	29(3)	23(1)	25(3)						24(1)	30(1)	23(2)	28(1)	31(2)	32(1)	28(1)		27(2)	18(3)	19(2)					
	Resultant SS	30(4)	24(3)	25(4)						25(1)	30(1)	24(3)	29(3)	32(2)	32(1)	29(1)		27(3)	18(3)	20(2)					
	Shear angle,θ	12	15	-11						-14	-9	17	16	60	9	12		-8	-13	20					

Table 7.13 : Average pressures ± (1SD) across all sites for HYDROCAST sockets during gait measured using B.E.S.T. Note; Tan $_{ss}$ = Tangential shear stress, Press. = Pressure and Lon $_{ss}$ = Longitudinal shear stress. Stress units all in kPa and shear angle in degree. The patellar tendon (PT) bar pressure and shear stresses were measured using PT transducer and distal end pressure was measured using electrohydraulic transducer.

		PT	A1	A2	AM-1	AM0	AM1	AM2	M-1	M0	M1	M2	PM1	P1	PL1	PL2	L-1	L0	L1	L2	AL-1	AL0	AL1	AL2	DE
#4	Tan $_{SS}$	8(1)	4(1)	4(2)		-5(3)	-5(2)			-7(1)	-8(1)	6(1)	9(2)	-6(1)	-4(1)			-8(1)	-9(1)	-6(1)					
	Press.	59(5)	52(4)	57(5)		58(7)	57(8)			48(4)	56(5)	67(6)	57(4)	54(5)	56(5)			57(5)	54(3)	51(4)					42(4)
	Lon $_{SS}$	22(2)	18(1)	17(4)		20(4)	24(2)			22(2)	15(3)	16(1)	22(2)	24(3)	31(2)			22(2)	23(1)	20(1)					
	Resultant SS	23(2)	18(1)	17(4)		21(5)	25(3)			23(2)	17(3)	17(1)	24(3)	25(3)	31(2)			23(2)	25(1)	21(1)					
	Shear angle,θ	20	13	13		-14	-5			-18	-28	21	22	-14	-7			-20	-21	-17					
#5	Tan $_{SS}$	9(3)	5(2)	7(1)		8(1)	7(3)			-8(2)	7(2)	-9(1)	-6(2)	6(1)	-8(2)			9(1)	7(2)	6(1)		8(1)	7(1)		
	Press.	57(4)	52(5)	57(5)		51(1)	54(9)			55(4)	46(3)	46(4)	51(5)	67(6)	57(7)			64(3)	62(4)	67(6)		58(3)	62(4)		31(4)
	Lon $_{SS}$	18(1)	17(3)	15(1)		19(3)	23(4)			22(1)	20(2)	18(1)	17(1)	16(1)	14(2)			13(1)	22(2)	21(1)		20(1)	18(2)		
	Resultant SS	20(3)	18(4)	17(1)		21(3)	24(5)			23(2)	21(3)	20(1)	18(2)	17(1)	16(3)			16(1)	23(3)	22(1)		22(1)	19(2)		
	Shear angle,θ	27	16	25		23	17			-20	19	-27	-19	21	-30			35	18	16		22	21		
#6	Tan $_{SS}$	7(5)	4(1)	4(2)		3(2)	5(2)		8(2)	7(2)	8(1)	8(1)	9(1)	11(2)	13(1)		8(1)	7(1)	6(1)			8(2)	7(1)	7(2)	
	Press.	62(8)	64(6)	64(6)		54(8)	59(11)		54(6)	57(2)	58(3)	49(4)	57(5)	59(6)	63(6)		57(6)	67(7)	64(8)			59(4)	57(3)	54(6)	42(3)
	Lon $_{SS}$	22(2)	16(4)	19(2)		17(4)	16(3)		18(2)	17(2)	22(1)	23(1)	19(1)	14(2)	18(1)		17(1)	15(1)	19(1)			21(2)	19(1)	18(4)	
	Resultant SS	23(5)	16(4)	19(3)		17(4)	17(4)		20(3)	18(3)	23(1)	24(1)	21(1)	18(3)	22(1)		19(1)	17(1)	20(1)			22(3)	20(1)	19(4)	
	Shear angle,θ	18	14	12		10	17		24	22	20	19	25	38	36		25	25	18			21	20	21	
#7	Tan $_{SS}$	9(3)	7(2)			8(1)	8(1)			8(2)	5(2)		-4(1)	-3(1)	-8(1)			2(1)	6(1)			7(1)	8(2)		
	Press.	80(10)	64(6)			64(9)	67(12)			64(4)	68(4)		67(1)	57(3)	67(3)			67(4)	56(8)			64(9)	67(9)		45(2)
	Lon $_{SS}$	35(2)	25(2)			28(3)	24(1)			27(3)	28(3)		27(2)	25(4)	24(5)			16(2)	17(2)			18(2)	23(3)		
	Resultant SS	36(4)	26(3)			29(3)	25(1)			28(4)	28(4)		27(2)	25(4)	25(5)			16(2)	18(2)			19(2)	24(4)		
	Shear angle,θ	14	16			16	18			16	10		-8	-7	-18			7	19			21	19		

...Contd... Table 7.13 : Average pressures ± (1SD) across all sites for HYDROCAST sockets during gait measured using B.E.S.T. Note; Tan $_{SS}$ = Tangential shear stress, Press. = Pressure and Lon $_{SS}$ = Longitudinal shear stress. Stress units all in kPa and shear angle in degree. The patellar tendon (PT) bar pressure and shear stresses were measured using PT transducer and distal end pressure was measured using electrohydraulic transducer.

		PT	A1	A2	AM-1	AM0	AM1	AM2	M-1	M0	M1	M2	PM1	P1	PL1	PL2	L-1	L0	L1	L2	AL-1	AL0	AL1	AL2	DE
#8	Tan $_{SS}$	10(8)	9(1)			8(2)	6(3)			-5(2)	-6(1)		-7(2)	-8(2)	-5(3)			4(1)	8(1)			6(1)	3(1)		
	Press.	64(11)	56(7)			57(11)	58(10)			46(6)	57(8)		48(10)	52(11)	52(8)			51(4)	56(6)			53(13)	57(2)		42(3)
	Lon $_{SS}$	23(4)	18(3)			15(4)	11(2)			20(2)	18(2)		17(3)	15(4)	11(2)			14(3)	13(2)			18(4)	20(6)		
	Resultant SS	25(9)	20(3)			17(4)	13(4)			21(3)	19(2)		18(4)	17(4)	12(4)			15(3)	15(2)			19(4)	20(6)		
	Shear angle,θ	23	27			28	29			-14	-18		-22	-28	-24			16	32			18	9		
#9	Tan $_{SS}$	9(3)	7(1)	-8(1)		4(3)	7(2)			8(1)			9(3)	10(1)	-8(1)			7(2)	6(3)						
	Press.	61(12)	57(6)	64(3)		54(12)	48(8)			57(7)			64(8)	54(7)	54(8)			64(9)	62(8)						35(4)
	Lon $_{SS}$	29(6)	22(5)	23(2)		18(4)	17(2)			15(4)			18(6)	19(2)	21(1)			19(2)	22(2)						
	Resultant SS	30(7)	23(5)	24(2)		18(5)	18(3)			17(4)			20(7)	21(2)	22(1)			20(3)	23(4)						
	Shear angle,θ	17	18	-19		13	22			28			27	28	-21			20	15						
#10	Tan $_{SS}$	11(1)	8(2)	7(1)		5(2)	6(2)			-8(1)	-6(1)		5(1)	7(1)	-8(1)			4(1)	-6(2)			5(2)	5(1)		
	Press.	57(14)	47(4)	52(4)		48(14)	54(7)			53(4)	54(5)		54(6)	62(7)	53(5)			59(6)	54(8)			52(7)	48(6)		49(2)
	Lon $_{SS}$	23(5)	21(2)	20(2)		18(6)	17(1)			15(3)	14(2)		22(1)	21(8)	19(4)			17(8)	18(2)			19(2)	20(4)		
	Resultant SS	25(5)	22(3)	21(2)		19(6)	18(2			17(3)	15(2)		23(1)	22(8)	21(4)			17(8)	19(3)			20(3)	21(4)		
	Shear angle,θ	26	21	19		16	19			-28	-23		13	18	-23			13	-18			15	14		

...Contd... Table 7.13 : Average pressures ± (1SD) across all sites for HYDROCAST sockets during gait measured using B.E.S.T. Note; Tan $_{SS}$ = Tangential shear stress, Press. = Pressure and Lon $_{SS}$ = Longitudinal shear stress. Stress units all in kPa and shear angle in degree. The patellar tendon (PT) bar pressure and shear stresses were measured using PT transducer and distal end pressure was measured using electrohydraulic transducer.

7.7.1 General curves of interface stresses

The interface stress results from the dynamic tests on test subjects are shown in Figures 7.20 to 7.69. Interface stress measurement sites labelled for each subject are located on each of the PTB and hydrocast sockets as shown in figure 6.9, table 7.1 and table 7.2. Positive sign conventions for the directions are also shown and described. (Figure 7.2 and section 7.2).

The interface stresses during the stance phase of walking at most sites showed a two peak pattern. Williams et al (1992) also stated that most measurements of pressures during gait, show that the major general shapes of the interface stresses are double peaked. Prior to heel strike, the pressures began to increase gradually. This was due to musculature contraction in preparation for heel strike. In a previous study by Pearson et al (1974) muscular contraction in the trans-tibial residual limb has been shown to produce pressures twice those that occur when the muscles were relaxed. The rate of increase in pressures in this short time frame was dependent on the location of the sites. At heel strike, the pressures increased almost instantaneously which was followed by a steep climb to the first peak. During stance phase, interface stresses curves were usually double-peaked with the first peak 10% to 25% into stance phase of the gait cycle (0.12 s to 0.32 s after heel strike and the second peak at 40% to 62% of gait cycle (0.48 s to 0.67 s) after heel strike. Generally, the first peak is associated with weight-acceptance followed by translational motion forward, and the second peak is associated with push off.

7.7.2 Peak Interface Stresses and shear angles directions.

Maximum interface pressures and shear stresses were achieved during the stance phase of the gait. As in table 7.12 for PTB socket, the maximum magnitudes recorded were 230 ± 17 kPa for pressure at the PT bar for subject # 7 and the maximum resultant shear stresses recorded were 53 ± 6 kPa at the PT bar for subject # 3. Excluding the PT bar position, which is well known as an area of high pressure, the maximum magnitudes measured are 116 ± 5 kPa at site AL1 of subject # 6 and the maximum resultant shear stresses 43 ± 2 kPa at site M1 of subject # 7 in the PTB socket. For the hydrocast socket (table 7.13), the maximum magnitudes were 80 ± 10 kPa, for pressure at the site of the PT bar for subject # 7, and for resultant shear stresses 36 ± 4 kPa at the site of the PT bar also for subject # 7. Again if the PT bar is not included, (even though the hydrocast socket is designed without rectification at the PT bar area, the PT bar is named just for comparison), the maximum magnitudes measured were 69 ± 8 kPa, for pressure, at site PL1 of subject # 1 and 32 ± 2 kPa, for shear stress, at site P1 of subject # 3. For the interface shear stresses (Figures 7.20 to 7.69), it was also observed that a longitudinal shear stress occurred as the limb pistoned into the socket during the stance phase and out again during swing phase. A double peak of longitudinal shear stress was evident during stance. The first peak was due to reaction forces during deceleration, followed by reduction as the body moves onto the forefoot. The second peak is probably due to the subject pushing down onto the prosthesis to gain some spring from the artificial foot providing upward acceleration on the body before toe-off. It may also be due to muscle flexion as the subject gains a stable purchase on the prosthesis before lifting it into

the swing phase. Tangential shear stress was seen to be much smaller than longitudinal shear, as was observed by Sanders and Daly (1989) and Sanders et al (1992). Table 7.14 (PTB socket) and table 7.15 (Hydrocast socket) summarises the results obtained.

Subject		Pressure, , ± 1 SD (kPa), [Site]		Resultant SS, ± 1 SD (kPa), [Site]		Shear angle, θ, (deg.) [Site]	
#1	Minimum	5(2)	AM0	9(5)	PM3	-25	PL3
	Maximum	203(10)	PT bar	51(4)	PT bar	28	PM1
#2	Minimum	10(1)	AM0	6(2)	AM0	-35	PL2
	Maximum	229(14)	PT bar	39(4)	PT bar	36	P1
#3	Minimum	10(3)	AL-1	8(2)	AL-1	-30	AL-1
	Maximum	226(15)	PT bar	53(6)	PT bar	40	A1
#4	Minimum	28(3)	L0	13(4)	L0	-21	PM1
	Maximum	224(10)	PT	40(5)	PT	29	L0
#5	Minimum	27(4)	AM0	13(1)	AM0	-18	PM1
	Maximum	202(10)	PT bar	47(2)	PT bar	34	L0
#6	Minimum	17(2)	AM0	11(1)	AM0	-34	AM0
	Maximum	210(16)	PT bar	48(4)	PT bar	22	PT bar
#7	Minimum	37(6)	AM0	19(4)	AL0	-21	PL1/A1
	Maximum	230(17)	PT bar	43(3)	PT bar	21	PT bar
#8	Minimum	27(3)	AL0	17(4)	AL0	-23	A1/PM1
	Maximum	200(9)	PT bar	40(4)	AL1	23	M0
#9	Minimum	25(9)	AM0	16(4)	AM0	-31	PL1
	Maximum	190(9)	PT bar	47(6)	AL1	32	PT bar
#10	Minimum	27(6)	AM0	17(1)	AM0	-29	PL2
	Maximum	187(10)	PT bar	42(1)	AL1	28	PL1

Table 7.14: Summarised minimum and maximum stresses values obtained from the PTB socket for all subjects during the gait.

Subject		Pressure, , ± 1 SD (kPa), [Site]		Resultant SS, ± 1 SD (kPa), [Site]		Shear angle, θ, (deg.) [Site]	
#1	Minimum	35(4)	DE	10(3)	AM-1	-18	AL0
	Maximum	64(3)	L2	27(8)	PL2	37	AM-1
#2	Minimum	49(6)	AL0	13(2)	P1	-30	M0
	Maximum	68(7)	PT bar	23(5)	PT bar	32	P1
#3	Minimum	6(1)	P1	18(3)	L1	-14	M0
	Maximum	71(8)	PT bar	32(2)	P1	60	P1
#4	Minimum	48(4)	M0	17(1)	M2	-28	M1
	Maximum	67(6)	M2	25(3)	AM1	22	PM1
#5	Minimum	46(3)	M1	16(1)	L0	-30	PL1
	Maximum	67(6)	P1/L2	24(5)	AM1	35	L0
#6	Minimum	49(4)	M2	16(4)	A1	10	AM0
	Maximum	67(7)	L0	24(1)	M2	38	P1
#7	Minimum	56(8)	L1	16(2)	L0	-18	PL1
	Maximum	80(10)	PT	36(4)	PT bar	21	AL0
#8	Minimum	46(6)	M0	12(4)	PL1	-28	P1
	Maximum	64(11)	PT	25(9)	PT	32	L1
#9	Minimum	48(8)	AM1	17(4)	M0	-21	PL1
	Maximum	64(8)	PM1	30(7)	PT	28	PT bar
#10	Minimum	47(4)	A1	15(2)	M1	-28	M0
	Maximum	62(7)	P1	25(5)	PT bar	26	PT bar

Table 7.15: Summarised minimum and maximum stresses values obtained from the Hydrocast socket for all subjects during gait.

For the PTB socket, the average stresses had a wide range, the normal stress from 5 ± 2 kPa to 230 ± 17 kPa, and the resultant shear stresses from 9 ± 5 kPa to 53 ± 6 kPa. The maximum pressures, as expected, occurred at the patellar tendon bar. Whilst for the Hydrocast socket, the average stresses were in the range of 35 ± 4 kPa to 80 ± 10 kPa, and resultant shear stresses from 10 ± 3 kPa to 36 ± 4 kPa. As mentioned before, during the static test section, shear angles were calculated from $\theta = \tan^{-1}$ (lon $_{ss}$ / tan $_{ss}$). Figure 7.70 and Figure 7.71 for the PTB and Hydrocast sockets give examples of the shear angles during stance phase at five selected measurement points for subject #7.

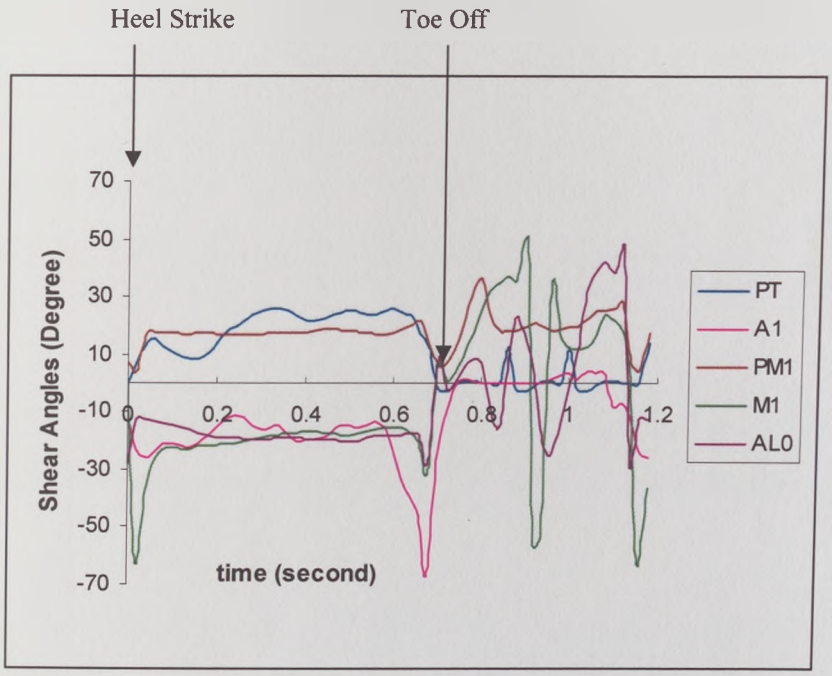

Figure 7.70: Example of shear angles during gait for subject #7 wearing a PTB socket.

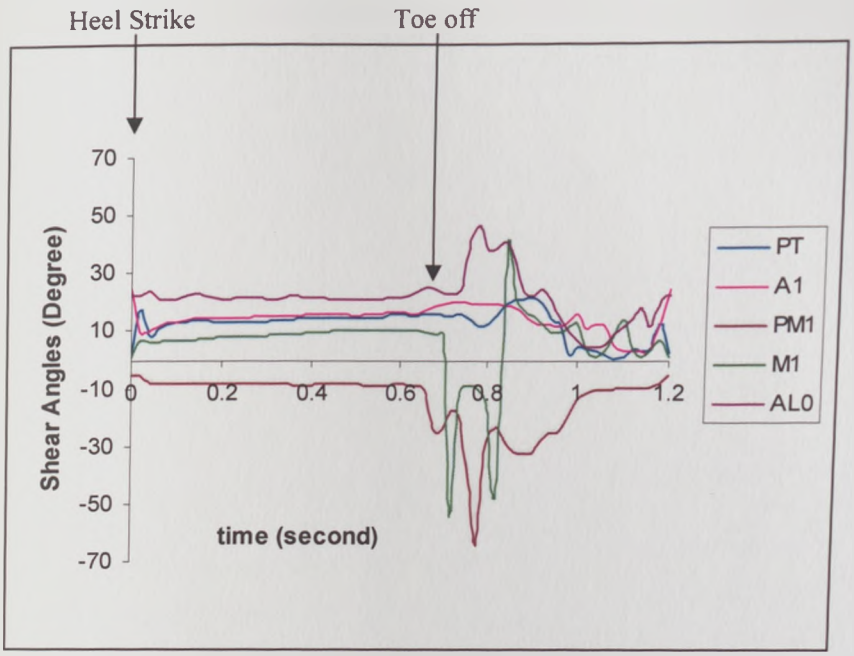

Figure 7.71: Example of shear angles during gait for subject #7 wearing a Hydrocast socket.

It is seen that the angles during swing phase were changeable, possible explanation caused by the effect in the longitudinal shear stress. Pictorial representation of peak resultant shear stresses and shear directions of PTB and Hydrocast socket for 10 subjects are shown in Figures 7.72 to 7.79. The main directions of the shear stresses were upward during stance. Due to the existence of tangential shear stress, the angles change in the range of $\pm 50^0$. The longitudinal shear stresses at all sites were upward (Figures 7.72 to 7.79) to help supporting the body weight during stance phase. The tangential shear stresses were also found at every site measured for every subject.

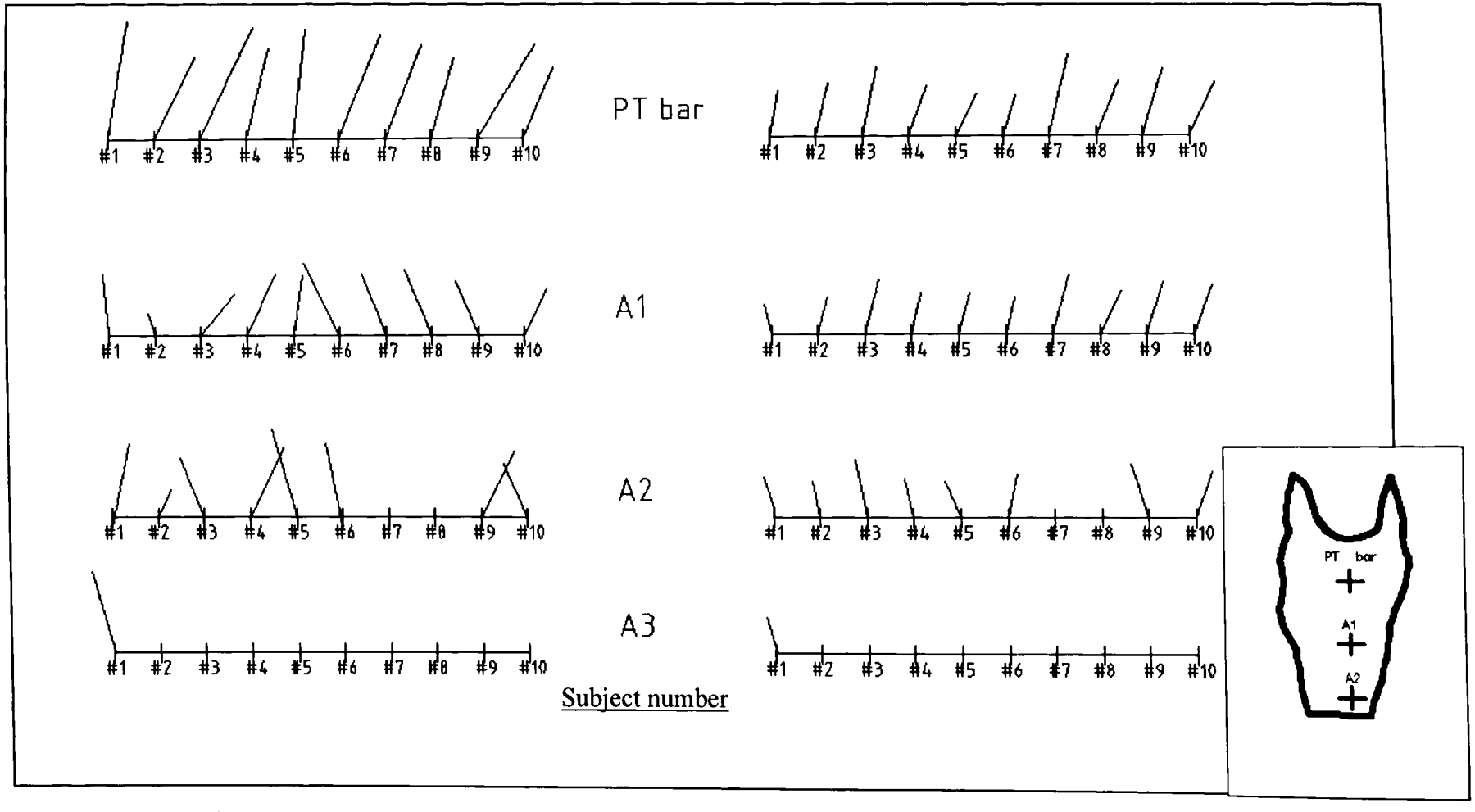

Figure 7.72: Peak resultant shear stress directions at sites: PT bar, A1,A2 and A3 for subject # 1 to #10 of PTB (left) and Hydrocast (right sockets). All vectors shown are directed upward and occurred at different times in the gait cycle. Magnitudes are to AutoCad software computer scale. Socket picture is for illustration only.

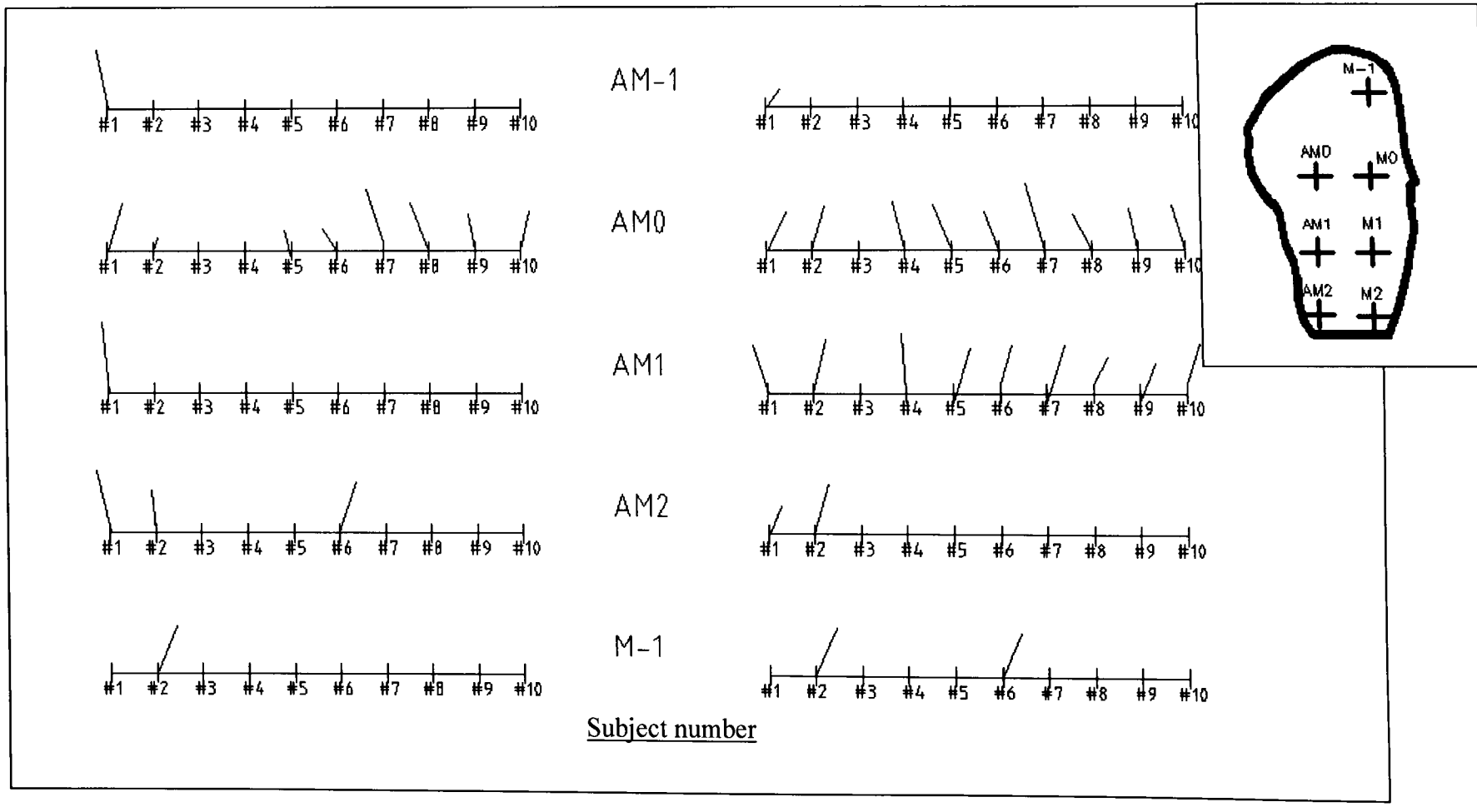

Figure 7.73: Peak resultant shear stress directions at sites: AM-1, AM0, AM1, AM2, and M-1 for subject # 1 to #10 of PTB (left) and Hydrocast (right sockets). All vectors shown are directed upward and occurred at different times in the gait cycle. Magnitudes are to AutoCad software computer scale. Socket picture is for illustration only.

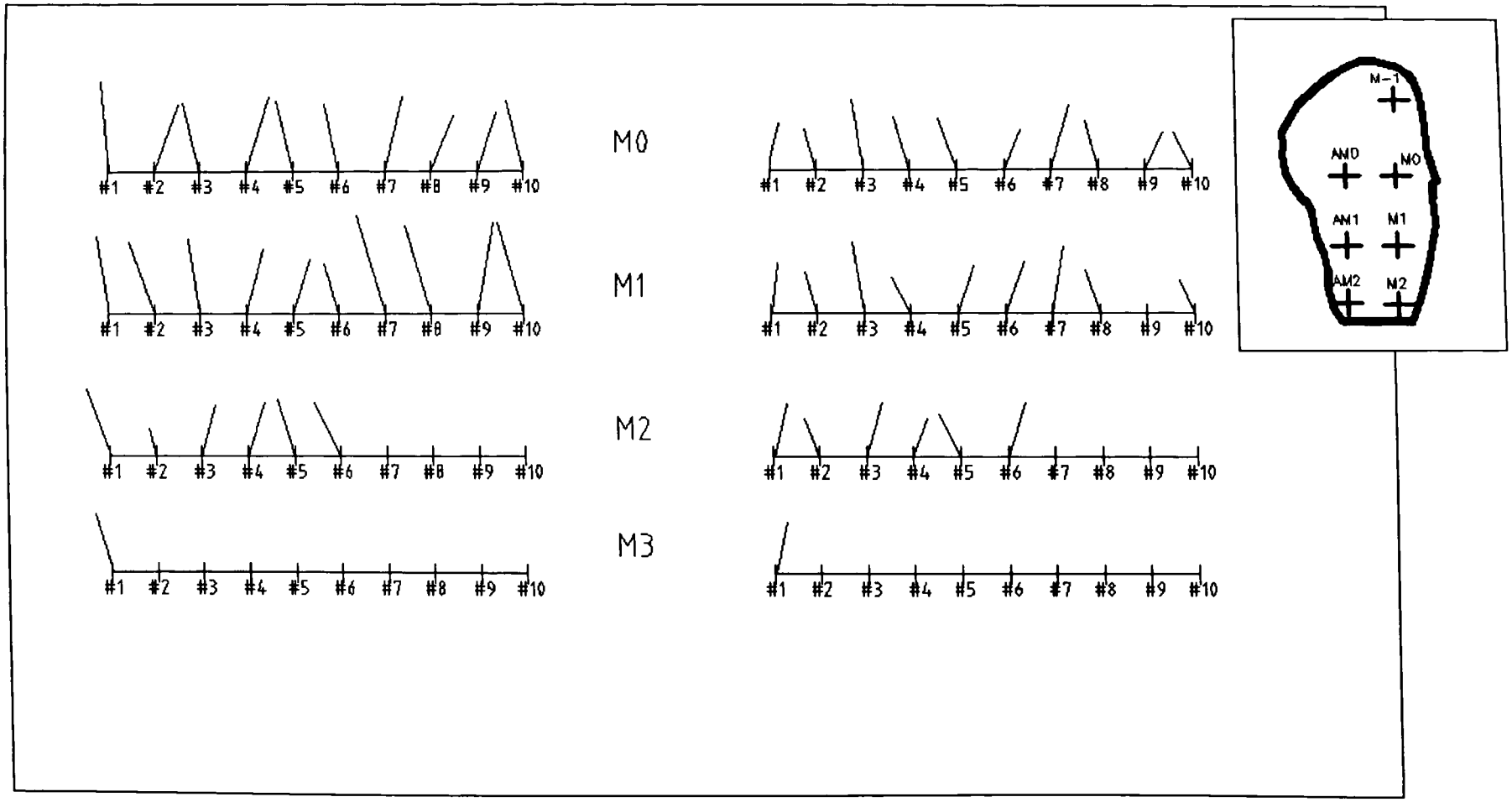

Figure 7.74: Peak resultant shear stress directions at sites: M0, M1, M2 and M3 for subject # 1 to #10 of PTB (left) and Hydrocast (right sockets). All vectors shown are directed upward and occurred at different times in the gait cycle. Magnitudes are to AutoCad software computer scale. Socket picture is for illustration only.

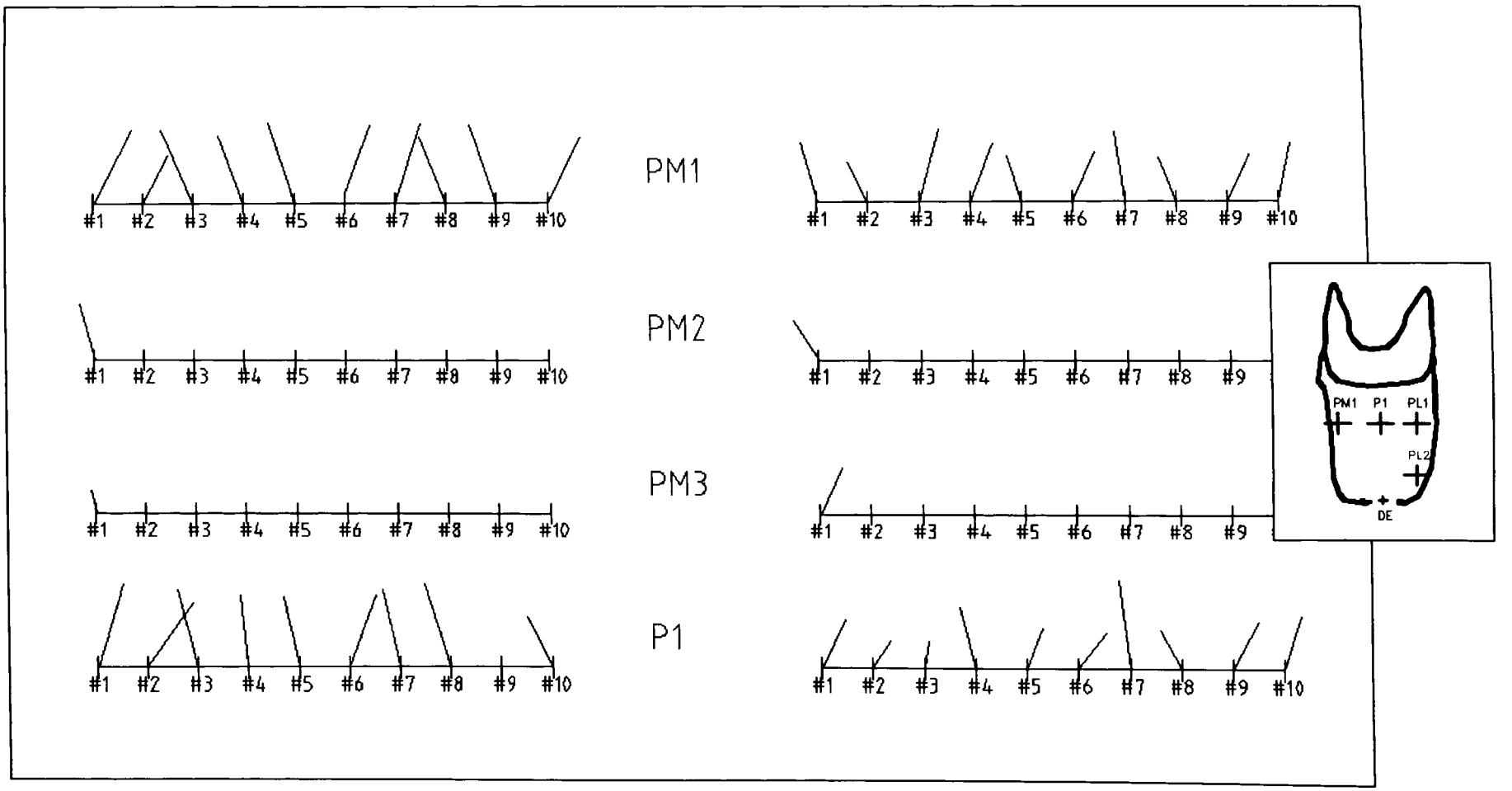

Figure 7.75: Peak resultant shear stress directions at sites: PM1, PM2, PM3 and P1 for subject # 1 to #10 of PTB (left) and Hydrocast (right sockets). All vectors shown are directed upward and occurred at different times in the gait cycle. Magnitudes are to AutoCad software computer scale. Socket picture is for illustration only.

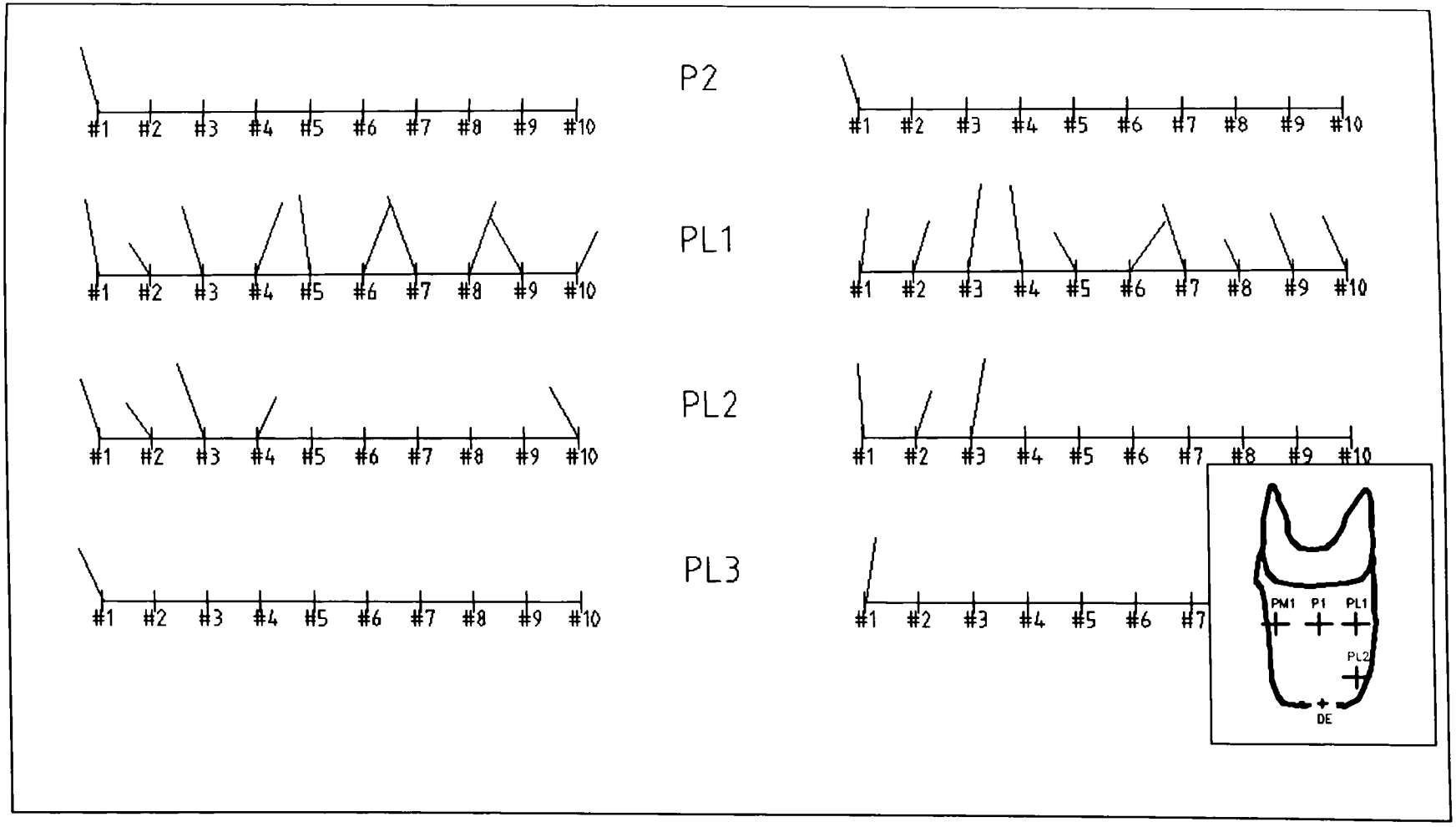

Figure 7.76: Peak resultant shear stresses directions at sites: P2, PL1,PL2 and PL3 for subject # 1 to #10 of PTB (left) and Hydrocast (right sockets). All vectors shown are directed upward and occurred at different times in the gait cycle. Magnitudes are to AutoCad software computer scale. Socket picture is for illustration only.

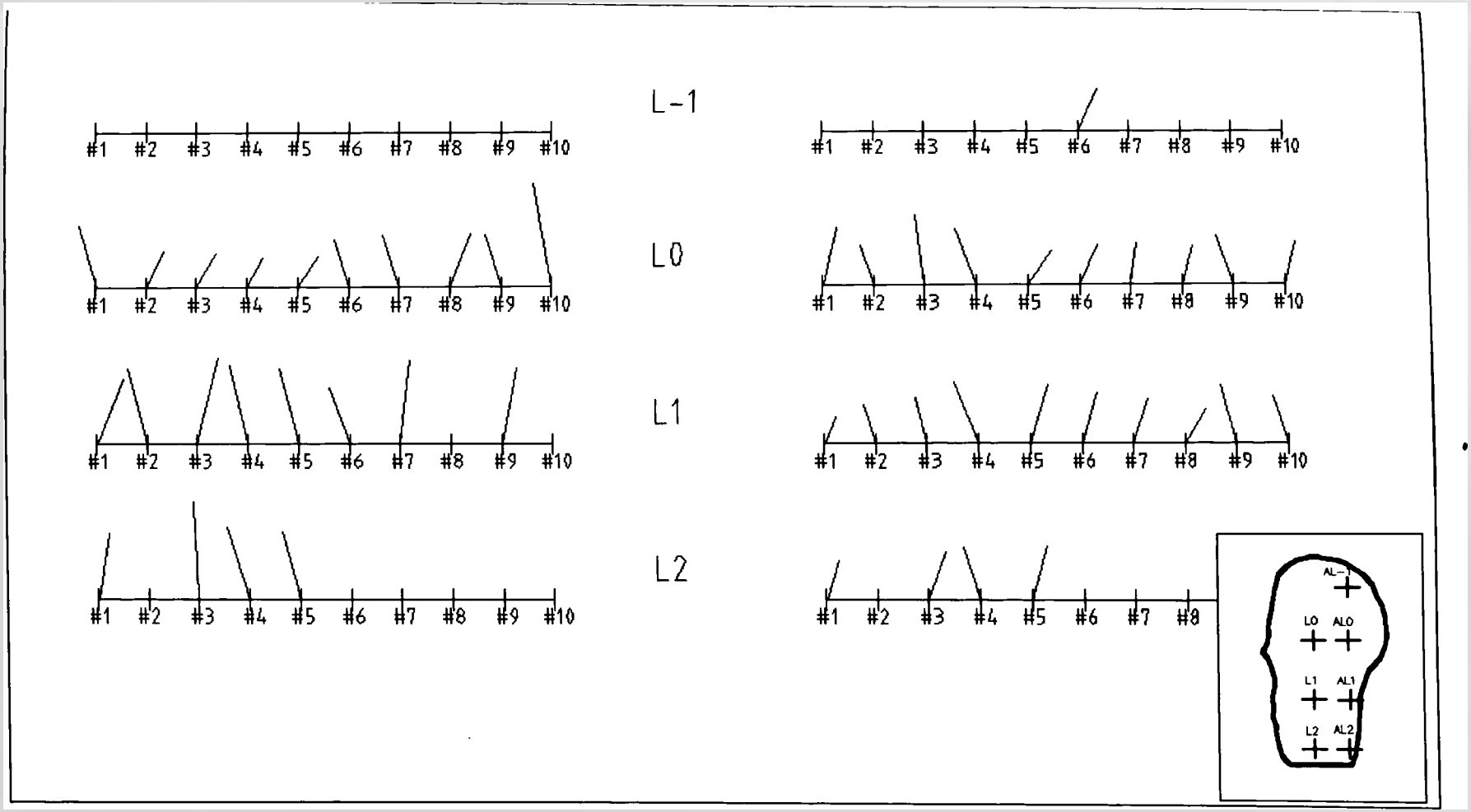

Figure 7.77: Peak resultant shear stress directions at sites: L-1, L0, L1 and L2 for subject # 1 to #10 of PTB (left) and Hydrocast (right sockets). All vectors shown are directed upward and occurred at different times in the gait cycle. Magnitudes are to AutoCad software computer scale. Socket picture is for illustration only.

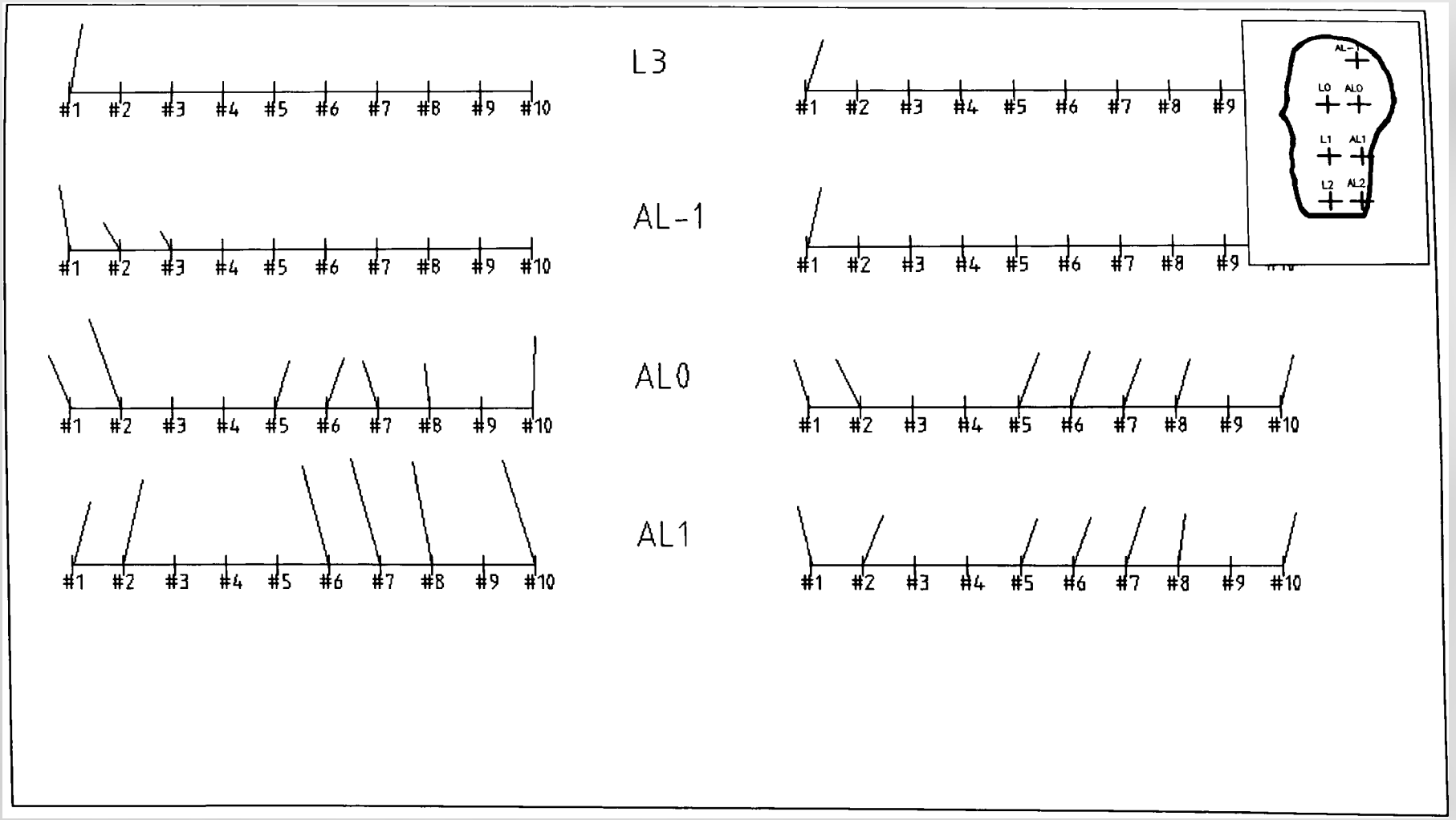

Figure 7.78: Peak resultant shear stress directions at sites: L3, AL-1, AL0 and AL1 for subject # 1 to #10 of PTB (left) and Hydrocast (right sockets). All vectors shown are directed upward and occurred at different times in the gait cycle. Magnitudes are to AutoCad software computer scale. Socket picture is for illustration only.

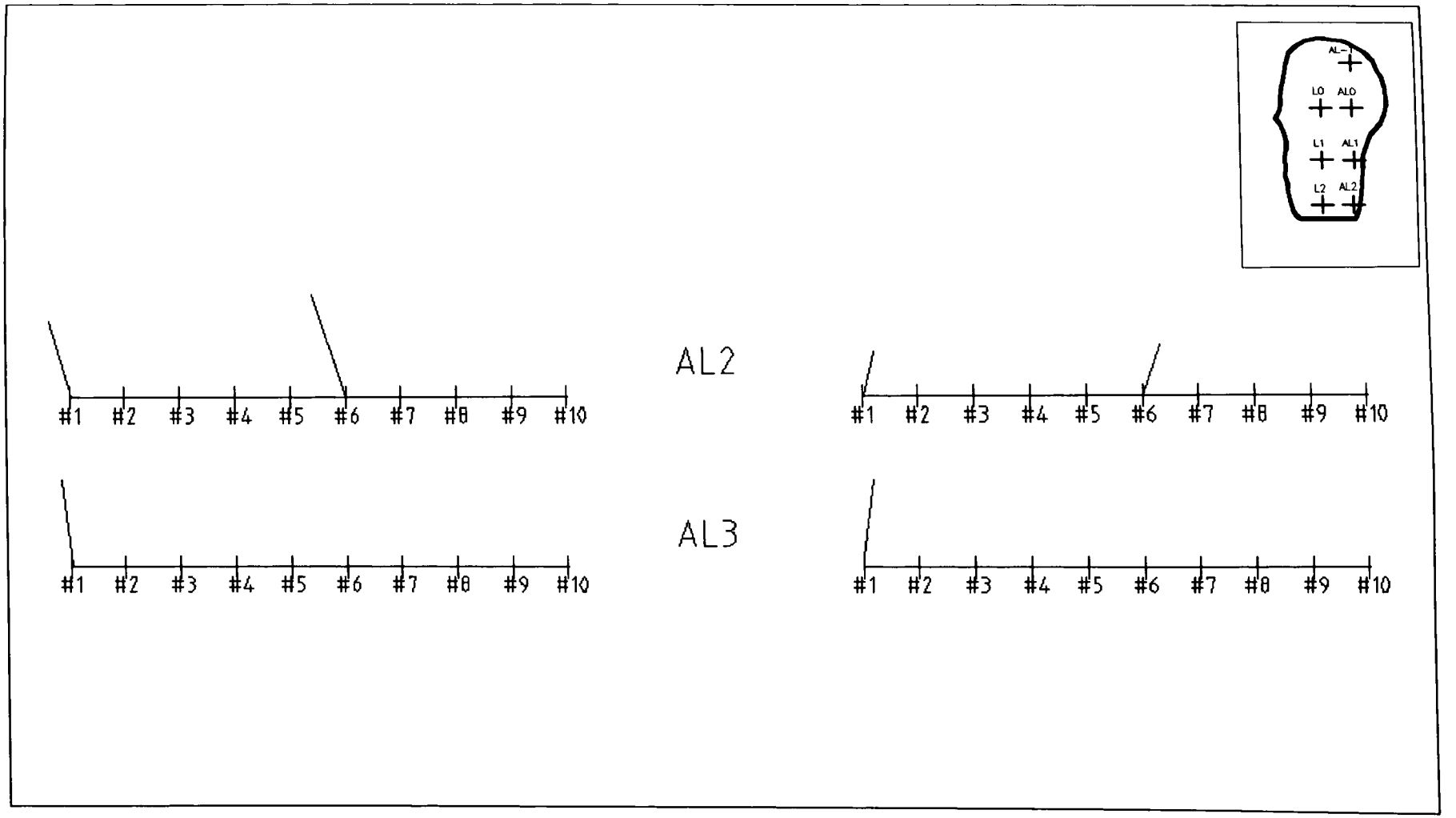

Figure 7.79: Peak resultant shear stress directions at sites: AL2 and AL3 for subject # 1 to #10 of PTB (left) and Hydrocast (right sockets). All vectors shown are directed upward and occurred at different times in the gait cycle. Magnitudes are to AutoCad software computer scale. Socket picture is for illustration only.

7.7.3 Resultant Shear Stress to Pressure (Ratios)

The ratios of resultant shear stresses to pressure at measured sites of the socket for all ten subjects are shown in table 7.16 (PTB socket) and table 7.17 (Hydrocast socket). An unstable change of the ratios may result from the influence of error in small pressure values. At most points, the ratios were less than 1.0 with the exception of subject # 1 with the PTB socket. This occurred because of pistoning during the initial experiments. Thus increasing the shear stress as a direct result. The average ratios for the PTB socket were 0.49 ± 0.15; minimum ratio of 0.17 at PT for subject #10 and the maximum ratio of 4.22 at site AL1 for subject #1. If subject #1 is excluded (due to problems of pistoning,), the maximum ratio is 0.82 at site L0 for subject # 2. Whilst for the Hydrocast socket the average ratio was 0.37 ± 0.05; with minimum ratio of 0.19 at PT for subject # 1 and the maximum ratio of 0.95 at AM1 for subject # 4.

Subj.	Site																					Aver.	SD
#1	0.25	0.53	0.47	0.49	1.61	4.18	0.54	0.92	2.27	0.53	0.38	0.96	1.53	0.51	0.49	0.58	0.40	0.50	0.47	0.61	0.50		0.92	1.02
	L1	L2	L3	AL-1	AL0	AL1	AL2	AL3	DE														
#1	0.41	0.51	0.35	4.22	0.60	0.35	0.25	1.36															
	PT	A1	A2	AM-1	AM0	AM1	AM2	M-1	M0	M1	M2	PM1	P1	PL1	PL2	L-1	L0	L1	L2	AL-1	AL0	AL1		
#2	0.17	0.18	0.20		0.63	0.67	0.46		0.51	0.50	0.59	0.44	0.45	0.27	0.63		0.82	0.55		0.40	0.32	0.41	0.46	0.18
#3	0.23	0.57	0.45						0.50	0.38	0.55	0.41	0.52	0.44	0.49		0.53	0.44		0.81			0.49	0.13
#4	0.18	0.50	0.43						0.48	0.37	0.54	0.44	0.39	0.45	0.44		0.45	0.57	0.41				0.43	0.10
#5	0.23	0.46	0.62		0.49				0.55	0.32	0.64	0.52	0.41	0.43			0.52	0.46	0.42		0.49		0.47	0.11
#6	0.23	0.59	0.48		0.64	0.59	0.50		0.45	0.23	0.49	0.34	0.38	0.37			0.44	0.38			0.45	0.34	0.43	0.12
#7	0.19	0.39			0.62	0.46			0.44	0.36		0.44	0.33	0.46			0.42	0.39			0.35	0.34	0.40	0.10
#8	0.18	0.47			0.64	0.36			0.39	0.41		0.46	0.48	0.55			0.61				0.63	0.41	0.47	0.13
#9	0.25	0.33	0.49		0.65	0.43			0.35	0.35		0.46		0.36			0.60	0.40					0.42	0.12
#10	0.17	0.41	0.31		0.65	0.43			0.45	0.40		0.42	0.35	0.24	0.59		0.62				0.56	0.36	0.43	0.14
																					Average	0.49	0.15

Table 7.16: Ratio of Resultant Shear Stress to Pressure for PTB socket.

Subj.	Site																						Aver.	SD
	PT	A1	A2	A3	AM-1	AM0	AM1	AM2	AM3	M0	M1	M2	M3	PM1	PM2	PM3	P1	P2	PL1	PL2	PL3	L-1	L0		
#1	0.33	0.24	0.23	0.31	0.21	0.36	0.45	0.23	0.26	0.32	0.46	0.39	0.32	0.55	0.32	0.39	0.41	0.51	0.34	0.47	0.36		0.35	0.36	0.11
	L1	L2	L3	AL-1	AL0	AL1	AL2	AL3																	
#1	0.19	0.25	0.40	0.56	0.34	0.36	0.25	0.57																	
	PT	A1	A2	AM-1	AM0	AM1	AM2	M-1	M0	M1	M2	PM1	P1	PL1	PL2	L-1	L0	L1	L2	AL-1	AL0	AL1	AL2		
#2	0.33	0.27	0.28		0.33	0.46	0.38	0.37	0.31	0.34	0.28	0.30	0.20	0.35	0.33		0.29	0.23			0.41	0.31		0.32	0.06
#3	0.42	0.40	0.45						0.49	0.53	0.39	0.57	0.58	0.51	0.58		0.49	0.34	0.38					0.47	0.08
#4	0.40	0.35	0.31		0.36	0.95			0.48	0.30	0.26	0.42	0.46	0.56			0.41	0.46	0.41					0.44	0.17
#5	0.35	0.34	0.29		0.40	0.45			0.43	0.46	0.44	0.35	0.26	0.28			0.25	0.37	0.33		0.37	0.31		0.35	0.07
#6	0.37	0.26	0.30		0.32	0.28		0.36	0.32	0.40	0.50	0.37	0.30	0.35		0.33	0.25	0.31			0.38	0.36		0.34	0.06
#7	0.45	0.41			0.46	0.38			0.44	0.42		0.41	0.44	0.38			0.24	0.32			0.30	0.36		0.38	0.06
#8	0.39	0.36			0.30	0.22			0.45	0.33		0.38	0.33	0.23			0.29	0.27			0.36	0.35		0.33	0.07
#9	0.50	0.41	0.38		0.34	0.38			0.30			0.31	0.40	0.42			0.32	0.37						0.37	0.06
#10	0.45	0.48	0.41		0.39	0.33			0.32	0.28		0.42	0.36	0.39			0.30	0.35			0.38	0.43		0.38	0.06
																							Average	0.37	0.05

Table 7.17: Ratio of Resultant Shear Stress to Pressure for Hydrocast socket.

7.7.4 Stresses distribution around the sockets.

The average stresses distribution measured using the B.E.S.T transducers from ten subjects for the PTB and Hydrocast socket are shown in Table 7.18. Low standard deviations were found in the Hydrocast socket compared to the PTB socket and thus, the results also show, during dynamic gait that a more uniform stresses distribution was recorded from the Hydrocast socket compared to the conventional PTB socket. (Figure 7.80 and Figure 7.81).

	PT bar, A1, A2 and A3	AM-1, AM0, AM1, AM2, AM3, M0, M1, M2, M3	PM1, PM2, PM3, P1, P2, PL1, PL2, PL3	L-1, L0, L1, L2, L3, AL-1, AL0, AL1, AL2, AL3
	Anterior	Medial	Posterior	Lateral
Hydrocast socket				
Pressure (kPa) Average ± 1 SD	60 ± 7	55 ± 6	57 ± 7	58 ± 6
Resultant SS (kPa) Average ± 1 SD	22 ± 5	21 ± 6	22 ± 5	19 ± 3
PTB socket				
Pressure (kPa) Average ± 1 SD	115 ± 72 64 ± 10 ***	52 ± 27	61 ± 16	59 ± 31
Resultant SS (kPa) Average ± 1 SD	33 ± 10 28 ± 7 ***	26 ± 7	26 ± 6	26 ± 9

*** Results for PT bar not included.

Table 7.18: Average pressure and shear stresses distribution on ten subjects for Hydrocast and PTB socket.

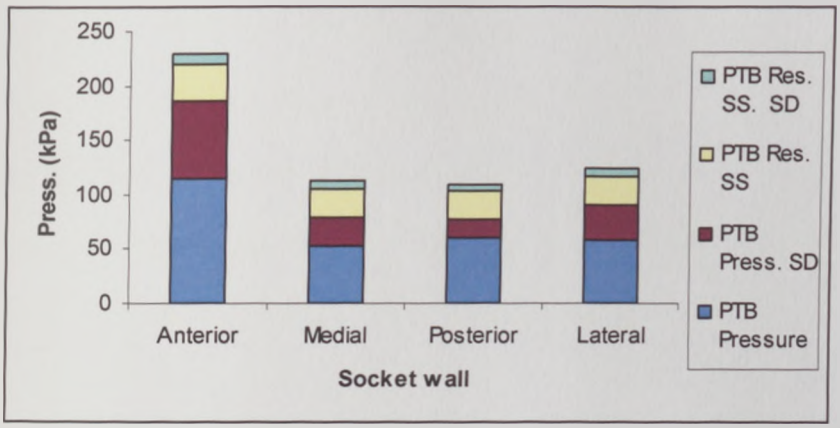

Figure 7.80: Average peak stresses on 10 subjects for the PTB socket.
Note : Res.SS = Resultant shear stress and SD =Standard deviation.

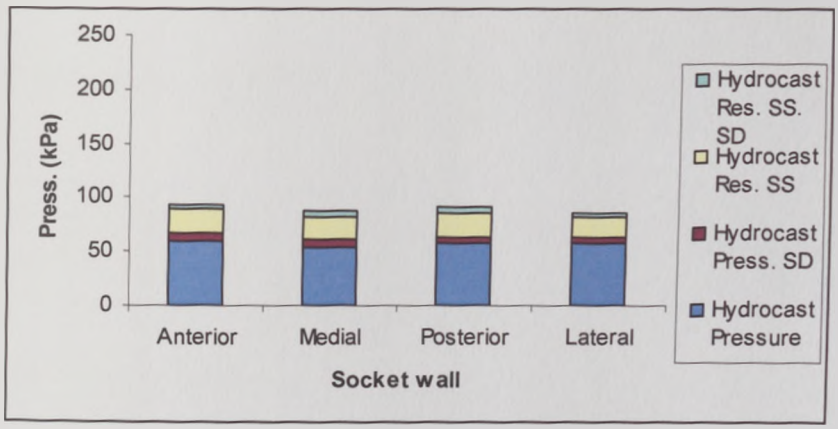

Figure 7.81: Average peak stresses on 10 subjects for the Hydrocast socket.
Note : Res.SS = Resultant shear stress and SD =Standard deviation.

7.8 Results of interface pressure measurement using commercial F-Socket™ sensor.

As explained in Chapter 6, section 6.3.2, during F-Socket™ sensor testing on the subjects, all the proximal sensors of the anterior, posterior, medial and lateral aspects were positioned at a level just below the Patellar Tendon Bar due to the experimental socket, with its moveable patellar tendon bar, preventing more proximal sensor measurement, therefore site measurement around the socket wall only occurred below the datum "0".

The average values of the peak pressure results during dynamic gait using the F-Socket™ sensor are presented in table 7.19 (PTB socket) and table 7.20 (Hydrocast socket). The tables also present comparison results from the same site with other the transducers utilised in these studies i.e. custom-made B.E.S.T, customised-commercial Entran transducer and custom built electrohydraulic transducer for distal end measurement.

Differences were seen in average peak magnitude interface pressure for F-Socket™ sensor but not for Entran and B.E.S.T. transducers. This was expected because of different sessions and possibility because of temporal changes in stump volume. Percentage of difference for the F-Socket™ sensor against Entran transducer for the PTB socket ranged from 6% at site L1, subject # 7, to 38% at site PL2, subject # 2, and at site AM3, subject # 1. Whilst for the Hydrocast socket, the difference ranged from 4 % at site A2, subject # 9, to 29 % at site AL1, subject # 6.

Subject		PTB Socket Site																						
		A1	A2	A3	AM1	AM2	AM3	M1	M2	M3	PM1	PM2	PM3	P1	P2	PL1	PL2	PL3	L1	L2	L3	AL1	AL2	AL3	DE
# 1 Pressure (kPa)	FScan	57(9)	82(11)	83(9)	64(7)	40(5)	18(9)	86(11)	39(8)	26(6)	69(8)	50(9)	18(8)	91(9)	62(8)	70(9)	51(10)	55(9)	76(11)	61(12)	67(13)	88(14)	121(10)	21(8)	32(2)
	Entran	45(3)	70(2)	78(4)	54(3)	31(2)	13(2)	76(2)	29(3)	19(2)	59(3)	42(2)	14(6)	85(6)	54(4)	62 (3)	42(5)	43(3)	68(3)	50(4)	54(2)	76(3)	106(6)	21(2)	
	BEST	49(5)	76(6)	74(8)	56(5)	29(3)	11(4)	78(6)	31(5)	17(8)	62(2)	45(4)	16(5)	87(2)	50(2)	60 (1)	38(3)	42(1)	66(5)	52(8)	58(6)	72(7)	113(10)	23(6)	23(4)*
% of different against Entran	FScan	27	17	6	19	29	38	13	34	37	17	19	29	7	15	13	21	28	12	22	24	16	14	29	37
	BEST	9	9	-5	4	-6	-15	3	7	-11	5	7	14	2	-7	-3	-10	-2	-3	4	7	-5	7	10	
# 2 Pressure (kPa)	FScan	68(10)	76(9)		35(8)	46(11)		70(6)	25(4)		61(5)			76(8)		64(9)	29(4)		60(11)			92(12)			31(5)
	Entran	54(4)	66(3)		28(7)	37(2)		63(2)	20(2)		52(3)			66(3)		53(2)	21(2)		52(2)			80(6)			
	BEST	58(2)	68(2)		25(2)	39(2)		64(2)	21(3)		49(3)			68(6)		54(5)	25(10)		54(7)			82(5)			23(3)*
% of different against Entran	FScan	26	15		25	24		11	25		17			15		21	38		15			15			35
	BEST	7	3		-11	5		2	5		-6			3		2	19		4			3			
# 3 Pressure (kPa)	FScan	49(9)	68(8)					92(7)	63(8)		84(9)			69(11)		67(8)	69(7)		85(10)	89(11)					16(3)
	Entran	39(4)	57(3)					83(4)	51(2)		74(3)			57(6)		56(4)	57(4)		74(3)	73(4)					
	BEST	41(3)	60(4)					85(6)	40(7)		75(3)			60(5)		60(4)	59(3)		77(3)	74(4)					12(2)*
% of different against Entran	FScan	26	19					11	24		14			21		20	21		15	22					33
	BEST	5	5					2	-22		1			5		7	4		4	1					
# 4 Pressure (kPa)	FScan	66(11)	88(13)					96(9)	53(11)		68(9)			82(10)		79(8)	46(9)		69(8)	86(7)					39(4)
	Entran	55(4)	74(3)					80(7)	47(2)		61(3)			69(7)		66(3)	34(4)		57(4)	76(3)					
	BEST	57(6)	76(7)					76(8)	45(6)		64(7)			72(6)		62(6)	38(8)		54(4)	72(5)					30(4)*
% of different against Entran	FScan	20	19					20	13		11			19		20	35		21	13					30
	BEST	4	3					-5	-4		5			4		-6	12		-5	-5					
# 5 Pressure (kPa)	FScan	69(10)	79(11)					86(11)	52(8)		77(6)			76(8)		79(9)			79(8)	76(7)					18(5)
	Entran	55(3)	62(5)					73(2)	42(4)		61(2)			65(3)		67(2)			64(4)	68(3)					
	BEST	57(6)	63(8)					75(7)	39(6)		63(8)			67(3)		68(3)			66(5)	64(2)					14(3)*
% of different against Entran	FScan	25	27					18	24		26			17		18			23	12					29
	BEST	4	2					3	-7		3			3		1			3	-6					

$n_{BEST} = 15$, $n_{ENTRAN} = 15$, $n_{FScan} = 50$

Table 7.19: Pressures comparison between commercial FScan 9811 F-Socket™ sensor, custom-commercial Entran transducer and custom-made B.E.S.T. for PTB socket. Note: * Pressure at distal end measured using electrohydraulic transducer. % of different for the distal end (DE) is against electrohydraulic transducer. n = number of tests represented in each transducer type.

Subject		PTB Socket Site																					
		A1	A2	A3	AM1	AM2	AM3	M1	M2	M3	PM1	PM2	PM3	P1	P2	PL1	PL2	PL3	L1	L2	L3	AL1	AL2	AL3	DE
# 6 Pressure (kPa)	FScan	66(10)	81(7)		61(6)	52(8)		102(8)	62(9)		93(8)			91(11)		81(11)			72(7)			126(12)	121		35(5)
	Entran	53(2)	72(4)		51(2)	44(3)		92(4)	51(5)		80(3)			77(4)		69(3)			60(4)			114(4)	104		
	B.E.S.T.	57(3)	74(2)		49(1)	46(2)		94(8)	52(8)		83(3)			79(4)		73(6)			61(2)			116(5)	105(4)		29(4)*
% of different against Entran	FScan	25	13		20	18		11	22		16			18		17			20			11	16		21
	B.E.S.T.	8	3		-4	5		2	2		4			3		6			2			2	1		
# 7 Pressure (kPa)	FScan	88(8)			64(9)			134(15)			90(10)			110(12)		79(5)			87(9)			142(14)			44(4)
	Entran	76(3)			54(3)			107(8)			70(4)			91(3)		63(3)			82(3)			119(9)			
	B.E.S.T.	71(8)			58(6)			118(3)			72(8)			92(9)		65(11)			83(6)			124(13)			35(4)*
% of different against Entran	FScan	16			19			25			29			21		25			6			19			26
	B.E.S.T.	-7			7			10			3			1		3			1			4			
# 8 Pressure (kPa)	FScan	72(7)			68(8)			99(11)			77(9)			81(13)		62(6)						134(11)			30(3)
	Entran	62(4)			57(4)			91(4)			60(3)			68(2)		50(4)						102(8)			
	B.E.S.T.	65(8)			59(11)			94(8)			62(7)			70(6)		51(9)						97(10)			24(5)*
% of different against Entran	FScan	16			19			9			28			19		24						31			25
	B.E.S.T.	5			4			3			3			3		2						-5			
# 9 Pressure (kPa)	FScan	82(6)	69(5)		59(11)			135(16)			81(9)					75(7)			79(10)						23(4)
	Entran	72(3)	63(2)		52(3)			114(10)			66(6)					63(3)			70(4)						
	B.E.S.T.	75(10)	65(11)		49(3)			110(4)			70(13)					64(5)			74(8)						19(3)*
% of different against Entran	FScan	14	10		13			18			23					19			13						21
	B.E.S.T.	4	3		-6			-4			6					2			6						
# 10 Pressure (kPa)	FScan	61(9)	91(8)		65(5)			121(17)			79(11)			82(10)		83(8)	41(3)					130(12)			34(3)
	Entran	54(2)	83(3)		54(3)			102(8)			65(4)			62(4)		72(4)	33(2)					117(9)			
	B.E.S.T.	55(8)	80(7)		52(5)			98(5)			67(5)			63(8)		70(7)	35(6)					115(12)			27(4)*
% of different against Entran	FScan	13	10		20			19			22			32		15	24					11			26
	B.E.S.T.	2	-4		-4			-4			3			2		-3	6					-2			

$n_{BEST} = 15$, $n_{ENTRAN} = 15$, $n_{FScan} = 50$

...Contd....Table 7.19: Pressures comparison between commercial FScan 9811 F-Socket™ sensor, custom-commercial Entran transducer and custom-made B.E.S.T. for PTB socket. Note: * Pressure at distal end measured using electrohydraulic transducer. % of different for the distal end (DE) is against electrohydraulic transducer. n = number of tests represented in each transducer type.

Subject		Hydrocast Socket Site																						
		A1	A2	A3	AM1	AM2	AM3	M1	M2	M3	PM1	PM2	PM3	P1	P2	PL1	PL2	PL3	L1	L2	L3	AL1	AL2	AL3	DE
# 1 Pressure (kPa)	FScan	63(9)	73(8)	62(11)	64(13)	68(11)	63(9)	57(8)	71(10)	79(7)	55(9)	66(11)	67(10)	62(12)	51(9)	80(11)	65(12)	72(11)	65(13)	70(10)	61(9)	75(11)	75(11)	55(10)	46(7)
	Entran	51(4)	64(4)	56(4)	51(2)	57(3)	55(3)	49(3)	62(4)	63(4)	41(3)	51(4)	53(3)	5	40(4)	72(4)	55(3)	63(4)	52(4)	60(4)	49(3)	58(3)	58(3)	43(4)	
	BEST	55(6)	62(3)	53(3)	47(5)	56(6)	52(7)	46(3)	59(8)	67(7)	44(8)	56(8)	50(8)	51(4)	43(6)	69(8)	58(8)	68(6)	58(7)	64(3)	54(8)	63(6)	63(6)	48(8)	35(4)*
% of different against Entran	FScan	24	14	11	25	19	15	16	15	25	34	29	26	15	28	11	18	14	25	17	24	28	29	28	31
	BEST	8	-3	-5	-8	-2	-5	-6	-5	6	7	-6	-6	-6	8	-4	5	8	12	7	10	19	9	12	
# 2 Pressure (kPa)	FScan	63(10)	69(11)		55(9)	60(10)		63(7)	72(8)		67(9)			72(9)		63(7)	66(8)		76(6)			75(11)			43(5)
	Entran	51(4)	57(3)		47(3)	53(5)		55(3)	64(4)		59(2)			60(3)		50(2)	57(3)		68(2)			61(2)			
	BEST	57(8)	59(7)		49(7)	58(6)		52(5)	61(1)		56(6)			65(7)		54(3)	54(3)		62(3)			67(3)			35(3)*
% of different against Entran	FScan	24	21		17	13		15	13		14			20		26	16		12			23			23
	BEST	12	4		4	9		-5	-5		-5			8		8	-5		-9			10			
# 3 Pressure (kPa)	FScan	67(9)	61(11)					67(8)	75(7)		59(9)			63(10)		74(8)	52(8)		63(7)	56(9)					51(6)
	Entran	63(3)	55(2)					59(3)	67(2)		47(2)			56(2)		60(3)	44(2)		50(3)	49(4)					
	BEST	59(7)	57(6)					57(3)	62(2)		51(3)			54(4)		64(5)	49(6)		54(8)	53(9)					41(5)*
% of different against Entran	FScan	6	11					14	12		26			13		23	18		26	14					24
	BEST	-6	4					-3	-7		9			-4		7	11		8	8					
# 4 Pressure (kPa)	FScan	61(7)	59(6)		62(9)			63(7)	74(8)		67(9)			61(11)		66(7)			68(8)	69(9)					48(4)
	Entran	55(3)	48(2)		53(3)			51(2)	64(3)		53(2)			49(2)		59(3)			61(3)	60(3)					
	BEST	52(4)	57(5)		57(8)			56(5)	67(6)		57(4)			54(5)		56(5)			54(3)	51(4)					42(4)*
% of different against Entran	FScan	11	23		17			24	16		26			24		12			11	15					14
	BEST	-5	19		8			10	5		8			10		-5			-11	-15					
# 5 Pressure (kPa)	FScan	65(8)	71(7)		63(9)			55(6)	51(11)		54(8)			72(9)		62(7)			73(9)	73(7)		74(10)			39(5)
	Entran	58(3)	61(2)		51(5)			49(3)	43(2)		49(4)			60(4)		51(2)			68(3)	60(2)		68(3)			
	BEST	52(5)	57(5)		54(9)			46(3)	46(4)		51(5)			67(6)		57(7)			62(4)	67(6)		62(4)			31(4)*
% of different against Entran	FScan	12	16		24			12	19		10			20		22			7	22		9			26
	BEST	-10	-7		26			-6	7		4			12		12			-9	12		-9			

$n_{BEST} = 15$, $n_{ENTRAN} = 15$, $n_{FScan} = 50$

Table 7.20: Pressures comparison between commercial FScan 9811 F-Socket™ sensor, custom-commercial Entran transducer and custom-made B.E.S.T. for Hydrocast socket. Note: * Pressure at distal end measured using electrohydraulic transducer. % of different for the distal end (DE) is against electrohydraulic transducer. n = number of tests represented in each transducer type.

Subject		Hydrocast Socket Site																						
		A1	A2	A3	AM1	AM2	AM3	M1	M2	M3	PM1	PM2	PM3	P1	P2	PL1	PL2	PL3	L1	L2	L3	AL1	AL2	AL3	DE
# 6 Pressure (kPa)	FScan	72(9)	76(7)		77(11)			66(6)	64(7)		63(8)			70(9)		71(10)			81(11)			67(9)	64(9)		51(4)
	Entran	59(4)	68(2)		63(2)			55(4)	57(3)		50(2)			63(2)		57(3)			69(4)			52(2)	50(3)		
	BEST	64(6)	64(6)		59(11)			58(3)	49(4)		57(5)			59(6)		63(6)			64(8)			57(3)	54(6)		42(3)*
% of different against Entran	FScan	22	12		22			20	12		26			11		25			17			29	28		21
	BEST	8	-6		-6			5	-14		14			-6		11			-7			10	8		
# 7 Pressure (kPa)	FScan	72(8)			70(9)			76(9)			81(7)			63(6)		70(8)			61(9)			75(8)			53(6)
	Entran	68(3)			61(4)			63(3)			64(2)			52(2)		61(1)			53(2)			71(3)			
	BEST	64(6)			67(12)			68(4)			67(1)			57(3)		67(3)			56(8)			67(9)			45(2)*
% of different against Entran	FScan	6			15			21			27			21		15			15			6			18
	BEST	-6			10			8			5			10		10			6			-6			
# 8 Pressure (kPa)	FScan	62(8)			64(9)			60(9)			57(6)			68(8)		67(7)			62(8)			63(9)			53(4)
	Entran	50(2)			53(3)			51(2)			46(3)			58(2)		59(2)			49(2)			53(4)			
	BEST	56(7)			58(10)			57(8)			48(10)			52(11)		52(8)			56(6)			57(2)			42(3)*
% of different against Entran	FScan	24			21			18			24			17		14			27			19			26
	BEST	12			9			12			4			-10		-12			14			8			
# 9 Pressure (kPa)	FScan	62(10)	71(9)		53(11)						80(120			72(9)		67(7)			74(11)						49(3)
	Entran	50(3)	68(1)		43(2)						71(2)			65(3)		59(2)			67(3)						
	B.E.S.T	57(6)	64(3)		48(8)						64(8)			54(7)		54(8)			62(8)						35(4)*
% of different against Entran	FScan	24	4		23						13			11		14			10						40
	BEST	14	-6		12						-10			-17		-8			-7						
# 10 Pressure (kPa)	FScan	63(7)	67(7)		68(6)			71(8)			79(11)			82(9)		63(10)			62(11)			54(9)			49(4)
	Entran	51(12)	55(3)		59(2)			61(3)			67(4)			69(3)		50(2)			49(3)			44(3)			
	BEST	47(4)	52(2)		54(7)			54(5)			54(6)			62(7)		53(5)			54(8)			48(6)			39(2)*
% of different against Entran	FScan	24	22		15			16			18			19		26			27			23			26
	BEST	-8	-5		-8			-11			-11			-10		6			10			9			

$n_{BEST} = 15$, $n_{ENTRAN} = 15$, $n_{FScan} = 50$

...Contd....Table 7.20: Pressures comparison between commercial FScan 9811 F-Socket™ sensor, custom-commercial Entran transducer and custom-made B.E.S.T. for Hydrocast socket. Note: * Pressure at distal end measured using electrohydraulic transducer. % of different for the distal end (DE) is against electrohydraulic transducer. n = number of tests represented in each transducer type.

7.9 Step duration. (heel strike to heel strike)

From the results of step durations displayed in table 7.21, (eight subjects using foot switches and another two subjects using a Kistler force platform), there were no statistically significantly differences in step durations between the PTB and hydrocast sockets.

Subject	PTB socket average ± 1 SD (s)	Hydrocast socket average ± 1 SD (s)
# 1 *	1.23 ± 0.04	1.22 ± 0.03
# 2 *	1.19 ± 0.02	1.21 ± 0.04
# 3	1.18 ± 0.03	1.19 ± 0.02
# 4	1.19 ± 0.03	1.20 ± 0.05
# 5	1.18 ± 0.04	1.17 ± 0.03
# 6	1.20 ± 0.02	1.21 ± 0.03
# 7	1.24 ± 0.05	1.23 ± 0.04
# 8	1.19 ± 0.02	1.20 ± 0.03
# 9	1.20 ± 0.03	1.19 ± 0.04
# 10	1.21 ± 0.02	1.22 ± 0.03
average	1.201 ± 0.03	1.204 ± 0.03
min	1.18 ± 0.03	1.17 ± 0.03
max	1.24 ± 0.05	1.23 ± 0.04

n = 15

Table 7.21: Step duration measured using foot switches. Note: n = number of tests represented in every subject. * measured using Kistler force platform.

CHAPTER 8: DISCUSSION

8. 1. Measurement Techniques

The instrumentation designed, developed and constructed using standard electrical resistance strain gauge technology in this research proved to be suitable in providing quantitative measurement of interface pressure and shear stresses on trans-tibial amputees. This instrumentation also enabled simultaneous measurement of stress in three directions to be obtained using some of the transducers. These transducers were: the Patellar tendon (PT) transducer; the Normal/Shear stress transducer [**B**ioengineering **S**hear **T**ransducer (B.E.S.T)] both of these designs are described for the first time. A third device based on an Entran load transducer which was utilised for the measurement of normal stress only; and finally an electrohydraulic transducer, which was used to measure the pressure at the distal end of the stump. One design of transducer, the **B**ioengineering **S**hear **T**ransducer (B.E.S.T) allows the measurement of normal and shear stress to be undertaken, and the other design, the PT transducer, in addition, allows a sensing surface, recording the stresses at the patellar tendon, to be translated by 10 mm from the neutral position for the purpose of examining the effect of patellar tendon bar indentation on the stress distribution at the interface.

Sockets, so called 'hard' sockets without soft liner, containing machined metal inserts were manufactured using standard laminating techniques. These inserts allowed all transducers except the electrohydraulic transducer to be placed within the socket wall so that the sensing surface was flush with the inside surface of the socket. The successful design specifications were determined from consideration of the work of previous researchers. This resulted in a transducer sensing surface of 5.6 mm in diameter thus minimising distortion of the socket wall. In addition the 'laminating in' of metal inserts into the socket wall during socket manufacture ensured that the active surface of the transducer was flush with the inner wall of the socket. The light and small size of the transducer and the technique employed to ensure flush fitting avoids protrusion into the soft tissues of the stump and minimizes measurement error. The sites measured for the PTB and Hydrocast sockets, for the same subject, were the same in order to make valid comparisons. Although attempts were made to maximise the number of sites at which measurement could be made and thus provide a detailed stresses distribution, there was a physical limit to the number. This was dependent of the area of the subject's stump with a maximum number of sites of 31 being utilised with subject # 1. By contrast the minimum number was 12 with subject # 9. (See table 6.3).

8.2 Measurement Results

8.2.1 Magnitudes of Stresses

From all measurements in this study, it was found that the maximum pressure was 230 ± 17 kPa over the patellar tendon bar of subject # 7, and maximum shear stress was 50 ± 3 kPa in the longitudinal direction of the patellar tendon bar site of subject # 1 and 25 ± 6 kPa over the patellar tendon bar in the tangential direction, of subject # 9. During testing of subject # 1 for the PTB socket, pistoning occurred due to "trial and error" for finding the best method of sticking the TEC suspension sleeve onto the proximal side of the PTB socket. With the exception of subject #1, maximum shear stresses were 48 ± 3 kPa in the longitudinal direction of the patellar tendon bar site of subject # 3. For the PTB socket, generally the high shear stresses occurred at the patellar tendon bar area, with maximum resultant shear stresses of 53 ± 6 kPa of subject # 3 (table 7.14).

In the hydrocast socket the maximum pressure was found to be 80 ± 10 kPa over the patellar tendon bar of subject # 7. Whereas in the PTB socket all maximum pressures were recorded at the patellar tendon, this was not the case for the hydrocast socket which displayed a far more even pressure distribution.

The maximum shear stresses were 35 ± 2 kPa in the longitudinal direction of patellar tendon bar site of subject # 7 and 13 ± 1 kPa over the PL1 site in the tangential direction, of subject # 6. The maximum shear stresses recorded from the

hydrocast socket thus display much reduced values compared with those from the PTB sockets.

Sanders et al (1992) in their measurement of pressure and shear stresses found values up to 205 kPa and resultant shear stresses up to 54 kPa. The values obtained in this study on the maximum pressure and maximum shear stresses fall within this range. However it was found that the values of pressure and shear stresses varied from subject to subject and from site to site.

Utilisation of the electrohydraulic transducer indicated that all subjects in both sockets displayed an amount of end bearing. This varied from subject to subject, with a range of 14 ± 3 kPa to 35 ± 4 kPa for the PTB socket and 31 ± 4 kPa to 49 ± 2 kPa for the hydrocast socket. All subjects reported no discomfort at the distal end. These results tend to support the theory of the PTB socket in that loading at the patellar tendon reduces the tendency to end load bearing, whereas there is no attempt to off load the distal end of the stump in a hydrocast socket.

The results obtained from the dynamic gait trial in (table 7.18, figure 7.80 and figure 7.81) clearly show that a more uniform pressure distribution for the Hydrocast socket was obtained. Table 7.18 showing the ranges of results for the four walls (Anterior, Posterior, Medial and Lateral) for both sockets clearly indicates a much smaller standard deviation of the pressure values for the hydrocast socket in all aspects. This provides further evidence of a more uniform and less variable pressure distribution.

Subjective feedback from all participants also favoured the hydrocast socket. It is thus believed that lower, more evenly distributed pressure enhances the comfort of the prosthesis user.

8.2.2 Pressure and shear curve pattern

This section will discuss the pattern of the stress curves presented in figures 7.20 – 7.69.

Examination of the pressure curves revealed the emergence of two distinct categories. The first follows the classical two peaked curve associated with the vertical ground reaction force (GRF) found in normal subjects. (See Figure 8.1). The second category including curves which do not display the classical two peaks but have a tendency to show a level of pressure that is maintained from shortly after ground contact to shortly before toe off. (See Figure 8.2).

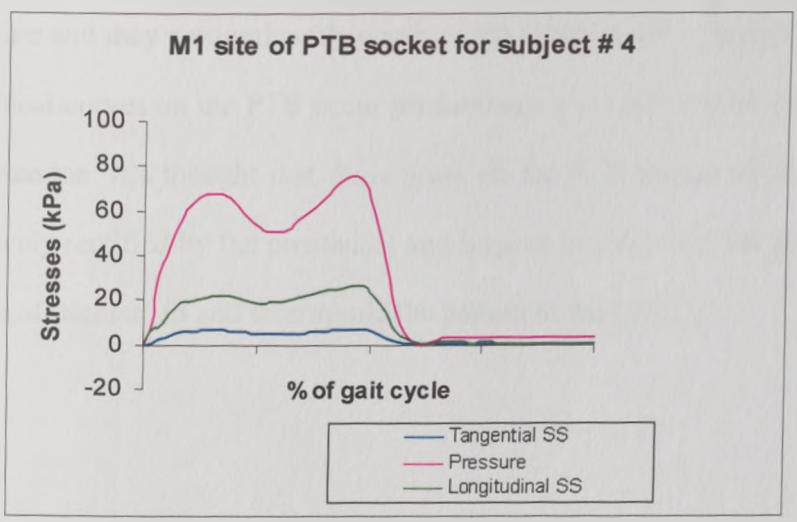

Figure 8.1: Example of Classical Two Peaked Curve

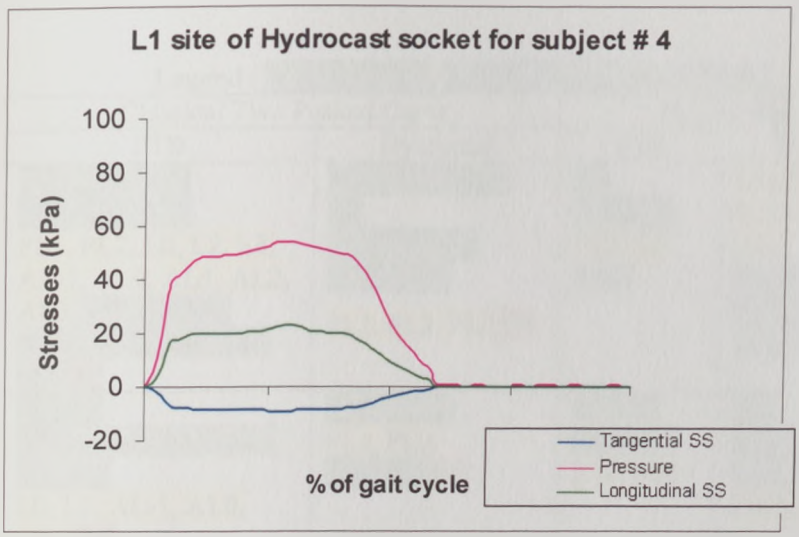

Figure 8.2: Example of non-Classical Curve

Table 8.1 shows the distribution of the site which displays the above curves for both socket types for all participants. These data are displayed in percentage terms in table 8.2. From the tables it can be seen that 70.5 ± 6.40 % of sites displaying the two peak curve in the PTB socket occur at the patellar tendon, lateral site, medial site and distal end. The remaining sites accounting for 29.5 ± 6.40 %, occur at the anterior A1, posterior P1 and PM1 and lateral PL1. The hydrocast socket shows markedly less classical curves with of 48.5 ± 6.40 % of sites displaying this feature and they predominantly occur on the anterior and posterior walls, whereas the classical curves on the PTB occur predominantly on the medial, lateral walls and patellar tendon. It's thought that those areas on the PTB socket are those which are aggressively rectified by the prosthetist and impose loading onto the stump and these are areas of 'tighter' fit and thus mimic the pattern of the GRF.

Legend : Anterior wall, Posterior wall, Medial wall, Lateral wall, DE

Subject no.	Classical Two Peaked Curve		Non-Classical Curve	
	PTB	Hydrocast	PTB	Hydrocast
#1	PT bar, A2 A3 P1, PM1, PM3 PL1, PL2, L0, L2, L3, AL-1, AL0, AL1, AL2, AL3,AM-1, AM0, AM2, AM3, M0, M1, M2 DE	PT bar, A1, A2, A3 P1, P2, PM1, PM2, PM3 PL1, PL2, PL3	A1 P2, PM2 PL3, L1 AM1	L0, L1, L2, L3, AL- 1, AL0, AL1, AL2, AL3 AM-1, AM0, AM1, AM2, AM3, M0, M1, M2, M3
#2	PT bar, AM0, AM1 AM2 M0, M1, M2 L0, L1, AL-1, AL0, AL1,DE	PT bar, A1, PL1, PL2, P1, PM1,DE	A1, A2, P1, PM1, PL1, PL2	A2, AM0, AM1, AM2, M-1, M0, M1, M2 L0, L1, AL0, AL1
#3	PT bar, A2 M0, M1, M2 L0, L1, L2, AL-1,DE	PT bar, A1, A2, PL1, PL2, P1, PM1,DE	A1, P1, PM1, PL1, PL2	M0, M1, M2 L0, L1, L2
#4	PT bar, M0, M1, M2 L0, L1, L2, PL1, PL2, PM1,DE	PT bar, A1, A2, PL1, P1, PM1,DE	A1, A2, P1	AM0, AM1, M0, M1, M2 L0, L1, L2
#5	PT bar, AM0, M0, M1, M2 L0, L1, L2, AL0, DE	PT bar, A1, A2, PL1, P1, PM1,DE	A1, A2, P1, PM1, PL1	AM0, AM1, M0, M1, M2 L0, L1, L2, AL0, AL1
#6	PT bar, AM0, AM1 AM2 M0, M1, M2 L0, L1, AL1, AL2, PM1,DE	PT bar, A1, A2, PL1, AL1 P1, PM1,DE	A1, A2, P1, PL1	AM0, AM1, M-1, M0, M1, M2 L-1, L0, L1, AL0, AL2
#7	PT bar, AM0, AM1, M0, M1, L0, AL0, AL1, PM1,DE	PT bar, A1, L0, L1, AL0, AL1, P1, PM1,DE	A1, P1, PL1, L1	AM0, AM1, M0, M1,
#8	PT bar, AM0, AM1, M0, M1, L0, AL0, AL1,DE	PT bar, A1, PL1, P1, PM1,DE	A1, P1, PM1 PL1	AM0, AM1, M0, M1, L0, L1, AL0, AL1
#9	PT bar, AM0, AM1, M0, M1, L0, DE	PT bar, A1, A2, PL1, P1, PM1,DE	A1, A2, PM1, PL1	AM0, AM1, M0, L0, L1
#10	PT bar, AM0, AM1, M0, M1, L0, AL0, AL1, DE	PT bar, A1, A2, PL1, P1, PM1,DE	A1, A2 P1, PM1 PL1, PL2	AM0, AM1, M0, M1, L0, L1, AL0, AL1

Table 8.1: Distribution of the site displays for Classical Two Peaked Curve and Non-Classical Curve.

	PTB		Hydrocast	
Subject no	Classical Two Peaked Curve (%)	Non-Classical Curve (%)	Classical Two Peaked Curve (%)	Non-Classical Curve (%)
#1	81	19	42	58
#2	68	32	37	63
#3	67	33	57	43
#4	79	21	47	53
#5	67	33	41	59
#6	76	24	42	58
#7	71	29	71	29
#8	69	31	43	57
#9	67	33	58	42
#10	60	40	47	53
Mean ± SD	70.5 ± 6.40	29.5 ± 6.40	48.5 ± 10.40	51.5 ± 10.40

Table 8.2: Percentage terms for Classical Two Peaked Curve and Non-Classical Curve

8.2.3 Comparing PTB and Hydrocast sockets.

Radcliffe and Foort (1961) produced an analysis of the mechanics of load transmission in a PTB socket, assuming that a trans-tibial subject was walking in a manner which was similar to a normal subject. This gives an indication of the direction and anticipated distribution of the forces acting on the residual limb but no values were presented.

From table 8.3, which indicates a comparison of magnitudes (without values) in a similar fashion to Radcliffe's for the medial aspect of the PTB socket, it is seen that the site of highest pressure occurs at an area corresponding to the medial tibial flare (i.e. M1 and AM1). This is shown by all subjects and is agreement with Radcliffe's concept.

Subject no.	Sites AM-1 to AM3	Sites M-1 to M3
#1	AM-1>AM0<AM1>AM2>AM3	M0<M1>M2>M3
#2	AM0<AM1<AM2	M0<M1>M2
#3	n/a	M0<M1>M2
#4	n/a	M0<M1>M2
#5	n/a	M0<M1>M2
#6	AM0<AM1>AM2	M0<M1>M2
#7	AM0<AM1	M0<M1
#8	AM0<AM1	M0<M1
#9	AM0<AM1	M0<M1
#19	AM0<AM1	M0<M1

Table 8.3: Comparison of magnitudes (without values) for the medial aspect of the PTB socket. Note: n/a = not available for comparison due to lack of measurement sites

Subject no.	Sites AL-1 to AL3	Sites L-1 to L3
#1	AL-1<AL0<AL1<AL2>AL3	L0<L1>L2>L3
#2	AL-1<AL0>AL1	L0<L1
#3	n/a	L0<L1<L2
#4	n/a	L0<L1<L2
#5	n/a	L0<L1<L2
#6	AL1<AL2	L0<L1
#7	AL0<AL1	L0<L1
#8	AL0<AL1	n/a
#9	n/a	L0<L1
#10	AL0<AL1	n/a

Table 8.4: Comparison of magnitudes (without values) for the lateral aspect of the PTB socket. Note: n/a = not available for comparison due to lack of measurement sites

Similarly table 8.4 shows the situation on the lateral distal aspect. (L1,L2, AL1 and AL2). This was exhibited by most subjects, (subject #1 showed a slightly different variation from this) once again supporting Radcliffe's concept of medial-lateral stabilisation in the PTB socket.

Considering the sagittal plane, Radcliffe's analysis indicated that at heel contact on the PTB socket forces would be predominantly acting at the patellar tendon in a posterior direction and at the posterior distal aspect in the anterior direction. This study has shown high pressure occurring at the patellar tendon, therefore concurring with Radcliffe's concept, but owing to a lack of measurement sites it is not possible to concur with this theory of loading posteriorly.

Furthermore, his analysis at shock absorption and at push off indicates a change in the force system such that stump loading would occur at the anterior distal and posterior proximal aspects. Again this study was unable to confirm the concept concerning the posterior loading due to a lack of measurement sites however this study found that the area of highest pressure anteriorly was the patellar tendon.

The hydrocast socket, on the other hand, does not yield results that accommodate Radcliffe's concept. (See Figure 7.81). The hydrocast socket shows a far more even distribution of pressure in the medial-lateral and the anterior-posterior planes.

The electrohydraulic transducer, situated at the distal end of the socket, showed a positive pressure value throughout the gait cycle for both types of socket for all subjects. This indicates that the end contact was maintained during swing phase, showing that pistoning of the prostheses was minimal. The values recorded during stance phase indicated that a degree of end bearing occurred on both socket types however the hydrocast socket had the higher amount of end bearing (average 40 ± 12 kPa) compared with the PTB of 30 ± 16 kPa.

Considering the results of the shear stresses it is clear that the values for tangential and longitudinal shear stress are much smaller than that of normal stress. The average values of the resultant shear stress acting on hydrocast sockets are 25 % lower than those acting on the PTB socket. It is thought that the higher values of shear stress in the PTB socket compared to the Hydrocast socket are related to the higher values of normal stress which occur due to the aggressive rectification performed by the prosthetist during production of the PTB socket. The hydrocast socket undergoes no such rectification and therefore a more uniform distribution results.

The low ratio of resultant shear stress to pressure indicates, it is believed, that normal stress and not shear stress is responsible for providing the majority of support.

8.2.4 Shear stress direction

Figures 7.73 to 7.80 show a representation of the resultant shear stress in terms of magnitude and direction for both socket types, all sites and all subjects. It is clearly seen that the longitudinal shear stress is always acting upward from the socket to the stump. The tangential shear stress is universally smaller in magnitude and has no consistent direction. This finding is in agreement with Sanders et al (1992).

8.3 Varying the load on the patellar tendon bar at the stump socket interface.

Data were obtained with the patellar tendon bar of the prosthesis in the neutral position (the original position as cast/rectified by the prosthetist), compressed by (+) 2 and 4mm and relieved by (-) 2mm. (Figure 8.1). In addition to the measurement obtained from the patellar tendon bar, the other test sites containing transducers were sampled simultaneously.

Table 8.1: Patellar tendon bar at different positions; From left (-2mm), (neutral) and (+ 4mm)

The discussions here are focused on the correlation of the patellar tendon bar with other test sites. In this study, the correlation of varying the load on the patellar tendon bar has on the pattern of pressure distribution at the stump socket interface has been investigated. The sites of interest for transducer location were the same for all experimental sockets for each individual subject with the centre of the patellar tendon acting as a datum. The data provided some interesting results for PTB and Hydrocast sockets which showed that, as the patellar tendon area of the prosthesis was compressed, the pressure at that site increased quite significantly for all subjects; however the amount of pressure varied from subject to subject as would be expected. The pressures recorded at the test sites from the transducers did not show any particular variation in pattern when the patellar tendon bar was compressed or relieved i.e. it had no significant effect on the other areas of the socket. (Figures 7.8 to 7.17). These results, by virtue of the fact that positive pressures were recorded from all sites, tend to support the hypothesis that they were total contact sockets. However, it should also be recognised that the attempt, by the prosthetist, to minimise the loading on the distal end of the stump was successful.

From the results shown in figures 7.8 to 7.17, it is the author's conclusion that increasing or decreasing the load at the patellar tendon had no effect on the overall pressure distribution between the stump and the socket of a PTB prosthesis or Hydrocast prosthesis.

In an attempt to understand why the increase or reduction in pressure applied to the tendon had no effect on the pressures around the socket the following procedure was adopted.

The internal surface area of a socket was estimated from the level of the patellar tendon distally. This was achieved by carefully applying 25 mm masking tape so that no overlap occurred, removing the tape and measuring the area thereof. This area was divided by the area of the sensing surface of a transducer to estimate the total number of sites which, theoretically, could be utilised. The value of pressure lost from the patellar tendon on removal of the PT transducer was then divided by the total number of potential sites to give the increase which would theoretically occur.

e.g.: socket for subject # 6

- Transducer sensing surface diameter = 5.6 mm
- Transducer sensing surface area = 24.64 mm^2
- Average pressures on 12 sites = 57.5 kPa
- Area of internal socket surface = 39345 mm^2
- Total number of potential measuring sites = 1597

$$\therefore \text{Increase in pressure per site} = \frac{210kPa}{1597} = 0.131 \text{ kPa / site}$$

It is clear that the increase in pressure per site of 0.131 kPa is almost insignificant, could not be detected by our measurement system and is unlikely to be detected by the subject.

Subjective feedback from the participants indicated that the patellar tendon bar could be indented a further 4mm from the original rectified position without causing pain. However the subjects unanimously preferred the relief position. This study of ten subjects therefore supports the supposition of Kristinsson (1993), which stated that the concept of load transfer to areas such as the patellar tendon, medial flare and condyles of the tibia is ineffective and uncomfortable, certainly as far as the patellar tendon area is concerned.

Analysis of the data revealed peak pressures to be located at the site of the patellar tendon only when the patellar tendon bar was indented. This peak pressure varied from subject to subject but always increased as the indentation increased. The position of the patellar tendon bar preferred by all subjects resulted in a pressure at the patellar tendon site which was often not significantly higher than other sites around the socket, and again was subject dependent.

8.4 Custom-made transducers vs. commercial F-Socket™ sensor

In this study the F-Socket™ sensor from Tekscan Inc. (USA) system was also used for measuring the stump/socket interface pressure for the PTB and Hydrocast sockets. In agreement with the results obtained from the custom-made transducers, the F-Socket™ sensor results showed that the pressure distribution in the hydrocast was more even than in the PTB socket. However, from the results obtained as in table 7.19 and table 7.20, all of the interface pressure values recorded at any measurement sites increased from 6 % to 38% for the PTB socket and 4 % to 29 % for the hydrocast socket in comparison with values obtained from the strain gauge technology.

It is thought that there may be several explanations for the increase in recorded value, some or all may be responsible. There include possible stump volume fluctuation; possible different position of the stump within the socket; different walking style although data from step duration, table 7.21, indicates no difference between tests; an existing pre-pressure brought about by sticking the sensors to the socket walls; introducing curvature to the sensor is known to influence the readings; the temperature inside the socket is elevated and thus may have an effect; the viscoelastic nature of the sensor material.

In order to minimise any deleterious effect from the degradation of the sensor themselves they were each only used twice.

However general observation indicates that the F-Socket™ sensor can be used for initial guidance in the research environment provided the accuracy requirement is not too high. It is also essential that the techniques of calibration and recognition of the measurement surface must be given proper due care and attention. It must be borne in mind that a likely error of up to 38% will occur. Although an error of 38 % is likely using the F-Socket™ sensor system this technique yielded a similar pattern of pressure distribution to that obtained with the B.E.S.T and Entran devices, which was that the hydrocast socket showed a far more even pressure distribution. This finding is of major importance in the prevention of tissue breakdown, which must be the goal of any prosthetist when providing a prosthesis to an amputee.

Early studies considered the formation of pressure sores by the loads transmitted from support surfaces such as beds, wheelchair seats etc. The level of constant pressure which causes capillary occlusion and therefore disruption of nutrients and oxygen to the tissue cells is generally reported to be less than 8kPa, [6 kPa (Dinsdale, 1974), 5.3 kPa (Bader and Bowker, 1983), 4 kPa (Fernandez, 1987), less than 8 kPa (Sanders, 2000)]. This work was later extended to look at the stump / prosthetic socket interface and to consider shear stress in addition to normal stress. All of the quoted values are low in comparison to interface pressures measured on a trans-tibial prosthetic socket. However Dinsdale (1974), reported that repeated loading of 38 kPa was sufficient to cause ulceration.

It is clear that in the day to day use of a prosthesis, during walking and sitting, that the level of load transmitted through the prosthesis will vary. However it is also clear that minimization of the pressures applied at the interface will reduce the

possibility of tissue damage. In this regard the hydrocast socket with its more even pressure distribution, and lower average pressures, compared to the PTB socket, whilst not reaching sub 8 kPa values is offering a better clinical solution to the trans-tibial amputee. Thus there would be fewer stump problems and fewer visits to the prosthetic clinic for the patient resulting in a less disrupted life style and reduced costs for the health care industry.

8.5 Suggestions for further work.

The three aims and objectives of the project have been successfully achieved, in that transducers capable of measuring components of forces in three directions were successfully designed, developed and manufactured. It was found that no correlation existed between indentation at the patellar tendon bar and other areas of the socket and thirdly the pressure distribution in the hydrocast socket was more uniform then in the PTB socket.

However, in the course of this work it became evident that there is much need for further investigation of certain aspects. Therefore, the following are suggestions for future work in this area.

1. The umbilical wiring cord between the subject and data acquisition system imposes limitation of testing environment. Elimination of this wiring would allow the subject to be tested outdoors and permit activities other than walking.

2. In order to gain a more complete position of the stress distribution many more sites around the socket have to be investigated. It is perceived that this necessitates the development of smaller and lighter transducers. This would allow data to be collected from more distal sites thus allowing confirmation or rebuttal of Radcliffe's theory.

3. In addition to the above point the new transducers/measurement techniques should be developed to have increased sensitivity so that the variations in pressure at the various sites arising from an alteration elsewhere in the socket (e.g. removal of PT bar) could be detected.

4. The results from this work, in terms of the values obtained for pressure and shear stress, are available to be input into a Finite Element Analysis (FEA) model of a trans-tibial stump/socket interface allowing further development of such a model.

5. The results of this work indicated that the hydrocast socket not only yields a more even pressure distribution but is also the socket of choice of ten participants. Further trials of the socket should be conducted on a clinical basis i.e. socket should be delivered to patients for use at home, work and during sporting activities.

6. The pressure data indicate a loss of the classical two peak curve associated with the GRF in the hydrocast socket. Full three dimensional gait analysis using a motion capture system and force plate together with pressure transducers should be conducted to investigate this phenomenon.

CHAPTER 9: CONCLUSION

Transducers capable of measuring normal force and two perpendicular shear forces, simultaneously, were designed, developed and constructed using standard electrical resistance strain gauging technology. They proved to be robust, and to provide repeatable and accurate results when utilised to measure stump/socket interface stresses. These transducers helped to provide an insight into the complex biomechanical interactions at the stump/socket interface which may lead to the design of more functional and comfortable prosthetic sockets minimising the risk of tissue injury. These transducers are therefore suggested as a useful tool in the field of rehabilitation and may prove to be of value in other areas of research such as limb/body/orthosis interfaces, the seat/buttock interface and perhaps any general hard-soft interface, provided proper, carefully structured inserts are incorporated to allow the correct installation of the transducers.

Varying the depth of the patellar tendon bar had no detectable effect on the pressure distribution around the remainder of the socket. The subjects felt no detrimental effects (quite the opposite) by removing the patellar tendon bar and it is therefore reasonable to conclude that it is an unnecessary feature which may be eliminated during the manufacture of a trans-tibial prosthetic socket.

The hydrostatic tank system, using the concept of uniform pressure distribution at the stump/socket interface was used to produce sockets which were compared to standard PTB sockets. The results from the ten subjects showed that the stress distribution of the hydrocast socket was more uniform compared to the conventional PTB socket and subjective feedback from the participants indicated a preference for the hydrocast sockets.

REFERENCES

Angel, J. C. (1979). "Amputation below the knee." in Operative Surgery: Orthopaedics Part 1, Rob C, Smith R (Eds), Butterworths, London, 311-315.

Appoldt, F. A., Bennet, L., and Contini, R. (1969). "Socket pressure as a function of pressure transducer protrusion." Bull Prosthet Res, 10(8), 20-55.

Appoldt, F. A., and Bennett, L. (1967). "Preliminary report on dynamic socket pressure." Bull Prosthet Res, 10(8), 20-55.

Appoldt, F. A., Bennett, L., and Contini, R. (1968). "Stump-socket pressure in lower-extremity prostheses." J. Biomech, 1(4), 245-257.

Appoldt, F. A., Bennett, L., and Contini, R. (1970). "Tangential pressure measurements in above knee sockets." Bull Prosthet Res, 10(13), 70-86.

Barbenel, J. C., and Sockalingam, S. (1990). "Device for measuring soft tissue interface pressure." J. Biomed. Eng, 12, 519-522.

Barclay, W. (1970). "Below-knee amputation - prosthetics. In G. Murdoch (Ed)." Prosthetic and Orthotic Practice. London: Edward Arnold Publishers Ltd, 70-78.

Bader, D. L and Bowker, P. (1983). "Mechanical properties of skin and underlying tissues in vivo." Biomaterials, 4, 305-308

Berme, N., Lawes, P., Solomonidis, S. E., and Paul, J. P. (1976). "A shorter pylon transducer for measurement of prosthetic forces and moments during amputee gait." Engineering in medicine, IMechE, 4(4), 6-8.

Branemark, R., Branemark, P.-I., Rydevik, B., and Myers, R. (2001). "Osseointegration in skeletal reconstruction and rehabilitation: A review." Journal of Rehabil Res Dev., 38(2), 175-181.

Bray, A. (1990). "Theory and practice of force measurement." Academic Press Ltd.

Buis, A. W. P. (1997). "Investigation of socket concept to improve trans-tibial socket quality in developing countries." PhD dissertation, University of Strathclyde, UK.

Buis, A. W. P., and Convery, P. (1997). "Calibration problems encountered while monitoring stump/socket interface pressures with force sensing resistors: techniques adopted to minimise inaccuracies." Prosth Orthot Int, 21, 179-182.

Burgess, E. M. (1968). "The below-knee amputation." Bull. Pros. Res., 10, 9.

Burgess, E. M. (1969). "The below-knee amputation." ICIB, 8(4), 1-22.

Burgess, E. M. (1985). "Below-knee amputation,." in Surgical Techniques Illustrated : A comparative Atlas, Malt.R.A, (Ed), Saunders, Philadelphia, 563-568.

Castronuova, J. (1980). "Below knee amputation : is the effort to preserve the knee justified ?" Arch. Surg.(115), 1184-1187.

Chino, N., Pearson, J. R., Cockrell, J. L., Mikisho, H. A., and Koepke, G. H. (1975). "Negative pressures during swing phase in below-knee prostheses with rubber sleeve suspension." Arch. Phys. Med. Rehabil., 56, 22-26.

Convery, P., and Buis, A. W. P. (1998). "Conventional patellar tendon bearing (PTB) socket/stump interface dynamic pressure distributions recorded during the prosthetic stance phase of gait of a trans-tibial amputee." Prosth Orthot Int, 22, 193-198.

Convery, P., and Buis, A. W. P. (1999). "Socket/Stump interface dynamic pressure distributions recorded during the prosthetic stance phase of gait of a trans-tibial amputee wearing hydrocast socket." Prosth Orthot Int, 23, 107-112.

Dinsdale S.M. (1974). "Decubius ulcers: role of pressure and friction in causation." Arch Phys Med Rehabil, 55, 147-151.

Ferguson-Pell, M. W., Bell, F., and Evans, J. H. (1976). "Interface pressure sensors: existing devices their suitability and limitations." Bedsore Biomechanics, 189-197.

Finley, F. R., and Cody, K. A. (1970). "Locomotive characteristics of urban pedestrians." Arch. Phys. Med. Rehabil., 51, 423.

Fleming, H. E. (1997). "Comparison of quadrilateral and ischial-ramal containment sockets for trans-femoral amputees : An interface pressure study." PhD dissertation, University of Strathclyde, UK.

Fernandez S. (1987). "Physiotherapy prevention and treatment of pressure sores." Physiotheraphy, 73(9), 450-454

Goh, J. C. H., Lee, P. V. S., and Chong, S. Y. (2003). "Static and dynamic pressure profiles of a patellar-tendon-bearing (PTB) socket." Proc. Instn Mech Engrs, Part H, 217(121-126).

Grant-Thompson, J. C. (1977). "Amputee gait analysis techniques using pylon data." MSc dissertation, University of Strathclyde, UK.

Grevsten, S., and Eriksson, U. (1974). "Stump-socket contact and skeletal displacement displacement in a suction patellar tendon bearing prosthesis." JBJS, 56-A, 1692-1696.

Ham, R., and Cotton, L. (1991). "Limb amputation, from aetiology to rehabilitation." Therapy in Practice series:23 London: Champman & Hall.

Ham, R., Luff, R., and Roberts, V. C. (1989). "A five year review of referrals for prosthetic treatment in England, Wales and Northern Ireland 1981-1985." Health Trends, 21, 3-6.

Hughes, J. (1970). "Below-knee amputation - biomechanics. In G. Murdoch (Ed)." Prosthetic and Orthotic Practice. London: Edward Arnold Publishers Ltd, 61-68.

Isherwood, P. A. (1978). "Simultaneous PTB socket pressures and force plate values." BRADU Report, London: Biomechanical Res and Dev Unit, 45-49.

Jones, D. (1976). "Data handling in amputee analysis of gait." PhD dissertation, University of Strathclyde, UK.

Kay, H. W., and Newman, J. D. (1975). "Relative incidences of new amputations-statistical comparison of 6000 new amputees." Orthot. Prosthet, 29(2), 3-16.

Kristinsson, O. (1992). "Pressurised casting instrument." in Proceedings of the 7th World Congress, ISPO, Chicago, USA, 43.

Kristinsson, O. (1993). "The ICEROSS concept: a discussion of philosophy." Prosth Orthot Int, 17, 49-55.

Lawes, P. (1982). "Alignment kinetics in patient - prosthesis matching." PhD dissertation, University of Strathclyde, UK.

Lee, V. S. P., Solomonidis, S. E., and Spence, W. D. (1997). "Stump-socket interface pressure as an aid to socket design in prostheses for trans-femoral amputees- a preliminary study." Proc. Instn Mech Engrs, Part H, 211, 167-180.

Levit, F. (1981). "Skin problems in amputees." Atlas of Limb Prosthetics :Surgical and Prosthetic Principles (American Academic of Orthopaedic Surgeons), C.V. Mosby Company, St. Louis, 443-447.

Lindan, O., Greenway, R. M., and Piazza, J. M. (1985). "Pressure distribution on the surface of the human body: I. evaluation in lying and sitting positions using a 'bed of springs and nails'." Arch. Phys. Med. Rehabil., 46, 378-385.

Little, J. M. (1985). "Below knee amputation." in Surgical Techniques Illustrated : A comparative Atlas, Malt.R.A, (Ed), Saunders, Philadelphia, 553-556.

Livingstone D.H, Keenan D, Kim D, Elcavage J, Malangoni M.A. (1994). "Extent of disability following traumatic extremity amputation." J Trauma, 35, 495-499

Magnissalis, E. A. (1992). "Studies of prosthetic loading by means of pylon transducer." PhD dissertation, University of Strathclyde, UK.

Marquardt, E., and Corell, J. (1984). "Amputation and prostheses for the lower limb." Intl. Orthop, 8, 139-146.

McColl, I. (1986). "Review of artificial limb and appliance centre services." London, Department of Health and Social security (DHSS).

McCollum, C. N. (1989). "Posterior flap below-knee amputation." in Vascular Surgical Techniques: An Atlas, Greenhalgh R M (Ed), Saunders, London, 340-346.

McCollum, P. T., Spence, V. A., Walker, W. F., and Murdoch, G. (1985). "A rationale for skew flaps in below-knee amputation surgery." Prosthet. Orthot. Int, 9, 95-99.

Meier, R. H., Meeks, E. D., and Herman, R. M. (1973). "Stump-socket fit of below-knee prostheses: comparison of three methods of measurements." Arch. Phys. Med. Rehabil., 54, 553-558.

Ming-Zhi, T. (1999). "Assessing two designs of trans-tibial prosthetic sockets by experimental measurement and numerical analysis." PhD dissertation, University of Strathclyde, UK.

Mizrahi, J., Susak, Z., and Bahar. (1985). "Biomechanical evaluation of an adjustable patellar tendon bearing prosthesis." Scand J Rehab Med, Suppl, 12, 117-123.

Mooney, V., Einbund, M. J., Rogers, J. E., and Stauffer, E. S. (1971). "Comparison of pressure distribution qualities in seat cushions." BPR, 10-15, 129-143.

Moore, J. H., Morimoto, S., Takami, K., and Ota, K. (2000). "A tri-axial force transducer for measuring interface stress caused by prosthetic socket." in Proceedings of 10th International Conference on Biomedical Engineering, Singapore, (Suppl).

Murdoch, G. (1968). "The Dundee socket for the below knee amputation." Prosthet. Int., 3(4/5), 15-21.

Murdoch, G. (1970). "Indications, levels and limiting factors in amputation In G Murdoch (Ed.)." Prosthetic and Orthotic Practice, 7-13.

Narang, I. C., and Jape, V. C. (1982). "Retrospective study of 14400 civilian disabled (new) treated over 25 years at an Artificial Limb Centre." Prosthet. Orthot. Int, 6, 10-16.

NASDAB. (2003). "The amputee statistical database for the United Kingdom." National Amputee Statistical Database, Statistics and Research Division, DHSS.

Olson, J. (1991). "Conventional pressure sensors." In: Prevention of Pressures Sores edited by Webster J G. IOP Publishing Ltd. Adam Hilger. Bristol, Philadelphia and New York.

Pashalides, S. (1989). "Design of a portable recording system for the measurement of prosthetic loading." PhD dissertation, University of Strathclyde, UK.

Pathak, A. P., Silver-Thorn, M. B., Thierfelder, C. A., and Prierto, T. E. (1998). "A rate-controlled indentor for in vivo analysis of residual limb tissues." IEEE Trans Rehabil Eng, 6(1), 12-19.

Pearson, J. R., Grevsten, S., Almby, B., and Marsh, L. (1974). "Pressure variation in the below knee patellar tendon bearing suction socket prostheses." J. Biomechanics, 7, 487-496.

Pearson, J. R., Holmgren, G., March, L., and Oberg, K. (1973). "Pressures in critical regions of the below-knee patellar-tendon-bearing prosthesis." Bull Prosthet Res, 10(33), 31-34.

Pritham, C. H. (1979). "Suspension of the below-knee prosthesis: an overview." Orth. Prosthet, 33(2), 1-19.

Quesada, P. M., and Skinner, H. B. (1992). "Finite element analysis of the effects of prosthesis model alterations on stump/socket interface stresses." in Proceedings of the 7th World Congress, ISPO, Chicago, USA, 275.

Radcliffe, C. W., and Foort, J. (1961). "The Patellar-Tendon-Bearing below-knee prosthesis." Biomechanics Laboratory, University of California , Berkely.

Rae, J. W., and Cockrell, J. L. (1971). "Interface pressure and stress distribution in prosthetic fitting." Bull Prosthet Res, 10(16), 64-111.

Renstrom, P. (1981). "A follow up study of 200 below knee amputees amputated between 1973-1977." In. The below knee amputee, Gothenburg, Sweden, 7- 25.

Robb, H. J., Jacobson, L. F., and Hordon, P. (1965). "Midcalf amputation : the lateral and medial flap." Arch. Surg., 91, 506-511.

Roberts, R. A. (1986). "Suction socket suspension for below knee amputees." Arch. Surg., 67, 196-199.

Robinson, K. P. (1988). "Skew-flap below knee amputation." in Limb Salvage and Amputation for Vascular Disease, 373-382.

Rutkow, I. M., and Marlboro, P. H. (1986). "Orthopaedic operations in the United States 1979 through 1983." J. Bone Joint Surg., 68-A, 237-241.

Sanders, J. E. (1995). "Interface mechanics in external prosthetics: review of interface stress measurement techniques." Med & Biol Eng & Comput, 33, 509-516.

Sanders, J. E., Bell, D. M., Okumura, R. M., and Dralle, A. J. (1998). "Effects of alignment changes on stance phase pressures and shear stresses on transtibial amputees : measurements from 13 transducer sites." IEEE Trans Rehabil Eng, 6(1), 21-31.

Sanders, J. E., Boone, D. A., and Daly, C. H. (1990). "The residual limb/prosthetic socket interface: normal stress and shear stress." in: Proceedings of the 13th Ann. Conference. RESNA, Washington, D.C, 234-235.

Sanders, J. E., and Daly, C. H. (1989). "Normal and shear interface stresses in lower limb prosthetics." IEEE Conference Engineering in Medicine and Biology, Seattle, 1443-1444.

Sanders, J. E., and Daly, C. H. (1993). "Measurement of stresses in three orthogonal directions at the residual limb-prosthetic socket interface." IEEE Trans Rehabil Eng, 1(2), 79-85.

Sanders, J. E., Daly, C. H., and Burgess, E. M. (1992). "Interface shear stresses during ambulation with a below knee prosthetic limb." Journal of Rehabil Res Dev., 29(4), 1-8.

Sanders, J. E., (2000). "Thermal response of skin to cyclic pressure and pressure with shear: A technical note." Journal of Rehabil Res Dev., 37(5), 511-515

Schrock, R. D., Zettl, J. H., Burgess, E. M., and Romano, R. L. (1968). "A preliminary report of basic studies from prosthetics research study." Bull Prosthet. Res, 10(10), 90-105.

Silver-Thorn, M. B., Steege, J. W., and Childress, D. S. (1992). "Measurements of below-knee residual limb/prosthetic socket interface pressures." in Proceedings of the 7th World Congress, ISPO, Chicago, USA, 280.

Silver-Thorn, M. B., Steege, J. W., and Childress, D. S. (1996). "A review of prosthetic stress investigation." Journal of Rehabil Res Dev., 33(3), 253-266.

Sonck, W. A., Cockrell, J. L., and Koepe, G. H. (1970). "Effect of liner materials and interface pressure in below knee prostheses." Arch. Phys. Med. Rehabil., 51, 666-669.

Spence, W.D., (2005). Personal communication. Bioengineering Unit, University of Strathclyde, UK

Staats, T. B., and Lundt, J. (1987). "The UCLA total surface bearing suction below-knee prosthesis." Clin. Prosthet. Orth., 11(3), 118-130.

Steege, J. W., and Childress, D. S. (1988). "Finite Element prediction of pressure at the below-knee socket interface." in: Report of ISPO Workshop on CAD/CAM in Prosthetics and Orthotics, Seattle, 71-82.

Steege, J. W., Schnur, D. S., Vorhis, R. L. V., and Rovick, J. S. (1987). "Finite Element analysis as a method of pressure prediction at the below knee socket interface." in: Proceedings of the 10th annual RESNA conference, Washington, 814-816.

Szulc, J. A. (1988). "Development of the above-knee telescopic limb prosthesis." PhD dissertation, University of Strathclyde, UK.

Termansen, N. B. (1977). "Below-knee amputation for ischaemic gangrene. Prospective randomised comparison of a transverse and sagittal operative technique." Acta Orthop Scand, 48, 311-316.

Vachranukunki, T., Seliktar, R., and Demopoulos, J. T. (1986). "Optimization of residual limb-socket load bearing of below knee prostheses." in Proceedings of the 5th World Congress, ISPO, Copenhagen, 355.

Van-Pijkeren, T., Naeff, M., and Kwee, H. H. (1980). "A new method for the measurement of normal pressure between amputation residual limb and socket." Bull. Pros. Res., 10(33), 31-34.

Vitali, M., Robinson, K. P., Andrews, B. G., Harris, E. E., and Redhead, R. G. (1986). "Amputations and prostheses." Bailliere Tindall, London.

Waddell, J. P. (1981). "Below knee amputation." in Amputation Surgery and Rehabilitation: The Toronto experience, Kostwick J P, (Ed), Churchill-Livingstone, New York, 63-80.

Wilson, A. B. (1970). "Evaluation of the patellar-tendon-bearing prosthesis and its variations". In G. Murdoch (Ed.). Prosthetic and Orthotic Practice, 105-114.

Williams, R. B., Porter, D., Roberts, V. C., and Regan, J. F. (1992). "Triaxial force transducer for investigating stresses at the stump/socket interface." Med. Biol. Eng. Comput., 30, 89-96.

Winarski, D. J., and Pearson, J. R. (1987). "Least-square matrix correlations between stump stresses and prosthesis loads for below-knee amputees." Journal of Biomechanical Engineering, 109, 238-246.

Zachariah, S. G., and Sanders, J. E. (1996). "Interface mechanics in lower-limb external prosthetics: a review of Finite Element models." IEEE Trans Rehabil Eng, 4(4), 288-301.

Zahedi, M. S., Spence, W. D., Solomonidis, S. E., and Paul, J. P. (1986). "Alignment of lower limb prostheses." Journal of Rehabil Res Dev., 23(2), 2-19.

Zhang, M., Lord, M., Turner-Smith, A. R., and Roberts., V. C. (1995). "Development of a nonlinear finite element modelling of the below knee prosthetic socket interface." Med Eng & Phys, 17, 559-566.

A1 Derivation of shear stress equations (Fig. 5.1)

To derive the shear stresses on the surface of the transducer the following analysis is required. (Magnissalis, 1992)

A general portion of the transducer is subjected to the bending-resulted normal stresses shown in figure A.1.

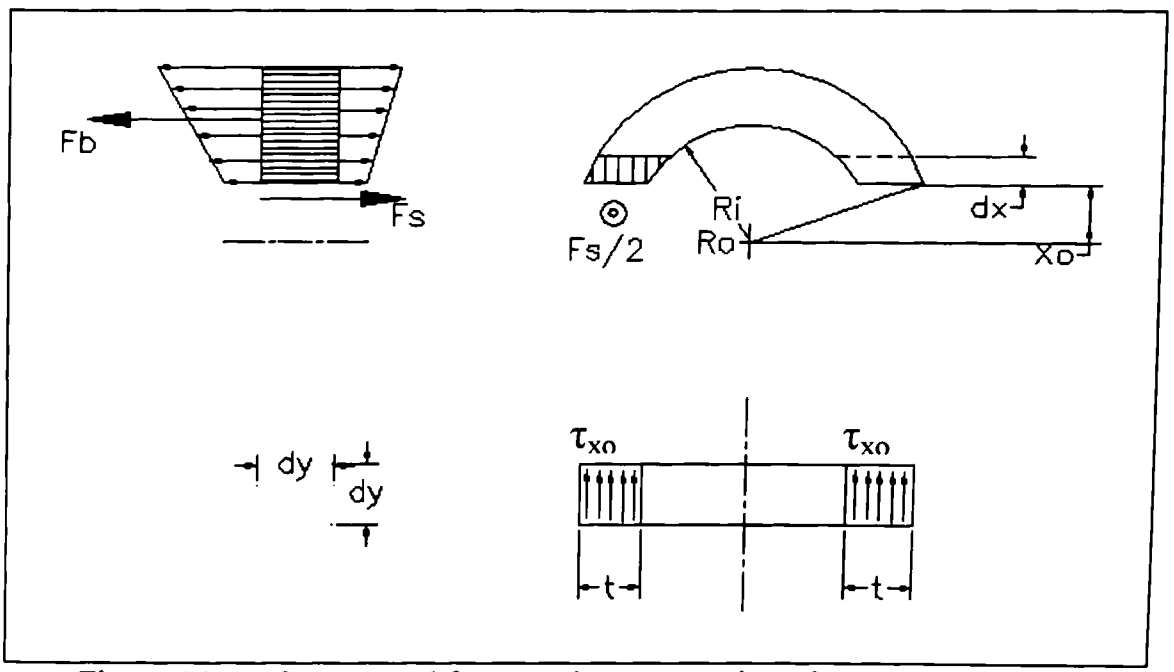

Figure A1: Stresses and forces acting on a portion of transducer. (Adapted from Magnissalis, 1992).

For equilibrium, the residual bending-generated force, F_b :

$$F_b = \int \frac{dM \cdot x}{I} dA = \frac{(F \cdot dy)}{I} \cdot \int x \cdot dA \qquad \text{equation A1.1}$$

must be balanced by a shear generated force, F_s :

$$F_S = (\tau_{xo}) \cdot (2 \cdot t) \cdot dy \qquad \text{equation A1.2}$$

where τ_{xo} is the shear stress at the lower surface of the considered portion and which is assumed uniform throughout the whole depth 2.t

The following substitutions equations according to figure A.1:

$dA = 2 \cdot t \cdot dx$ and

$$t = \sqrt{R_O{}^2 - x_O{}^2} \; - \; \sqrt{R_i{}^2 - x_O{}^2} \qquad \text{equation} \qquad \text{A1.3}$$

With these substitutions equations A1.1 and A1.3 can be written as follows:

$$F_b = 2\frac{(F \cdot dy)}{I} \cdot \int x \cdot \left(\sqrt{R_O{}^2 - x_O{}^2} - \left(\sqrt{R_i{}^2 - x_O{}^2} \right) dx \right) \qquad \text{equation} \qquad \text{A1.4}$$

$$F_S = 2 \cdot \tau_{xo} \cdot \left(\sqrt{R_O{}^2 - x_O{}^2} - \left(\sqrt{R_i{}^2 - x_O{}^2} \right) dy \right) \qquad \text{equation} \qquad \text{A1.5}$$

Since Fb and Fs must be equal the following equations are derived, by evaluating the integral in two distinct ranges:

$0 \leq x_O \leq R_i$:

$$\tau_{xo} = \left(\frac{F}{3 \cdot t \cdot I} \right) \cdot \left[\left(R_O{}^2 - x_O{}^2 \right)^{\frac{3}{2}} \right] - \left[\left(R_i{}^2 - x_O{}^2 \right)^{\frac{3}{2}} \right]$$

where $t = \sqrt{R_O{}^2 - x_O{}^2} \; - \; \sqrt{R_i{}^2 - x_O{}^2}$

and $R_i < x_O \leq R_O$:

$$\tau_{xo} = \left(\frac{F}{3 \cdot t \cdot I} \right) \cdot \left[\left(R_O{}^2 - x_O{}^2 \right)^{\frac{3}{2}} \right] \qquad \text{equation} \qquad \text{A1.6}$$

where $t = \sqrt{R_O{}^2 - x_O{}^2}$

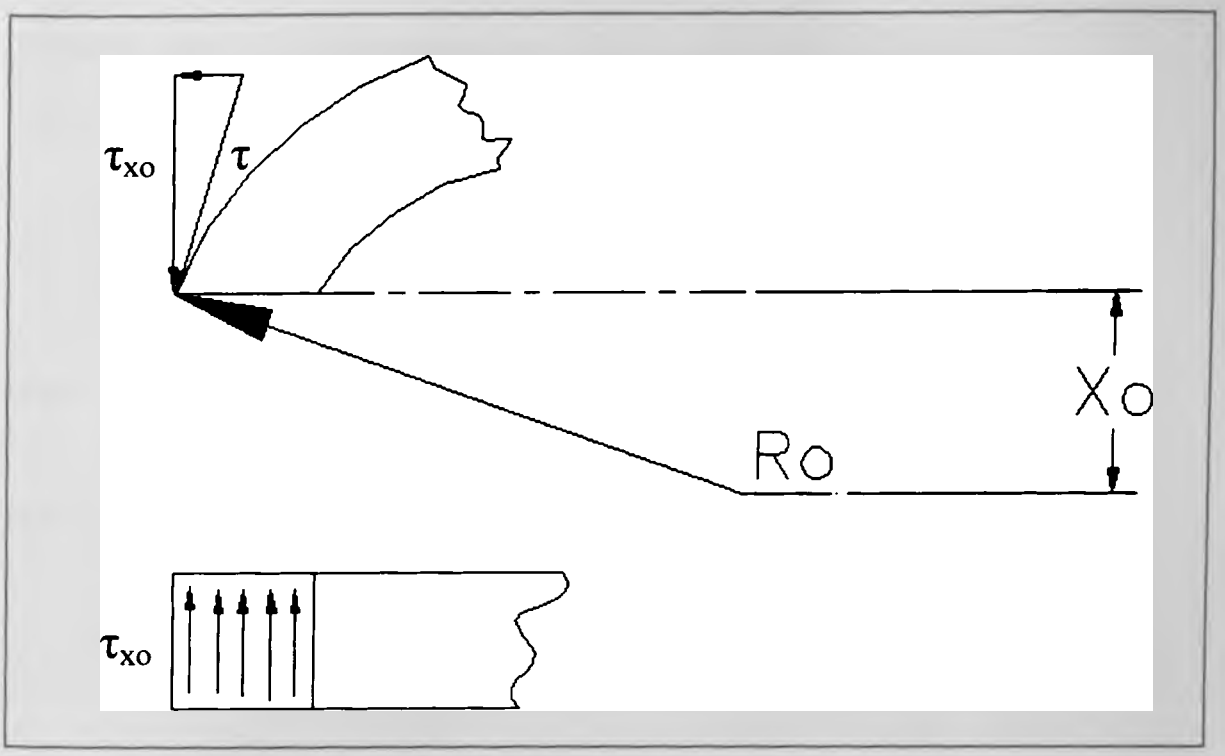

Figure A2: The surface of shear stress, τ. (Adapted from Magnissalis, 1992).

Figure A2 shows that shear stress, τ_{xo} is equal to the stress component shown on the cross-section surface. However shear stress, τ_{xo} is not equal to the total shear stress, τ present on the surface of the component. This surface stress, τ as shown, can only be tangential to the circumference of the cross-section because the surface of the component is not loaded and it is known that shear stresses cannot cross over unloaded surface. Therefore the total shear stress, τ can be calculated using equation A1.6 and the following geometrical relationship, which simply implements what is stated above. (See Figure A2).

$$\frac{\tau}{\tau x_O} = \frac{R_O}{\sqrt{R_O{}^2 - x_O}} \qquad \text{equation A1.7}$$

The shear stress, τ for a given position x_O can be expressed as follows :

$0 \leq x_O \leq R_i$:

$$\tau_{xo} = \left(\frac{F}{3 \cdot t \cdot I} \cdot \frac{R_O}{\sqrt{Ro^2 - x_O^2}} \right) \cdot \left[\left(R_O^2 - x_O^2 \right)^{\frac{3}{2}} \right] - \left[\left(R_i^2 - x_O^2 \right)^{\frac{3}{2}} \right]$$

where $t = \sqrt{R_O^2 - x_O^2} - \sqrt{R_i^2 - x_O^2}$

and $R_i < x_O \leq R_O$

$$\tau = \left(\frac{F \cdot R_O}{3 \cdot I} \right) \cdot \sqrt{R_O^2 - x_O^2} \qquad \text{equation} \quad \text{A1.8}$$

Equation A1.8 is the equation for the shear stress developed, and under the same conditions, on a solid cylindrical component.

Appendix B
Results of the calibration for the transducers

B1 B.E.S.T. 1

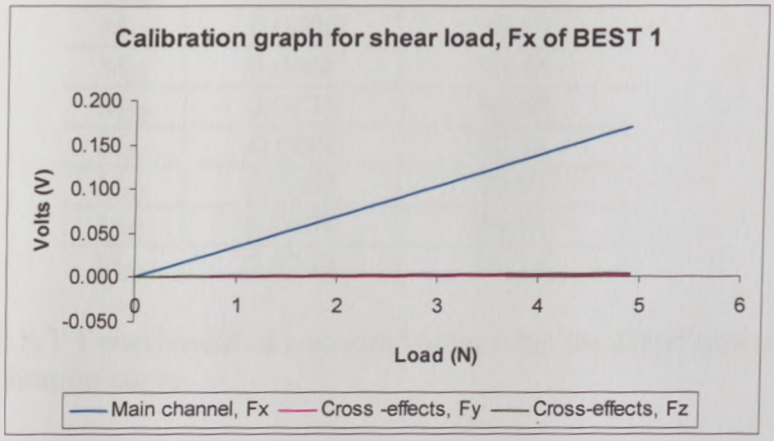

Figure B1.1: Calibration curve for B.E.S.T 1 under shear load, Fx.

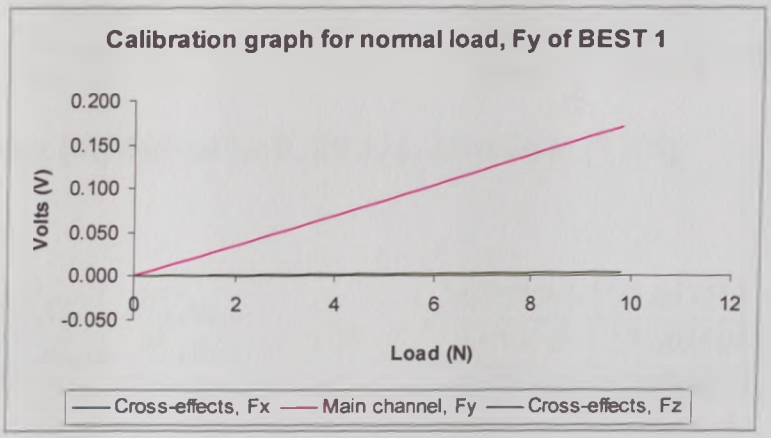

Figure B1.2: Calibration curve for B.E.S.T 1 under normal load, Fy.

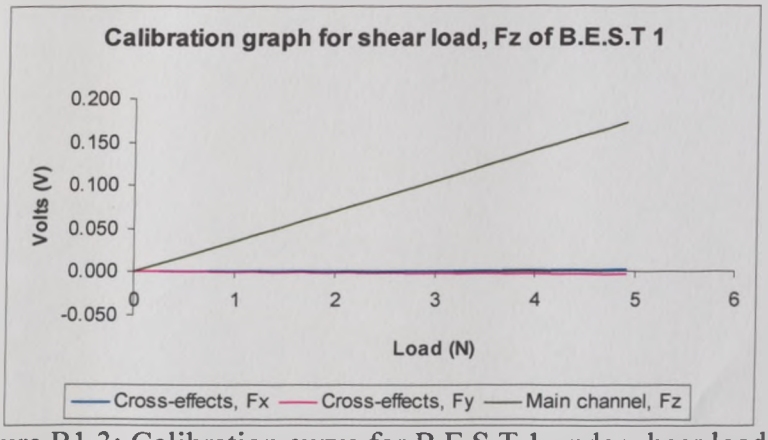

Figure B1.3: Calibration curve for B.E.S.T 1 under shear load, Fz.

Coef.	Mean (V/N)	r-square (%)
M_{11}	0.0348	99.97
M_{12}	0.0004	99.94
M_{13}	0.0006	99.97
M_{21}	0.0006	99.86
M_{22}	0.0173	99.68
M_{23}	-0.0006	99.78
M_{31}	0.0007	99.95
M_{32}	0.0004	99.84
M_{33}	0.0349	99.74

Table B1.1: B.E.S.T 1 coefficient of r-square values from the fitted lines of B.E.S.T 1 calibration curve.

M_{11}	M_{12}	M_{13}	=	0.0348	0.0004	0.0006
M_{21}	M_{22}	M_{23}		0.0006	0.0173	-0.0006
M_{31}	M_{32}	M_{33}		0.0007	0.0004	0.0349

Table B1.2: Matrix [M] derived for B.E.S.T. 1. All units in (V / N).

M^{-1}_{11}	M^{-1}_{12}	M^{-1}_{13}	=	28.757065	-0.653213	-0.505621
M^{-1}_{21}	M^{-1}_{22}	M^{-1}_{23}		-1.016955	57.803600	1.011242
M^{-1}_{31}	M^{-1}_{32}	M^{-1}_{33}		-0.565134	-0.649404	28.651846

Table B1.3: The calibration matrix $[M^{-1}]$ derived for B.E.S.T. 1. All units in (N / V).

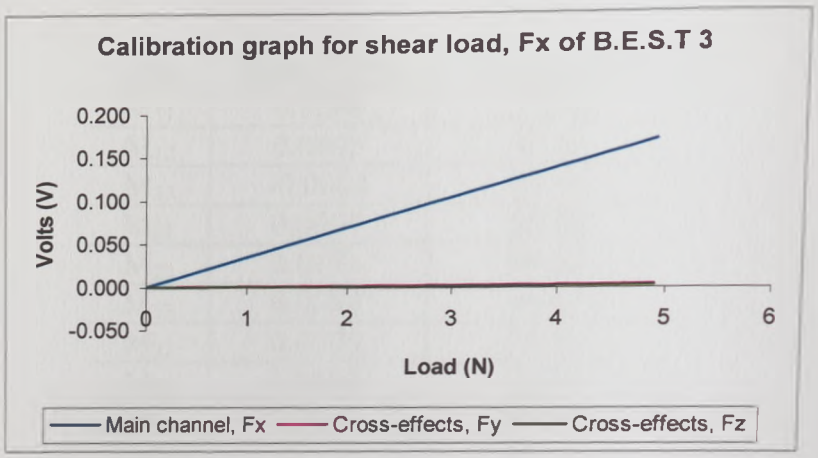

Figure B2.1: Calibration curve for B.E.S.T 3 under shear load, Fx.

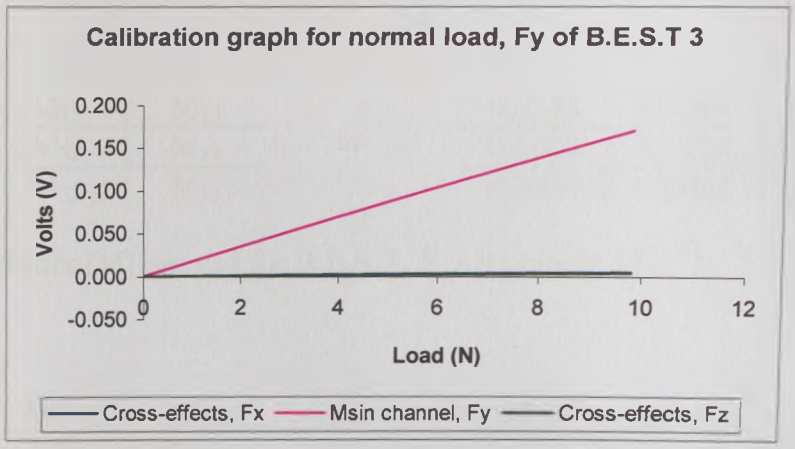

Figure B2.2: Calibration curve for B.E.S.T 3 under normal load, Fy.

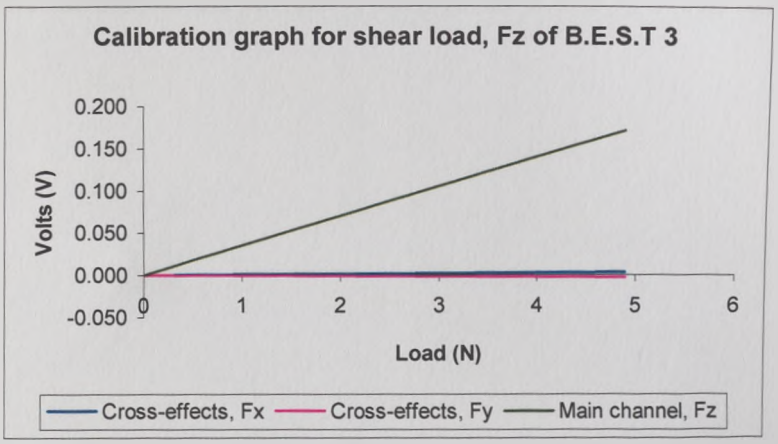

Figure B2.3: Calibration curve for B.E.S.T 3 under shear load, Fz.

Coef.	Mean (V/N)	r-square (%)
M_{11}	0.0348	99.92
M_{12}	0.0005	99.84
M_{13}	-0.0004	99.95
M_{21}	0.0007	99.94
M_{22}	0.0174	99.87
M_{23}	0.0004	99.81
M_{31}	0.0005	99.89
M_{32}	0.0004	99.82
M_{33}	0.0347	99.94

Table B2.1: B.E.S.T 3 coefficient of r-square values from the fitted lines of B.E.S.T 3 calibration curve.

M_{11}	M_{12}	M_{13}		0.0348	0.0005	-0.0004
M_{21}	M_{22}	M_{23}	=	0.0007	0.0174	0.0004
M_{31}	M_{32}	M_{33}		0.0005	0.0004	0.0347

Table B2.2: Matrix [M] derived for B.E.S.T. 3. All units in (V / N).

M^{-1}_{11}	M^{-1}_{12}	M^{-1}_{13}	28.747507	-0.833917	0.340996
M^{-1}_{21}	M^{-1}_{22}	M^{-1}_{23}	-1.147290	57.519779	-0.676277
M^{-1}_{31}	M^{-1}_{32}	M^{-1}_{33}	-0.401004	-0.651036	28.821326

Table B2.3: The calibration matrix $[M^{-1}]$ derived for B.E.S.T. 3. All units in (N / V).

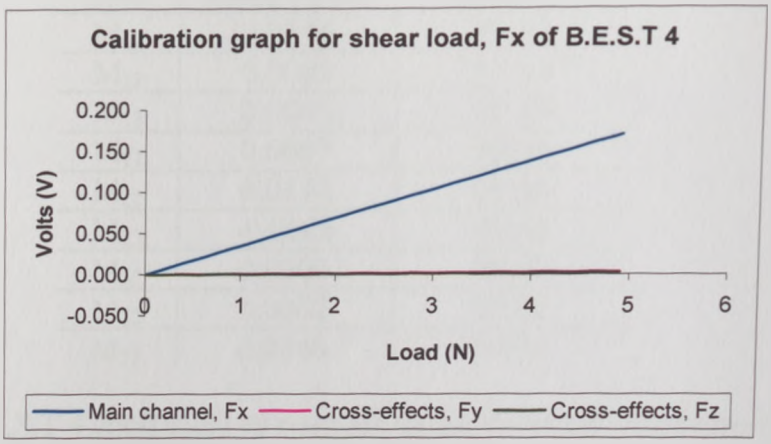

Figure B3.1: Calibration curve for B.E.S.T 4 under shear load, Fx.

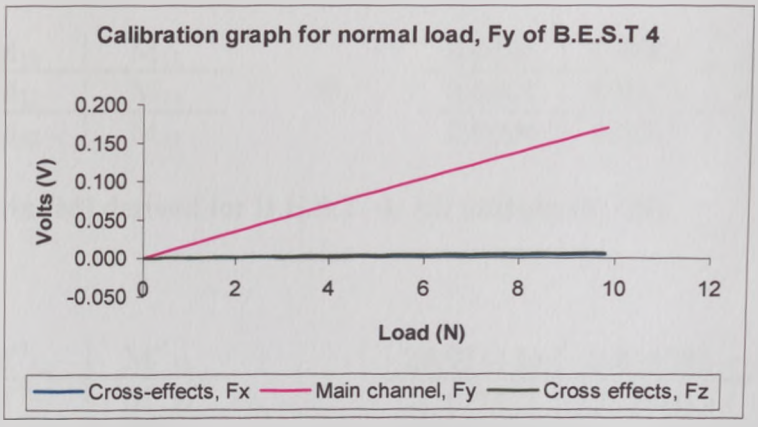

Figure B3.2: Calibration curve for B.E.S.T 4 under normal load, Fy.

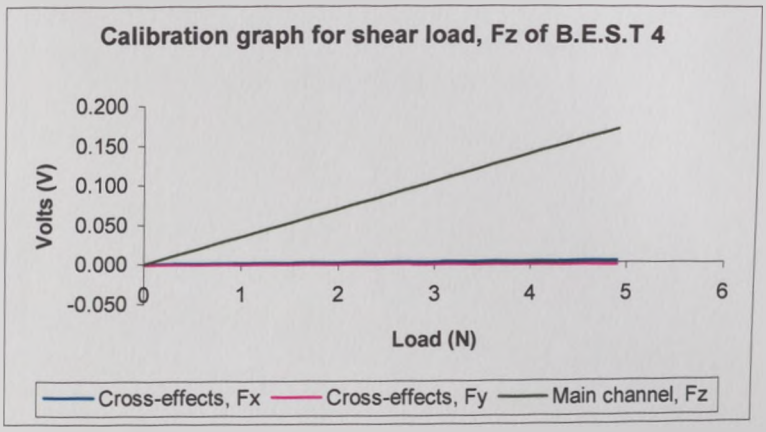

Figure B3.3: Calibration curve for B.E.S.T 4 under shear load, Fz.

Coef.	Mean (V/N)	r-square (%)
M_{11}	0.0346	99.91
M_{12}	0.0005	99.84
M_{13}	0.0006	99.86
M_{21}	0.0007	99.95
M_{22}	0.0173	99.85
M_{23}	-0.0004	99.93
M_{31}	0.0004	99.97
M_{32}	0.0007	99.92
M_{33}	0.0346	99.94

Table B3.1: B.E.S.T 4 coefficient of r-square values from the fitted lines of B.E.S.T 4 calibration curve.

M_{11}	M_{12}	M_{13}	=	0.0346	0.0005	0.0006
M_{21}	M_{22}	M_{23}		0.0007	0.0173	-0.0004
M_{31}	M_{32}	M_{33}		0.0004	0.0007	0.0346

Table B3.2: Matrix [M] derived for B.E.S.T. 4. All units in (V / N).

M^{-1}_{11}	M^{-1}_{12}	M^{-1}_{13}	28.924136	-0.815281	-0.511000
M^{-1}_{21}	M^{-1}_{22}	M^{-1}_{23}	-1.177521	57.809633	0.688739
M^{-1}_{31}	M^{-1}_{32}	M^{-1}_{33}	-0.310560	-1.160134	28.893708

Table B3.3: The calibration matrix $[M^{-1}]$ derived for B.E.S.T. 4. All units in (N / V).

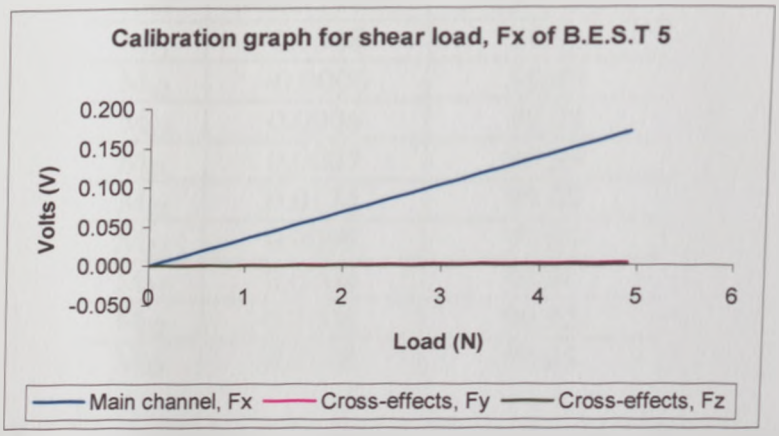

Figure B4.1: Calibration curve for B.E.S.T 5 under shear load, Fx.

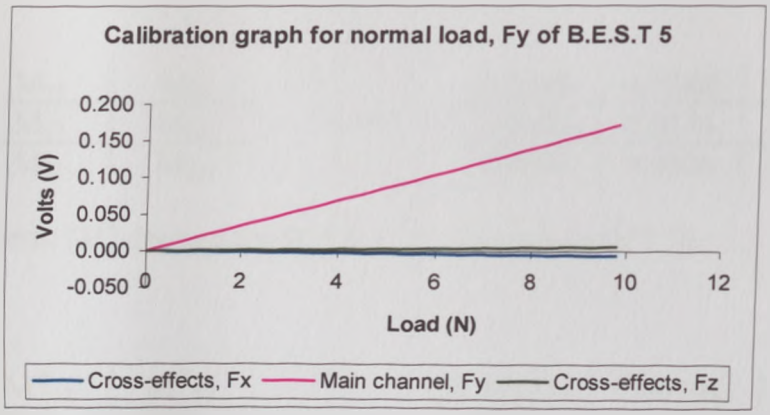

Figure B4.2: Calibration curve for B.E.S.T 5 under shear load, Fy.

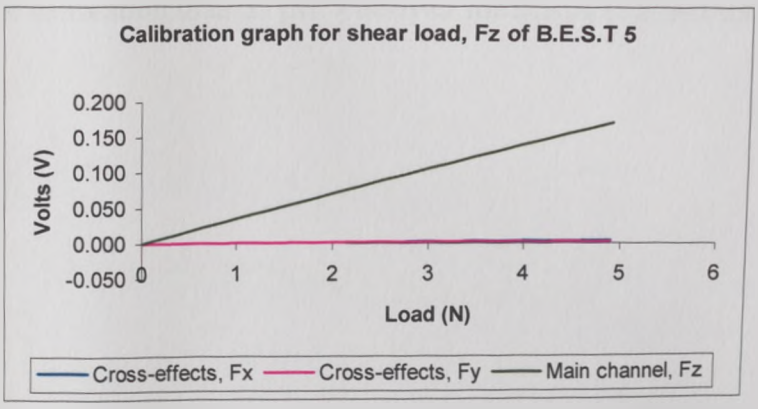

Figure B4.3: Calibration curve for B.E.S.T 5 under shear load, Fz.

Coef.	Mean (V/N)	r-square (%)
M_{11}	0.0348	99.91
M_{12}	-0.0006	99.89
M_{13}	0.0006	99.78
M_{21}	0.0007	99.94
M_{22}	0.0174	99.98
M_{23}	0.0005	99.99
M_{31}	0.0004	99.84
M_{32}	0.0006	99.92
M_{33}	0.0348	99.95

Table B4.1: B.E.S.T 5 coefficient of r-square values from the fitted lines of B.E.S.T 5 calibration curve.

M_{11}	M_{12}	M_{13}	=	0.0348	-0.0006	0.0006
M_{21}	M_{22}	M_{23}		0.0007	0.0174	0.0005
M_{31}	M_{32}	M_{33}		0.0004	0.0006	0.0348

Table B4.2: Matrix [M] derived for B.E.S.T. 5. All units in (V / N).

M^{-1}_{11}	M^{-1}_{12}	M^{-1}_{13}	28.721215	1.007962	-0.509676
M^{-1}_{21}	M^{-1}_{22}	M^{-1}_{23}	-1.146533	57.459515	-0.805800
M^{-1}_{31}	M^{-1}_{32}	M^{-1}_{33}	-0.310361	-1.002267	28.755384

Table B4.3: The calibration matrix $[M^{-1}]$ derived for B.E.S.T. 5. All units in (N / V).

B5 Patellar tendon (PT) transducer.

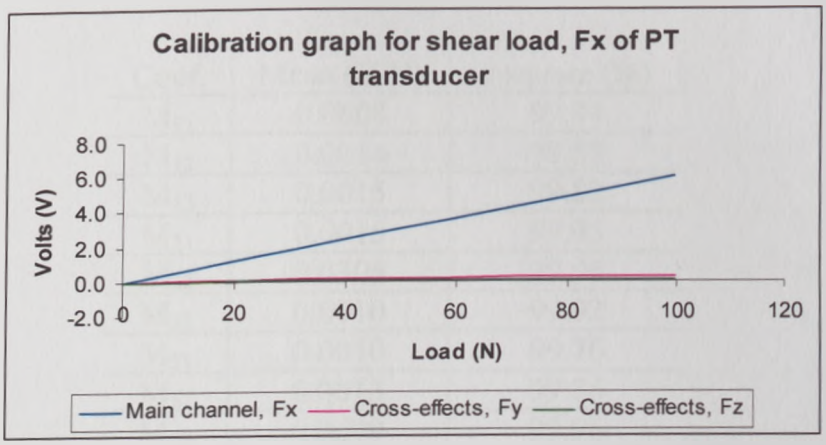

Figure B5.1: Calibration curve for PT transducer under shear load, Fx.

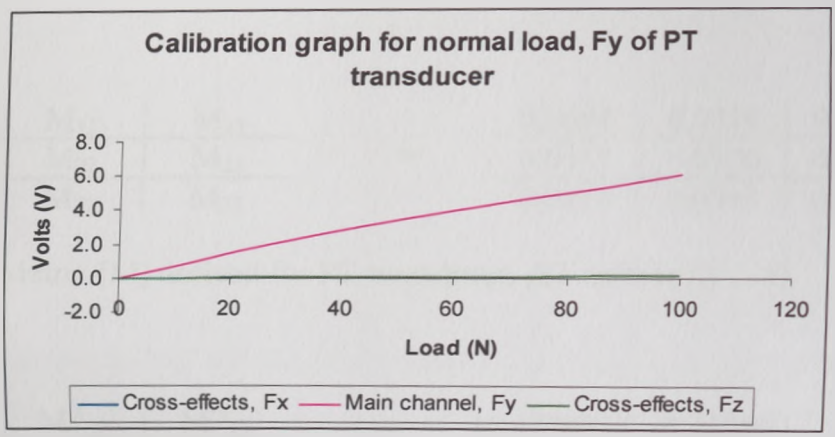

Figure B5.2: Calibration curve for PT transducer under normal load, Fy.

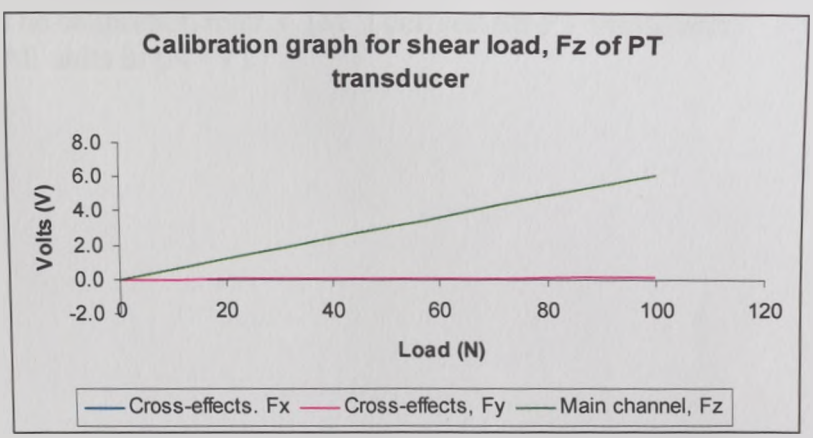

Figure B5.3: Calibration curve for PT transducer under shear load, Fz.

Coef.	Mean (V/N)	r-square (%)
M_{11}	0.0608	99.94
M_{12}	0.0014	99.89
M_{13}	0.0015	99.82
M_{21}	0.0015	99.95
M_{22}	0.0306	99.96
M_{23}	0.0010	99.92
M_{31}	0.0010	99.76
M_{32}	0.0013	99.86
M_{33}	0.0609	99.96

Table B5.1: PT transducer coefficient of r-square values from the fitted lines of PT transducer calibration curve.

M_{11}	M_{12}	M_{13}	=	0.0608	0.0014	0.0015
M_{21}	M_{22}	M_{23}		0.0015	0.0306	0.0010
M_{31}	M_{32}	M_{33}		0.0010	0.0013	0.0609

Table B5.2: Matrix [M] derived for PT transducer. All units in (V / N).

M^{-1}_{11}	M^{-1}_{12}	M^{-1}_{13}	16.472022	-0.736900	-0.393615
M^{-1}_{21}	M^{-1}_{22}	M^{-1}_{23}	-0.799170	32.738304	-0.517891
M^{-1}_{31}	M^{-1}_{32}	M^{-1}_{33}	-0.253417	-0.686747	16.437880

Table B5.3: The calibration matrix $[M^{-1}]$ derived for PT transducer. All units in (N / V).

B6. Calibration of Entran transducers

The Entran transducer was calibrated using dead weights in its complete assembly. Each of the fourteen transducers was individually calibrated since it was stated by the manufacturer that they posses different sensitivities. The bridge voltage for the Entran transducers was set at 5V and the gain was set at 500. A simple system was used to transfer loading to the sensitive area of the transducer. A steel beam supported at one end by a knife edge and the other by the transducer sensitive face, enabled weights to be hung (Figure B6.1). The contact point on the transducer face was reduced to a point load by a ball bearing embedded in the beam. A series of known weights were hung at 75 mm and 25 mm away from the knife edge and the transducer respectively. Thus, the total load acting on the transducer sensitive face was 75% of the hung weights. The transducer output signals were recorded using 16 channel strain gauge amplifier; model DAQN-Bridge (Dewetron, Austria) with PCMCIA Lab View DaqCard 700 (National Instruments, Austin, TX) for data acquisition and a Dell Inspiron PIII for data storage with Lab View version 6.1 as analyzing software. The transducer was loaded and unloaded five times by sequentially placing or taking weights on or off the beam. The voltage is then read after 5 seconds when the value had established. Figure B6.2 and Figure 6.3 shows the plot of the transducer output voltage (V) against load (N). A high degree of linearity could be observed.

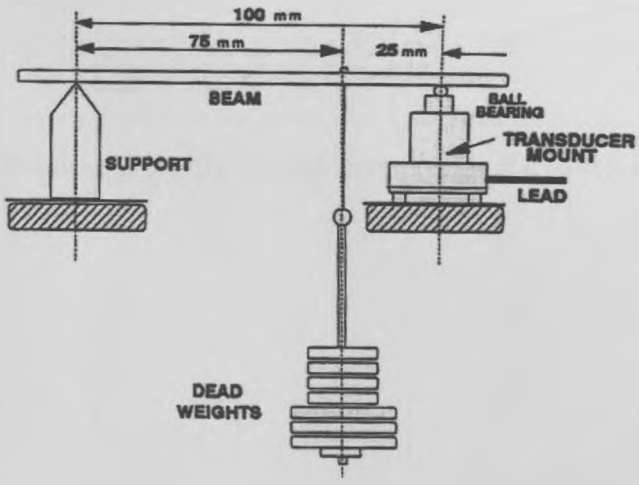

Figure B6.1: Entran transducer calibration setup

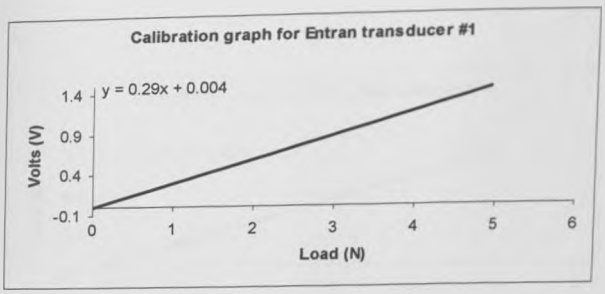

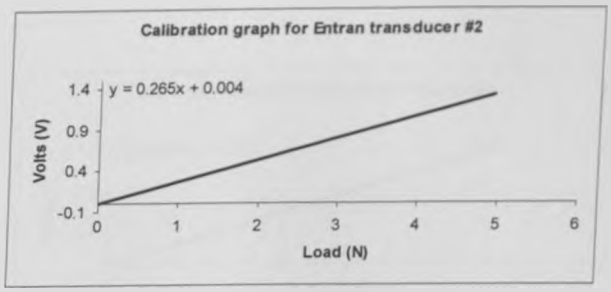

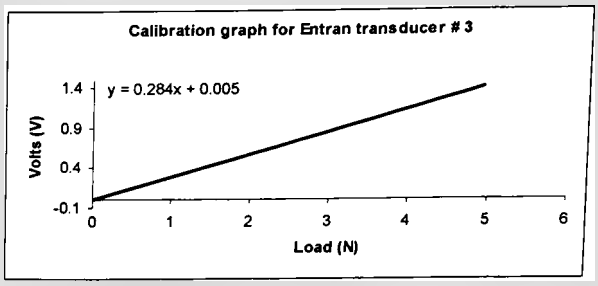

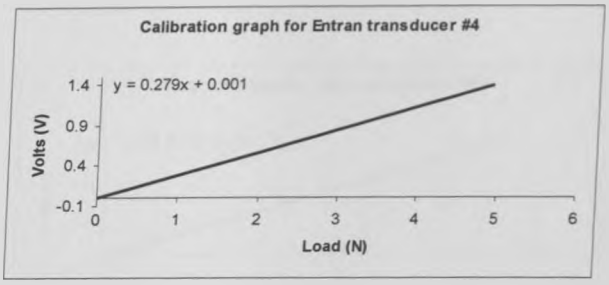

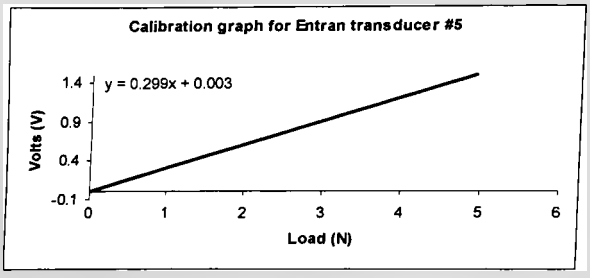

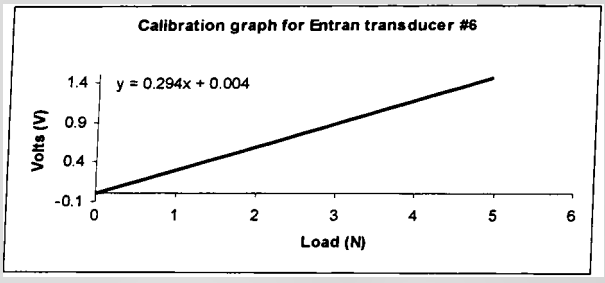

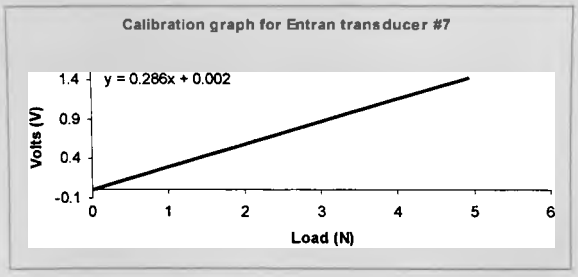

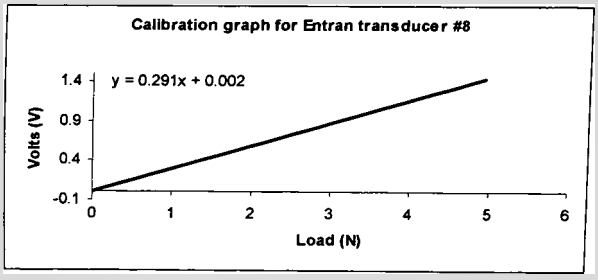

Figure B6.2: Calibration graph for Entran transducers # 1 to # 8 under normal load.

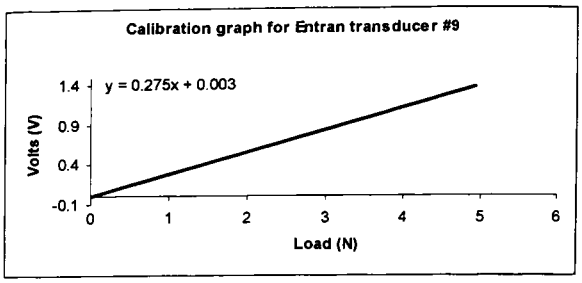

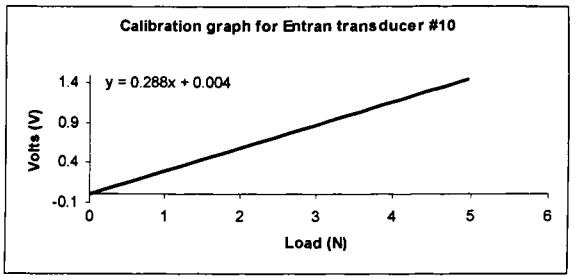

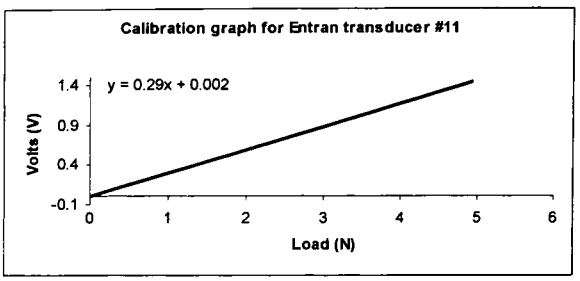

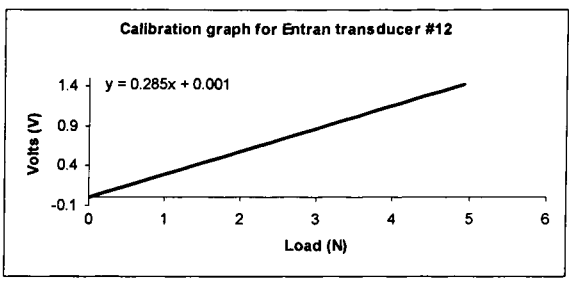

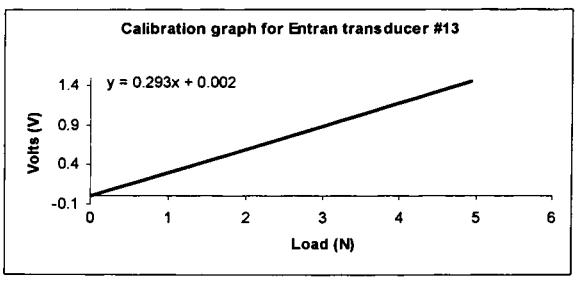

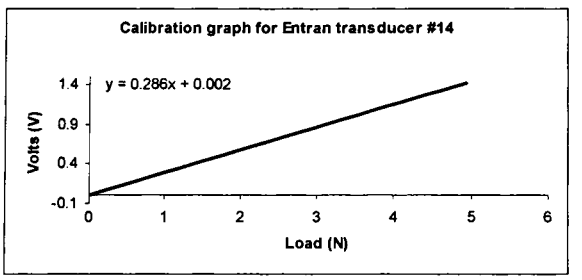

Figure B6.3: Calibration graph for Entran transducers # 9 to # 14 under normal load.

B7. Calibration of electrohydraulic transducer

The electrohydraulic transducer used a pressure vessel (Figure B7.1) to apply uniform pressure on the sensor bag and the calibration results show linear output. (Figure B7.2)

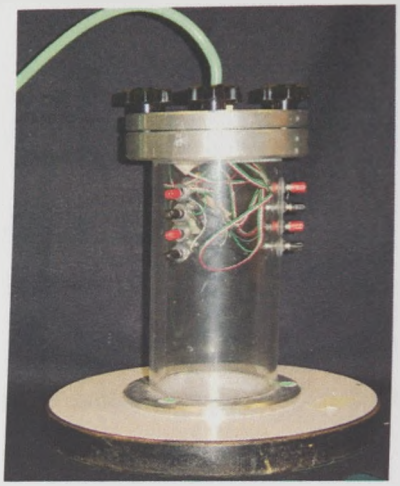

Figure B7.1: Pressure vessel

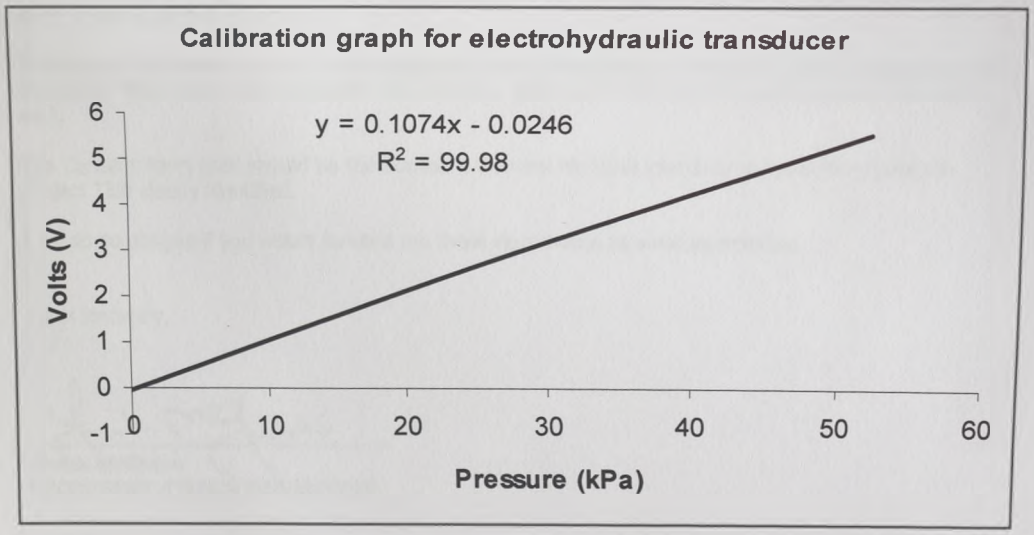

Figure B7.2: Calibration graph for electrohydraulic transducer

Appendix C

C1 Ethical approval (Southern General Hospital, UK)

South Glasgow
University Hospitals
NHS Trust

Southern General Hospital

GENERAL SERVICES DEPARTMENT

1345 Govan Road
Glasgow G51 4TF
Telephone 0141-201-1100
Fax 0141-201-2999
www.nhsscotland.co.uk

NHS
Greater
Glasgow

Enquiries to: Mr Frank McGuire
Direct Line 0141 201 1150/1273
Ref: NOV02LET FMcG.LC

28TH November 2002

Mr W D Spence,
University of Strathclyde,
Bioengineering Unit,
Wolfson Centre,
106 Rottenrow,
Glasgow G4 ONW

Dear Mr Spence,

EVALUATION OF PRESSURE DISTRIBUTION AT THE STUMP-SOCKET INTERFACE OF TRANSTIBIAL AMPUTEES
PAPER NO. EC/02/S/126

Further to your recent application for approval of the above study, I am pleased to advise that full ethical approval was granted by the Southern General Hospital Ethics Committee at its meeting held on Tuesday 26TH November 2002.

The Committee did ask for a better set out Patient Information Sheet. In general the sheet falls short of the expected standard.

The Patient Information should have paragraphs set out advising for example; what is the purpose of the study. Why have I been chosen? Do I have to take part? Can I withdraw, what are the risks etc?.

The Consent Form used should be the Southern General Hospital standard consent form with the Project Title clearly identified.

I would be obliged if you would forward me these documents as soon as possible.

Yours sincerely,

Frank McGuire
SECRETARY ETHICS COMMITTEE

C2 Ethical approval (University of Strathclyde, UK)

MEMORANDUM

To : Mr W Spence, Bioengineering Unit

copy : Members of Ethics Committee
Ms A Stevenson, Finance Office

From : Mrs Gwen McArthur, Senior Assistant Registrar (Court) [Secretary to the Group]

Date : 11 November 2002

PROTOCOL APPROVAL

Project No: ECO7 : 02/03

Project Title: Evaluation of pressure distribution at the stump-socket interface of trans-tibial amputees

Investigators: Mr W Spencer, Lecturer,
Mr W Solomonidis, Honorary Senior Lecturer,
Mr N A Abu Osman, Research Student, Bioengineering Unit;
Dr A M Weir, Consultant in Rehabilitation Medicine, Westmarc, Southern General Hospital.

Location: Bioengineering Unit

Insurance: To be confirmed

Note : Approval from the Ethics Committee at the Southern General Hospital has been sought.

I can confirm that the Ethics Committee has now approved the above protocol. This is subject to ensuring that appropriate insurance cover is in place for this project. If you have not already done so, please contact Ms A Stevenson (extension 2941) in the Finance Office to discuss these arrangements.

I would remind you that if there are any changes made to the protocol the Committee must be informed of these and given the opportunity to consider them.

I would draw to your attention that the Committee would expect you to report back on the outcome of the project with an account of anything which may have occurred within the project that may prompt ethical questions for any similar future project and with anything else you feel the Committee should know.

Should you have any queries or require further information please to not hesitate to contact me. On behalf of the Committee I wish you every success with your project.

GMcA

Subject # 1

Subject # 2

Subject # 3

Subject # 4

Subject # 6

Subject # 7

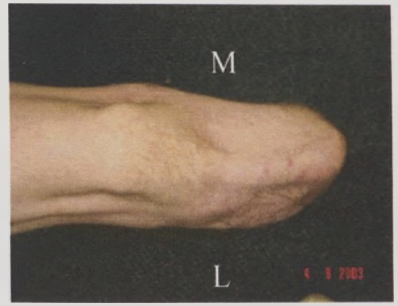

Subject # 8

Subject # 9

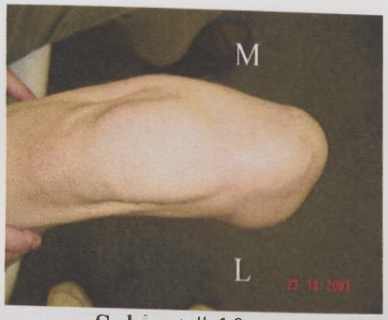

Subject # 10

Figure D1: Anterior view of subjects stump. Note M= medial; L=lateral. Subject 5 stump view not available.